COMPARATIVE EVALUATION OF COOLING TOWER DRIFT ELIMINATOR PERFORMANCE

by

Joseph K. Chan
and
Michael W. Golay

Energy Laboratory
and
Department of Nuclear Engineering
Massachusetts Institute of Technology
Cambridge, Massachusetts 02139

Final Report for Task #3 of the
Waste Heat Management Research Program

Sponsored by

New England Electric System
Northeast Utilities Service Co.

under the

MIT Energy Laboratory Electric Power Program

Energy Laboratory Report No. MIT-EL 77-004

June 1977

COMPARATIVE EVALUATION OF COOLING TOWER DRIFT ELIMINATOR PERFORMANCE

by
Joseph K. Chan and
Michael W. Golay

Energy Laboratory Report No. MIT-EL 77-004

June 1977

ABSTRACT

The performance of standard industrial evaporative cooling tower drift eliminators is analyzed using experiments and numerical simulations. The experiments measure the droplet size spectra at the inlet and outlet of the eliminator with a laser light scattering technique. From these measured spectra, the collection efficiency is deduced as a function of droplet size. The numerical simulations use the computer code SOLASUR as a subroutine of the computer code DRIFT to calculate the two-dimensional laminar flow velocity field and pressure drop in a drift eliminator. The SOLASUR subroutine sets up either no-slip or free-slip boundary conditions at the rigid eliminator boundaries. This flow field is used by the main program to calculate the eliminator collection efficiency by performing trajectory calculations for droplets of a given size with a fourth-order Runge-Kutta Numerical method.

The experimental results are in good agreement with the collection efficiencies calculated with no-slip boundary conditions. The pressure drop data for the eliminators is measured with an electronic manometer. There is good agreement between the measured and calculated pressure losses. The results show that both particle collection efficiency and pressure loss increase as the eliminator geometry becomes more complex, and as the flowrate through the eliminator increases.

Acknowledgements

This work was begun in recognition of the growing concern regarding the possible environmental effects of cooling tower drift in central power station cooling. The literature in this area has been very sparse, in regard to the aerodynamic performance and basic physics of drift eliminators, as well as in the related areas of field measurement of drift transport and field data regarding the environmental effects of salt exposures. The goal of this work has been to improve this situation by providing a basic experimental and theoretical understanding of drift eliminator performance, spanning the range of designs in current industrial use.

This work has been conducted since 1974 with the generous support of the New England Electric System and of Northeast Utilities, through the MIT Energy Laboratory's Waste Heat Management Program.

The work has been carried out by Joseph K. Chan and myself, with the doctoral thesis research of Joseph being derived from the project. The success of this project has been greatly aided by the generous cooperation of the Ceramic Cooling Tower Company, Ecodyne Cooling Products, and the Marley Cooling Tower Company in donating eliminators for testing and in providing critical reviews as the work has progressed. In addition, special thanks are due to Thermo-Systems Inc. for the loan of a Berglund-Liu Monodisperse

Droplet Generator, and to Spray Engineering Co. for supplying SPRACO spray nozzles for use in the Drift Elimination Experimental Facility.

At MIT, Professors Warren M. Rohsenow and S. H. Chen have contributed valuably to the work in consultative discussions regarding the design of the experiments and in the interpretation of the results. Graduate students Ralph Bennett and Yi Bin Chen have also provided valuable assistance to the work in a similar fashion.

In conclusion, the competent typing of this report by Ms. Marsha Myles also deserves grateful recognition.

Michael W. Golay
Associate Professor
of Nuclear Engineering

TABLE OF CONTENTS

LIST OF FIGURES

No.

LIST OF TABLES

CHAPTER 1

INTRODUCTION

1.1 Background

Current practice in the design and operation of new electric power stations selects a single method of waste heat disposal and then designs the cooling apparatus to meet the worst station heat load throughout the year (D1). This is an outgrowth of past trends, in which once-through cooling was virtually the universal method of power station waste heat disposal in the United States. In the late 1960's waste heat disposal suddenly became a controversial topic with the introduction of unprecedentedly large (>800MWe) and thermally inefficient nuclear power stations. In 1973 the Environmental Protection Agency (EPA) added impetus to the use of cooling towers when it took under advisement a Burns & Roe study indicating that evaporative cooling towers may well be the only closed circuit cooling option available in the near future. Based on this study, the EPA recommended the evaporative cooling tower as the best practical technology under the Water Pollution Control Amendments. Subsequent concern for protection of the aquatic environment, and a desire to avoid costly licensing delays has motivated many utilities to design their new, large power stations using cooling towers rather than once-through cooling. As recently as October, 1973, a complete listing of all operating or committed nuclear generating units revealed that 48% of the generating capacity was to be served by cooling towers. The participation by fossil-fueled plants is not as great as this, and projections

indicates that about 50% of the newly added power generating installations at early 1980's will be using cooling towers.

The major cooling tower vendors in the United States are Ecodyne, Inc., Santa Rosa, Calif.; The Marley Co., Mission, Kansas; Research Cottrell, Inc., Bond Brook, N.J.; Ceramic Co., Fort Worth, Texas, and Zurn Industries, Erie, Pa. Other large corporations which are either entering the field or considering doing so are Westinghouse Electric Corp., General Electric Corp., and the Babcock and Wilcox Co.

To meet the increasing demand for electricity in the United States, the utilities are planning to build a large quantity of new, large power stations with more emphasis on nuclear power plants. With the prospect of rapidly increasing cooling requirements due to these plants, special attention has been paid to the environmental effects of cooling methods. The major areas of concern related to the environmental effects of cooling towers are fog, icing, and drift deposition.

Drift consists of the water droplets that are mechanically entrained in the cooling tower's exhaust air stream from the station's cooling water. Drift particles contribute very little to the visibility of cooling tower plumes because the quantity of drift is very small compared to the other forms of water present. The following order of magnitude numbers for the mass concentration of typical cooling tower effluents illustrates this point (S3):

$$X(\text{vapor}) \sim 20\ g/m^3$$

$$X(\text{fog}) \sim 1\ g/m^3$$

$$X(\text{drift}) \sim 0.01\ g/m^3$$

Drift has several important deleterious effects on the local environment. When the mixture of water vapor and drift particles in the cooling tower plume, mixed with the ambient cold air,is carried away, the drift particles may form nucleation sites for condensation. Also, the mixing of the cooling tower plume with the stack plume may form acids through chemical reactions.

In order to meet future electric power requirements and because of the scarcity of cooling water, it will be necessary for many of the new power generating plants to utilize cooling water that contains various concentrations of salt, e.g., brackish inland waters, estuarine water, or sea water. Therefore the drift will contain salt as well as chemicals from the coolant water chemistry. The main concern about drift is its potential for damage to nearby facilities, transmission lines and biota. In some instances, drift has caused serious problems in electric distribution systems; the drift deposits being responsible for equipment failures. Cases involving corrosion and fouling of nearby structures have been reported from both fresh and sea water cooling towers (L3). Drift can also be a considerable nuisance when it spots cars, windows, and buildings.

Estimates of drift from cooling towers range from 0.001% of the circulating water to more than 3%. The industry practice, until early 1970, was for cooling tower vendors to guarantee drift release to be less than 0.2%. At the American Power Conference in Chicago (April, 1970) a new performance standard

of 0.03% was introduced, and in November, 1970, a further reduction was proposed, leading to the estimate that future cooling towers may be certified for drift release less than 0.002%.

Drift from cooling towers is traditionally reduced by passing the exhaust flow through drift eliminators installed in the cooling towers. These eliminators operate by passing the two-phase flow stream through a curved duct, with the heavy water droplets becoming trapped on the duct walls due to centrifugal acceleration. The accumulated water on the walls flows back into the cooling tower.

There are many different ways to install the drift eliminators in a cooling tower, depending upon the type and geometry of the cooling tower. All cooling towers are either crossflow or counterflow types, which is determined by the flow direction of the cooling air relative to the downward travel of the water to be cooled. In general, eliminators are installed either horizontally or vertically. The horizontal scheme is commonly used in crossflow type cooling towers and the vertical scheme in counterflow type cooling towers, as shown in Fig. 1.1.1. The horizontal installation scheme is easier and more sturdy in construction. It can also be used to adjust the air flow pattern within the tower. The main problem with the horizontal installation scheme is the inefficient drainage of water from the eliminator walls: a thick water film forms on the eliminator walls and reduces the drift collection effectiveness. The vertical installation scheme has little water drainage

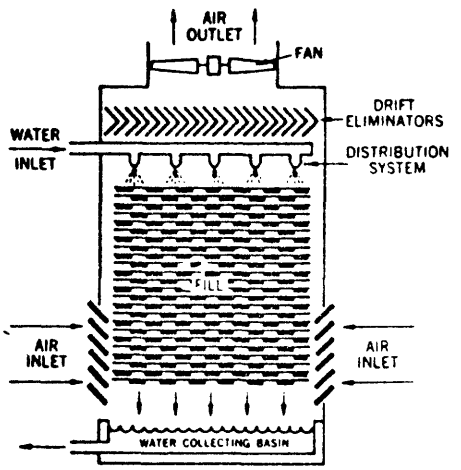

Counter-Flow tower

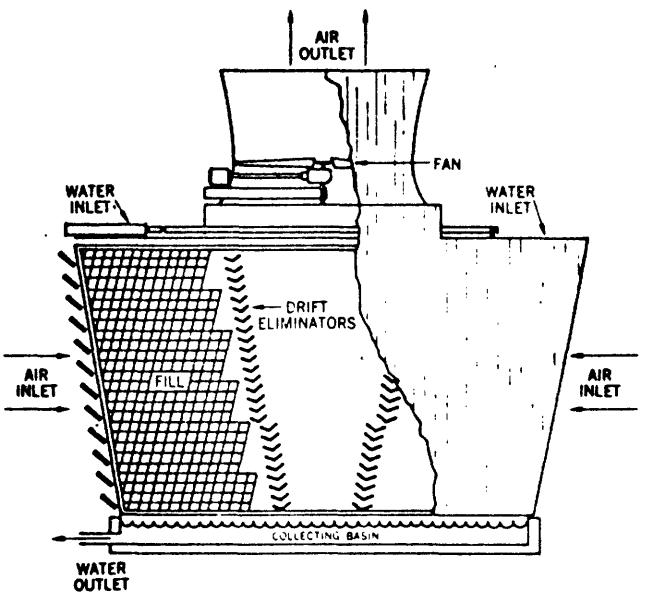

Cross-Flow tower

Fig. 1.1.1 Installation Schemes of Drift Eliminators in Cooling Towers

problem due to the enhanced film flow by gravity.

There are many different types of drift eliminators sold by cooling tower vendors. The common ones are shown in Fig. 1.1.2. The single and double-layer louvre eliminators are generally made with wood.The sinus-shaped eliminator is made from asbestos cement. The Hi-V eliminator is made of polyvinyl chloride (PVC) plastic. The zig-zag eliminator is made from fiber. Some other industrial eliminators are also shown in Fig. 1.1.3.

The performance of drift eliminators can be quantified by two factors: the droplet collection efficiency and the pressure drop across the eliminator. The collection efficiency is generally defined as the ratio of drift mass collected by the eliminator to the total drift mass entering the eliminator. For environmental protection, this factor should be high. The pressure drop across the eliminator represents the resistance of the eliminator to the exhaust air flow. The presence of an eliminator will reduce the air flow within the cooling tower, thus decreasing the tower's cooling capacity. This particular effect can be very detrimental in natural draft cooling towers, since they pass only the small draft caused by the air density difference at the entrance and exit. For mechanical draft cooling towers, a high pressure drop will cause a high horsepower requirement in the fans. Therefore, for inexpensive cooling tower performance, the pressure drop across the eliminators should be as low as possible.

Eliminators operate on the principle of centrifugal separation caused by turning of the flow in the duct. In

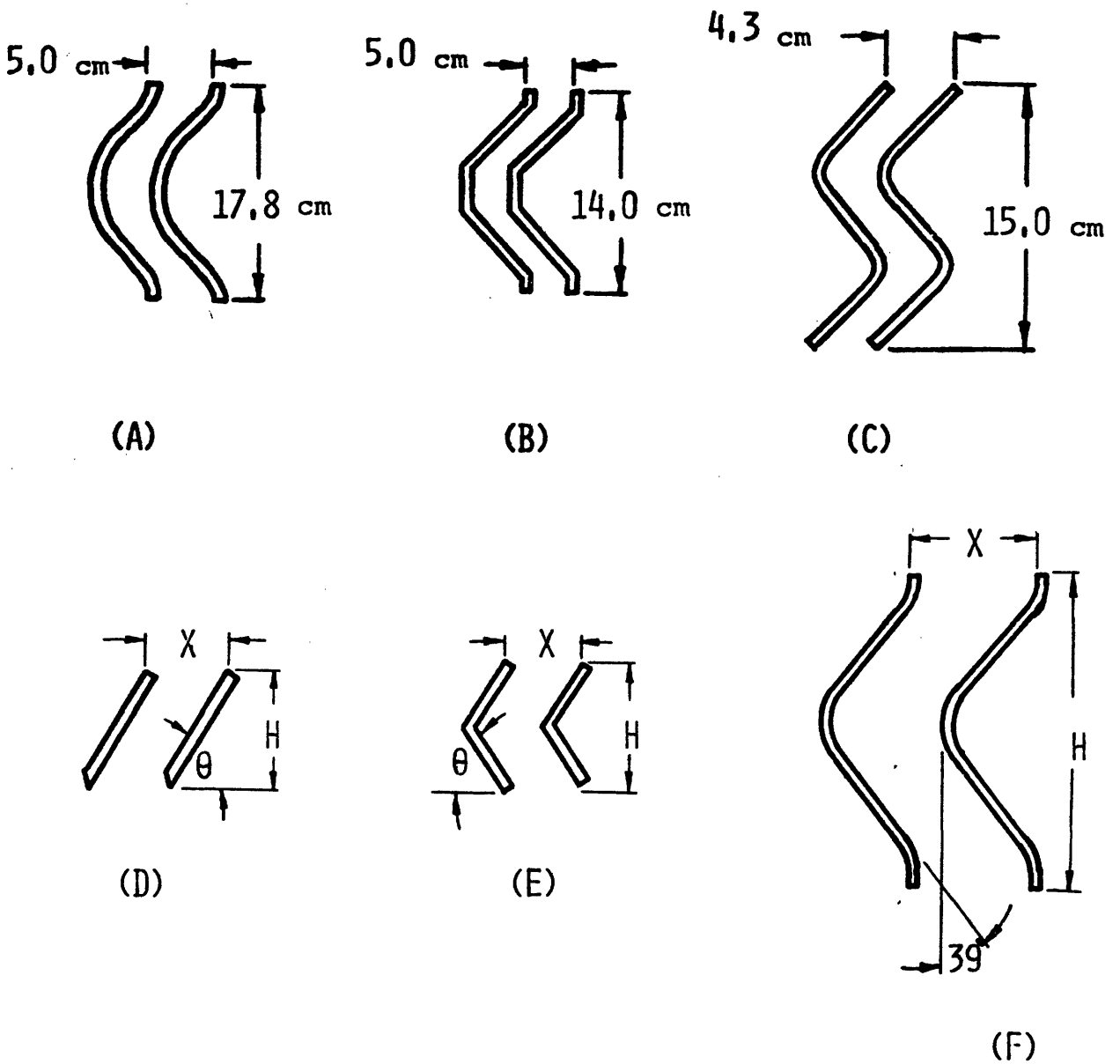

Fig. 1.1.2 Some Common Drift Eliminator Geometries

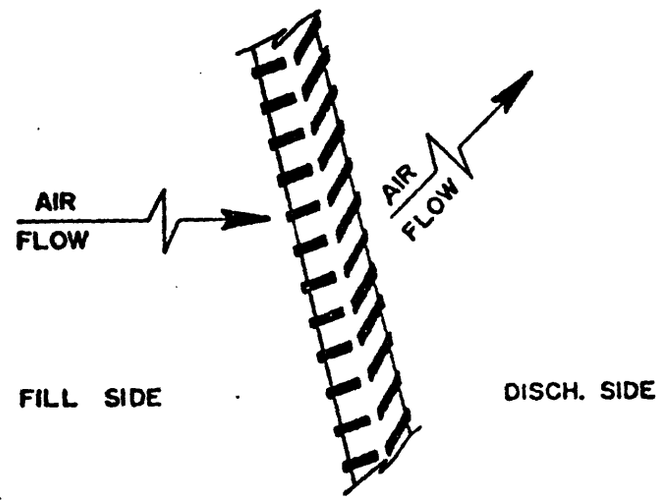

Herringbone
Eliminator

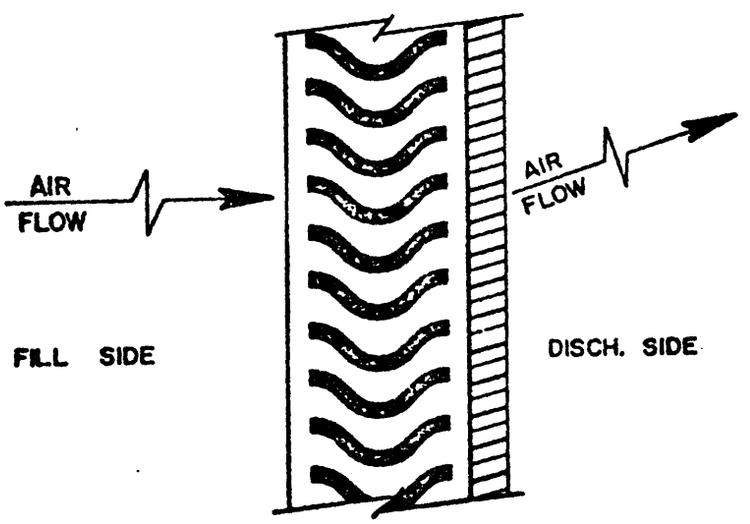

Duplex Eliminator

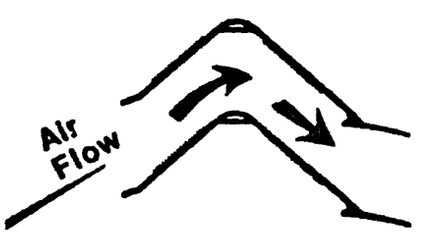

PVC Chevron Type
Eliminator

Fig. 1.1.3 Some Modern Industrial Drift Eliminators

general, more turning results in a higher collection efficiency, but a higher pressure drop. In order to achieve a high collection efficiency and a low pressure drop, the design of drift eliminators calls for an optimization between these two factors. In current industrial practice, there is no standard design procedure for doing this. That is, all existing drift eliminators are generated through random innovation, experience, and experiments. This thesis develops a numerical technique to study the cooling tower drift eliminator performance, which can eventually be used to evaluate and design drift eliminators.

1.2 Previous Theoretical Studies of Drift Eliminator Performance

Studies of eliminator performance have been carried out mainly with experiments. However, the experiments suffer from the difficulties encountered in measuring the drift quantity and distribution. None of the drift measurement techniques has yet been proven to be generally satisfactory to the point of their being adapted for general use (A1). Theoretical studies are rarely performed because it is feared that such studies would be unreliable due to a number of uncertainties. These include the possibility of flow turbulence within the eliminator, the droplets rebounding from or being generated in the water film on the eliminator walls, and the water film drainage system design. Despite this, a theoretical model is still a very useful tool in evaluating the relative performances of different drift eliminators, and in designing improved drift eliminators. Recently a few attempts have been made in this

direction; the approaches are briefly described next.

1.2.1 Roffman's analytical formulation

An analytical formulation for the estimation of drift eliminator collection efficiency has been developed by Roffman et al. (R4). In this model it is assumed that the drift droplets flow longitudinally at the assumed-constant vertical air velocity within the eliminator, and that it experiences transverse viscous drag due to the transverse air velocity component. This component is obtained by assuming that the air velocity at any point in the eliminator is locally parallel to the eliminator wall. For complex geometries the model uses a Fourier series expansion of the transverse velocity component in terms of the duct contour. By using these assumptions an explicit form of the equation describing the droplet transverse displacement can be obtained as a function of longitudinal location of the droplet. From the displacement information it can be determined which of the entering droplets will hit the eliminator walls. The collection efficiency of the eliminator can be determined as a function of droplet size. The results are claimed to be satisfactory when overall collection efficiencies are compared with the experimental data obtained by Chilton (C4).

1.2.2 Foster's Model

Foster, et al. (F3) have developed a potential flow numerical simulation model for theoretical investigations of drift eliminators. The model defines the effective eliminator boundaries with experimental flow visualization photography,

and it is assumed that all droplets entering this region are eliminated. The main stream flow fields are obtained by solving the Laplace equation for the velocity potential within an experimentally defined laminar flow region. Using this information the collection efficiency for any droplet size is estimated from numerically computed droplet trajectories by solving the droplet equation of motion using a Runge-Kutta-Gill procedure. However, the estimated efficiencies are much greater than those observed experimentally. This is thought to be due to the improper treatment of the turbulent wake region. It has been found that results obtained from direct calculation of the flow field without definition of the turbulent wake region provide better agreement with experiments (F2).

1.2.3 Yao and Schrock's model

Yao and Schrock (Y2) also developed a numerical model for evaluating the eliminator collection efficiency. The flow field is calculated by a relaxation method for iterative solution of the Laplace equation for the stream function. The droplet trajectories are calculated step by step in space, with the droplet drag-induced acceleration assumed constant within a given mesh interval. In this model the pressure drop across the eliminator is also calculated by using a boundary layer analysis.

1.3 Survey of Experimental Evaluation of Drift Eliminator Performance

Experimental evaluations of drift eliminator performance are performed by measuring the drift at the exhaust side of the

eliminator in a particular cooling tower or a simulated cooling tower facility. In most cases only the drift rate (defined as the drift mass flowrate escaping the tower divided by the recirculating water flowrate in the tower) is measured. The droplet size-dependent collection efficiency of the eliminator is generally never measured. Many methods exist for measuring drift in these two ways. Most of them stem from droplet measurement techniques in cloud physics. Those that are widely used are summarized below.

1.3.1 Droplet Size Distribution Measurement Techniques

The following methods measure the drift droplet size distribution. The total drift rate can be determined by integrating the distribution over the droplet size.

1.3.1.1 Sensitive Paper

This method has been used extensively to measure the liquid water content and size distribution in clouds and fog. Recently this method was adapted for cooling tower drift measurements (F1,R3,S3,S4,W2). In this method filter paper is sensitized by soaking it with a 1% solution of potassium ferricyanide. The paper is dried thoroughly and dusted with finely ground ferrous ammonium sulfate. The treated paper is pale yellow in color. When a water droplet falls on the paper, it dissolves both chemicals and forms an insoluble blue precipitate known as Turnbull's blue which is easily identifiable against the pale yellow background. The area of the stain is related to the droplet diameter. Adjustments must be made for the speed of

impingement and porosity of the paper. The best method of obtaining calibration factors for these variables and various droplet sizes is to use a monodisperse droplet generator to form stains from a known droplet size, speed of impingement, and porosity of the paper. The calibration is independent of sensitizing agent (C4).

There are two types of sensitive paper sampling methods. The most common method exposes the paper briefly in the air stream with the paper normal to the air flow. However, in this method, the impingement speeds are different for different droplet sizes. A second method (S3) moves the sensitive paper through the air by a rotating head machine with the axis of rotation parallel to the air flow. The head velocity is perpendicular to the average air flow and droplet trajectory, therefore the droplet impingement speed is always equal to the rotational speed of the heads.

The collection efficiency of sensitive paper depends on the droplet sizes and velocities. Calibration of this method should include consideration of the dynamics of particle motion and impingement: particles can impinge at an angle, producing elongated stains, and at higher velocities droplets will produce larger stains. The collection efficiency decreases for smaller droplets. For these reasons calibration and data reduction are time-consuming in the sensitive paper technique.

1.3.1.2 Coated Slide or Film

The measurement technology for this method was also established by cloud physics investigators. This technique is

easily adaptable to field measurements of cooling tower drift droplet size distribution (R3,S4,W2). In this method a glass slide or photographic film is coated with a material that preserves the shape of impinging droplets against coalescence and evaporation. Of all the slide coatings evaluated, a liquid plastic coating called FORMVAR gives the clearest and most distinct representation of the drift droplets. When a water droplet impacts the coating, it is encapsulated as the plastic solvent evaporates. The water in the droplet eventually evaporates through the thin FORMVAR skin,but the exact shape of the impacting droplet is preserved by the plastic film for future size analysis with a microscope. Calibration involves corrections for the flattening of droplets on the slide, and for evaporation, which is a function of time and droplet mineral concentration.

This technique has an upper droplet size limitation in the range of 200 to 300 microns. When droplets larger than this impinge on the slides, the droplets tend to shatter, making a size determination impossible. As with the sensitive paper method, data reduction is lengthy and tedious.

1.3.1.3 Laser Light Scattering

In the laser light scattering technique for drift measurement (S2,S4,S5,S7), droplets are illuminated by coherent, monochromatic laser light. Light scattered by a particle within the sampling volume (defined by the intersection of the laser beam and the detector acceptance cone) is detected by a photodetector, producing a current pulse which is related uniquely

to the droplet size. The current pulses are analyzed and stored in a pulse height analyzer and the data can be processed by a minicomputer. The size of the sampling volume should be small, so that lengthy sampling times can be avoided, and so that the probability of having more than one particle present in the volume is small.

The system is calibrated by noting the response of the instrument to droplets of known size that are generated by a monodisperse droplet generator. However, this method is complicated by the variation of the laser light intensity across the laser beam and by an edge effect.

The main advantage of the laser light scattering system is that it can operate on-line, providing fast results.

1.3.1.4 Laser Light Imaging

This method has not been used in cooling tower drift measurement but appears in principle to have some advantages over the laser light scattering system (K1). In this method a linear array of photodetectors spaced equally measures the droplet shadow diameter. The droplet passes between a He-Ne laser and the detector array of fiberoptics. An optical system focusses the laser beam to cast the droplet's shadow at the desired magnification on the detector array. A voltage drop across a given detector in the array due to shadowing is compared to the quiescent voltage of the unshadowed detectors. Since the ambient light level is always used as a reference, this method has an increased sensitivity to soiling of its optics. The size of particle is determined by the number of

occulted fibers. Only shadows lying fully within the array are used, which eliminates the unavoidable edge effects of scattering or extinction methods.

The device operates on-line and samples particles in situ. However, it is expected that considerable experimentation and possibly modification would be required before an imaging instrument was developed to the point of practical applications for drift measurement.

1.3.1.5 Holography

The principle of this method is that light from coherent laser light source scattered by the droplet interferes at the film plane with light which proceeds unscattered and forms the hologram interference pattern. The photographic film is then processed and replaced in the electromagnetic wave. The diffraction by the interference pattern density variations in the film is such as to produce a focusing of light to produce a real image of the hologram of the droplet. This can be viewed with a closed circuit television system. If the recording and reconstruction light waves have the same properties the reconstructed image will be at the same distance as the recording distance and the cross-section of the droplet under reconstruction will be the same as the cross-section of the original scattering droplet. In this way, one may therefore map out a dynamic droplet field with respect to both position and size distribution.

The method has been used in measuring fog droplets in the size range of 5 to 35 microns (T3). The system has the

disadvantage that the reconstruction necessitates a two-step process and is therefore lengthy. This method is expensive and is shown to be inferior to the light scattering method (S4).

1.3.1.6 Photography

Droplets can be filmed using a high-speed cine camera, with the droplets being diffusely illuminated from the opposite direction. Droplets down to a diameter of 50 microns have been measured. The films are studied frame by frame using an analyzing projector, and the diameter, velocity, and trajectory of the droplets that are clearly in focus can be analyzed. This method has been used in studying drift eliminator collection efficiency (F3). However, the data reduction is lengthy.

1.3.2 Total Drift Mass Measurement Techniques

In most experimental work drift eliminators are evaluated by measuring the total drift mass flux escaping cooling towers. Some of these methods are described below.

1.3.2.1 Isokinetic Systems

In isokinetic systems air is drawn into the collector with a kinetic energy identical to that of a fluid element at that position, had the collector not been there. If the density and temperature of the air do not change as the air is drawn into the collector, isokinetic sampling requires only that the velocity of the air flow into the collector being equal to that in the absence of the collector at the point of measurement. In an isokinetic system, the mean air flow within the collector is adjusted by a blower to be

equal to the mean air flow outside the collector. There are many different isokinetic systems which use various collectors. One of them is cyclone collector (R1,W2), where droplets entering the cyclone collector are separated from the air stream by centrifugal force and are collected in a container. The collection efficiency of the collector is determined in a fog chamber. Drift droplets collected are analyzed by atomic absorption spectroscopy for dissolved mineral concentration. Since the collected water contains not only drift water, but also condensed water, the drift mass flux cannot be determined simply from the quantity of the collected water. Rather, the drift mass flux is determined from the dissolved mineral concentration by assuming that the mineral concentration in the drift is the same as in the makeup water source. This constitutes the greatest uncertainty in this method.

Another kind of collector is the isokinetic sampler tube (H4,M1,S3,S4) in which a heated glass tube filled with glass beads is used to collect drift mineral residue. The heating element evaporates all of the liquid water sampled. Only the mineral residues are retained for subsequent chemical analysis. This method also suffers from the uncertainty in assuming an equality of mineral concentration in the drift and the makeup water source.

The mineral background in a real cooling tower is generally high, and this introduces even more error into either of these methods.

1.3.2.2 High Volume Sampler

The high volume sampler method measures the drift mineral concentration per unit volume of air (L1,R2). Air is pumped through a filter and particles in the air are trapped. The air flow rate through the filter is recorded continuously to give the total volume of air sampled. The filter is heated to keep it dry. Data reduction of the drift mineral concentration is performed with atomic absorption spectroscopy and by comparing the results to a clean filter background count. This method is affected by ambient humidity, wind, and background airborne particulate concentration.

1.3.2.3 Airborne Particulate Sampler

The airborne particulate sampler (APS) was originally developed for monitoring atmospheric salt loading at coastal locations. It operates on the principle of collection by impaction. Two woven polyester meshes mounted on rotating arms sweep out a known volume of air per revolution. By counting the number of revolutions, the total volume of air sampled can be determined. A fan maintains the air flow past the meshes and keeps it parallel to their plane. A wind vane rotates the entire system about the vertical axis so that it always faces into the wind. Calibration can be done with a monodisperse droplet generator. Data reduction is performed by a spectroscopic analysis of the meshes for salt content. The main advantage of the APS over the high volume sampler is that the APS system does not require as much power, and can be

run on a car battery at remote locations.

1.3.2.4 Deposition Pans

In this method petri dishes or polyethylene jars are put at various locations in the horizontal plane surrounding the cooling tower to measure the quantity of drift residue that settles on the ground. Residue is collected for a known length of time and is analyzed by atomic absorption spectrophotometry.

1.3.2.5 Chemical Balance

This method measures the rate of decrease in concentration of a chemical such as sulfate or other tracer chemicals added to the circulating water (C2). The drift rate is calculated from the amount of change in the concentration of the tracer with time. The disadvantages of this method are that a long test period is required and that circulating water systems invariably have other leaks that deplete the chemical tracer.

1.3.2.6 The Calorimetric Technique

The calorimetric technique incorporates special thermodynamic and hydrodynamic principles by utilizing a calorimeter with a throttling nozzle (R3). The droplets passing through the throttle point evaporate because of a pressure drop, and in doing so, they remove heat from the surrounding air. This in turn causes a detectable air temperature drop which is used to determine the drift rate.

1.4 Industrial Efforts in Drift Eliminator Evaluation

The first extensive investigation of drift eliminator

performance was done by Chilton (C4) in the late 1940's and early 1950's. The test apparatus included a closed loop experimental tower which simulated a natural draught cooling tower. The drift droplets were collected by a Calder Fox Scrubber at the tower exit. By measuring the water collected for a certain period of operating time at different velocities, the collection efficiencies of various eliminators for several ranges of droplet size were determined. The pressure drop was measured by pitot static tubes leading to a Chattock Fry tilting micro-manometer. Many different eliminator geometries were tested, and a double-layer louvre eliminator was recommended, which was subsequently adopted on many cooling towers in England. Measurements of precipitation from the cooling towers after installation of the recommended eliminator were then performed using the sensitive paper technique. The sensitive paper used was Whatman No. 1 filter paper.

The experiment was considered to be a great success. Since then, not much work on eliminator performance evaluation has been reported until recently. In 1969, drizzle from two modern 2000 MW stations was detected by the Central Electricity Generating Board Regional Scientific Service Staff. Research work on drift eliminators was subsequently rekindled by the Central Electricity Research Board. Tests similar to those by Chilton were performed on some eliminator geometries (G1),with a recommendation for a closer pitched (1.75 in.) asbestos-cement eliminator. Droplet size measurements were made on water sensitive papers exposed inside cooling towers at various levels

including both under and over the eliminators (M3). Droplet removal efficiencies were found for conventional louvre eliminators. The sensitive paper technique described in this work is the same as the one reported in Chilton's paper except that the calibration was extended to smaller droplet sizes (25-400μm). Theoretical evaluation was also carried out to calculate the collection efficiency as a function of droplet size (F3). The theoretical efficiencies were found to be much greater than the observed efficiencies from their experiments which was done with a photographic method.

In 1971, Fish and Duncan at Oak Ridge National Laboratory developed an isokinetic sampling sensitive paper technique using Whatman No. 41 filter paper (F1). The technique was used to measure the drift size distribution above drift eliminators of a counterflow hyperbolic cooling tower. The drift rate was found to be 0.002-0.006%.

The Marley Company has established a strong program in drift measurement and drift eliminator development since late 1960's. In 1968, a chemical balance method was used in the Marley Laboratory to check drift levels with and without drift eliminators in the testing tower. The technique was also used in drift determinations on an operating mechanical draft industrial crossflow tower at a Municipal Power Plant. In 1970, the Marley Co. was interested in operating a cooling tower on salt water makeup, which required an accurate knowledge of drift rate. Since that time they have sponsored and cooperated with the Environmental Systems Corporation (ESC) to develop

reliable drift measurement instruments that include the Particulate Instrumentation by Laser Light Scattering (PILLS) system, the Isokinetic Sampling (IK) system, and sensitive paper techniques. Later the Marley Co. added a special drift test cell to the Marley Laboratory exclusively for drift eliminator development. Drift measurements were mostly done with the isokinetic sampling system developed by ESC. Many different eliminators have been tested. Some of the important conclusions are listed here (H4):

(1) Numerous observations have shown that the circulating water rate has little effect on the drift level. Specific tests on the Duplex eliminator revealed, within the limits of test accuracy, that there was no change in drift rate with circulating water rates ranging from 12 GPM/ft^2 to 22 GPM/ft^2.

(2) Theoretically, drift eliminator collection efficiency increases with air velocity. However, the water load on the eliminator also increases with the air velocity, but at a greater rate than the increase in efficiency. Altogether it was found that drift increases with air velocity. The rate of this increase can be drastic with an inefficient eliminator, with the failure to control the pattern of the water on the fill side of the eliminator, or with inadequate provision for draining the eliminator.

(3) The effect of efficient air handling in the tower by the eliminators seriously changes the tower performance and drift release rate.

The Environmental Systems Corporation was first sponsored by the Marley Co., but later established itself as an independent organization providing services to parties of every interest. In 1971 ESC received grants from Environmental Protection Agency to further develop drift measurement techniques, particularly on the PILLS system. Other techniques to be evaluated were isokinetic sampling using filter papers, cyclone collector and glass wool fill material, sensitive paper using milli-pore membrane filter paper, and on-line holography. APS was developed later for airborne particulate measurement. Numerous drift measurements at operating cooling towers by ESC using these techniques have been performed. Some of them are listed in Table 1.4.1.

In the early 1970's, Ecodyne developed several drift measurement techniques for field testing. These include the isokinetic sampling system using a cyclone separator, assembled and calibrated by Meteorology Research, Inc., the impaction method using FORMVAR coated slides, and sensitive paper techniques. As of 1973, more than twenty types of drift tests had been conducted on industrial towers. The tests included towers equipped with both the standard two pass drift eliminator configurations typical of the industry for the past twenty years, and a new drift eliminator developed by Ecodyne, the Hi-V eliminator. Test results showed that drift rates for the standard two pass

Table 1.4.1

Field Work of the Environmental Systems Corporation

Field Trip Description	Measuring Instrumentation	Drift Rate Measured (%)
Mechanical draft tower at Oak Ridge (J1,S4)	IK	0.0076
	PILLS	0.0055
Aquatower, a small commercial cooling tower (S4)	IK	0.01
A commercial double flow mechanical draft tower (S4)	PILLS	0.005
Natural draft hyperbolic tower (S4)	IK	0.005
	PILLS (d>145μm)	0.0012
Homer City, Pa., a 500 MWe counter flow natural draft tower (M1,S3)	IK	0.0011
Hornaing, France, a 250 MWe cross flow natural draft tower (S3)	IK	0.0011
Chalk Point Unit #3 (H3,S6)	PILLS	-
Oyster Creek, Forked River, N.J. (S1)	APS	-
Le Havre, France, a cross flow natural draft testing tower (M1)	IK	0.0014

designs varied from 0.02% to 0.12% with a typical value of 0.05%. The Hi-V drift eliminator drift rates varied from 0.001% to 0.008% with a typical value of 0.004%.

Other companies that are involved in cooling tower drift measurements are Research Cottrell, Inc., who uses the High Volume Air Sampling Method (L1), and the Balcke Co., who uses the cyclone separator (R3), etc.

Although much progress has been made recently in drift measurement techniques, disagreements and unreconciled differences frequently show up, which often involve factors of two or three in the value of certain results. Reliable methods should be developed soon in order to accurately access the environmental effects of cooling towers.

1.5 Present Approach

In the present study, an analysis of the performance of standard industrial drift eliminator devices using both theoretical and experimental techniques is carried out. The theoretical approach makes use of the code SOLASUR (H2) to calculate the air velocity distribution within a drift eliminator and the pressure loss through the eliminator, using both free-slip and no-slip boundary conditions at the eliminator walls. This information is used to perform trajectory calculations with a fourth order Runge-Kutta numerical technique for droplets of a given size injected into the eliminator in a uniform transverse distribution.

In the experimental approach, the laser light scattering technique is used to measure the droplet size spectra both at

the inlet section and outlet section of the eliminator. This drift measurement technique is selected because of its on-line data acquisition and reduction capacity, and because of its successful application in the PILLS system by the Environmental Systems Corporation. The main differences between the present technique and the PILLS system are that the laser presently used is a steady-state laser instead of a pulsed laser as in the PILLS system (S4), and that there is no fog problem in this laboratory scale work. The pressure drop across the eliminator is measured with a differential electronic manometer.

Comparison of the calculated results and the experimental data for several drift eliminators is presented.

1.6 Organization of this Report

Chapter 2 describes the numerical model for theoretical evaluation of drift eliminator performance. The assumptions made in the theoretical model are also listed in Chapter 2. The results of this calculation for some common cooling tower drift eliminators are presented in Chapter 3.

In Chapter 4, the details of the experimental measurement techniques in this work are described. The experimental data is displayed in Chapter 5, where it is compared with the calculated results. The sources of experimental error, and efforts to quantify this error are included in both Chapters 4 and 5.

Chapter 6 discusses the discrepancies between the measured and calculated results, the validations of the assumptions

made in the theoretical calculations, and the usefulness of the theoretical model. The overall performances of many drift eliminators are compared, and future improvements are recommended for drift eliminator design.

CHAPTER 2

THEORETICAL EVALUATION OF DRIFT ELIMINATOR PERFORMANCE

2.1 Introduction

Despite the fact that many of the important parameters which affect the performance of drift eliminators cannot be easily accounted for, a theoretical model remains very useful in evaluating the relative performances of different drift eliminators, and in designing improved devices.

In order to do this, a computer program, DRIFT, has been written to numerically simulate the performance of drift eliminators. This chapter describes the theory of the calculations performed by the code and the assumptions that are made in the analysis. A detailed discussion of the use of the code can be found in Ref. C5.

2.2 Assumptions

There are many parameters that affect eliminator performance that cannot be easily included in a theoretical model. Therefore, the following assumptions have to be made in the numerical analysis:

(1) The air flow within the eliminator is laminar. It was demonstrated (F3) experimentally that the flow in a typical drift eliminator is laminar throughout most of the eliminator volume, with

Reynolds numbers lying in the range 2000 to 4000.

(2) The exhaust flow field is not affected by the presence of the drift since the drift density is low.

(3) The flow is two dimensional.

(4) The flow is incompressible since the flow Mach number is low.

(5) Any water film effects on the air flow are neglected.

(6) The initial velocity of the droplet at the inlet of the eliminator is the vector sum of the exhaust flow velocity at the inlet and the vertical droplet terminal velocity.

(7) The probability of a droplet of a given size entering the eliminator inlet at any location is uniform.

(8) There is no droplet mass loss due to either evaporation or friction.

(9) Interactions among the droplets can be neglected since the drift density is low.

(10) The drift is eliminated if it impinges on the eliminator walls, i.e., the "bounce" effect and any water film effects are neglected. Re-entrainment of water droplets from the water film on wall into the exhaust flow can be neglected if the drainage is properly designed and if the film

thickness is sufficiently small so that film surface instabilities do not develop over the anticipated range of exhaust speeds.

Further discussion of the validity of some of these assumptions is presented in Chapter 6.

2.3 Calculation of Air Flow Distributions

In order to calculate the droplet trajectory within an eliminator, it is necessary to know the air velocity distribution within the eliminator. In all previous studies either a uniform flow distribution (R3), or potential flow (F3,Y2) is assumed. In this study, the flow distribution is calculated by the SOLASUR code (H2) which is included in the DRIFT code as a subroutine. In the original SOLASUR code a free-slip boundary condition is used at the rigid boundaries of the eliminators. In this work the option of a no-slip boundary condition at the rigid boundaries has been added to the code so that the mass-averaged total pressure drop between the inlet phase and the outlet phase of the eliminator can be evaluated. It is found that the flow distributions calculated with no-slip boundary conditions look more realistic than those with free-slip boundary conditions. Also, the collection efficiencies calculated with these more realistic flow distributions agree better with measured values. All of these results are shown in later chapters.

The SOLASUR code is a modified version of the SOLA code for calculating confined fluid flows having curved rigid or free surfaces as boundaries. It solves the two-dimensional, transient Navier-Stokes equations for an incompressible fluid using an implicit finite difference technique. This technique is based on the Marker-and-Cell (MAC) method (H1, W1). The description of a flow transient proceeds step by step from an assumed initial velocity field to an asymptotically steady final exhaust flow distribution. The time step size is determined from numerical stability considerations (H2). The fluid region is made up of uniform rectangular cells, and is surrounded by a single layer of fictitious cells as shown in Fig. 2.3.1. Fluid velocities and pressures are located at cell positions as shown in Fig. 2.3.2; horizontal velocities at the middle of the vertical sides of a cell, vertical velocities at the middle of the horizontal sides, and pressure at the cell center.

The procedures involved in one calculational cycle (one time step) consist of:

(1) Computing guesses for the new velocities for the entire mesh from the difference form of the Navier-Stokes equations, which involve only the previous values of contributing pressures and velocities in the various flux contributions. The velocities at boundary cells are adjusted so that the boundary conditions are satisfied.

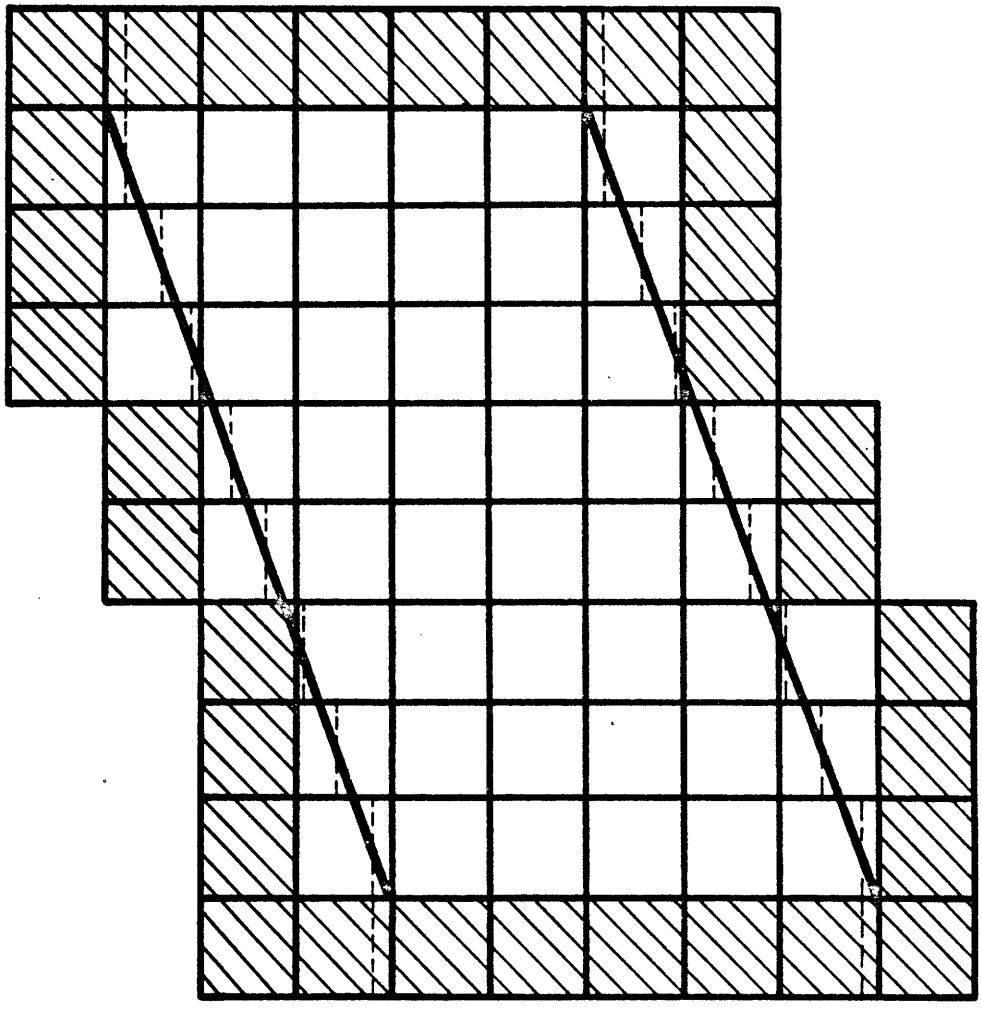

Fig. 2.3.1 General Mesh Arrangement in SOLASUR. Fictitious Boundary Cells are Shaded

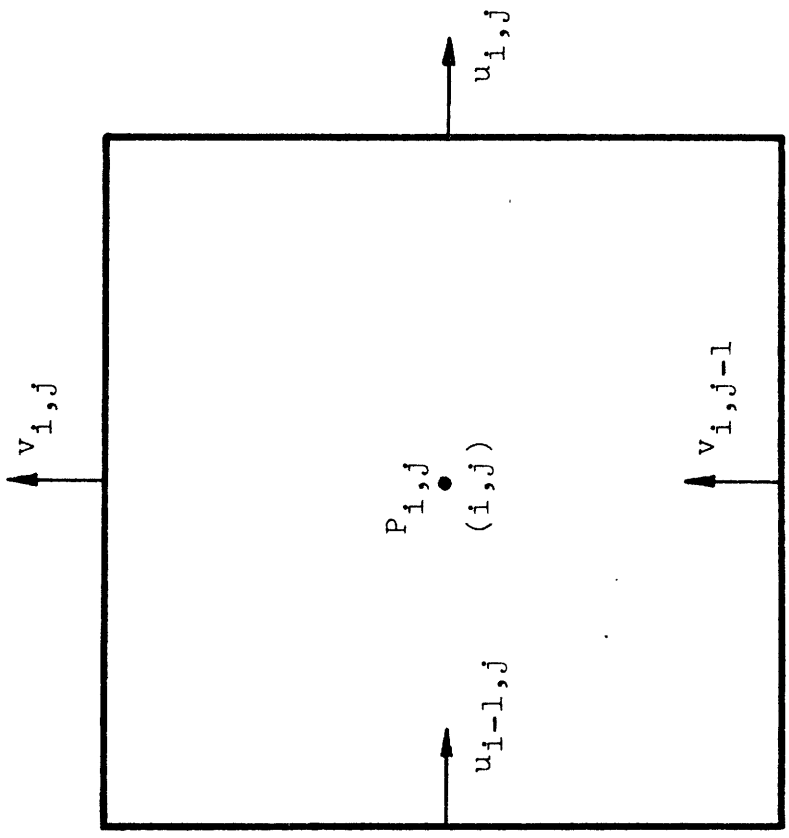

Fig. 2.3.2 Arrangement of Finite Difference Variables in a Typical Cell

(2) Adjusting these velocities iteratively to satisfy the continuity equation by making appropriate changes in the cell pressures. In the iteration, each cell is considered successively and is given a pressure change that drives its instantaneous velocity divergence to zero, thus satisfying the continuity equation.

(3) When convergence has been achieved, the velocity and pressure fields are at the advanced time level and are used as starting values in the next calculational cycle.

The above procedures are repeated in each time step until an asymptotic distribution is reached. The results are then used for droplet trajectory calculations in the main program. The flow chart of the SOLASUR subroutine is shown in Fig. 2.3.3.

In the original code, free-slip boundary conditions are used at the rigid boundaries (the top and bottom boundaries), where in each top surface cell the u-velocity in the top fictitious cell (the cell above the surface cell) is set equal to the u-velocity in the top surface cell, and for each bottom surface cell the u-velocity in the bottom fictitious cell (the cell below the bottom cell) is set equal to the u-velocity in the bottom surface cell. In the DRIFT code, no-slip boundary conditions were added as an

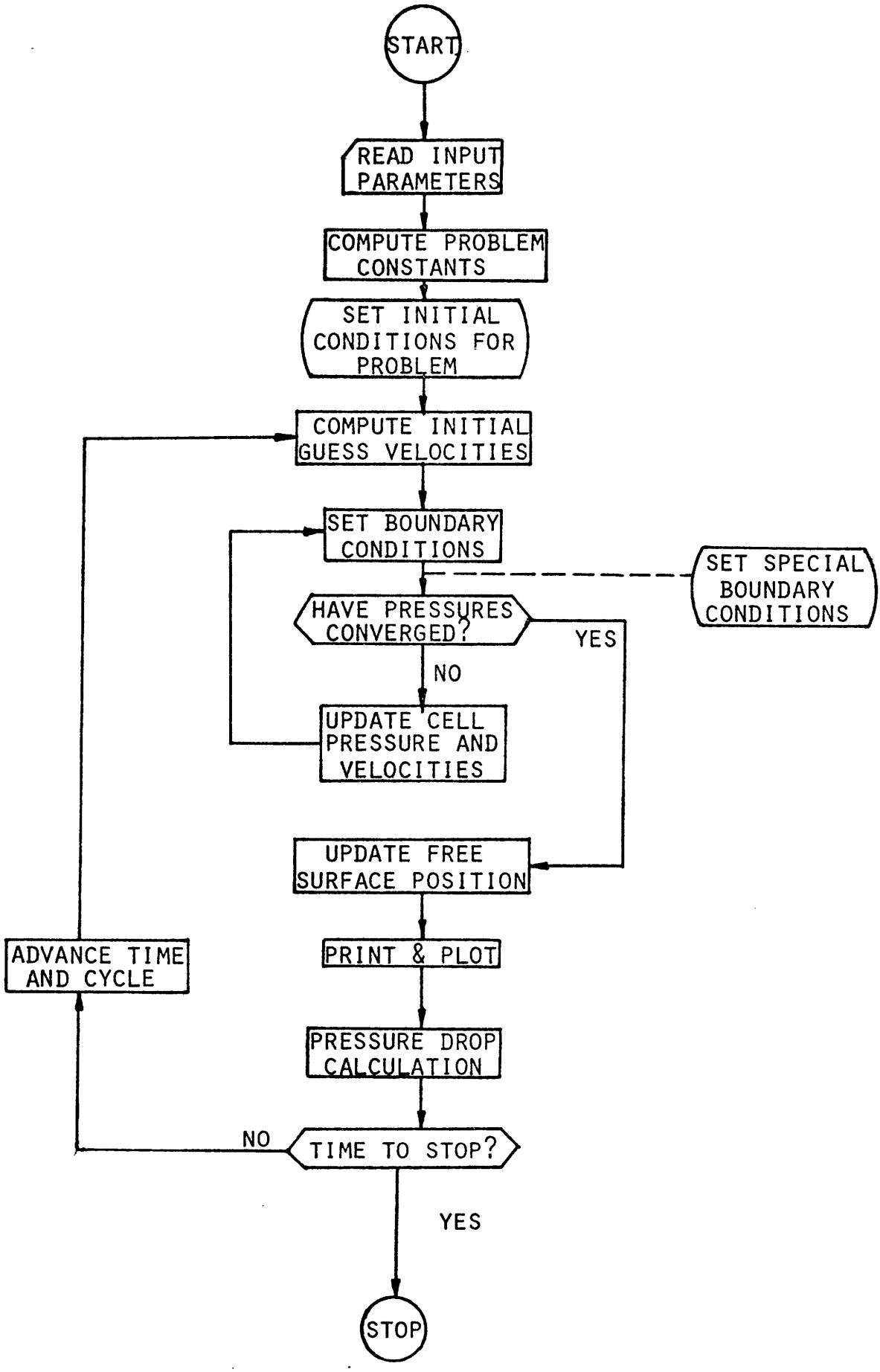

Fig. 2.3.3 Flow Chart of the SOLASUR Code

option, where the u-velocity in the fictitious cells at the top and bottom boundaries are set equal to the negative u-velocity in the top and bottom surface cells.

A detailed discussion of the SOLASUR code is given in Ref. H2. Results of air velocity distribution calculations are presented in Chapter 3.

2.4 Pressure Loss Calculations

The pressure loss of the air stream flowing through an eliminator is an important factor in designing a drift eliminator. A large pressure drop will reduce the tower cooling capacity and will thus either increase the capital cost or the operating cost of the tower. An estimate (G1) reveals that a flow resistance of three velocity heads ($=\Delta P/\frac{1}{2}\rho V^2$) will increase the final temperature of the condensate by approximately 0.2°C. This seems to be a very small increase, yet it is significant in terms of overall station economics, bearing in mind that 1°C is valued at about $3M over the life of a 2000MW station. The flow resistances of current industrial drift eliminators range from two to ten velocity heads.

Prediction of the pressure drop across an eliminator is complicated by the fact that flow separation occurs in most eliminator geometries, and this induces a large pressure drop. Yao and Schrock (Y1, Y2) calculated the pressure drop across drift eliminators using the method of Lieblein and Roudebush (L2), in which the total pressure loss is expressed as a

function of boundary layer thickness, provided that no flow separation occurs in the eliminator. The hydrodynamic boundary layer thickness is determined by an approximation method proposed by Thwaites (T5).

In the SOLASUR code values of pressure are calculated at all cells. Using no-slip boundary conditions at the rigid walls, the pressure drop can be calculated. Assuming equal air density at the inlet and outlet regions of the eliminators, the mass averaged pressure loss is defined as

$$\Delta P = \frac{\sum_{j=JB}^{JT} u_{2,j} \cdot P_{2,j}}{\sum_{j=JB}^{JT} u_{2,j}} - \frac{\sum_{j=JB}^{JT} u_{IBAR,j} \cdot P_{IBAR,j}}{\sum_{j=JB}^{JT} u_{IBAR,j}}, \qquad (2.4.1.)$$

where the summation is from the bottom boundary cell (JB) to the top boundary cell (JT). i=IBAR is the outlet region, and i=2 is the inlet region. $u_{i,j}$ and $P_{i,j}$ are horizontal velocity component and pressure at cell (i,j), respectively. This pressure loss calculation is performed at each time step until a steady state value is reached. Results of this calculation are presented in Chapter 3.

2.5 Droplet Trajectory and Collection Efficiency Calculations

The droplet collection efficiency of an eliminator is generally defined as the ratio of drift mass collected by the eliminator to the drift mass entering the eliminator. It is customary to study eliminator efficiency only in terms of its effect on the total mass of droplets leaving the cooling

tower. However, it is currently known that the droplet size distribution also plays an important part in determining the nature of drift deposition. Therefore it is necessary in evaluating an eliminator to investigate the variation of eliminator efficiency as a function of droplet size. The collection efficiency is defined as

$$\eta(d) = \frac{N_c(d)}{N_i(d)} \quad , \qquad (2.5.1)$$

where $N_c(d)$ represents the number of droplets of diameter d being captured by the eliminator, and $N_i(d)$ represents the number of droplets of diameter d entering the eliminator.

In the numerical simulation process, a certain number of droplets of a given size are injected into the eliminator with a uniform transverse distribution. By calculating their trajectories within the eliminator, the number of droplets that encounter the eliminator boundaries and are then assumed to be captured can be found. The collection efficiency of the eliminator for this droplet size is then determined from Eq. 2.5.1.

The drift trajectory is calculated by solving the droplet equation of motion. For a sphere moving in a flow field, the general solution is governed by the momentum equation (M4)

$$m_d \frac{d\bar{V}_d}{dt} = 6\,\pi\mu_a R(\bar{V}_a - \bar{V}_d)\,\frac{C_d Re}{24} + m_d\bar{g} \quad , \qquad (2.5.2)$$

where

$$\frac{C_d Re}{24} = 1 + 0.197Re^{0.63} + 2.6x10^{-4}Re^{1.38} \quad (2.5.3)$$

and

$$Re = \frac{2\left|\bar{V}_a - \bar{V}_d\right| R\rho_a}{\mu_a} \quad (2.5.4)$$

For a spherical water droplet, Eq. 2.5.2 can be simplified:

$$\frac{d\bar{V}_d}{dt} = \frac{9}{2} \frac{\mu_a}{\rho_w R^2} \frac{C_d Re}{24} (\bar{V}_a - \bar{V}_d) + \bar{g} \quad (2.5.5)$$

The symbols appearing in the above equations are:

m_d = droplet mass

$\bar{V}_d$ = droplet velocity

t = time

μ_a = air viscosity

R = droplet radius

$\bar{V}_a$ = air velocity

C_d = drag coefficient

Re = Reynolds number

$\bar{g}$ = gravitational acceleration

ρ_a = air density

ρ_w = water density

Equation 2.5.5 is a nonlinear differential equation. A fourth-order Runge-Kutta numerical analysis is applied to

determine the droplet trajectory. At any time step, the position of the droplet and its velocity are found. At each location the air velocity is interpolated from the cell values calculated by the SOLASUR code. The air velocity at the beginning of each time step is used throughout that time step, and the local drag coefficient and droplet acceleration are calculated from these velocities and from the local values of the remaining parameters.

A variable time step size is used in the calculation. The step size is determined from a consideration of the propagation of errors in the following manner: For a differential equation of the form

$$\frac{dV_d}{dt} = f(t,V_d), \qquad (2.5.6)$$

the error at time step i + 1 in the fourth order Runge-Kutta method is (C1)

$$\varepsilon_{i+1} = \varepsilon_i \left(1+h\frac{\partial f}{\partial V_d}\bigg|_{t_i,\alpha}\right) - \frac{h^2}{2} f'(\xi,V_d(\xi)) , \qquad (2.5.7)$$

where α is a velocity value somewhere in the interval between t_i and t_{i+1}, ξ is a time value somewhere in the interval between t_i and t_{i+1}, and h is the time step size.

The first term on the right hand side of Eq. 2.5.7 represents the propagation error, and the second term is the local truncation error, which is generally small for small values of h. Then, if $\frac{\partial f}{\partial V_d}\Big|_{t_i,\alpha}$ is negative, a value of h

can be found which will make $(1+h\frac{\partial f}{\partial V_d}\Big|_{t_i,\alpha})<1$, and the error will tend to diminish or die away, so the solution will be stable. For the cases considered, $\frac{\partial f}{\partial V_d}$ is always found to be negative, so by specifying a proper value for the step factor, $h\frac{\partial f}{\partial V_d}$, a stable solution can be obtained. A large value for this step factor will yield a smaller propagation error but a larger truncation error. A small step factor will result in too small a step-size, thus prolonging the computation. A step factor of 0.1 has been found to be satisfactory for the cases under study. In the present model, $\partial f/\partial V_d$ is determined at the beginning of each time step using the local values of droplet velocity and air velocity. The step size of this time step is then the constant step factor divided by $\partial f/\partial V_d$.

If the eliminator is installed in a vertical scheme, the droplets are assumed to enter the eliminator at a velocity which is the difference between the air velocity and their terminal velocities. The terminal velocity of a droplet of radius R is determined from Eq. 2.5.5 by requiring $d\bar{V}_d/dt$ to be zero. Thus

$$\bar{V}_t = \bar{V}_a - \bar{V}_d = -\frac{2}{9}\frac{\rho_w g R^2}{\mu_a \frac{C_d Re}{24}} \qquad (2.5.8)$$

This nonlinear algebraic equation is solved by Newton's method of tangents with a calculational accuracy of 0.1%.

If a droplet enters the eliminator other than vertically (as in a horizontal scheme), then the initial velocity of the droplet will have a vertical component which equals the difference between the vertical component of the air velocity and the droplet terminal velocity, and a horizontal component which equals the horizontal component of the air velocity.

Droplets of a certain size are introduced uniformly across the inlet of the eliminator. The trajectory of each droplet is calculated until it either hits the eliminator walls or passes through the eliminator. The collection efficiency for this droplet size is then the ratio of the number of captured droplets to the number introduced at the entrance. The number of droplets introduced at the entrance determines the accuracy of the collection efficiency calculation. If N_d droplets are introduced uniformly at the entrance, then the error in the collection efficiency calculation will be proportional to $1/N_d$. In the DRIFT code, a provision is made for testing a finer distribution of droplets at the locations where the condition of trap and escape changes between two adjacent droplets. This method greatly improves the accuracy but does not demand too much computation time. A flow chart of the DRIFT code is presented in Fig. 2.5.1.

Trajectory plots and calculated collection efficiencies are presented in Chapter 3.

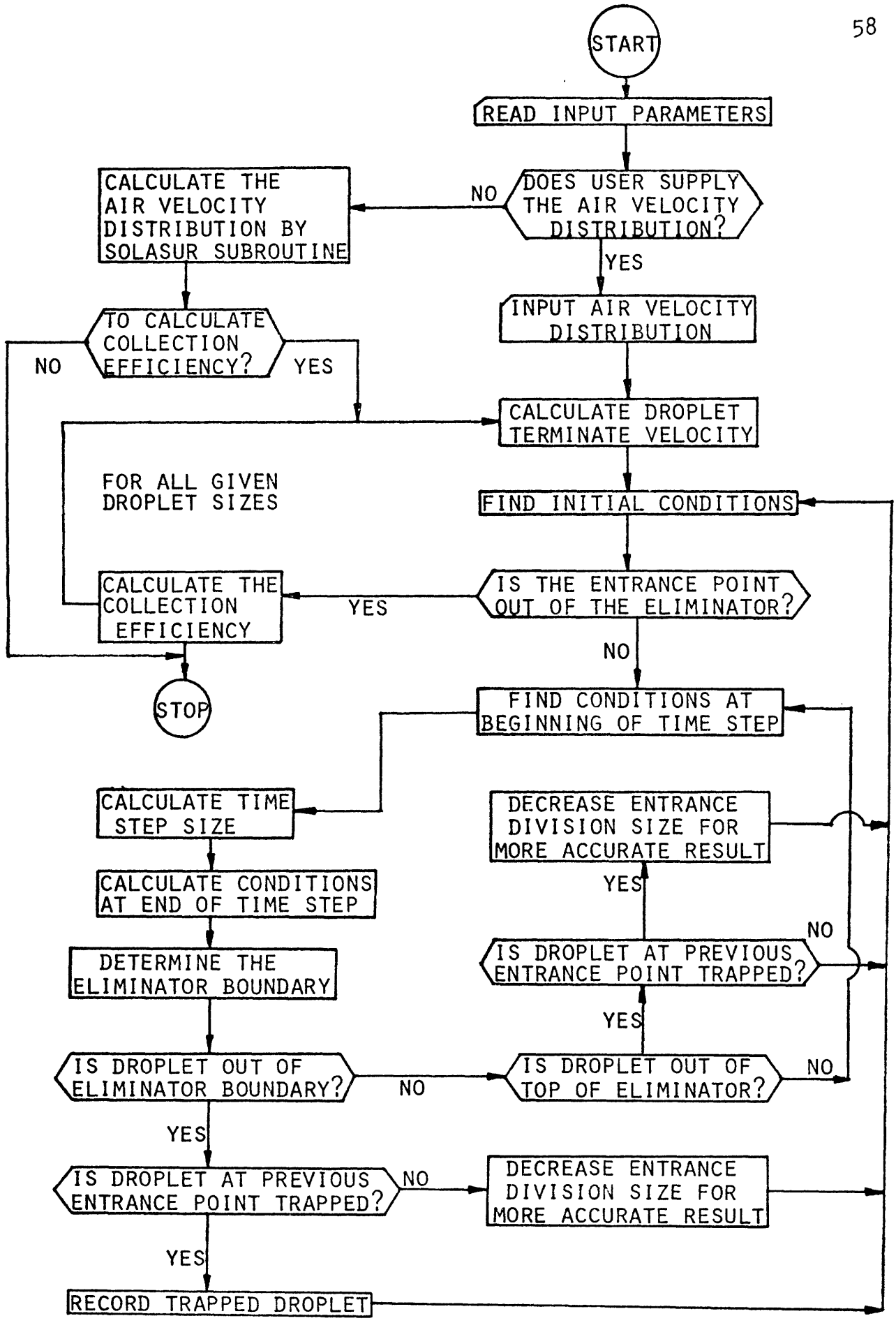

Fig. 2.5.1 Flow Chart of the DRIFT Code

CHAPTER 3

RESULTS OF THEORETICAL CALCULATIONS

3.1 Introduction

This chapter presents the results of the calculations performed with the DRIFT code. The air velocity distributions in some common cooling tower drift eliminators are calculated by the SOLASUR subroutine. The calculations employ both free-slip and no-slip boundary conditions at the eliminator walls, and results are compared and discussed in Section 3.2. The calculated droplet trajectories within these eliminators are presented in Section 3.3. The collection efficiencies calculated from these trajectories are compared with those obtained from other sources in Section 3.4. The last section of this chapter presents the calculated pressure loss across some common industrial drift eliminators.

Table 3.1.1 tabulates the physical dimensions of the eliminators under study. The case numbers in the table will be referred to throughout this thesis.

3.2 Air Velocity Distributions

In this section, air velocity distribution plots for some drift eliminators are presented and discussed. In the plots, the length of the line segments are proportional to the magnitudes of the velocities at the mesh points, and the directions of the lines represent the directions of the flow at the mesh points. In all of the cases presented here

Table 3.1.1

Physical Dimensions of the Eliminators Under Study

Case No.	Eliminator Type	Pitch (cm)	Height (cm)	Inclination Angle, °
S1	Single-Layer Louver	3.92	5.44	45
D1	Double-Layer Louver	6.2	13.2	60
D2	Double-Layer Louver (Lath type)	7.6	18.0	60
N1	Sinus-Shaped	5.7	14.6	-
N2	Sinus-Shaped (Belgian-wave)	5.08	17.8	-
A1	Asbestos-Cement	5.08	14.6	-
H1	Hi-V	5.08	14.0	45
Z1	Zig-Zag	4.3	15.0	45
E1	E-E	3.91	9.75	-

the air flow direction at the inlet of the eliminator is normal to the flow channel cross section. The gravity effect on the air flow is negligible; therefore the air velocity fields will be assumed to be the same whether the eliminators are installed horizontally or vertically.

Figures 3.2.1 and 3.2.2 display the air velocity distributions for a single-layer louver eliminator as calculated by the SOLASUR subroutine using free-slip and no-slip boundary conditions at the eliminator walls, respectively. With the free-slip condition, the calculated velocity is quite uniform (see Fig. 3.2.1). With the no-slip boundary condition, the calculated velocity field,shown in Fig. 3.2.2, is more realistic. Near the lower boundary a wake region can clearly be seen. Such a wake region is expected in the real flow. Note that the velocity in both cases is mainly parallel to the duct boundary, thus, the collection efficiency can be expected to be low for this type of eliminator.

Figures 3.2.3 and 3.2.4 show similar air velocity fields for a two-layer louver eliminator. The free-slip prediction, Fig. 3.2.3, shows a nearly uniform distribution except at the turn in the eliminator where the velocity decreases as the radius of curvature increases. With the no-slip condition, the velocity distribution plot, Fig. 3.2.4, shows very small velocities at the lower boundary in the first half of the eliminator, and at the upper boundary in the second half of the eliminator. In fact, these are the regions where a wake is expected.

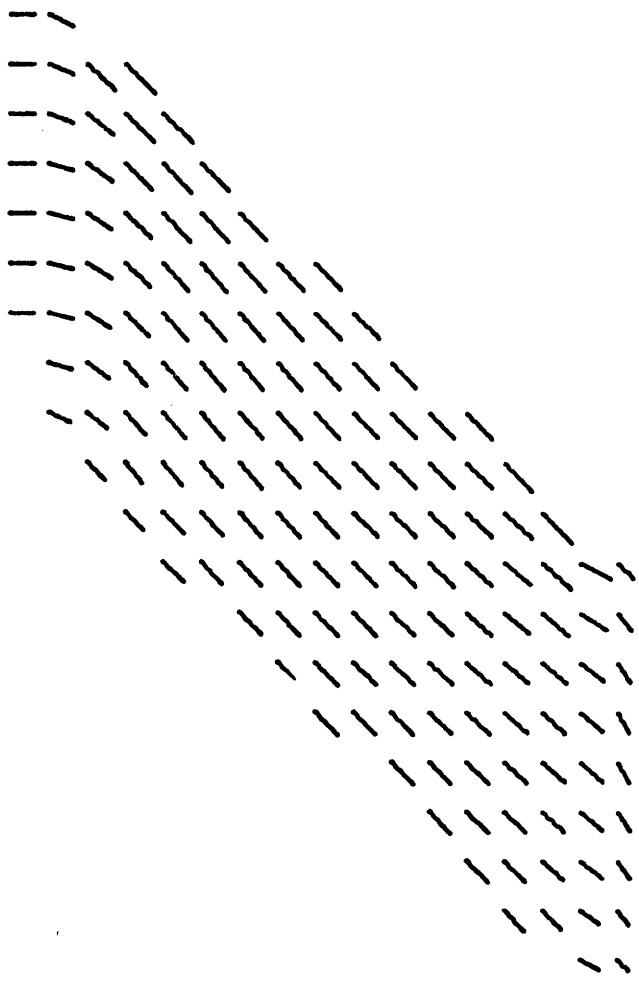

Fig. 3.2.1 Velocity Distribution of Air Flow in Single-Layer Louver Eliminator Using Free-Slip Conditions at Upper and Lower Boundaries

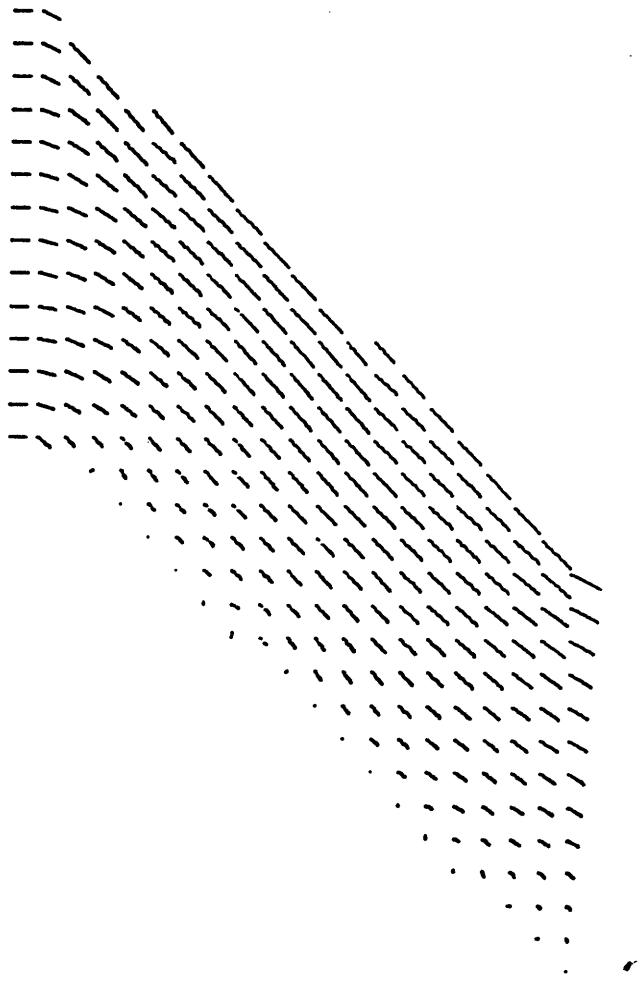

Fig. 3.2.2 Velocity Distribution of Air Flow in Single-Layer Louver Eliminator Using No-Slip Conditions at Upper and Lower Boundaries

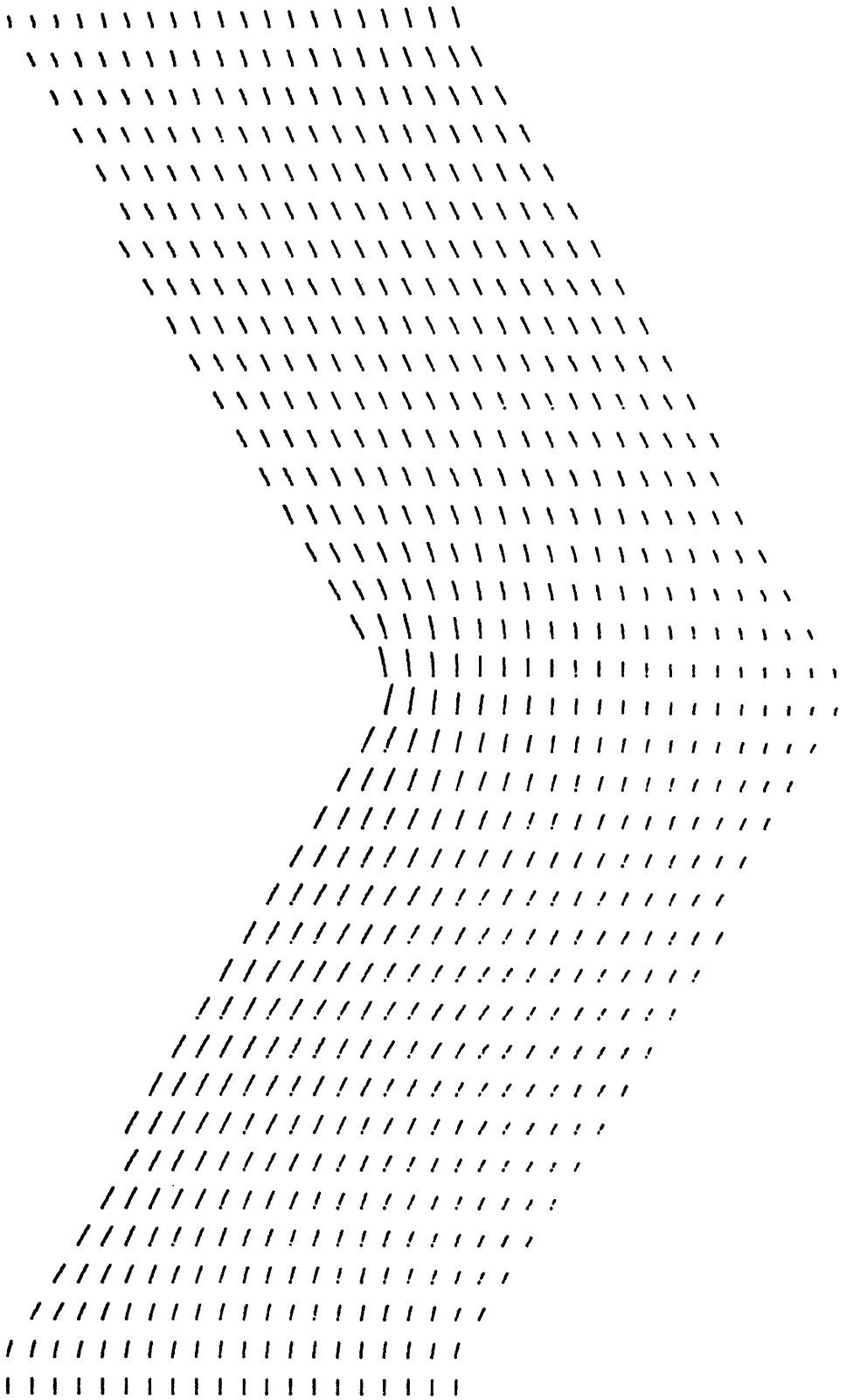

Fig. 3.2.3 Velocity Distribution of Air Flow in Double-Layer Louver Eliminator Using Free-Slip Conditions at Upper and Lower Boundaries

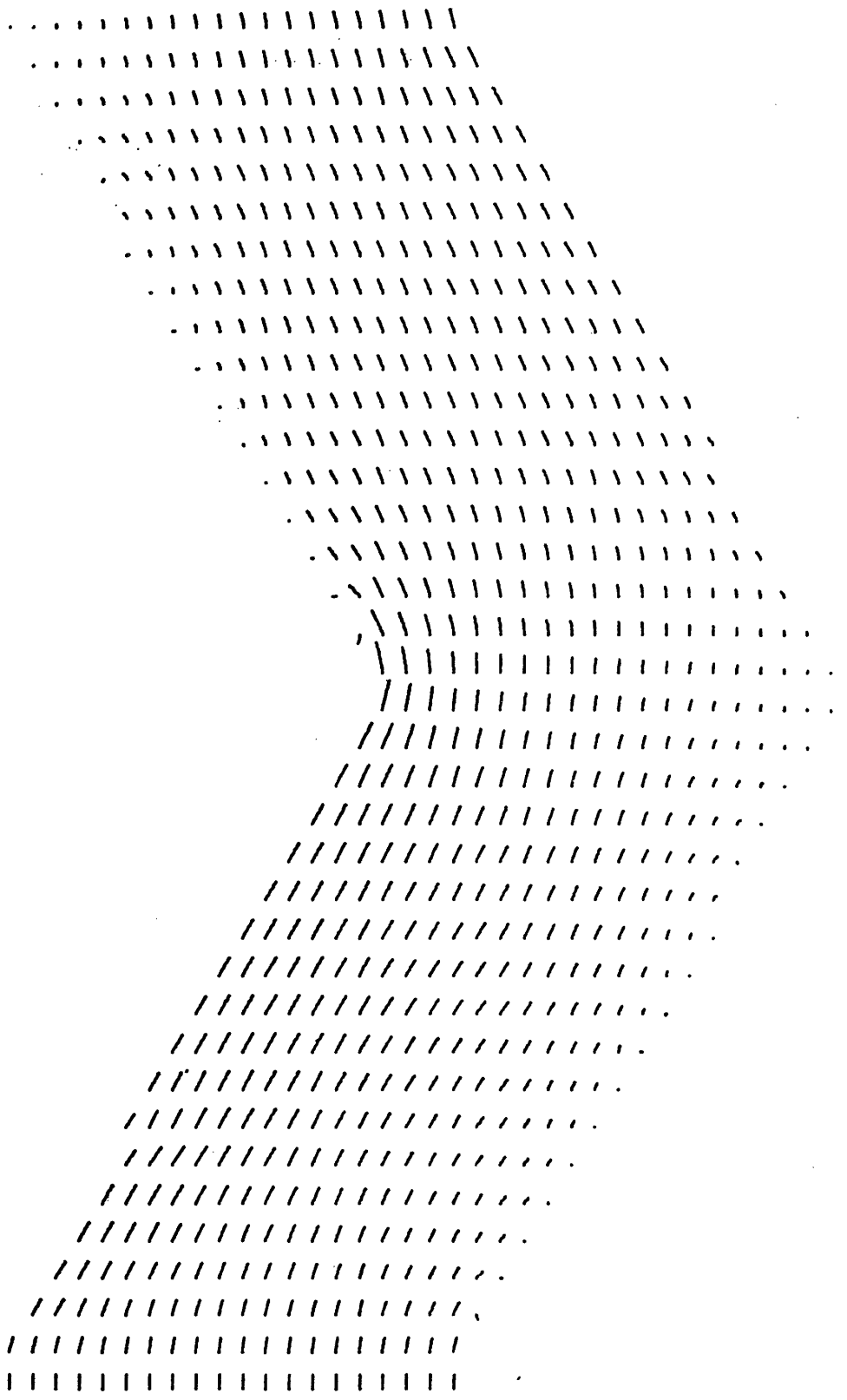

Fig. 3.2.4 Velocity Distribution of Air Flow in Double-Layer Louver Eliminator Using No-Slip Conditions at Upper and Lower Boundaries

Figure 3.2.5 compares the air velocity fields for a sinus-shaped eliminator calculated with free-slip and no-slip boundary conditions. In the free-slip case, A,the velocity distribution is approximately uniform. At the mid-length of the eliminator the velocity decreases as the radius of curvature increases. Also, at the high pressure sides of the eliminator the velocity is slightly greater than that at the low pressure sides. It can also be observed at each transverse cross section that the maximum velocity always occurs at the wall. This is not true in the no-slip case, B, where the maximum velocities occur at short distances away from the high pressure walls, and approach a value of zero at the walls. At the mid-length of the eliminator the maximum velocity occurs close to the center of the cross section. Note that the velocities shown at the upper and lower boundaries of the eliminator do not represent the velocities exactly at the walls, but rather at short distances away from the walls. It can also be seen from these plots that the no-slip results predict a more realistic flow because they show the wake regions. This will be illustrated with the help of flow visualization photographs in Chapter 6.

Similar observations can be made regarding the velocity fields of the Hi-V and Zig-Zag type eliminators shown in Figs. 3.2.6 through 3.2.8. For these more complicated geometries it is anticipated that significant recirculating eddies and turbulent wake regions exist at and near the bends

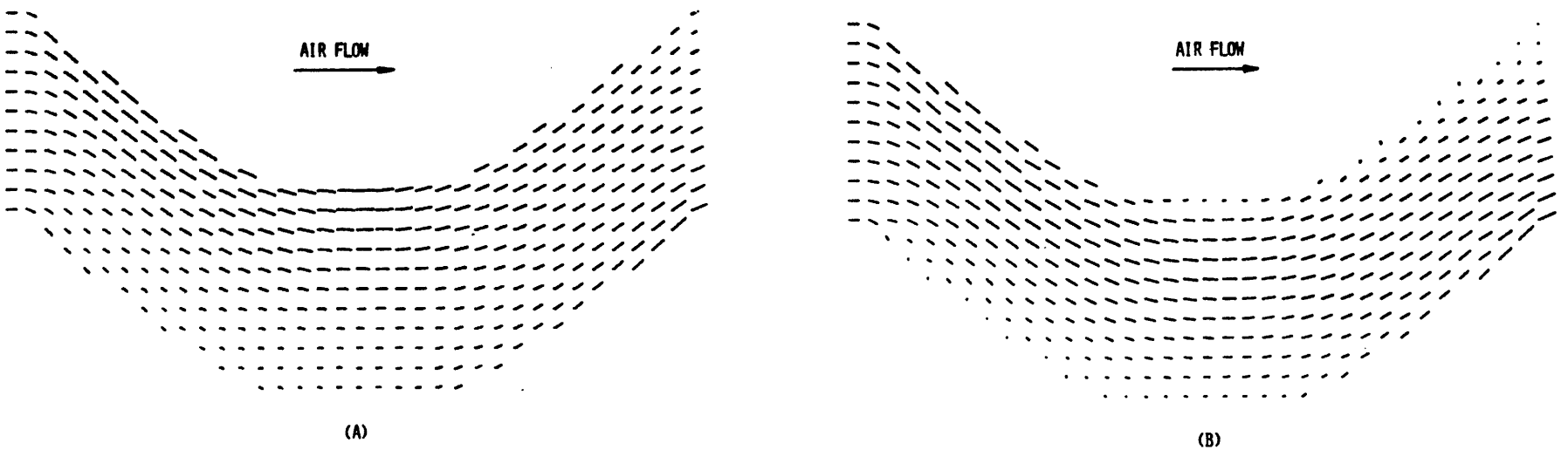

Fig. 3.2.5 Velocity Distribution of Air Flow in Sinus-Shaped Eliminator.
(A) Free-Slip Conditions at Upper and Lower Boundaries.
(B) No-Slip Conditions at Upper and Lower Boundaries

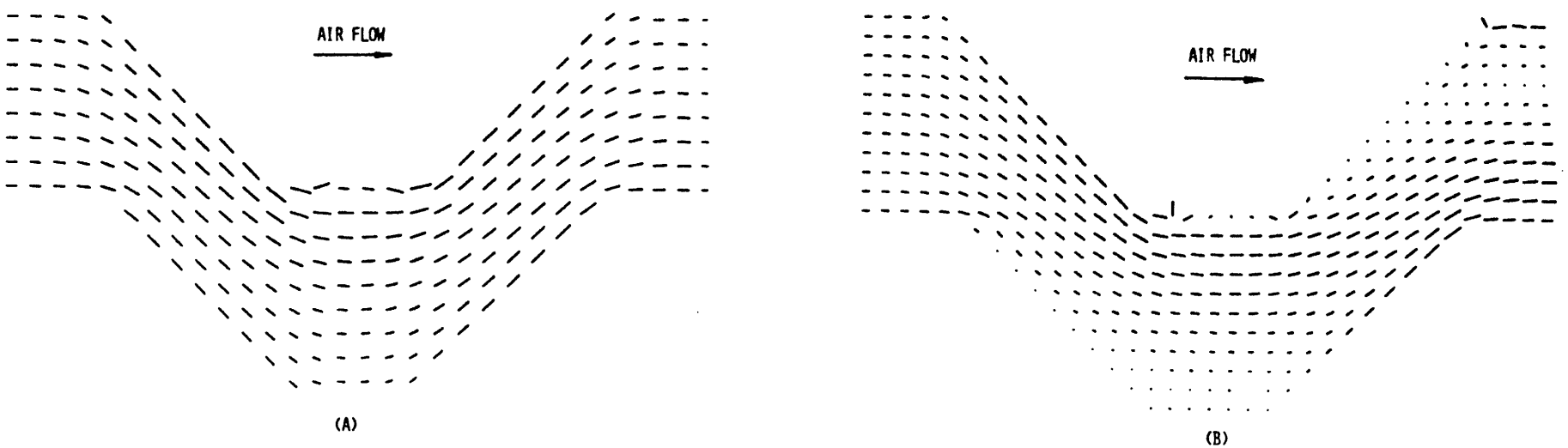

Fig. 3.2.6 Velocity Distribution of Air Flow in Hi-V Eliminator.
(A) Free-Slip Conditions at Upper and Lower Boundaries.
(B) No- Slip Conditions at Upper and Lower Boundaries

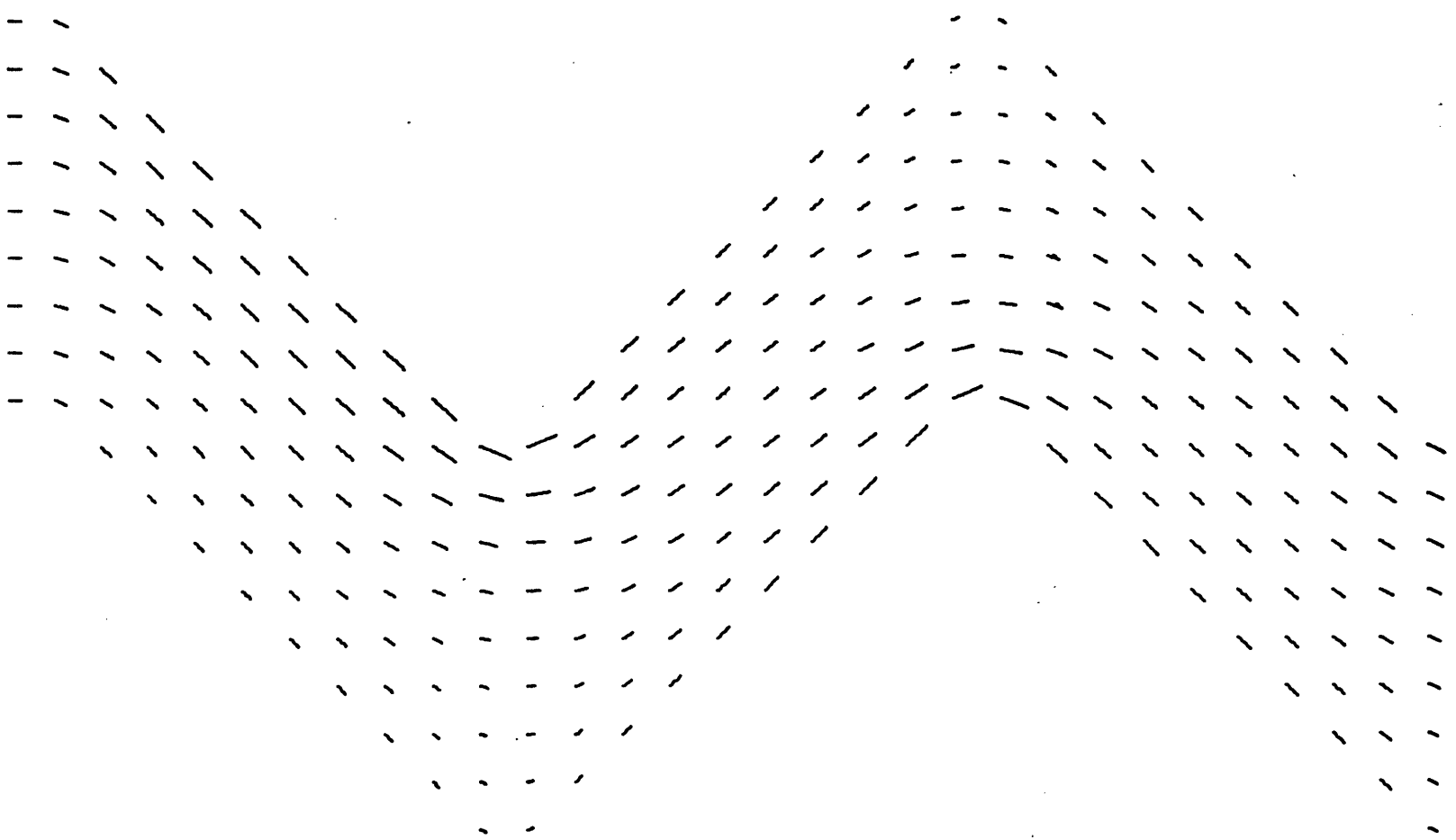

Fig. 3.2.7 Velocity Distribution of Air Flow in Zig-Zag Eliminator Using Free-Slip Conditions at Upper and Lower Boundaries

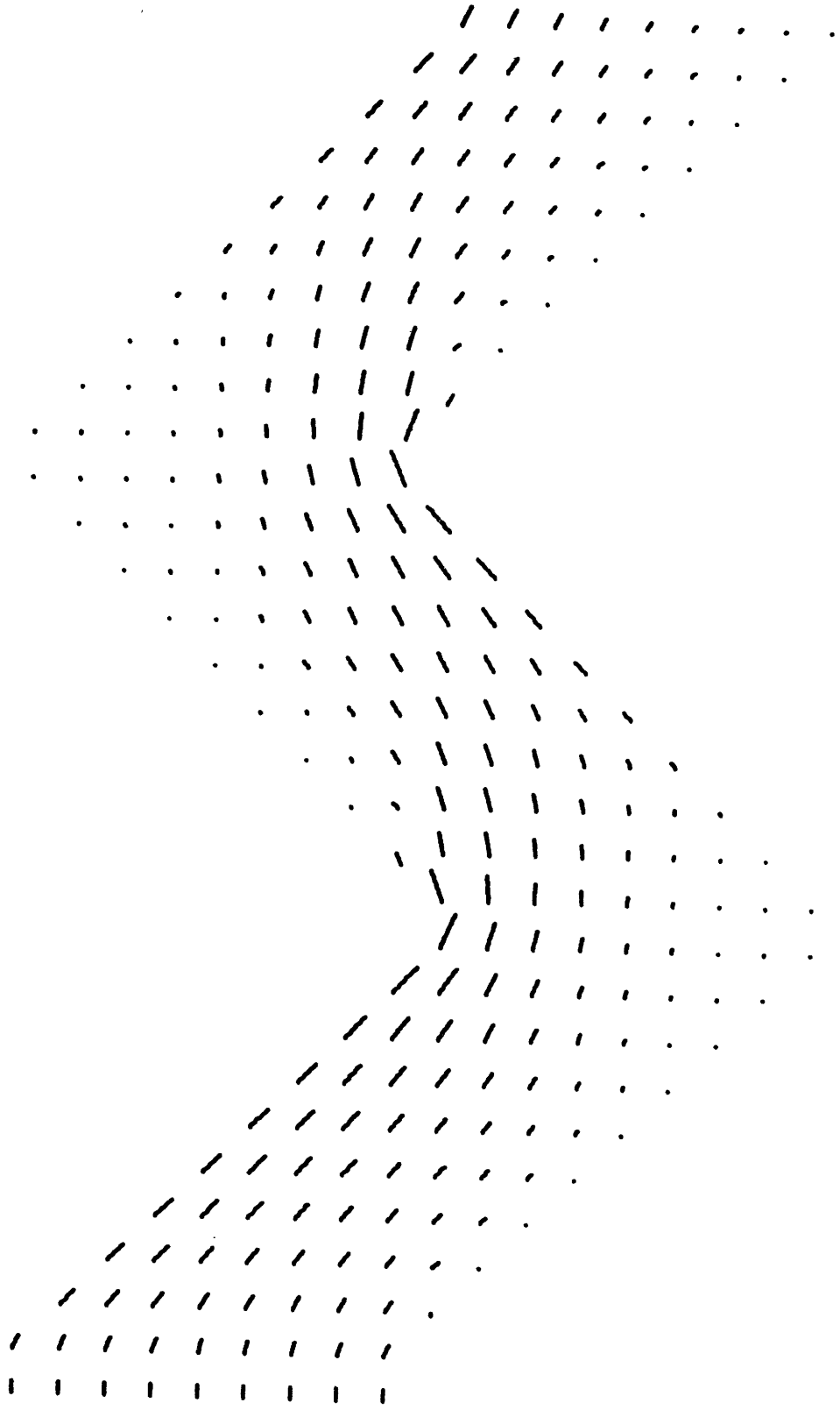

Fig. 3.2.8 Velocity Distribution of Air Flow in Zig-Zag Eliminator Using No-Slip Conditions at Upper and Lower Boundaries

in the flows. From the distributions shown it is concluded that the no-slip results predict more realistic distributions than the free-slip results, which will also be discussed in Chapter 6.

For the Zig-Zag eliminator with no-slip boundary conditions, the calculation fails to achieve a steady-state value. Or, if a small mesh size is used for a more accurate determination of the actual flow, the calculation fails. These effects are due to the fact that in the actual flow, turbulence is very significant for this eliminator. This will be shown in Chapter 6. The effects of turbulence are not taken into account in the current calculation. The recirculating eddies in interior corners are not fully resolved in the solution. This could be done by using a finer calculational mesh. However, this was not done since the mesh size already is in a range for which the calculated droplet capture efficiencies are relatively insensitive to the choice of mesh size. In addition, the droplet capture dynamics are relatively insensitive to whether the calculation of an eddying region is exact or if the region is treated as being approximately stagnant-which is what occurs with an inadequate spatial resolution of the calculated flow field.

The flow structure of any turbulent wake flow cannot be resolved by simply using a finer mesh, but it could be treated explicitly with a "turbulence model" calculation (for which several different computer programs are available). However,

in view of the success of DRIFT in predicting the experimentally observed behavior of the drift eliminators, it was decided that a turbulence model calculation would not be required. Effectively, the error introduced into the capture efficiency prediction by a failure to describe turbulent eddy regions is relatively small. This is mainly true because the devices examined have droplet trajectories that result in captures lying far from these wake regions. This will be discussed further in the following section and in Chapter 6.

Figures 3.2.9 and 3.2.10 show the results for the E-E eliminator designed by Yao and Schrock (Y1, Y2). The criterion for the design is that in order to minimize the air stream total pressure loss, any flow separation of the hydrodynamic boundary layer from the walls is to be avoided. Separation can be avoided if the air velocity increases monotonically along the flow direction. This is done by making the cross section of the flow channel decrease monotonically. After using this criterion and examining several geometries, it was found the E-E eliminator performs satisfactorily. Looking at the velocity distribution calculated by the SOLASUR subroutine using a free-slip boundary condition (Fig. 3.2.9), it is found that the velocity increases monotonically along the flow direction except near the outlet of the eliminator. However, the result predicted with a no-slip calculation (Fig. 3.2.10) indicates that separation does occur and that a wake region exists at the upper boundary just after the

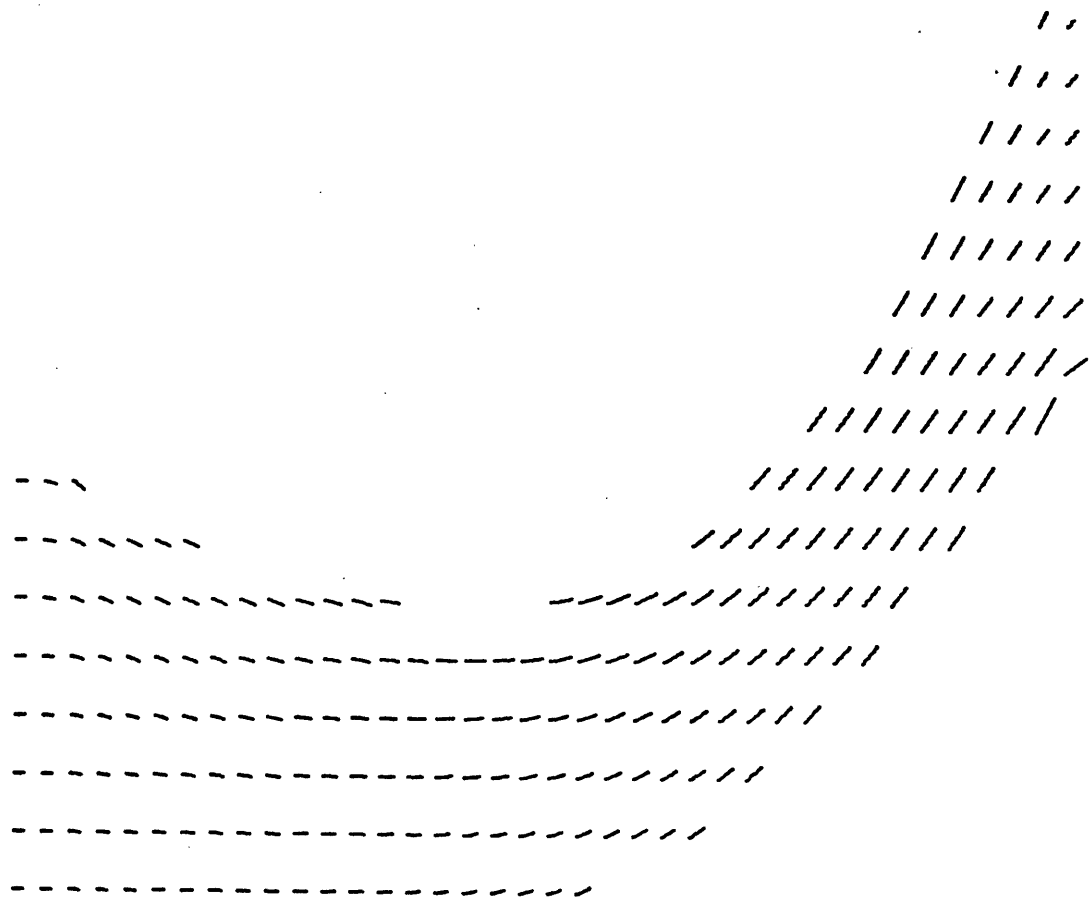

Fig. 3.2.9 Velocity Distribution of Air Flow in E-E Eliminator Using Free-Slip Conditions at Upper and Lower Boundaries

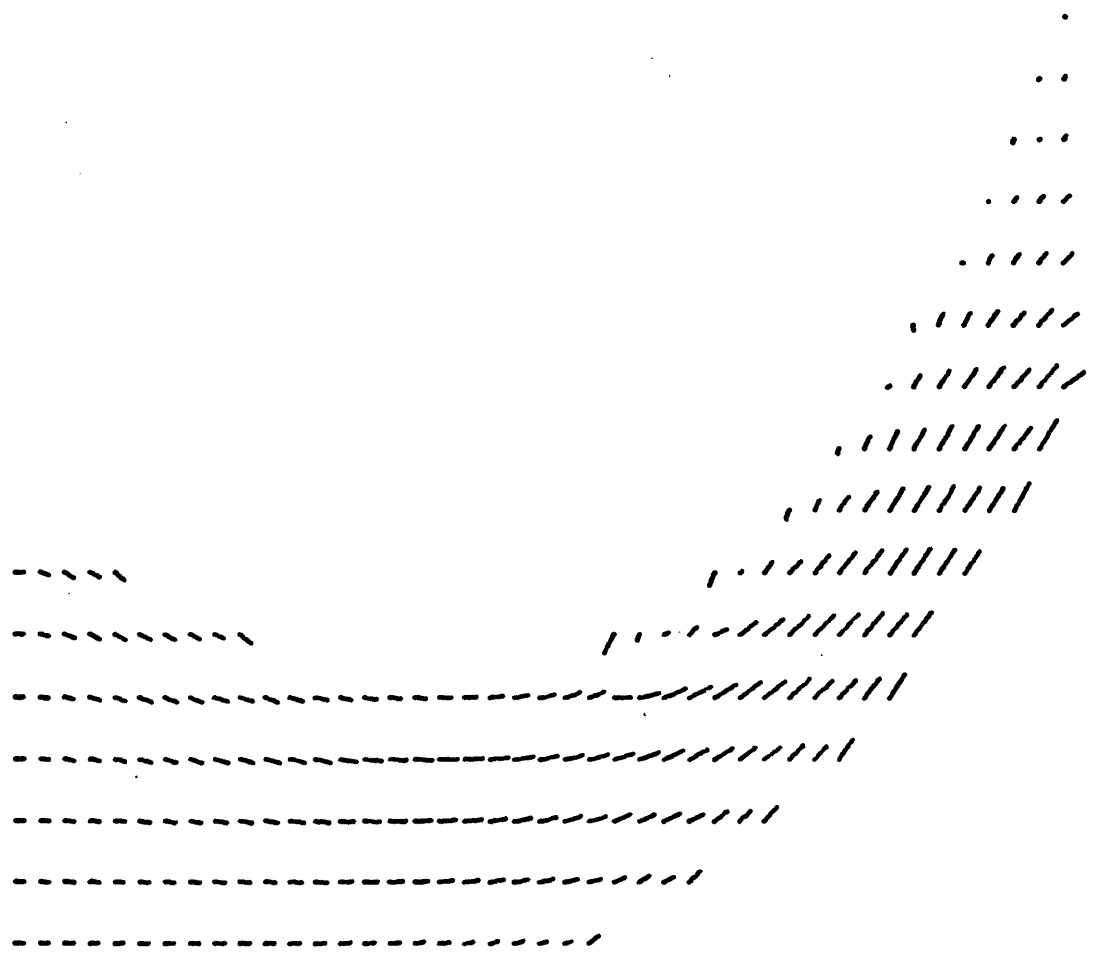

Fig. 3.2.10 Velocity Distribution of Air Flow in E-E Eliminator Using No-Slip Conditions at Upper and Lower Boundaries

sharp turn. As a result of this, the pressure loss calculated by the DRIFT code is much higher than that predicted by Yao and Schrock (Y1 and Y2). The collection efficiency calculated by the DRIFT code using the free-slip condition has a velocity distribution that is very close to that calculated by Yao and Schrock. Using a no-slip condition, the collection efficiency calculated by the DRIFT code is not significantly different. These results will be developed in the following sections.

3.3 Droplet Trajectories

The collection efficiency of a drift eliminator at a certain droplet size is determined theoretically by uniformly injecting droplets of that size into the inlet of the eliminators and observing their trajectories inside the eliminators. If the trajectory of a droplet ends at an eliminator wall, then that droplet is assumed to be captured. If the trajectory exits the eliminator without touching the walls, then the droplet is assumed to have escaped the eliminator. By comparing the numbers of escaped and captured droplets, the collection efficiency can be determined.

Droplet trajectories are calculated by solving numerically the droplet equation of motion within the eliminator flow field as described in Chapter 2. Figs. 3.3.1 through 3.3.13 illustrate the droplet trajectory plots for seven different eliminator geometries, with all eliminators assumed

to be in vertical scheme, and droplets entering the eliminators at the left of the figures. For each geometry the trajectories for two droplet sizes are shown. It can be seen in all of the eliminator geometries that larger droplets are more easily captured. In fact, it will be shown in a later section that for any eliminator and any air speed, the calculated droplet collection efficiency increases monotonically with droplet size. This occurs because the net acceleration on a drop varies approximately as 1/R, where R is the droplet radius. To see this, note that at a given air speed, the aerodynamic drag force increases approximately as R^2 (see Fig. 2.3.1), while the particle mass varies in proportion to R^3, and the time during which the particle is affected by drag is approximately constant. Thus, the net acceleration on a particle, and the resulting displacement vary approximately as $\frac{1}{R}$, resulting in easier capture for larger droplets.

Figures 3.3.1 and 3.3.2 show the droplet trajectories within a single-layer louver eliminator determined by using a free-slip air velocity distribution. It is observed that the paths of the droplets are essentially parallel to the duct boundary except at the entrance where the inertial motion of the droplets carries them towards the duct boundary. It is because of this inertial effect that the droplets are trapped, and it can be expected that they will be trapped at the boundary towards which they are initially directed, in this case being the upper boundary. Thus, it is concluded that as

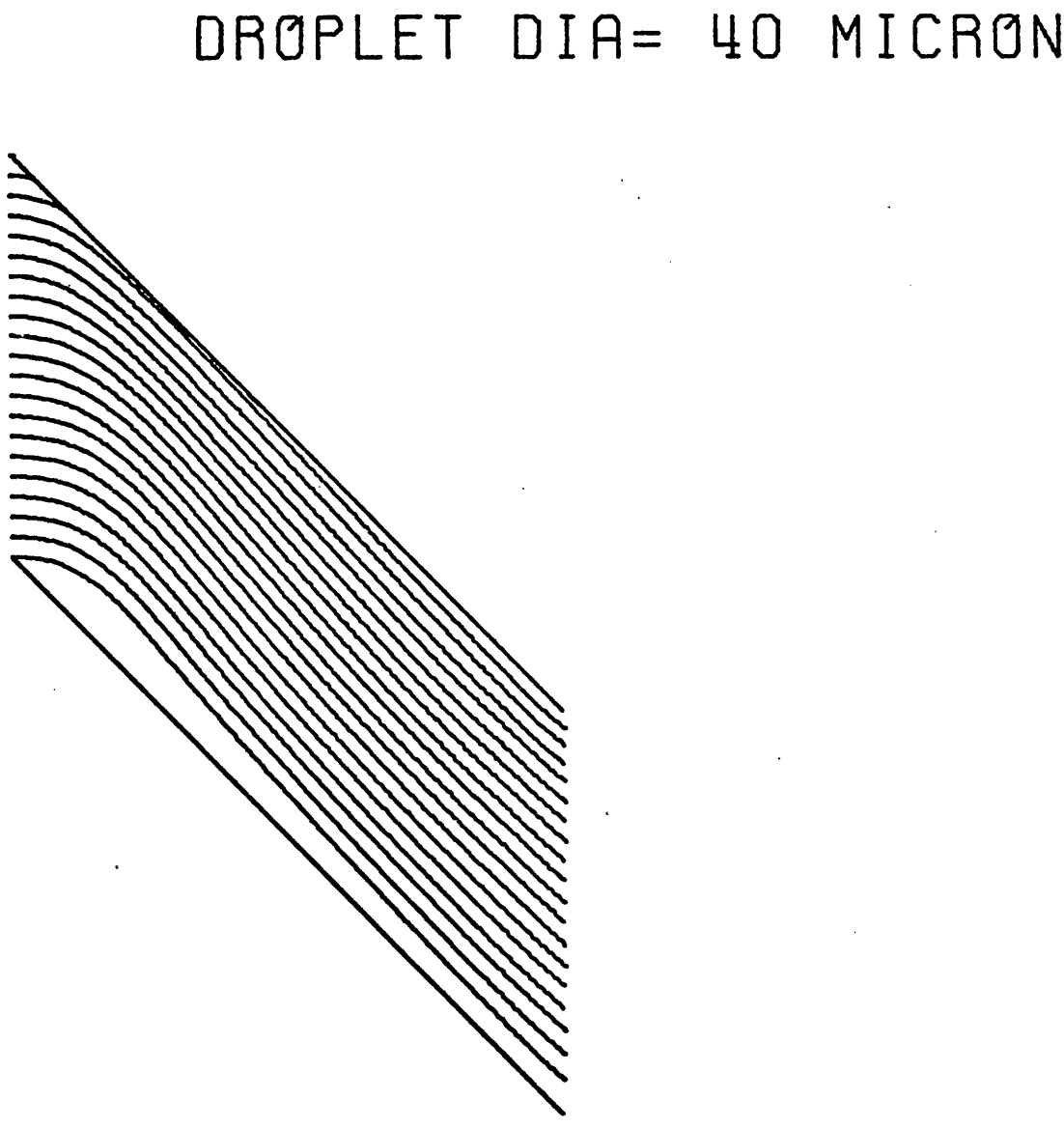

Fig. 3.3.1 Droplet Trajectory Plot for Single-Layer Louver Eliminator with Droplets Entering the Eliminator at Left of Figure. Droplet Size is 40 μm

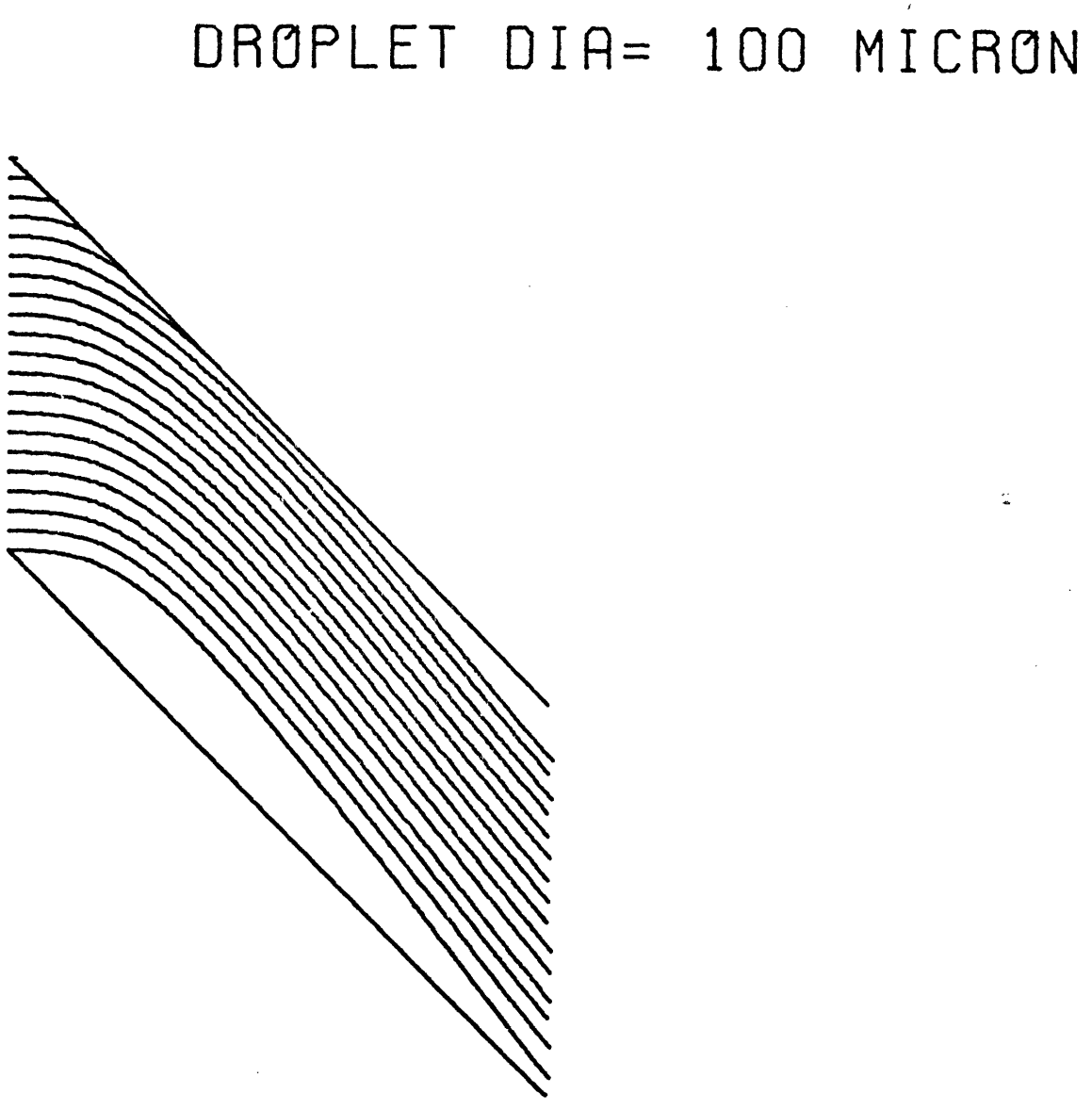

Fig. 3.3.2 Droplet Trajectory Plot for Single-Layer Louver Eliminator with Droplets Entering the Eliminator at Left of Figure. Droplet Size is 100 μm

the duct boundary steepness increases the collection efficiency will also increase since the area of the boundary towards which the droplets are initially directed is increased.

Figures 3.3.3 through 3.3.6 display similar sets of data for the two-layer louver and sinus-shaped geometries. In these two cases the length, pitch, and entrance conditions are the same in each of the two geometries in order to compare their drift collection efficiencies. The trajectories are calculated using free-slip boundary conditions in the air velocity determination. Their collection efficiencies are tabulated in Table 3.3.1 as a function of droplet size. The fact that the sinus-shaped geometry has a higher collection efficiency can be explained with the fluid velocity vector and droplet trajectory plots. Comparing these figures, it is seen that the sinus-shaped geometry has a steeper slope at the entrance than does the two-layer louver eliminator, and this is where most of the smaller droplets are trapped (see Figs. 3.3.3 and 3.3.5). For larger droplets, the number trapped near the turn in the duct becomes significant. However, the number is about the same for both geometries, as shown in Figs. 3.3.4 and 3.3.6. Therefore, in order to collect small droplets a geometry that has a steep slope at the entrance should be used, while for large droplets both slopes are important. Thus, if the drift size distribution is known, an optimal drift eliminator for that distribution can be indicated in this manner.

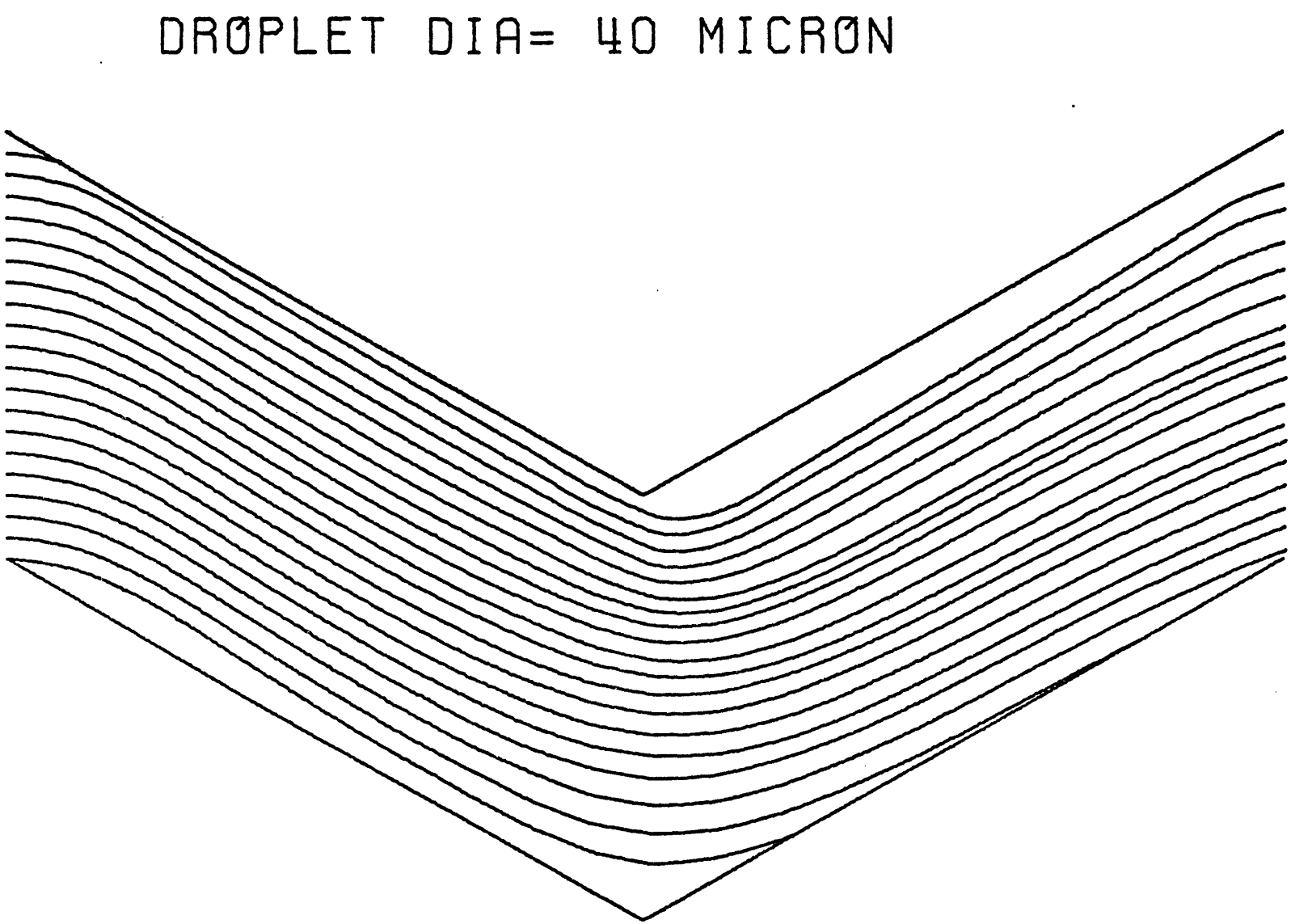

Fig. 3.3.3 Droplet Trajectory Plot for Double-Layer Louver Eliminator with Droplets Entering the Eliminator at Left of Figure. Droplet Size is 40 μm

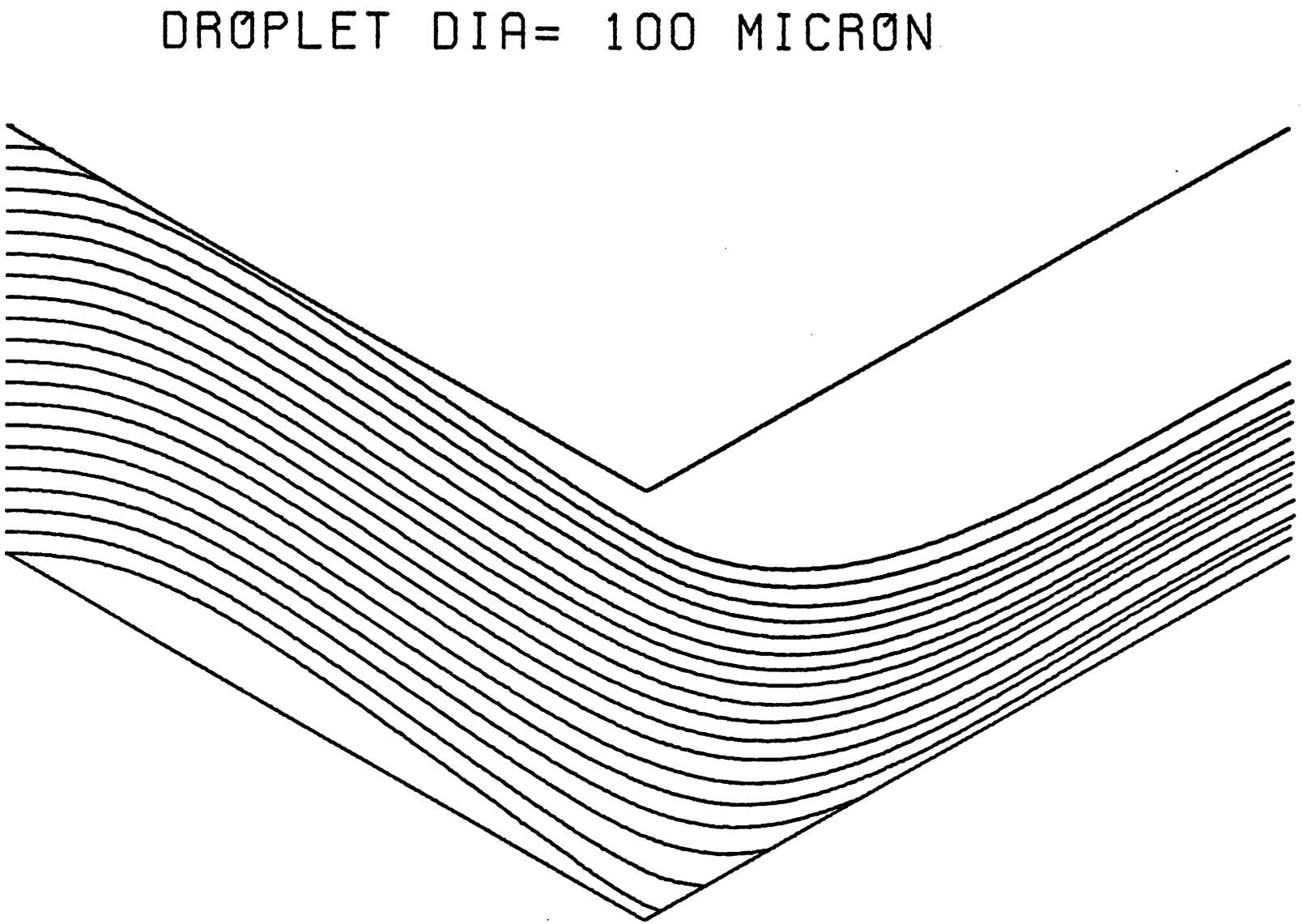

Fig. 3.3.4 Droplet Trajectory Plot for Double-Layer Louver Eliminator with Droplets Entering the Eliminator at Left of Figure. Droplet Size is 100 μm

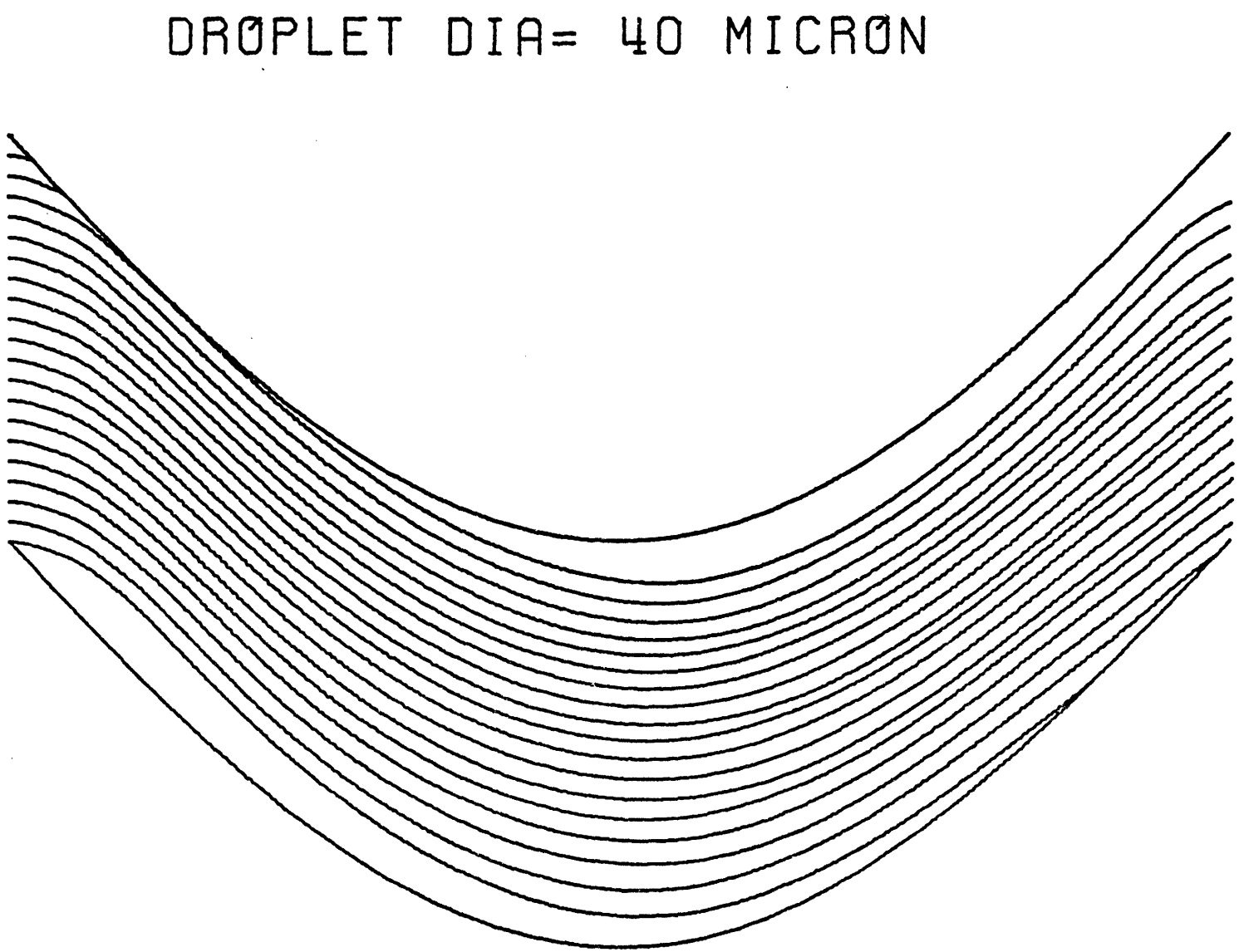

Fig. 3.3.5 Droplet Trajectory Plot for Sinus-Shaped Eliminator with Droplets Entering the Eliminator at Left of Figure. Droplet Size is 40 µm

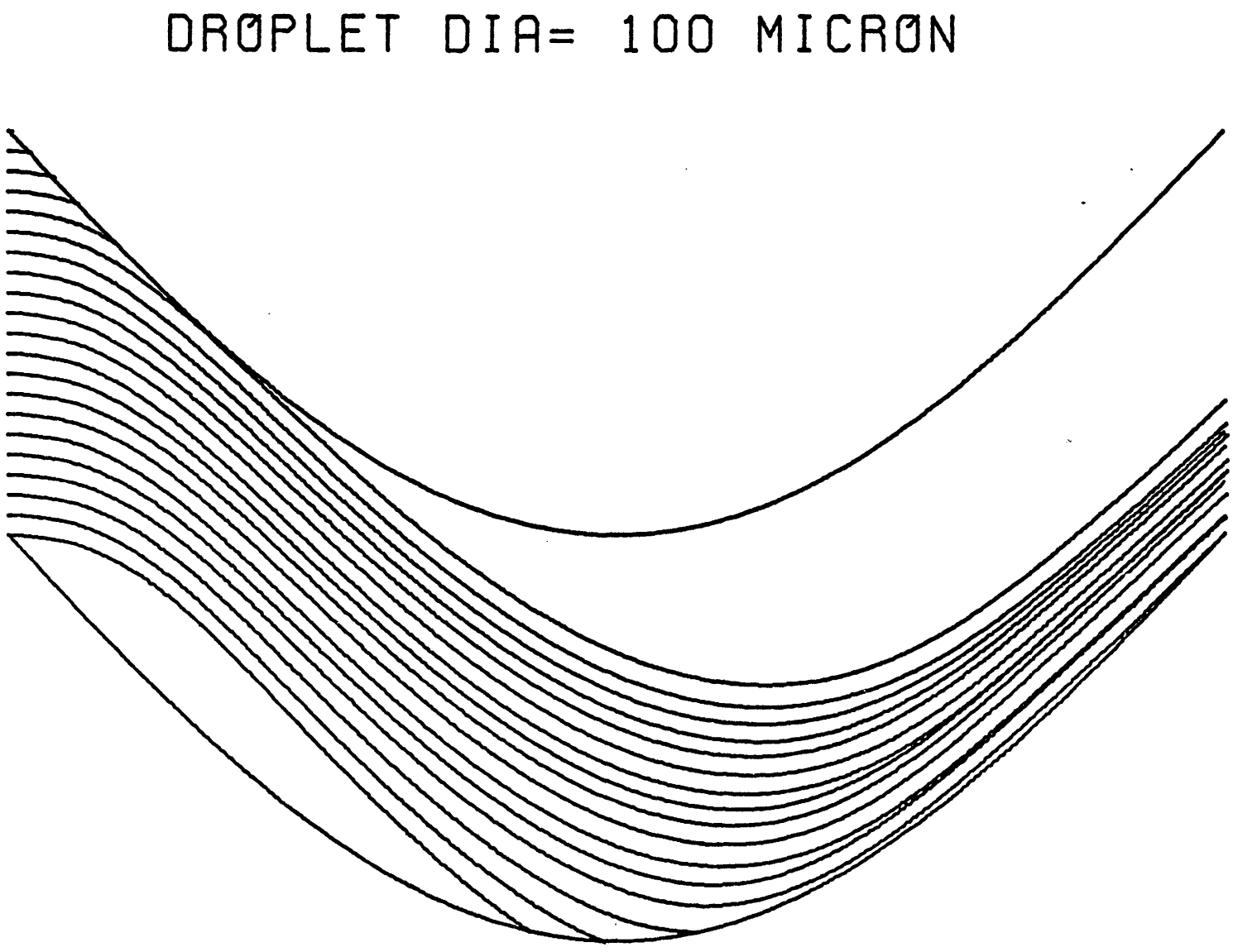

Fig. 3.3.6 Droplet Trajectory Plot for Sinus-Shaped Eliminator with Droplets Entering the Eliminator at Left of Figure. Droplet Size is 100 µm

Figures 3.3.7 and 3.3.8 show the droplet trajectory plots for the asbestos-cement eliminator using a free-slip air velocity distribution. Trajectory plots for those using no-slip air velocity distributions in a Hi-V eliminator are shown in Fig. 3.3.9. By observing the results of all of the essentially two-layer type eliminator geometries (two-layer louver, sinus-shaped, asbestos-cement, Hi-V), it is concluded that in the first half of those eliminators, the droplets are trapped on the upper duct boundaries, while for the second half of the eliminators, the droplets are trapped on the lower duct boundaries. It can therefore be expected that most of the water loading on these eliminators will occur at these two regions. In designing an effective drainage technique for this water loading, special attention must be paid to these two regions. One drainage technique is to put small grooves on the eliminator surfaces at these two regions to direct the water away.

Another point can be made by observing the trajectories in these two-layer eliminators. The droplet trajectories shown in Fig. 3.3.9 for the Hi-V eliminator are a good example. It is seen that few water droplets enter the two regions where turbulent wakes are expected to occur as discussed in the previous section. These two regions are near the lower boundary for the first layer of the eliminators

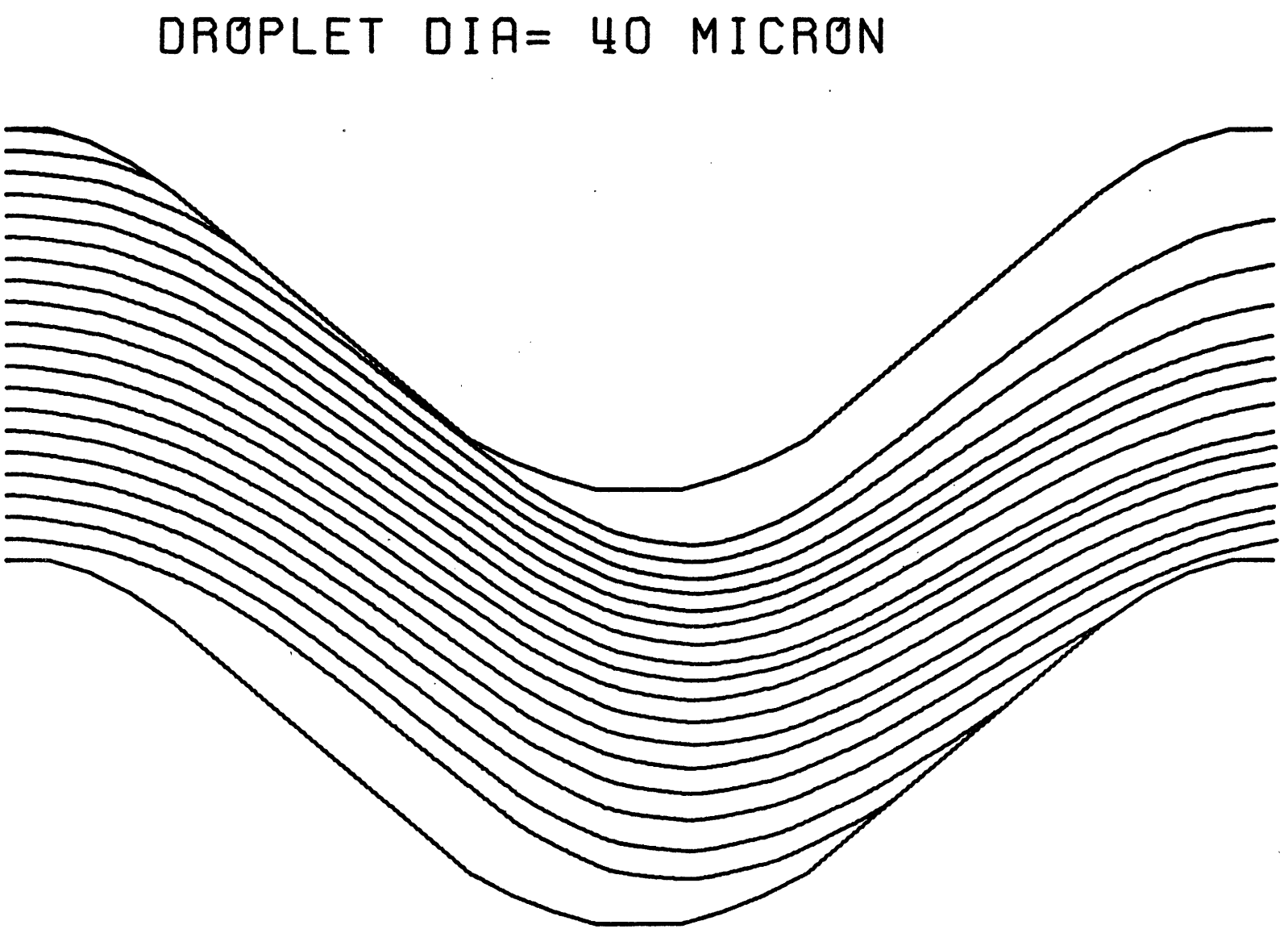

Fig. 3.3.7 Droplet Trajectory Plot for Asbestos-Cement Eliminator with Droplets Entering the Eliminator at Left of Figure. Droplet Size is 40μm

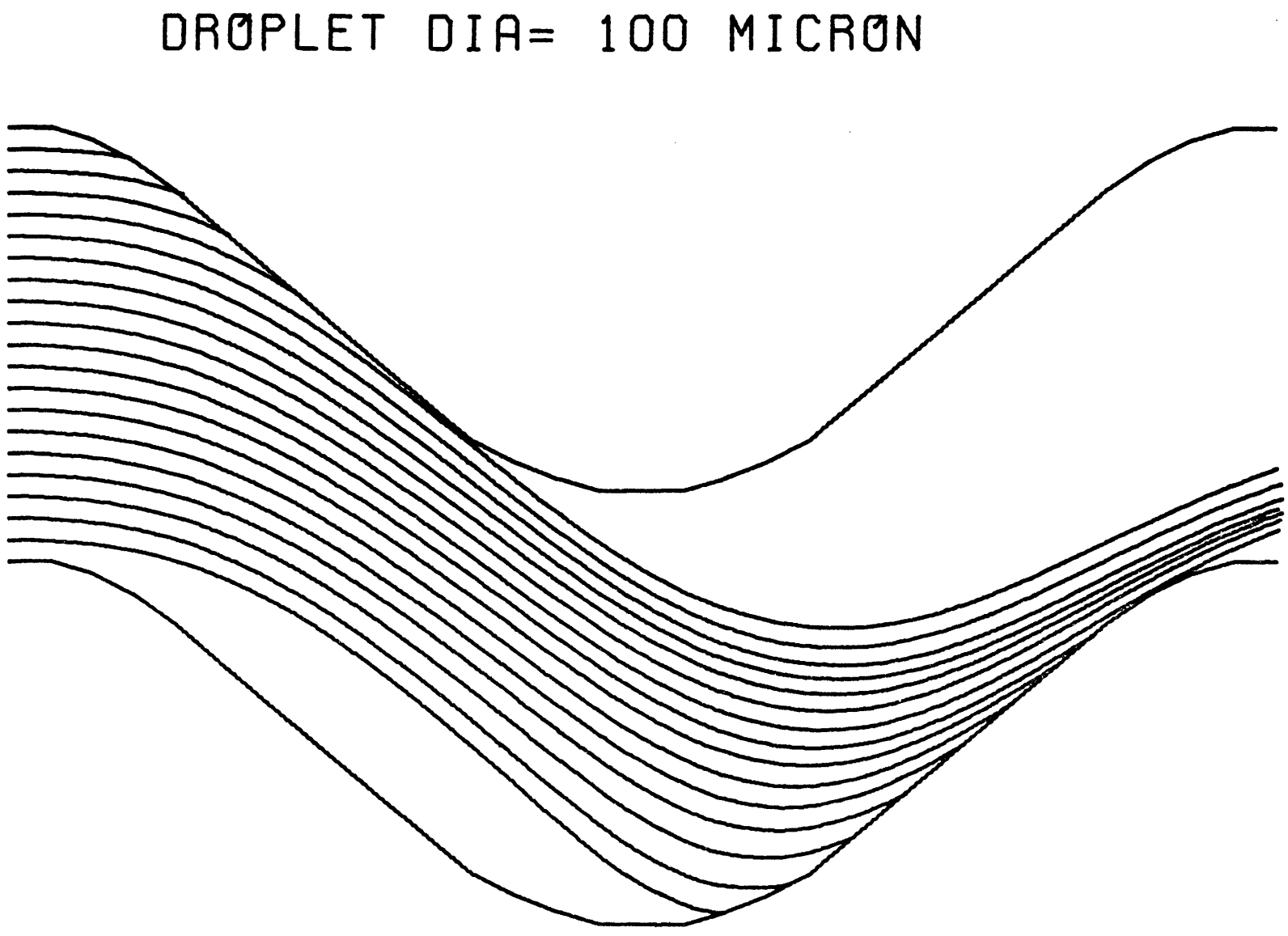

Fig. 3.3.8 Droplet Trajectory Plot for Asbestos-Cement Eliminator with Droplets Entering the Eliminator at Left of Figure. Droplet Size is 100 μm

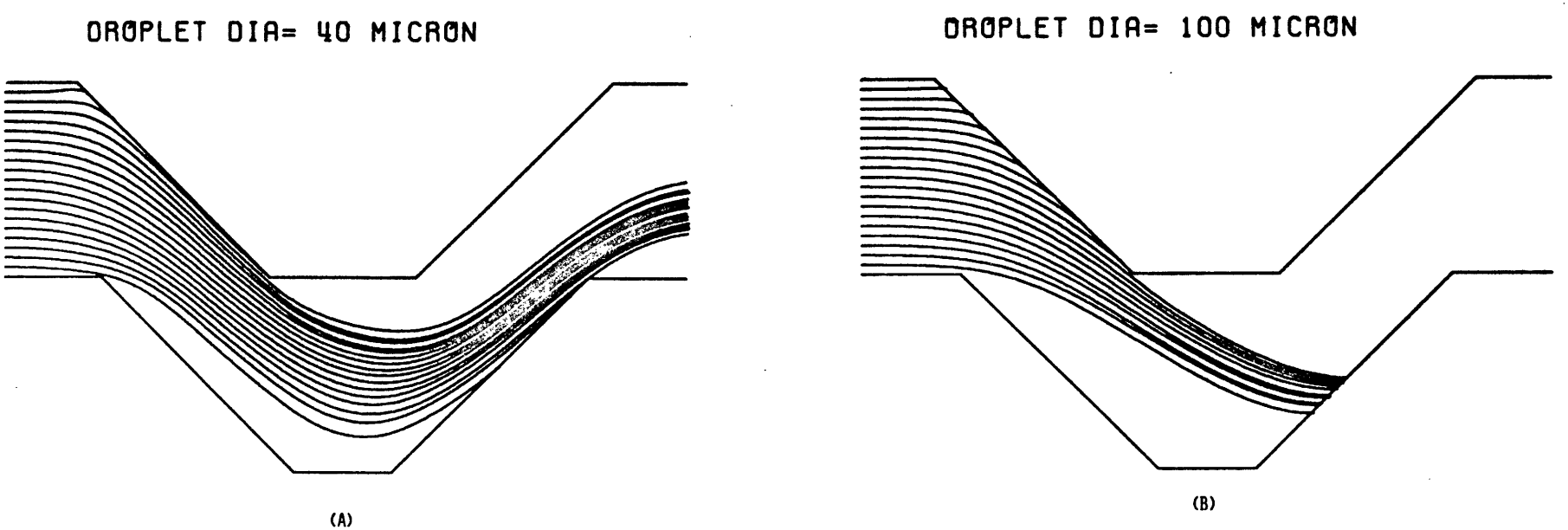

Fig. 3.3.9 Droplet Trajectory Plot for Hi-V Eliminator with Droplets Entering the Eliminator at Left of Figures. (A) 40 μm Droplet Size. (B) 100 μm Droplet Size

and near the upper boundary for the second layer of the eliminators. This means that the turbulent wakes will not have a great effect on the droplet trajectories. Therefore, even if these wake regions are not described exactly, the calculated collection efficiency results may approximate the results of an exact flow field, as long as the velocity distribution is calculated using no-slip boundary conditions which will show the general pattern of the flow field. Further discussion will be made in Chapters 5 and 6.

Figures 3.3.10 and 3.3.11 show the droplet trajectories in the Zig-Zag eliminator, using no-slip boundary conditions for the air velocity calculation. It is seen that all droplets that are captured were trapped in the first two layers of the eliminator. Therefore it is doubtful that a third layer is necessary. Figs. 3.3.12 and 3.3.13 display similar data, but with the third layer of the Zig-Zag eliminator removed. It is observed that the capture efficiencies are about the same for the two droplet sizes shown. This is in fact true for all droplet sizes, though the Zig-Zag eliminator has a slightly higher efficiency at smaller droplet sizes. It is expected that the drift collection efficiency for the two cases will not differ significantly,and therefore it is suggested that two layers of the Zig-Zag eliminator will probably suffice. If this is done, then the pressure loss will be significantly reduced.

Figures 3.3.14 and 3.3.15 display the trajectory plots

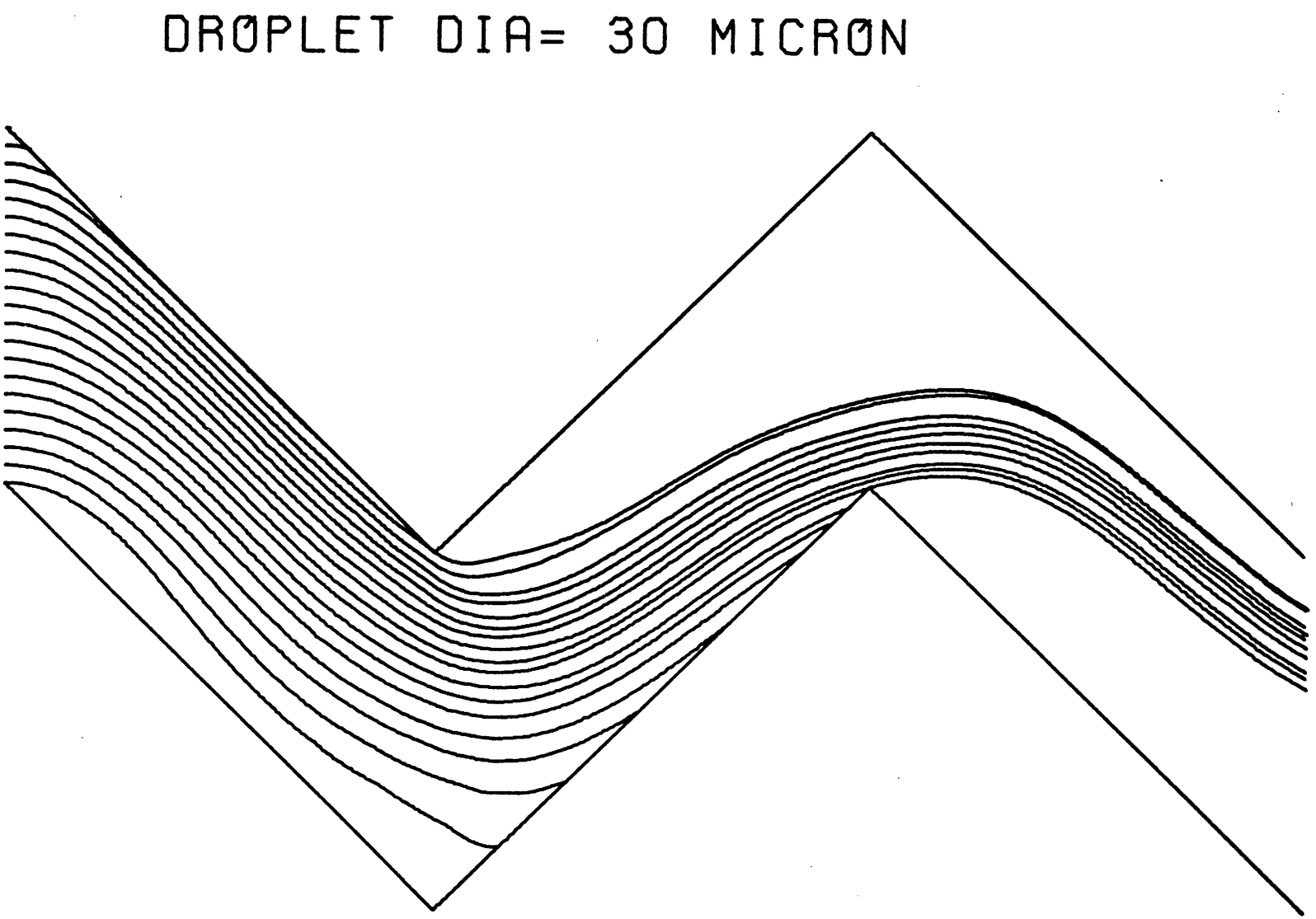

Fig. 3.3.10 Droplet Trajectory Plot for Zig-Zag Eliminator with Droplets Entering the Eliminator at Left of Figure. Droplet Size is 30 μm

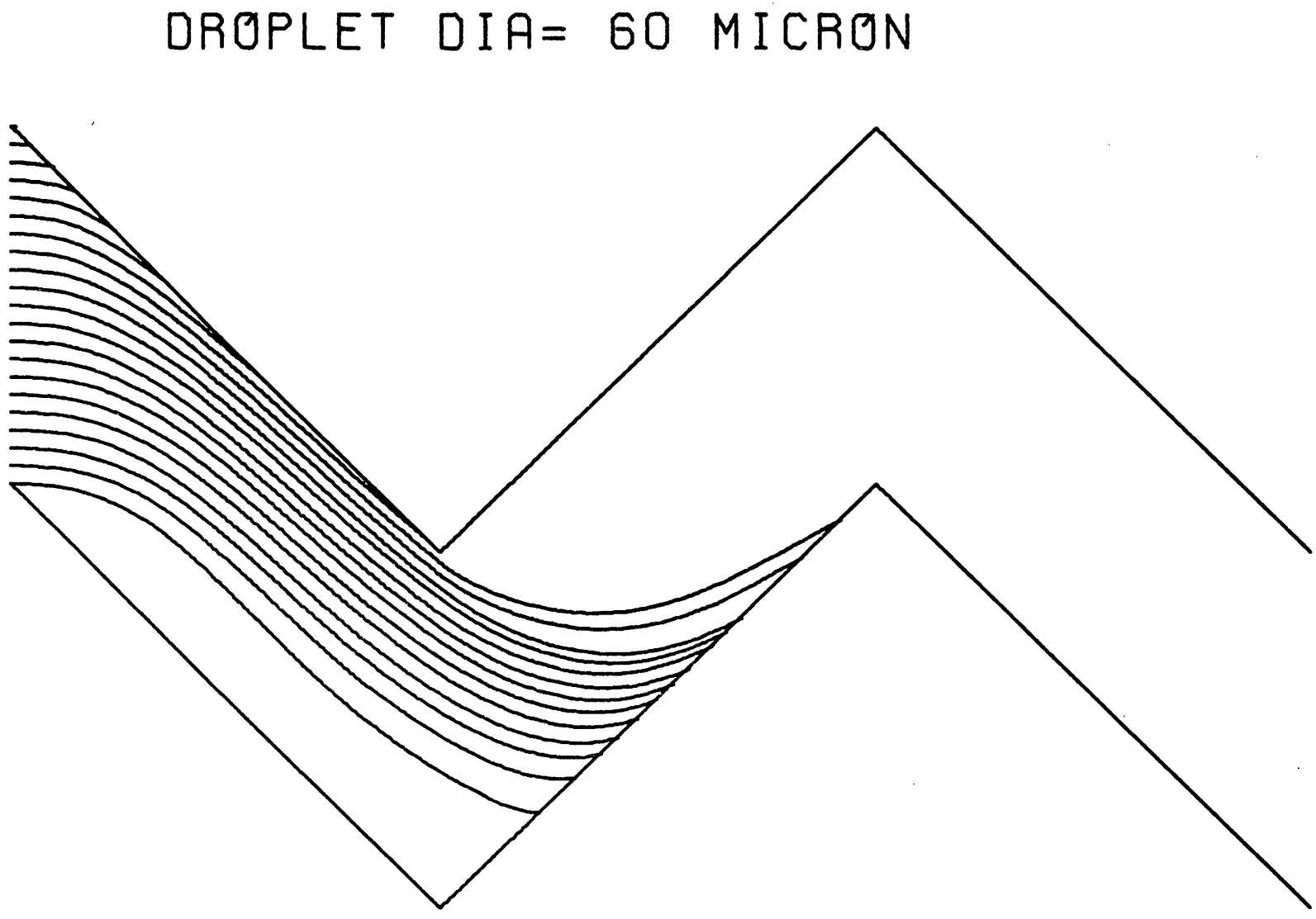

Fig. 3.3.11 Droplet Trajectory Plot for Zig-Zag Eliminator with Droplets Entering the Eliminator at Left of Figure. Droplet Size is 60 μm

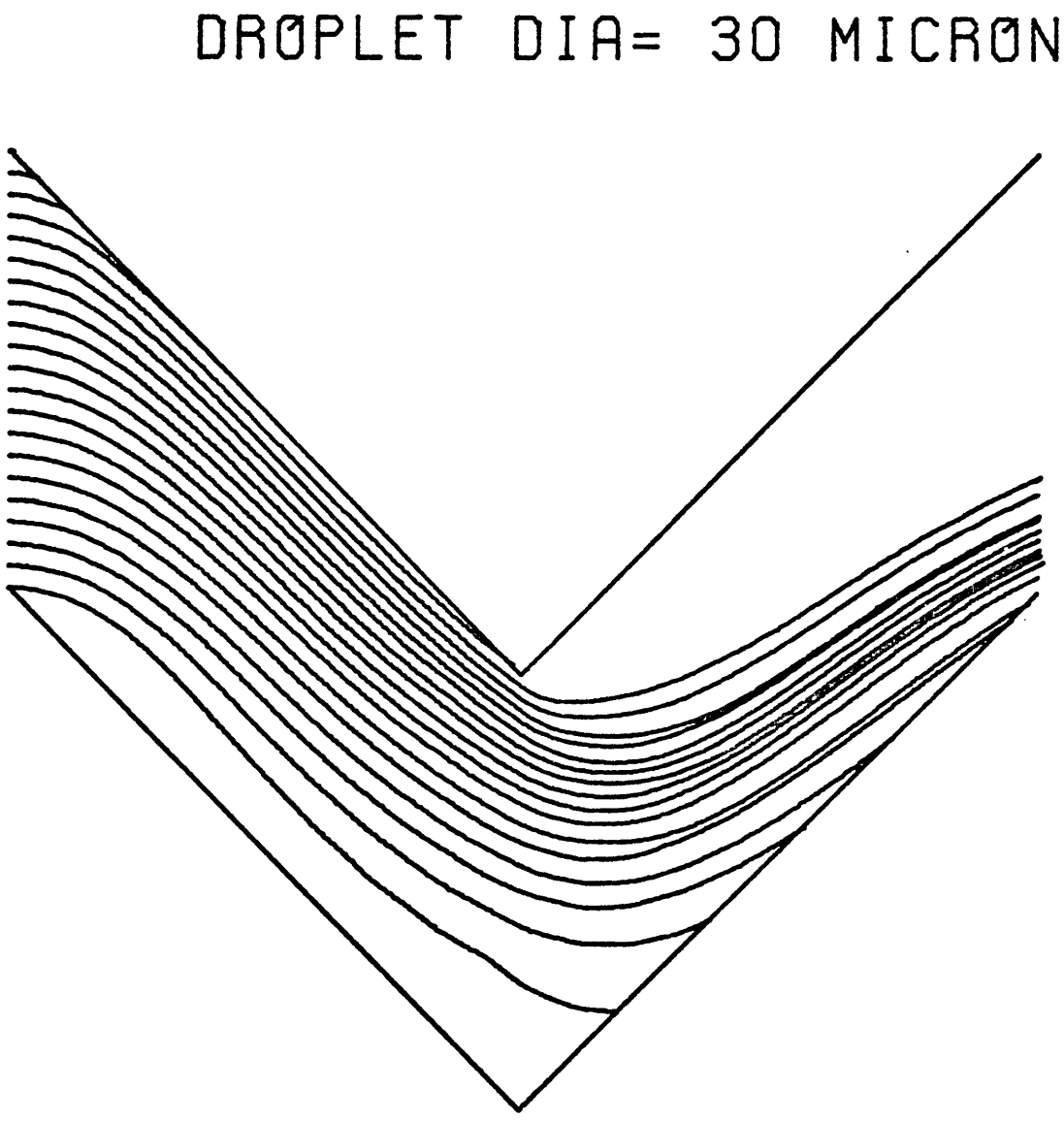

Fig. 3.3.12 Droplet Trajectory Plot for Two-Layer Zig-Zag Eliminator with Droplets Entering the Eliminator at Left of Figure. Droplet Size is 30 μm

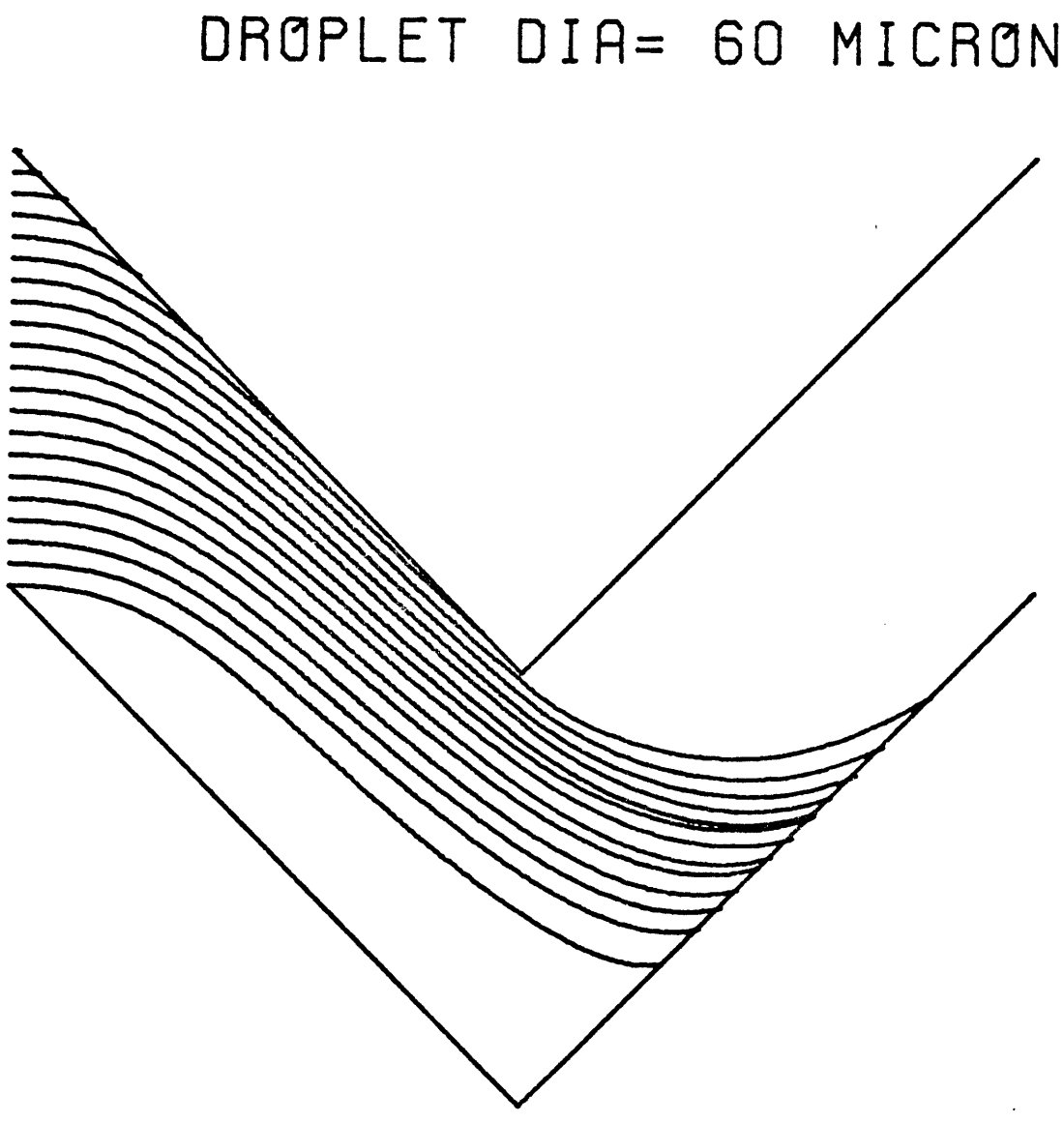

Fig. 3.3.13 Droplet Trajectory Plot for Two-Layer Zig-Zag Eliminator with Droplets Entering the Eliminator at Left of Figure. Droplet Size is 60 μm

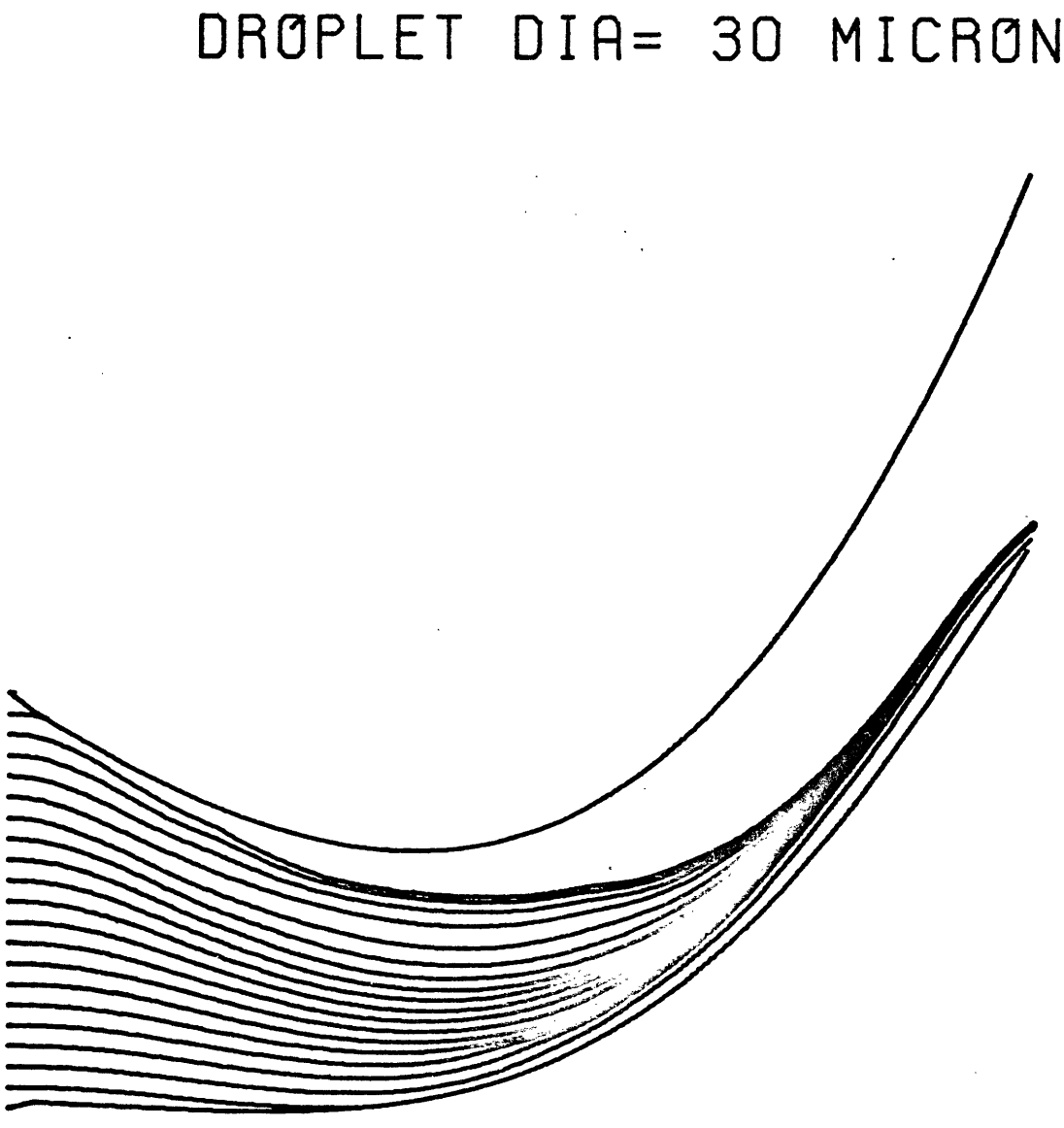

Fig. 3.3.14 Droplet Trajectory Plot for E-E Eliminator with Droplets Entering the Eliminator at Left of Figure. Droplet Size is 30 μm

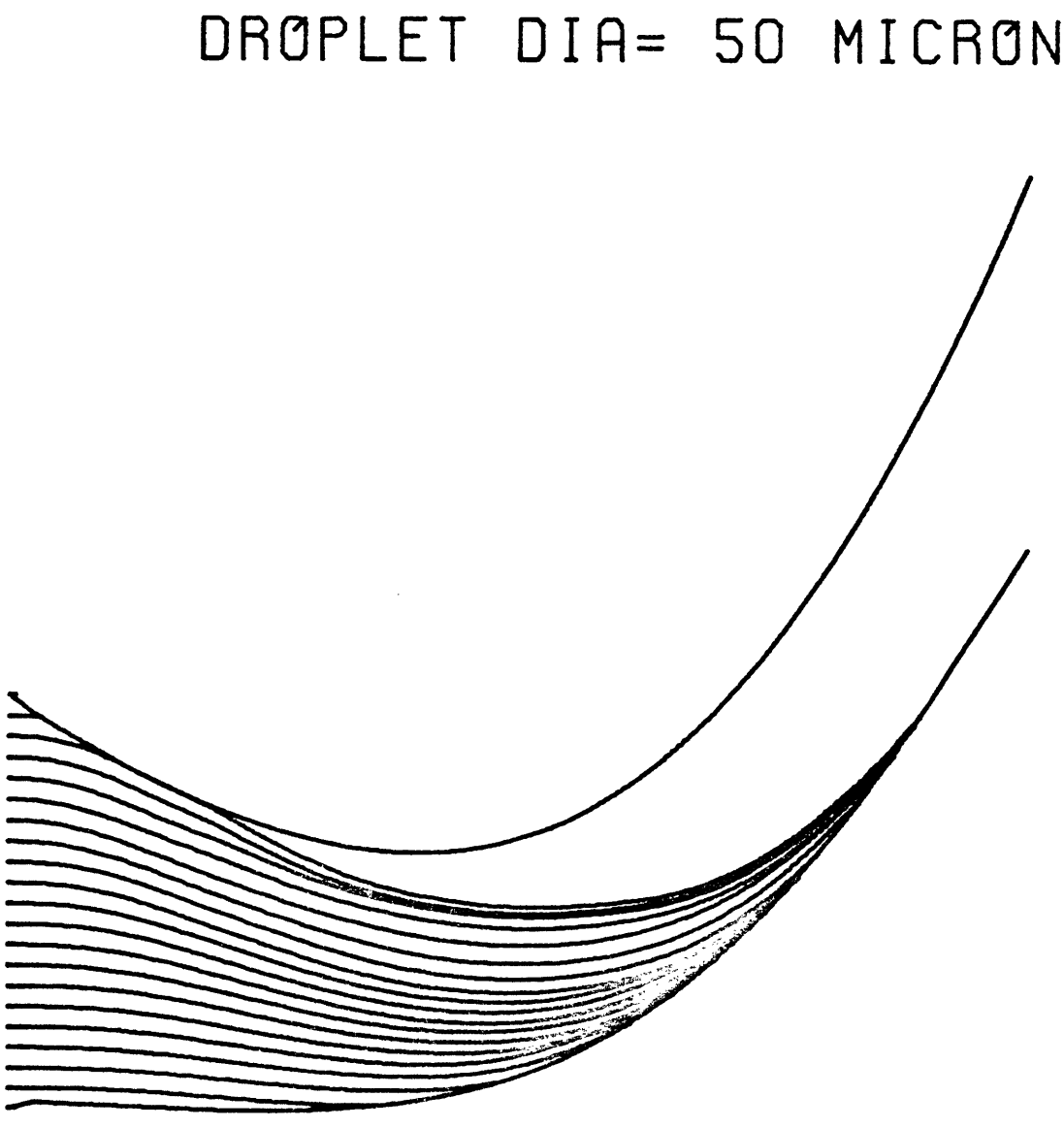

Fig. 3.3.15 Droplet Trajectory Plot for E-E Eliminator with Droplets Entering the Eliminator at Left of Figure. Droplet Size is 50 μm

for the E-E eliminator. It is seen that the capture efficiency of this eliminator is indeed very high, as predicted by Yao and Schrock (Y1, Y2). However, it will be shown in Sec. 3.5 that the pressure drop across this eliminator calculated by the DRIFT code is much higher than that predicted by Yao and Shrock.

3.4 Collection Efficiencies

The droplet collection efficiencies of drift eliminators are calculated from the droplet trajectories through the eliminators. These trajectories are obtained by using either no-slip or free-slip predictions of the air velocity field.

Figure 3.4.1 compares the collection efficiency results calculated by the DRIFT code using a free-slip air velocity field with those calculated by Roffman et al. Roffman et al. used an analytical formulation for the estimation of drift eliminator efficiency by assuming that the drift flows longitudinally at the assumed-constant vertical air velocity within the eliminator, and that it experiences transverse viscous drag due to the transverse air velocity component which is obtained by assuming that the air velocity at any point in the eliminator is locally parallel to the eliminator wall. For complex geometries the model uses a Fourier series expansion of the transverse velocity component in terms of the duct contour. Results obtained by the DRIFT code using free-slip boundary conditions for air flow field calculations are shown

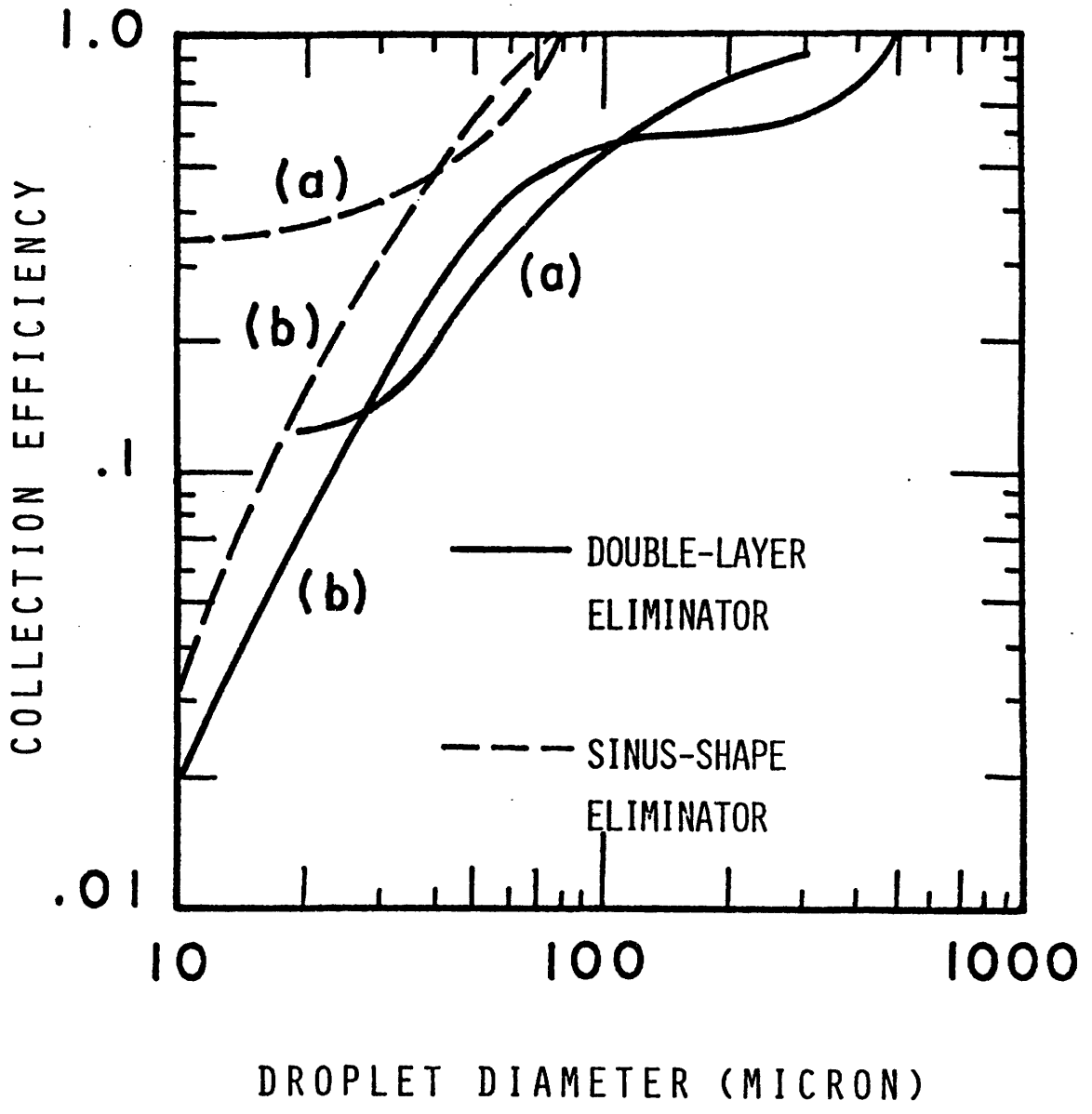

Fig. 3.4.1 Collection Efficiency of Droplets as a Function of Droplet Size
(a) DRIFT Calculation
(b) Roffman Calculation

in Fig. 3.4.1 as the curves A, and Roffman's results are the curves B. The solid curves are the results for the double-layer louver eliminator, Case D1 as identified in Table 3.1.1. The broken curves are for the sinus-shaped eliminator, Case N2 as identified in Table 3.1.1 For both geometries there is a fair agreement between the two calculations over the range of droplet sizes considered. However, at small droplet sizes, the results deviate from each other. The reason for this is that for small droplets, the trajectory depends strongly on the air velocity distribution. Therefore, for an air velocity distribution that is mainly parallel to the duct walls, even near the entrances and turns as assumed by Roffman's model, the smaller droplets will follow the air stream and escape the eliminator. In this way, a smaller collection efficiency than the real value is predicted.

It is found from these comparisons that the calculated results are quite sensitive to the assumptions regarding the air-stream velocity distribution. It is noted that the numerical simulation model in this work is physically more realistic than others which are available.

Figure 3.4.2 shows the drift collection efficiencies for the two-layer louver and sinus-shaped type geometries of the same length, pitch, and entrance conditions. The comparisons of their air velocity distributions and trajectory plots were given in previous sections. The fact that the sinus-shaped geometry has a higher collection efficiency can be explained

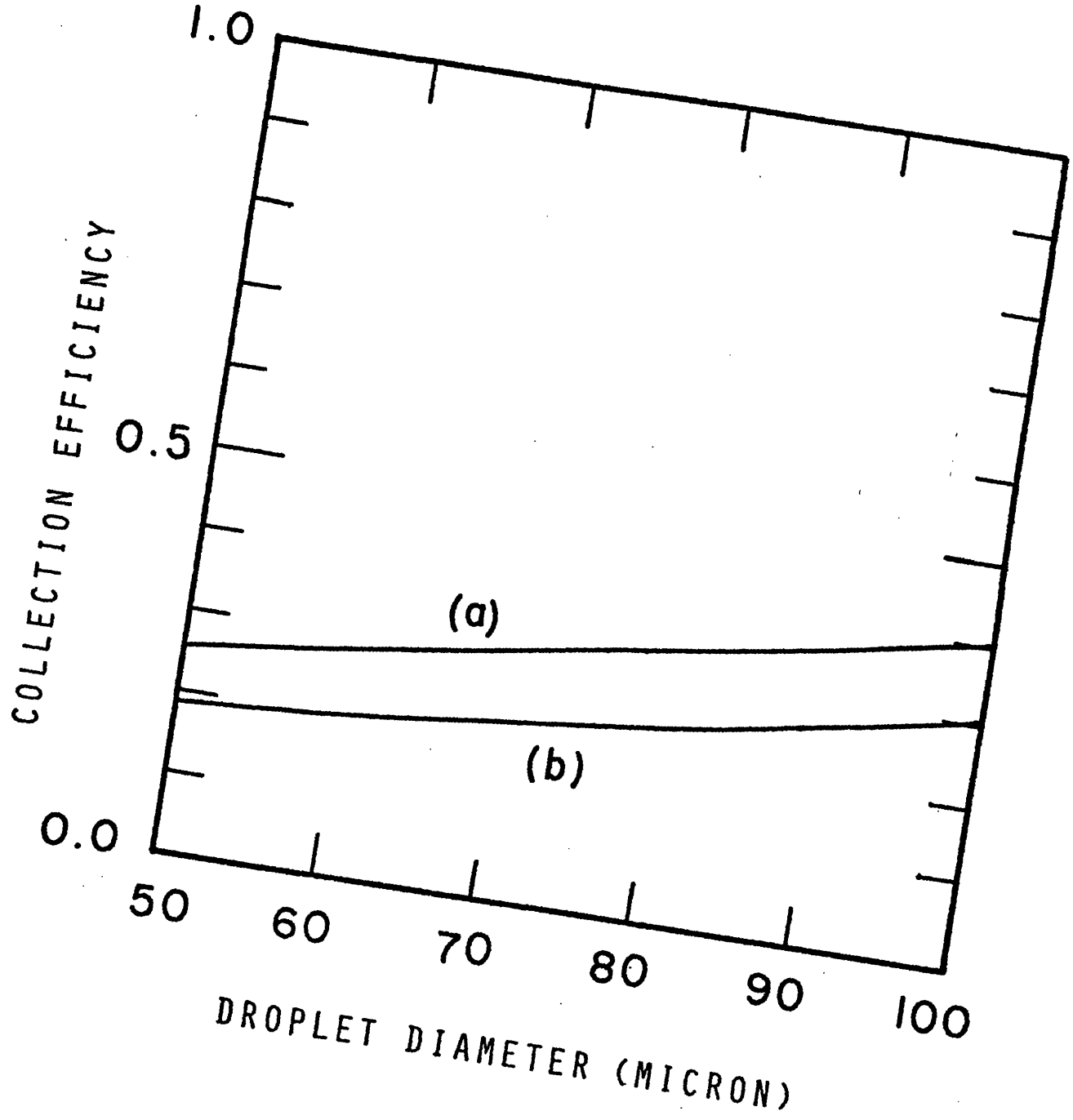

Fig. 3.4.2 Collection Efficiency of Droplets as a Function of Droplet Size
(a) Sinus-Shaped Eliminator
(b) Double-Layer Louver Eliminator of Same Dimensions.
(Air Inlet Velocity=1 m/s)

by the fluid velocity vector and droplet trajectory plots as explained in the previous section.

The comparison of collection efficiency results will be discussed in Chapter 5. Generally, for simple geometries like the one or two-layer louver eliminators, and sinus-shaped eliminator, the difference in the calculated collection efficiency using a no-slip or free-slip velocity distribution is not significant. This is demonstrated by the results shown in Table 3.4.1 for the two-layer louver eliminator at a 1.5 m/s air velocity. For more complicated geometries, this difference becomes significant, and will be shown in Chapter 5.

Also shown in Table 3.4.1 is the capture efficiency comparison of the DRIFT code calculation with Yao's calculation for the E-E eliminator. It is seen that with free-slip conditions in the DRIFT calculation, the results are very close to Yao's results. This is expected because potential flow is assumed in Yao's calculation. Using a no-slip condition in the DRIFT calculation, the results are different, but not significantly. However, the difference in the pressure drop results is very great, and is demonstrated in the next section.

3.5 Pressure Drops

The SOLASUR subroutine determines the pressure at each nodal point. From this information the total mass-averaged

Table 3.4.1
Collection Efficiency Calculated by DRIFT at 1.5 m/s Air Velocity
for Double-Layer Louver Eliminator and E-E Eliminator

Droplet Diameter (μm)	Double-Layer Louver (Case D2 in Table 3.1.1)		E-E		
	Free-Slip	No-Slip	Yao's Prediction	Free-Slip	No-Slip
20	-	-	0.1	-	0.09
30	0.130	0.130	0.45	0.485	0.215
40	0.140	0.145	0.75	0.725	0.615
50	0.170	0.155	1.00	1.00	1.00
60	0.195	0.185			
70	0.250	0.220			
80	0.310	0.260			
90	0.385	0.410			
100	0.500	0.515			

pressure drop across the eliminator can be determined if a no-slip boundary condition is assumed at the eliminator walls. The results of such calculations will be compared with experimental data in later chapters. In this section the pressure drop distribution along some of the eliminators will be presented to get some insight into the effect of the geometry upon pressure loss across eliminators. The pressure drop distributions presented here are normalized as the ratio of the pressure drop at any location in the eliminator to the total pressure drop across the eliminator.

Figure 3.5.1 shows the pressure drop distribution for the sinus-shaped eliminator. It can be seen that most of the pressure loss occurs near the inlet and outlet regions of the eliminator. This is due to the fact that the slope of the duct boundaries is steeper at these regions. Similar results are obtained for the asbestos-cement eliminator (Fig.3.5.2) which has a shape similar to the sinus-shaped eliminator except that the slope at the entrance and exit regions is not as steep while it is steeper at other regions. These regions of steeper slope extends farther along the eliminator length than in the sinus-shaped eliminator. It will be shown later that the total pressure loss across the asbestos-cement eliminator is larger than that of the sinus-shaped eliminator.

Figure 3.5.3 shows the results for another smooth geometry, the E-E eliminator designed by Yao and Schrock (Y1,Y2). The flow channel cross-sectional area decreases along the eliminator

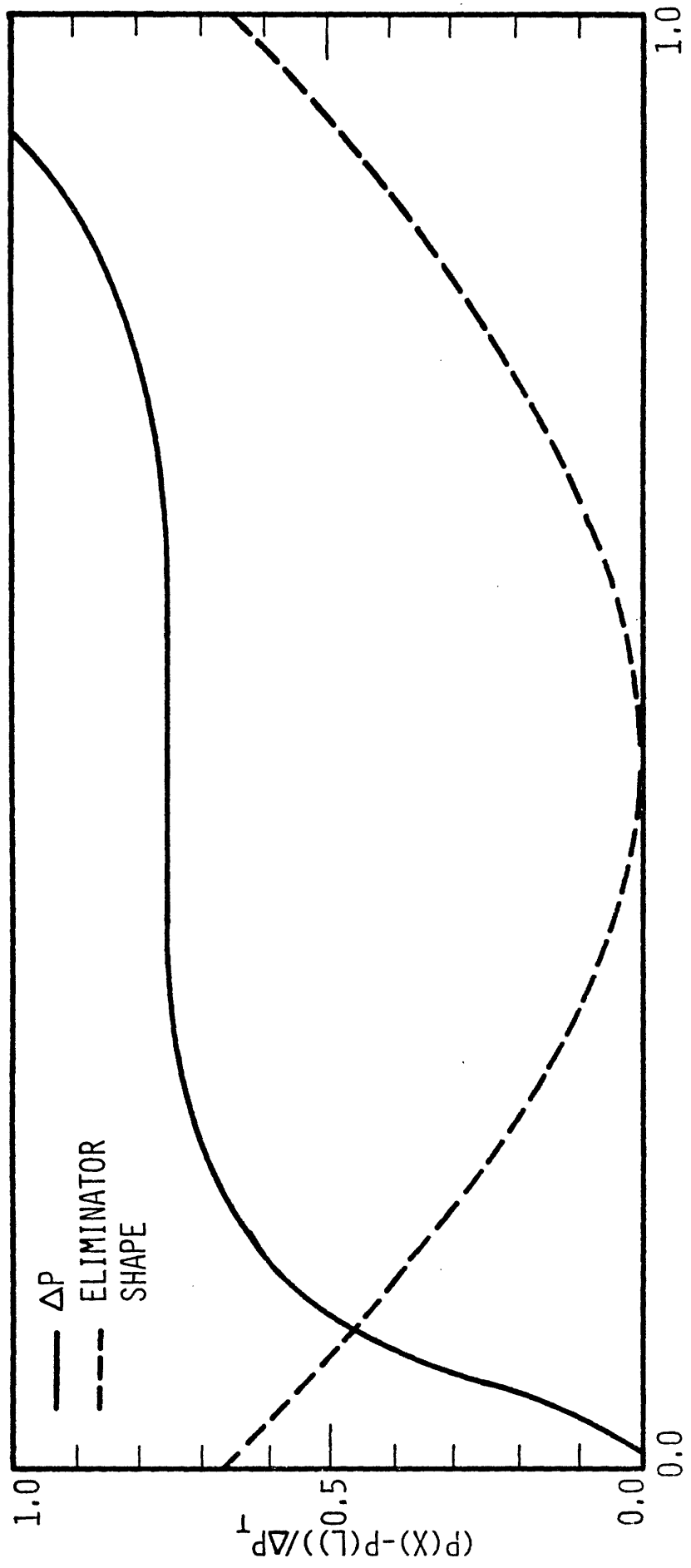

Fig. 3.5.1 Pressure Drop Distribution Along the Length of Sinus-Shaped Eliminator

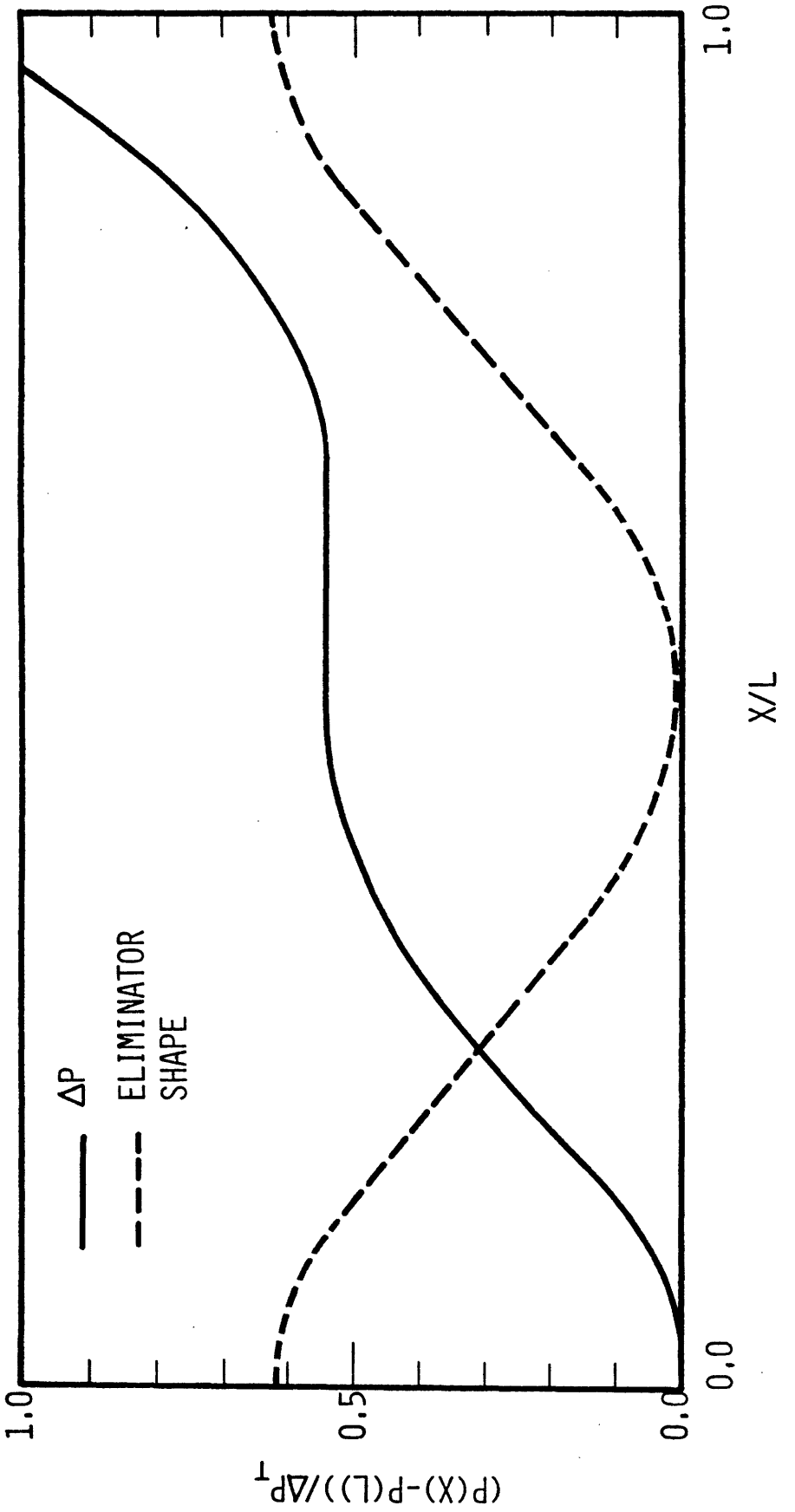

Fig. 3.5.2 Pressure Drop Distribution Along the Length of Asbestos-Cement Eliminator

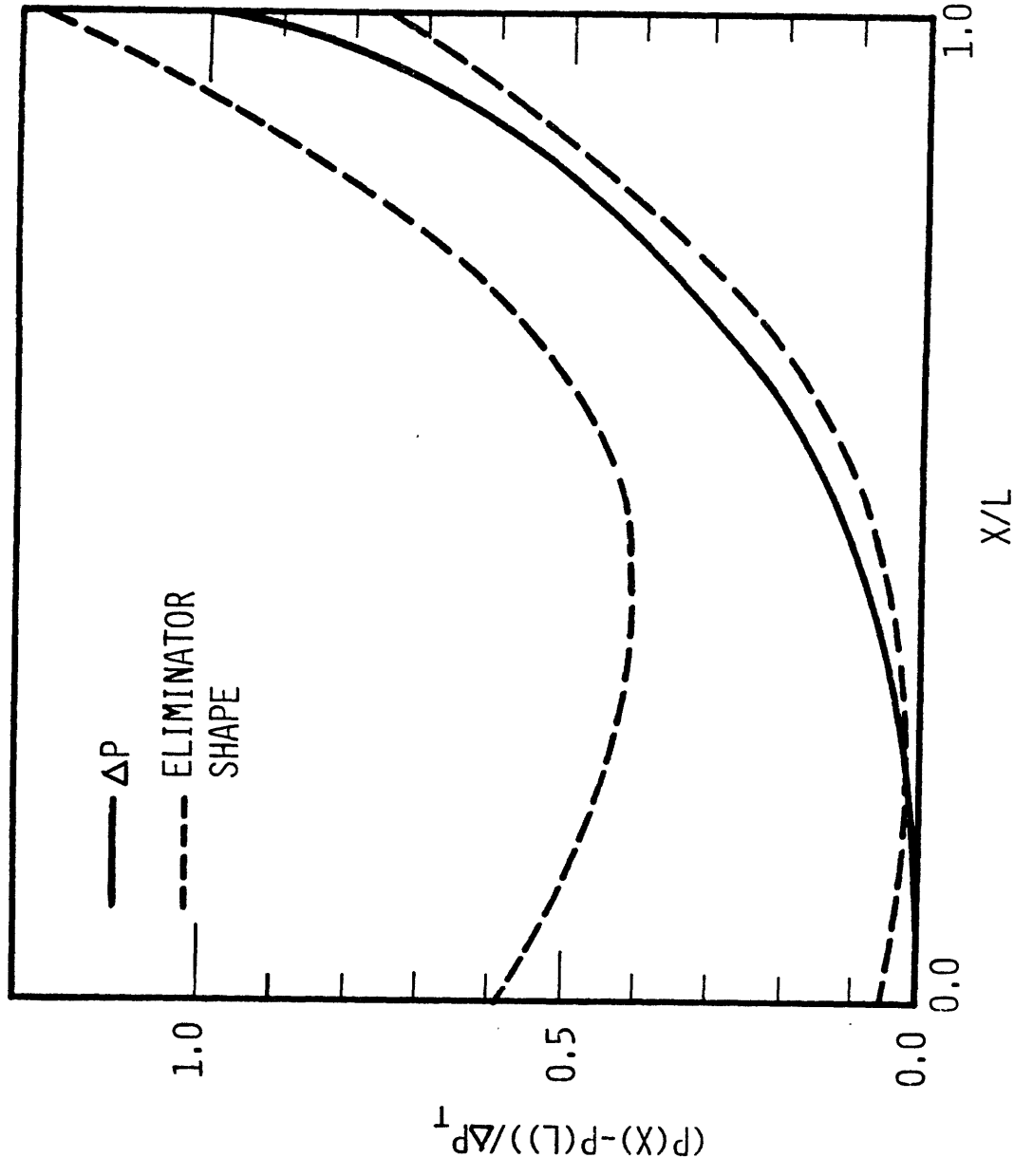

Fig. 3.5.3 Pressure Drop Distribution Along the Length of E-E Eliminator

length, which causes the pressure loss to increase steadily along the eliminator length. The pressure loss increases sharply near the outlet region of the eliminator. This is probably due to the occurrence of flow separation as discussed in Sec. 3.2.

Figures 3.5.4 and 3.5.5 show the results of the two eliminators with sharp corners, the double-layer eliminator and the Hi-V eliminator. For both of these eliminators, the pressure distribution curves exhibit a complicated behavior. For the double-layer louver eliminator in Fig. 3.5.4, the first discontinuity occurs near the inlet region, and is probably due to the occurrence of flow separation. The maximum pressure loss occurs at the turn in the eliminator, where it decreases sharply in a very short length. It then increases again to the outlet of the eliminator. Similar results are obtained for the Hi-V eliminator in Fig. 3.5.5. These distributions are not physically reasonable. Therefore, the pressure drop results for geometries with sharp corners are not reasonable, and should be used with care.

Table 3.5.1 lists the calculated pressure losses across some common drift eliminators. They are expressed in terms of the velocity head, which is $\Delta P/\frac{1}{2}\rho V^2$. It can be seen from this table that the pressure loss increases as the eliminator geometry becomes more complex. Since the collection efficiency also increases in this manner, it is necessary to compromise between these two parameters in the design of a

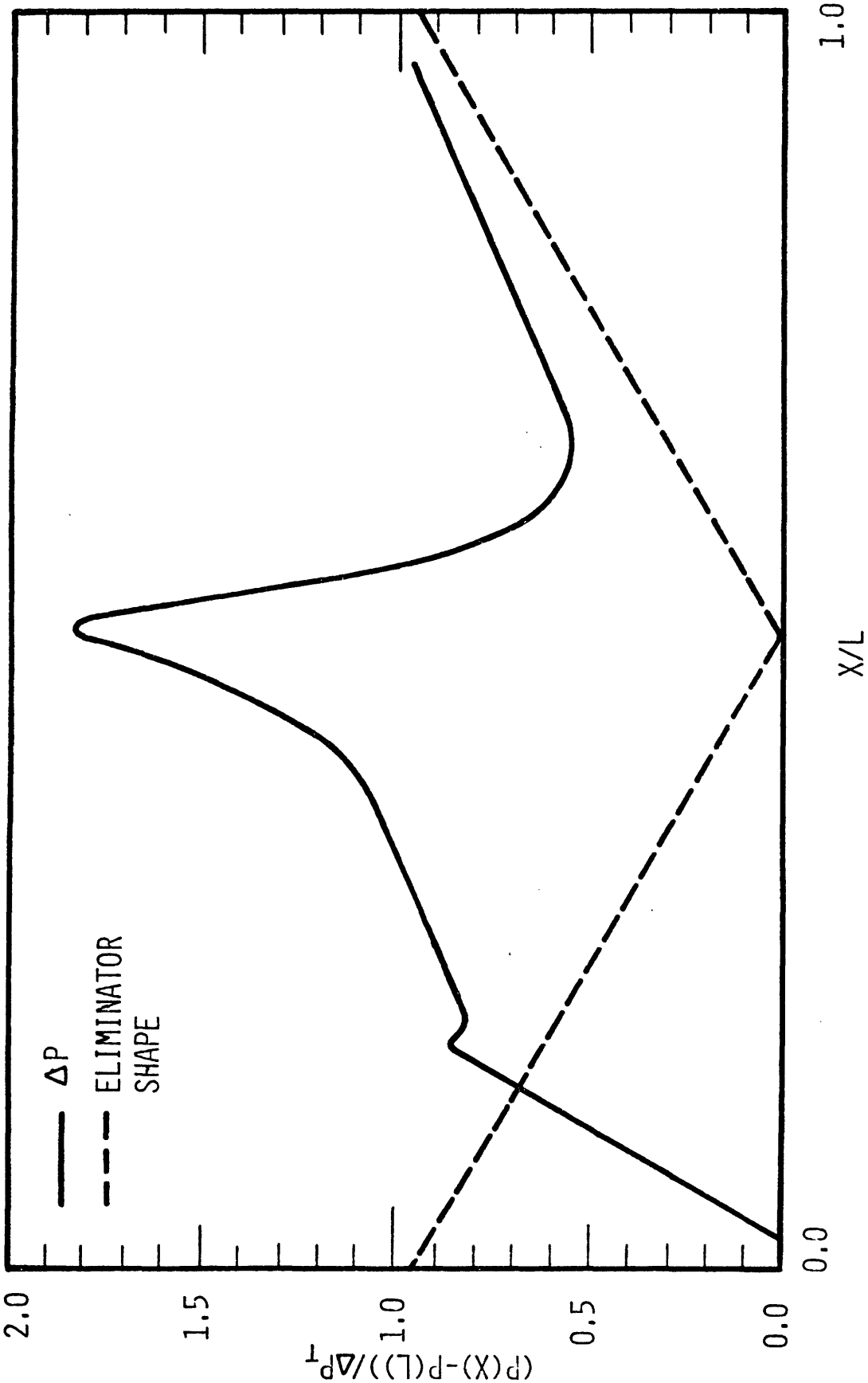

Fig. 3.5.4 Pressure Drop Distribution Along the Length of Double-Layer Louver Eliminator

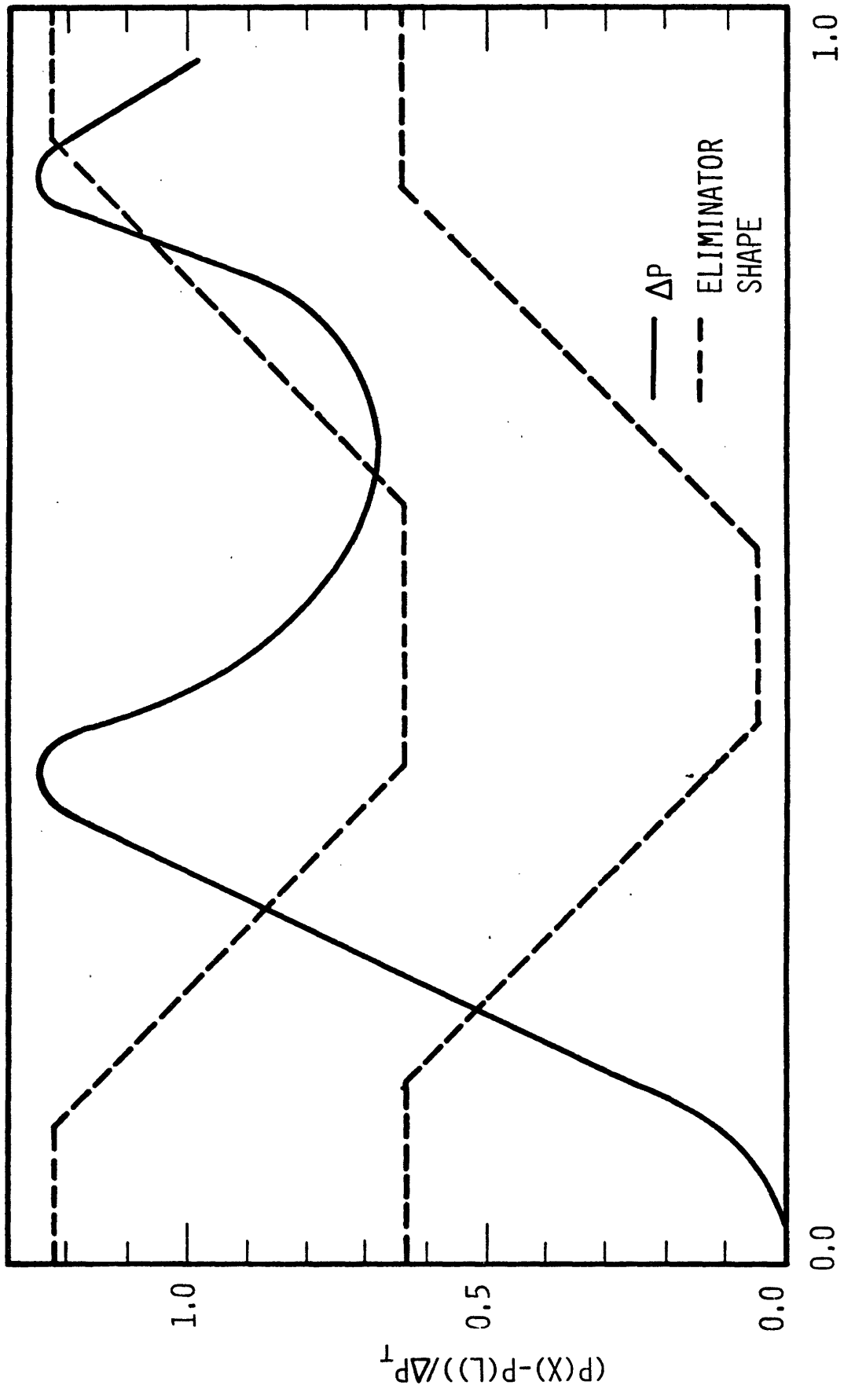

Fig. 3.5.5 Pressure Drop Distribution Along the Length of H1-V Eliminator

Table 3.5.1

Calculated Pressure Loss Across Some Common Drift Eliminators

Eliminator Geometry	Case No. in Table 3.1.1	$\Delta P / \frac{1}{2}\rho V^2$
Single-Layer Louver	S1	2.35
Double-Layer Louver	D2	0.97
Sinus	N2	2.82
Asbestos-Cement	A1	3.91
Hi-V	H1	3.43
Zig-Zag	Z1	2.54
E-E	E1	14.61
E-E (Yao's result)	E1	1.20

drift eliminator with low pressure loss and high collection efficiency.

The pressure loss across the E-E eliminator calculated by Yao and Schrock (Y1,Y2) is also found in the table. Its value is much lower than the one calculated by the DRIFT code. This is because Yao and Schrock assumed that there was no flow separation. This was, however, shown not to be true in Sec. 3.2. If this is true, then this eliminator will be unsuitable for use in cooling towers despite its high capture efficiency.

As mentioned earlier, for eliminators with sharp turns, the pressure loss calculation will not yield reasonable results. This is illustrated in Table 3.5.1; for the double-layer louver, Hi-V, and Zig-Zag eliminators, the results are unreasonably low. The experimental values of the pressure loss are higher, and are reported in Chapter 5.

CHAPTER 4
EXPERIMENTAL TECHNIQUES

4.1 Introduction

Experimental evaluations of drift eliminator performance are usually performed by measuring the drift distribution at the exhaust side of an eliminator which is installed in a particular cooling tower or in a simulated cooling tower facility. In most cases only the drift rate (defined as the drift mass current divided by the recirculating water flowrate in the tower) was measured. Very limited experimental work has been done on the droplet size-dependent collection efficiencies of drift eliminators.

Recently it has been realized that the droplet size distribution plays an important part in determining the nature of any drizzle which may arise from the drift (M3). Investigations have therefore been made into the droplet capture efficiency of drift eliminators as a function of droplet size. This data can also validate the calculations performed by the DRIFT code.

This chapter describes the drift elimination facility, the drift measurement techniques, the methods for analyzing the measured data, and the technique for pressure loss measurements. Results obtained from the experiments will be presented and discussed in Chapter 5.

4.2 Drift Elimination Facility

In order to perform comparative performance studies of cooling tower drift eliminators experimentally, a Drift Elimination Facility has been constructed. The facility simulates a cooling tower fill-outlet environment in which drift eliminators can be installed for testing. A schematic diagram of the facility is presented in Fig. 4.2.1.

This facility is a low-speed wind tunnel, 0.8 m by 0.8 m (2.5' x 2.5') with plexiglass walls, supported by a Dexion angle skeleton. Chrome felt gaskets are placed between the plexiglass and Dexion angles to prevent leakage. In order to have access to various regions, most of the plexiglass plates can be removed. Air speeds are adjusted by means of a two-speed exhaust fan at either 1.5 m/s or 2.5 m/s, which simulates natural-draft or mechanical-draft cooling tower conditions, respectively. The fan is placed at the inlet of the tunnel and forces air into the tunnel. To dampen the flow turbulence, some soda straws and honeycomb sheets have been installed downstream from the fan. The turning vanes are made of plastic sheets, and are spaced in such a way that the air flow will remain uniform after turning out of the horizontal section of the facility into the vertical section of the facility. The air is recirculated continuously through a 0.46 m (18") diameter flexible air duct to insure that water vapor saturation is maintained. Recirculating droplets are thought to contribute only an insignificant amount to the drift generated in the

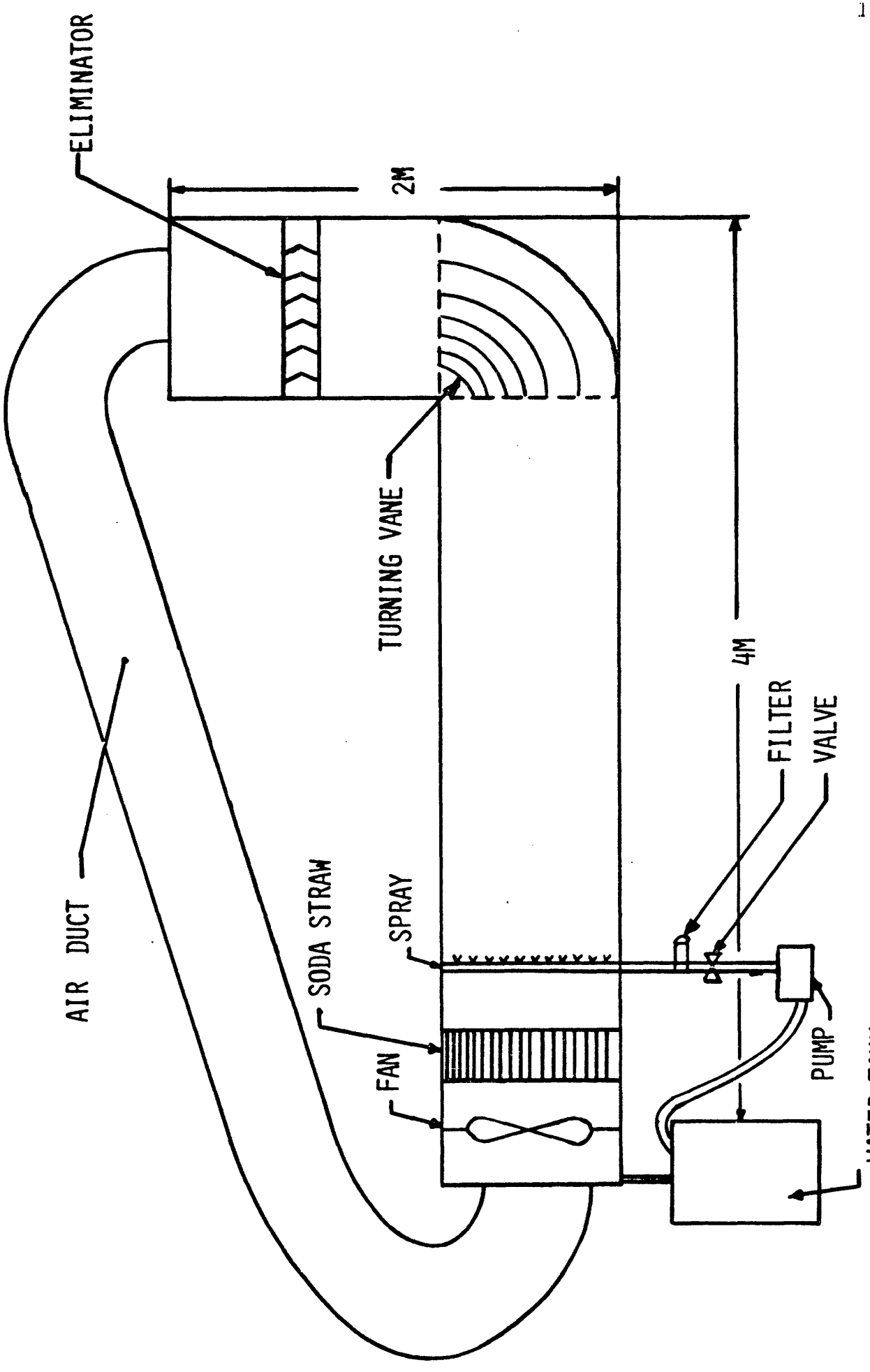

Fig. 4.2.1 Schematic Diagram of Drift Elimination Facility

tunnel and are neglected.

Water droplets are injected into the flow by a spray head which consists of 20 full-cone center-jet nozzles (SPRACO Model 3B), each delivering about 0.3 gallons per minute of water (S8). The drift quantity and droplet size spectrum can be controlled by means of the spray flowrate valve located above the pump. The valve is a PVC ball valve and the pump is rated at two horsepower. The droplets produced by the nozzles lie mainly in the 5 to 200μm diameter range. A Fulflo water filter with a cellulose acetate honeycomb cartridge that has a removal rating of 20 μm filters out any solid particles in the circulating water that might plug the spray nozzles. The facility is slightly tilted so that water will run down to a drain and be collected in the water tank. This recirculating water is changed to fresh, clear water before an experiment is performed.

The vertical test section in which the eliminators are installed is shown in Fig. 4.2.1. Eliminators could also be installed horizontally in the horizontal test section of the facility. However, in the work reported in this thesis the eliminators have all been installed in the vertical test section. This is done so that no significant water film can accumulate on the eliminator walls; also the droplet entrance conditions are simpler and are consistent with the theoretical calculations.

Three types of industrial drift eliminators have been

received from cooling tower vendors. They are the following:

(A) Belgian-Wave (sinus-shaped) eliminator

(B) Hi-V eliminator

(C) Zig-Zag eliminator

The eliminators are cut into suitable lengths so that they can be fitted into the test section of the facility. These eliminators are secured by special eliminator holders, which can hold eliminators of different lengths. The holders can adjust the pitch of the eliminators and the angle inclined to the air flow direction. The holders are made of aluminum to resist corrosion in the humid environment of the facility.

4.3 Drift Measurement Techniques

There are many methods for measuring the water droplet size distribution of water entrained in an air flow stream. In the work reported here, the laser light scattering technique is used because of its capability to measure very small water droplets online. This technique is similar to the PILLS system developed by the Environmental Systems Corporation (S2,S4).

Soon after the laser was developed, it was recognized to be extraordinarily useful for light scattering studies because of its monochromaticity, high power density, spatial coherence in the TEM_{00} mode, temporal coherence, and the small divergence of a laser beam. The laser used in the present study is a steady-state, Helium-Neon gas laser (Spectra-

Physics Model 125A) which provides 50 milliwatts of single transverse mode optical power at 632.8 nm. The schematic diagram of the droplet measuring instrument shown in Fig. 4.3.1 illustrates the general principle of this light scattering technique for sensing flowing droplets. The laser light source illuminates a narrow beam in the medium where the water droplets are flowing. The illuminated water droplets scatter light in all directions. The scattered light intensity is related to the parameters of the scattering medium and to the geometry of the apparatus through the familiar Mie theory (M5, V1). It has been found that the scattered light intensity I_s, at any angle can be related to the size of the spherical water droplet by the relation

$$I_s = Kd^2 \qquad (4.3.1)$$

where K is the proportionality constant and d is the droplet diameter. Fig. 4.3.2 shows a plot of scattered light intensity versus droplet size calculated by the DAMIE code. A description of the code is given in Appendix B. It can be observed from this figure that Eq. 4.3.1 holds. A scattering volume, designated V in Fig. 4.3.1, is defined by the intersection of the laser beam and a collimated photodetector acceptance cone. The acceptance cone is defined by the two 1000 μm diameter apertures in front of the detector. The photodetector is an RCA Model 7265 photomultiplier tube. This is a 14-stage, head-on type detector having an S-20 spectral response. It is placed at an angle of approximately 30° to

L - Laser
S - Stopper
M - Mirror
V - Scattering Volume
A - Aperture
C - Photomultiplier Tube
P - Amplifier
MCA - Multichannel Analyzer

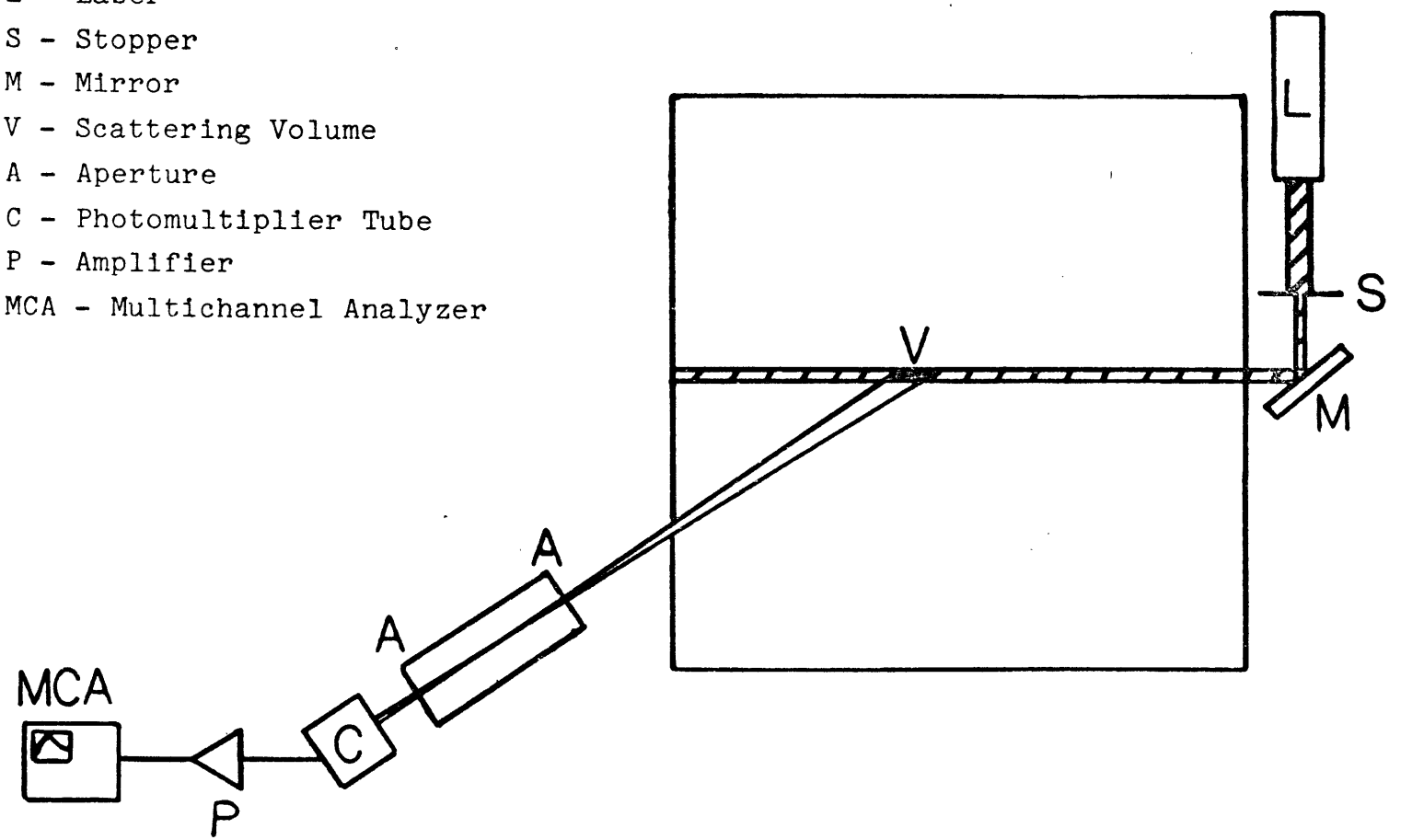

Fig. 4.3.1 Schematic Diagram of Light Scattering Drift Measurement Instrumentation

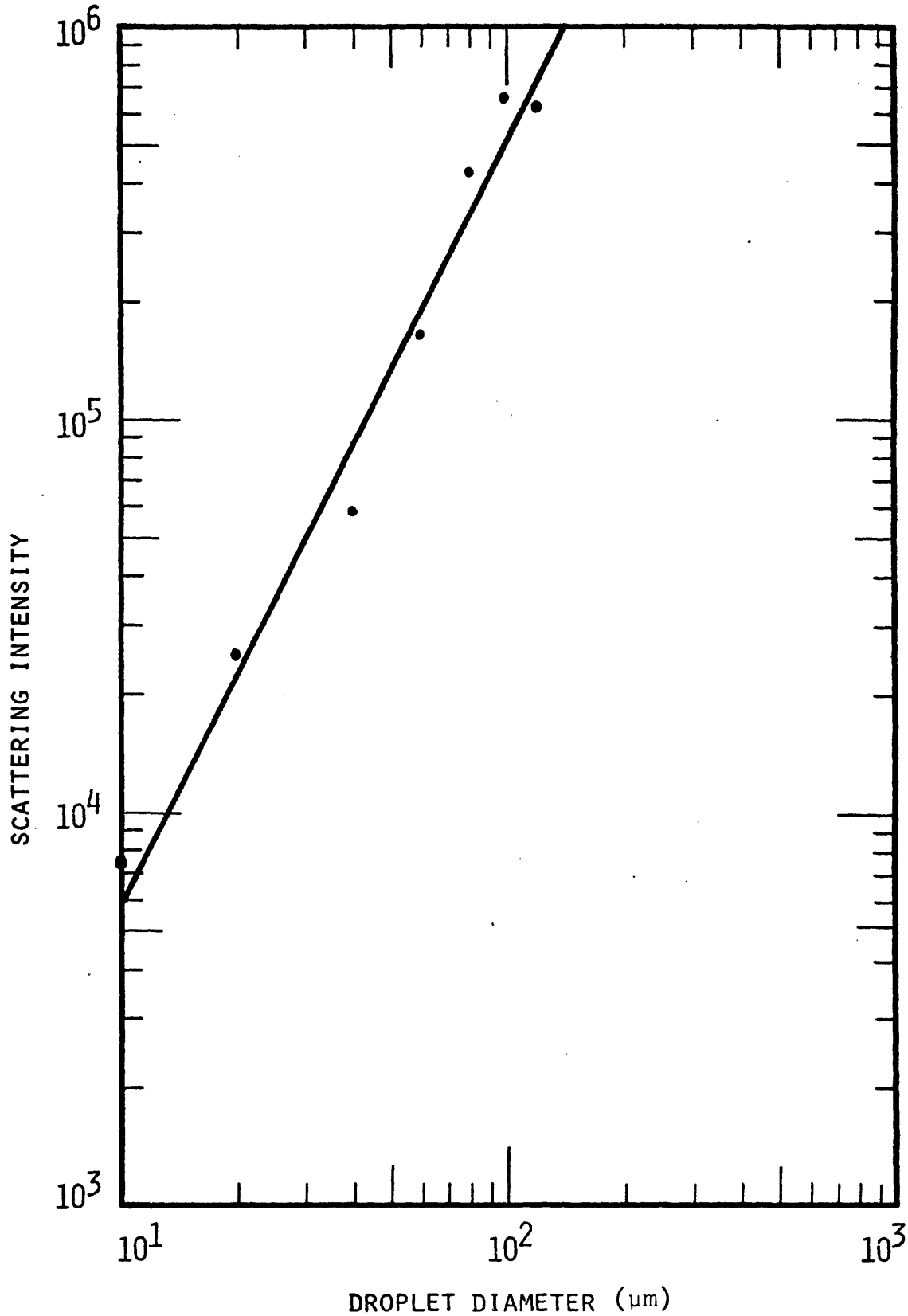

Fig. 4.3.2 Scattered Light Intensity Versus Droplet Size Calculated by DAMIE

the laser beam, which was found to be optimum. When a droplet passes through the scattering volume, light is scattered and detected by the photomultiplier tubes, producing a voltage pulse. The height of the pulse represents the scattered intensity. The pulse is amplified and recorded in a multichannel analyzer. The multichannel analyzer determines the pulse height and records each pulse in an appropriate channel. The analyzer used in this work is an NS 900 pulse height analyzer with 1024 channels. It can record pulse heights of zero to eight volts. In the current work, only 256 channels are used. It has been demonstrated, by using a standard pulse generator, that this analyzer is capable of analyzing the typical pulse shapes encountered in the experiments. The spectrum being recorded represents the droplet size spectrum of the droplets passing through the scattering volume.

This measuring technique was developed from the PILLS system (S2). Limitations of the PILLS system due to fog-induced background signals have been reported in field measurements of drift in cooling towers, but are nonexistent in this laboratory work since cold water is used in the experiments. Multi-particle scattering can be avoided by controlling the size of the scattering volume and by adjusting the drift density appropriately. A single droplet is never counted more than once because a steady-state laser is used rather than a pulsed laser as in the PILLS system, where a slow moving particle may remain in the scattering volume during more than one laser pulse.

Other background signals are derived from the high-voltage power supply, photomultiplier tube, amplifier, and from any surrounding light sources. These contribute very little to the measured signal and are neglected.

4.4 Calibration of the Drift Measurement Instrumentation

A calibration is necessary in order to find the voltage response of the drift measurement instrumentation versus the droplet size. The instrument is calibrated by introducing monodisperse water droplets of certain sizes into the scattering volume and noting the output signals. Monodisperse means that the droplets all have the same size. Monodisperse droplets are generated by a Berglund-Liu Monodisperse Aerosol Generator, on loan from Thermo Systems, Inc. This generator produces water droplets of a certain uniform size by utilizing a vibrating orifice. Its operation is based on the instability and uniform breakup of a cylindrical water jet under mechanical disturbances (B1). When these mechanical disturbances are generated at a constant frequency and with sufficient amplitude in a liquid jet of constant velocity, the jet will break up into equally sized droplets. To form a source of monodisperse droplets, these uniform droplets must be dispersed and diluted before they recombine. The generator is unique in that it can produce droplets of a known size, the droplet size being calculable from the generator operating conditions to an accuracy of 2%. The droplets generated are exceedingly uniform in size-the standard deviation is approximately 1% of the mean droplet diameter (B1).

A schematic diagram of this generator is shown in Fig. 4.4.1. It consists of four major parts : the liquid feed system, the droplet generator, the droplet dispersion system, and the wave generator. The liquid feed system is a syringe pump which forces water through a membrane filter at a constant rate into the droplet generator. The rate is determined by noting the time (using a stop watch) in which a known volume of liquid is forced into the droplet generator. The droplet generator pictured in Fig. 4.4.2 consists of a stainless steel cup with a 1.15 in. diameter flange and a hole in the bottom. A 0.375 in. O.D. orifice disc is placed in a groove inside the bottom of the cup, a Teflon O-ring is placed on top of the orifice disc, and a stainless steel cap is tightened onto the O-ring holding the orifice disc in place. A ring-shaped piezoelectric ceramic with two silvered faces is epoxied to the flange on the cup with conductive epoxy. The liquid from the liquid feed system is fed through the cap into the cup and is then sprayed through the orifice. An A.C. voltage from the wave generator is applied to the piezoelectric ceramic which vibrates the cup and disturbs the liquid jet at a constant adjustable frequency. Because the syringe pump delivers the liquid at a constant rate, the liquid jet breaks up into uniform droplets at the frequency of the A.C. voltage. The uniform droplet stream then enters the dispersion system. The droplet dispersion system consists of a stainless steel holder and cover for the droplet generator, a pressure

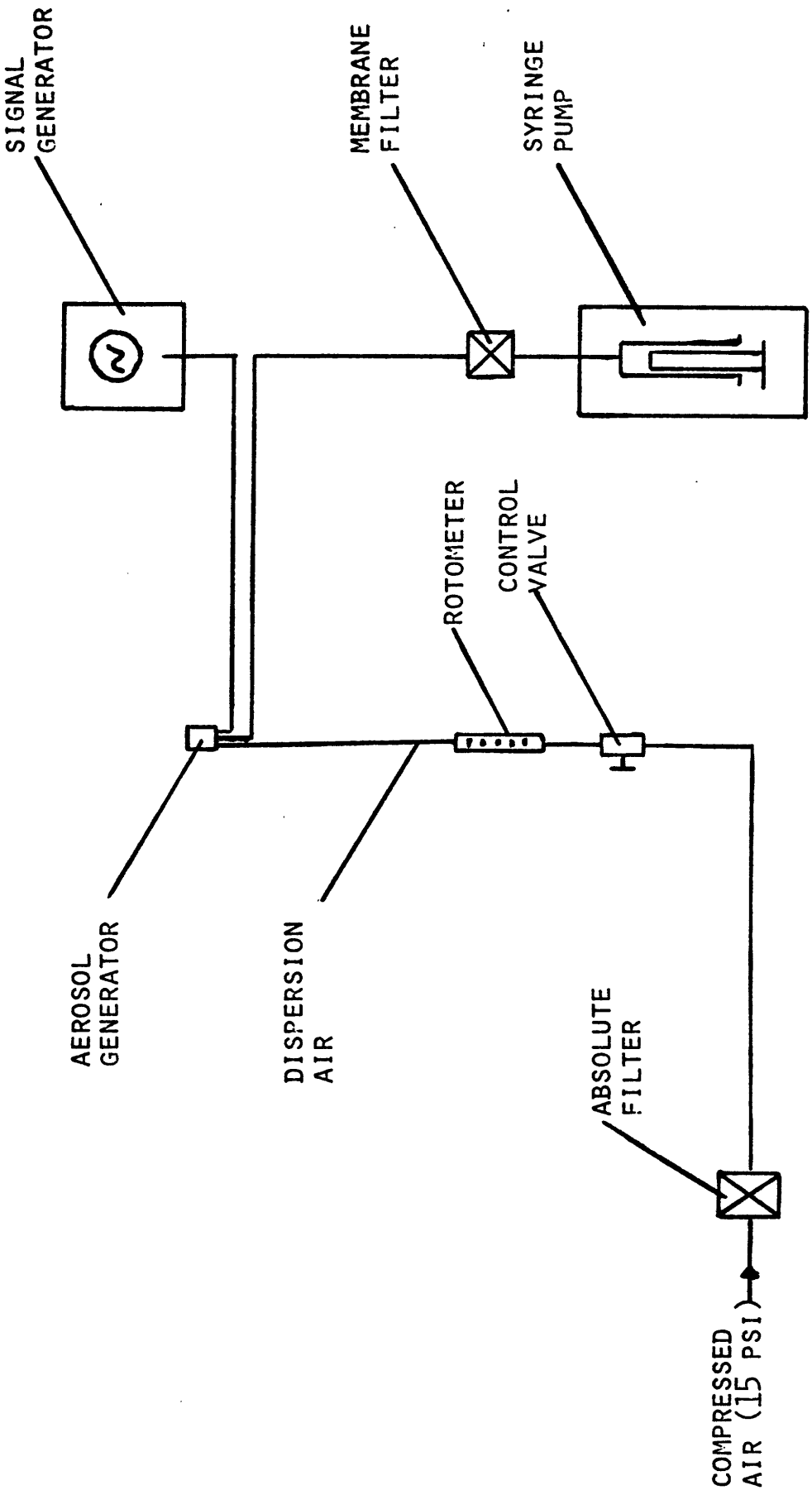

Fig. 4.4.1 Schematic Diagram of the Model 3050 Vibrating Orifice Monodisperse Aerosol Generator

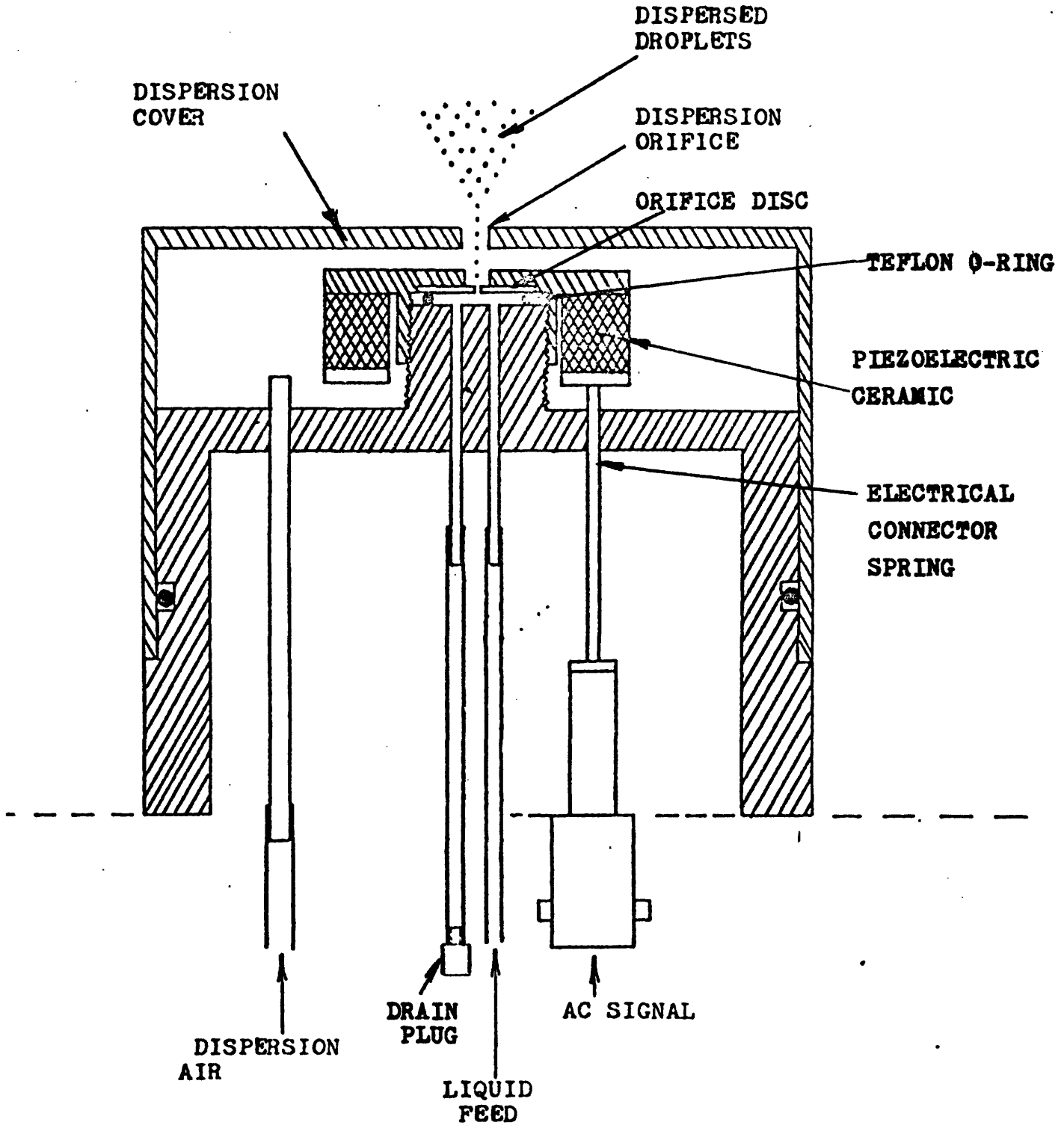

Fig. 4.4.2 Schematic Diagram of the Droplet Generating System

regulator, a flow meter, and an absolute filter. The cover has a dispersion orifice through which both the droplet stream and a turbulent air jet pass. When the droplet stream mixes with this air jet, it is dispersed into a conical shape. The dispersed droplets are then ready to enter the wind tunnel flow stream. The droplet generator is placed under the laser light beam at an appropriate distance so that the droplets are well enough dispersed to avoid multiple scattering, yet it is close enough to avoid significant evaporation of the droplets. The droplets are carried up to the scattering volume by the normal air flow in the Drift Elimination Facility described in Sec. 4.2. The scattered light from these droplets is detected and recorded by the drift measuring instrument in the manner described in Sec. 4.3.

The water droplet size produced by the vibrating orifice monodisperse aerosol generator is deduced from a knowledge of the orifice size, the liquid feed system flowrate, and the wave generator frequency by

$$D_d = \left(\frac{6Q}{\pi f}\right)^{1/3}, \qquad (4.4.1)$$

where D_d is the droplet diameter, Q is the liquid feed flowrate and f is the disturbance frequency. Table 4.4.1 tabulates some droplet sizes under typical operating parameters. The droplet sizes generated in this work range from 50 μm to 100 μm diameter. More detailed information on this generator is contained in Refs. B1 and T1.

Table 4.4.1

Droplet Diameter As A Function of Typical Droplet Generator Parameters

Nominal Orifice Diameter (μm)	Liquid Feed Rate (cc/min)	Operating Frequency (KHz)	Droplet Diameter (μm)
50	0.17	21	102
20	0.139	60	42
10	0.08	160	25
5	0.039	350	15

4.5 Data Acquisition and Analysis Techniques

Because the laser light intensity is not uniform across the beam cross section, monodisperse water droplets passing through the beam will emit different scattered intensities. The laser light has the Gaussian intensity distribution along its diameter shown in Fig. 4.5.1, where the laser light intensity was measured across the beam cross section using a Spectra-Physics Model 404 laser power meter. Because of this, the pulse heights recorded in the multichannel analyzer will not yield a single sharp peak as would be expected from a beam of uniform intensity if the edge effect is negligible (which is true when the beam size is much greater than the droplet size).

Figure 4.5.2 shows a typical measured monodisperse droplet pulse height distribution using 80 μm diameter droplets. The location of the peak in the distribution is unique to this droplet size. This measurement is repeated for several monodisperse droplet sizes. Fig. 4.5.3 plots the heights of the peaks versus the droplet sizes. The slope of the curve in this logarithm plot is very close to two, which verifies the correlation of Eq. 4.3.1.

Since the measured relationship between an output voltage pulse and an input droplet size is not unique, a complicated matrix operation must be used to analyze the measured voltage distribution. To transform the measured voltage distribution data into a droplet size distribution the following transformation procedure is used.

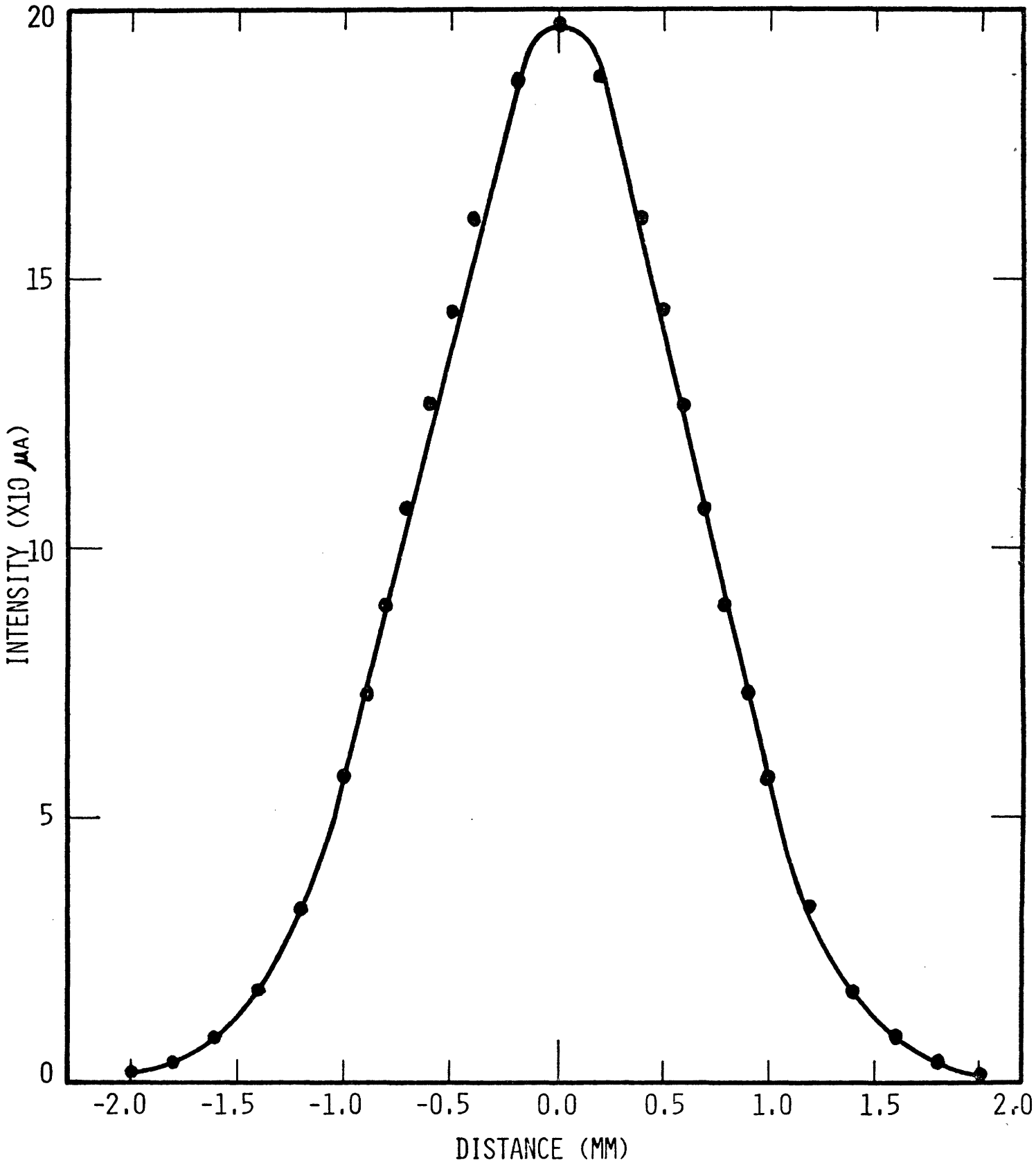

Fig. 4.5.1 Intensity Distribution Across the Laser Beam Cross Section

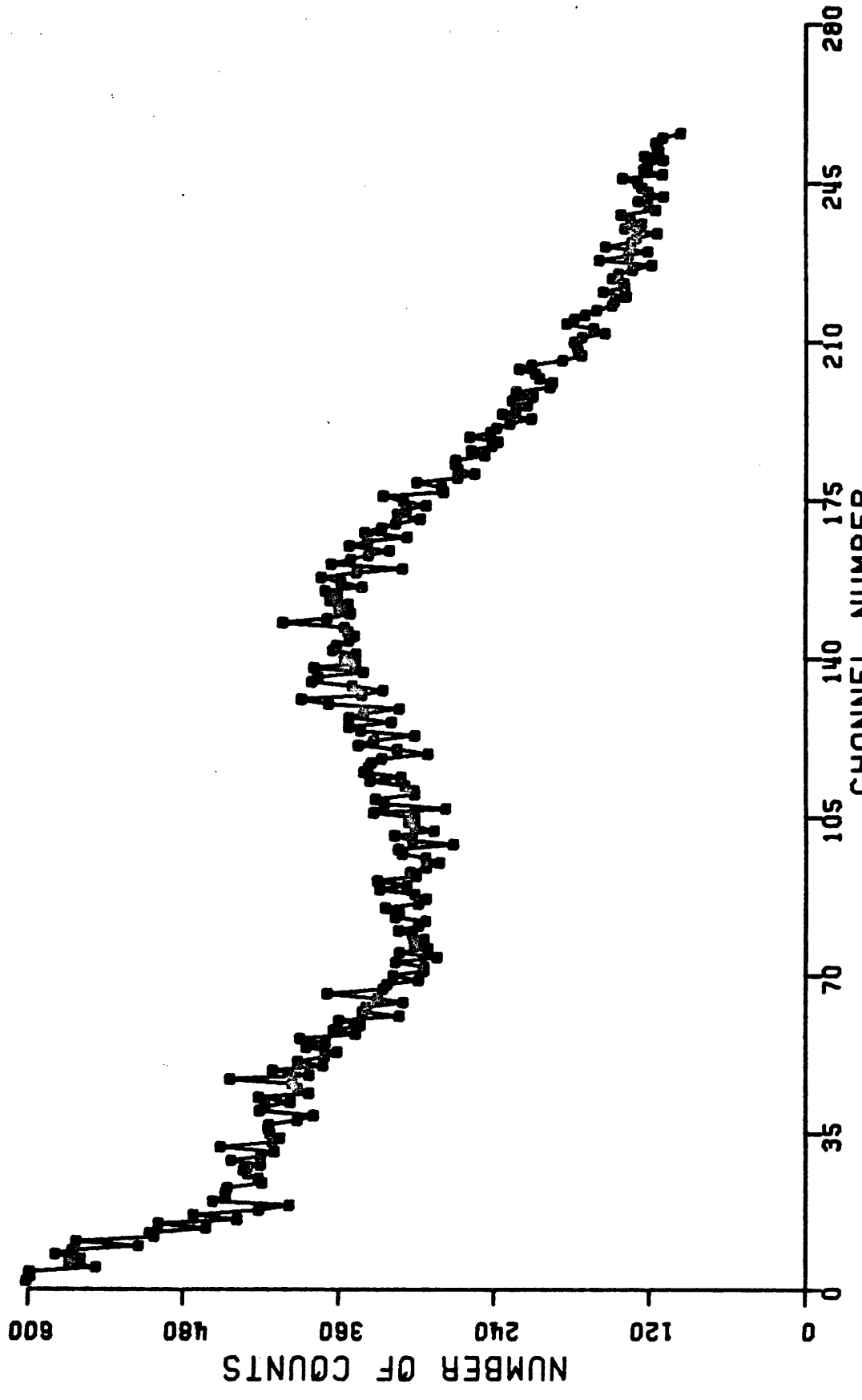

Fig. 4.5.2 Measured Pulse Height Distribution for Monodisperse Water Droplets of 80 µm Diameter

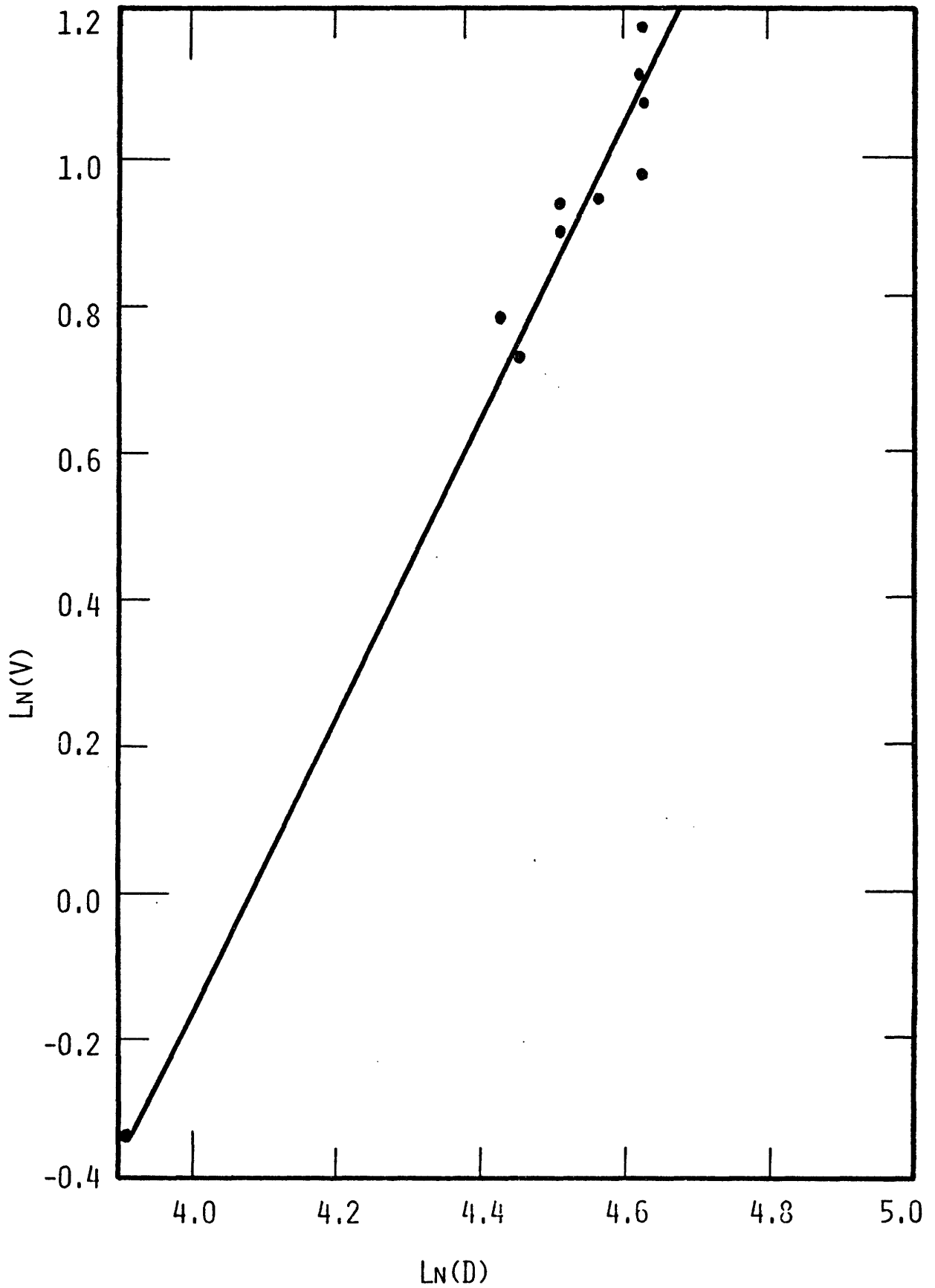

Fig. 4.5.3 Calibration Curve - the Peak Voltage of Pulse Height Distribution Versus Droplet Size

If the matrix $\underline{\underline{R}}$ (v;d) represents the voltage response function for droplets of diameter d, and if vector $\underline{A}(d)$ is the actual size spectrum of the drift, then the measured voltage distribution vector, $\underline{M}(v)$, is given as

$$\underline{M}(v) = \underline{\underline{R}}\ (v;d)\ \underline{A}(d) \qquad (4.5.1)$$

So the actual size spectrum can be determined as

$$\underline{A}(d) = \underline{\underline{R}}^{-1}(v;d)\ \underline{M}(v), \qquad (4.5.2)$$

where $\underline{\underline{R}}$ and $\underline{M}$ are found by calibration and field measurements, respectively.

For 256 channels, the $\underline{\underline{R}}$ matrix is a 256 by 256 square matrix. This matrix is determined from calibration measurement with the relationship in Eq. 4.3.1. The matrix inversion for Eq. 4.5.2 is done by the LEQT1F subroutine of the IMSL Library (I2). A description of the subroutine is given in Appendix A.

To determine the collection efficiency of the eliminators as a function of droplet size, the droplet size spectra should be measured at the inlet and outlet of the eliminators. In the present experiment, the scattering volume is fixed in space while the eliminators are either placed below the volume or above it. By placing the eliminators above the scattering volume the spectrum measured represents the inlet droplet spectrum, $P_{in}(d)$, and similarly the spectrum measured when the eliminators are below the scattering volume is the outlet spectrum, $P_{out}(d)$. From these two spectra, the collection efficiency as a function of droplet size, $\eta(d)$, can be

calculated by

$$\eta(d) = 1 - \frac{P_{out}(d)}{P_{in}(d)} \quad . \qquad (4.5.3)$$

The measured spectra are recorded on paper tape and analyzed by a computer program called DATANA which performs the response matrix multiplication and calculates the collection efficiency if a pair of measured spectra are provided. A description of this code can be found in Appendix A.

A sensitivity analysis of the effect of the response function $\underline{\underline{R}}(v;d)$ on the collection efficiency calculation was performed. This was done by using a typical set of measured voltage distributions at the inlet and outlet of the eliminator, and the calibration curve. By changing the parameters in the calibration curve, the sensitivity of the collection efficiency results are recorded. The parameters include the size of the monodisperse droplets used for calibration, DC, and NC1, NC2, and CC1, which are three parameters that specify the calibration curve (as explained in Appendix A). Table 4.5.1 lists the maximum changes in the calculated collection efficiency from its mean value as the parameters are individually changed by 10% from their mean values. It is observed that the only parameter that yields a significant change in the collection efficiency is DC, and this change is only significant at small droplet sizes. It is concluded that the collection efficiency results are not very sensitive to the response function, and

Table 4.5.1

Sensitivity Analysis of the Collection Efficiency Results

Parameter whose value is changed by 10%	Maximum Change in Collection Efficiency
DC	17% at 40 μm 8% at 50 μm 4% at 60 μm
NC2	8% at 40 μm 3% at 50 μm
NC1	No significant change
CC1	No significant change

the error introduced by the calibration will not amplify the error in the collection efficiency results.

4.6 Pressure Loss and Air Speed Measurement Techniques

The pressure loss across the eliminators is measured with a differential electronic manometer (D4). Two static pressure pitot tubes monitor the static pressure at the inlet and outlet of the eliminators. The tubes are made of 1/16" ID, 18" long, stainless steel. One pitot tube is located 6" downstream of the eliminators and the other is located 10" upstream. They are 21" apart overall. The pressures are measured at these two points, and averaged over a certain time period. The differential pressure is first set to zero with the air flowing, but without the eliminators. In this way the pressure loss due to other structures will not be included in the pressure loss measurement of the eliminators.

The sensor is a Barocell differential pressure transducer (Datametrics Model 570D). The pressure range that can be measured by this sensor is from zero to 10 torr (i.e., zero to 0.1934 psi). The pressure-sensing element in this unit is a high-precision stable capacitive potentiometer; its variable element is a thin, highly prestressed metal diaphragm positioned between two gas-tight enclosures which are connected to the external pressure ports. A difference in pressure between the two enclosures produces a deflection of the diaphragm which varies the capacitance of the diaphragm and the

fixed capacitor plates. The Barocell is wired into a 10 KHz carrier-excited bridge so that the variable capacitance unbalances the bridge and produces a 10 KHz signal whose amplitude is proportional to the applied pressure. This A.C. voltage is measured by a high-precision electronic manometer (Datametrics Model 1173), which gives a zero to 1.0 volt D.C. output. This D.C. voltage is read by a digital voltmeter.

The accuracy of the system is about 0.5% of the reading. The sensitivity of the system is 3×10^{-6} torr.

The pressure difference can be accurately measured, but there are other errors in the interpretation due to pressure fluctuations in the flow turbulence and pressure loss contributions by the eliminator holder structure, which have been found to be significant. The measured results will be presented in Chapter 5.

The air velocity is measured with a hot wire anemometer (Datametrics Series 800-VTP Flowmeter (D5)). It measures the average and instantaneous velocities in the flow of air by considering the cooling effect of the stream on a very thin electrically-heated wire filament. The probe that holds the flow-sensing wire filaments is a 3/8" diameter stainless steel wand. It is inserted into the drift measurement facility at any point to measure the local, time-averaged air velocity. The velocity range metered by this system is from zero to 6000 ft/min (0-30 m/s). It has a two volt D.C. output connection for a digital voltmeter. The voltage reading can be converted

to a velocity with a calibration curve. The accuracy of this unit is about 2% of the reading. However, due to flow turbulence and a non-uniform flow distribution, an error of about 10% is introduced.

The results of these measurements will be presented and compared with calculations in Chapter 5.

4.7 Sources of Experimental Error

It is difficult to analyze the contributions of the experimental uncertainties in the final drift measurement results. In this work, the approach is to repeat the measurements several times, so that the experimental accuracy is indicated by the variations in the final results. These measurements include the calibration measurement and the measurements of voltage distributions at the inlet and outlet of the eliminators. The results of this test are presented in Chapter 5. In this section, all possible sources of experimental error are identified.

(1) The position of the laser beam moves in the first few hours after it is turned on. Therefore, a warm up period of at least one hour should be allowed before any measurement. Movement of other drift measuring components is not significant throughout the experiment, which takes about ten to fifteen hours.

(2) Calibration is the most difficult measurement in the experiment. The droplet generator orifice is frequently plugged, and sometimes may be partially plugged, which decreases the pumping flow rate and thus changes the droplet size and the uniformity of generated droplets. Therefore, the flow rate should be constantly checked throughout a measurement.

One important uncertainty in the calibration is that the chance of more than one droplet appearing in the scattering volume is significant, although efforts have been made to reduce this. However, the final results are found not to be very sensitive to the calibration curve except at small droplet sizes, as discussed before.

Since the monodisperse droplets are carried by the flow up to the scattering volume a few inches away from the droplet generator, the droplet size will decrease due to evaporation. It was estimated that this decrease can be as large as 5% for 100 μm droplets. This error could introduce an error of 10% in the final results for small droplet sizes, as was shown previously.

(3) Statistical counting errors are difficult to estimate because they are not uniform for all

droplet sizes, but become larger for bigger droplets. In the data analysis, the distribution is smoothed, and this will eliminate some of this error. Dead time in the pulse height analyzer contributes another uncertainty to the results. Since the drift rate is much higher at the eliminator inlet than at the outlet, the dead time is very different for the two distributions, and it is found that the analyzer used in this work cannot account for this very well.

(4) There is a possibility that more than one droplet may appear in the scattering volume and cause the analyzer to record a wrong signal. This possibility cannot be avoided but can be reduced by decreasing the size of scattering volume and by reducing the quantity of drift. This error is thought to be small.

(5) The quantity of drift fluctuates with time due to the pumping power fluctuations and changing conditions within the Drift Elimination Facility. However, if the data acquisition time is long (three to five hours in the present experiment), this fluctuation will average out in the measured results.

The pressure drop across the filter in the circulating water system increases with time because of the gradual plugging of the filter by foreign particles in the circulating water. This affects the quantity of the drift generated by the facility. But the effect is small during one test.

(6) Signal noises that may contribute to the measurement uncertainty consists of electronic noise in the amplifier and high voltage supply, the dark current of the photomultiplier tube, and scattered light from other sources. It is found that these noises contribute about 10% to the lowest recordable signal and become insignificant for larger signals.

(7) The laser light intensity at the measuring point depends on the drift concentration which shadows some of the laser light. However, by measuring the intensity at the scattering volume with a power meter for different drift concentrations, this effect was found to be almost undetectable.

The above discussion gives possible sources of experimental uncertainties. In Chapter 6, a quantitative analysis of experimental errors is developed.

CHAPTER 5

COMPARISON OF EXPERIMENTAL RESULTS WITH THEORETICAL CALCULATIONS

5.1 Introduction

In this chapter the experimental results for the drift collection efficiency and pressure loss across some industrial cooling tower drift eliminators are presented. These results are compared with the calculations from the DRIFT code. The experimental measurement techniques are discussed in Chapter 4, and the numerical simulation techniques in the DRIFT code are described in Chapter 2.

Three industrial drift eliminators were donated for this study by cooling tower vendors. These are the Belgian-wave eliminator, the Hi-V eliminator, and the Zig-Zag eliminator. Their geometries and dimensions are shown in Fig. 5.1.1. The Belgian-wave eliminator is made of sinusoidally shaped asbestos cement board, and it has a uniform flow channel cross section. The Hi-V eliminator is made of polyvinyl chloride. Its flow channel cross section is not uniform, as shown in Fig. 5.1.1. The Zig-Zag eliminator is made of fiberglass. Its flow channel cross section is uniform, except at the corners.

The measured pressure losses across these eliminators are compared with calculated pressure losses in Section 5.2, and the collection efficiency comparisons are presented in Section 5.3. The data is developed at two air speeds, 1.5 m/s and 2.5 m/s.

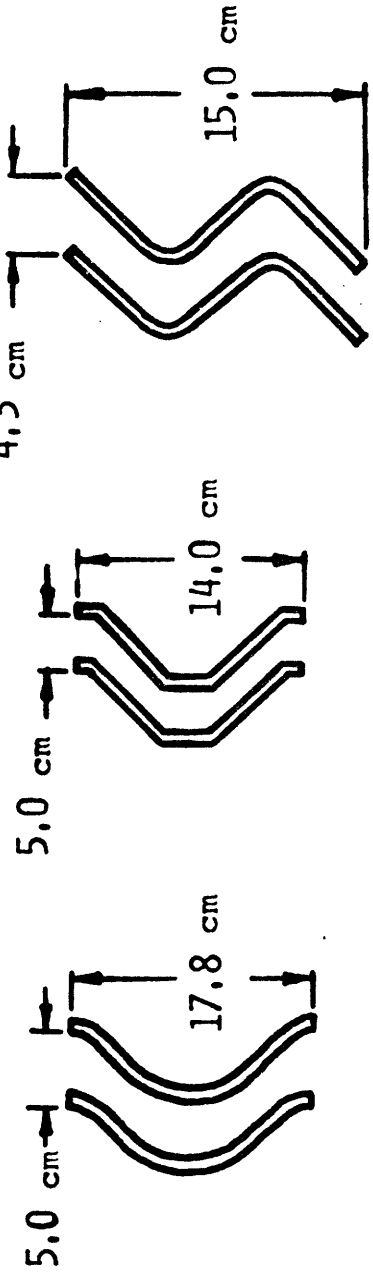

FIG. 5.1.1 DRIFT ELIMINATOR GEOMETRIES. (A) BELGIAN-WAVE ELIMINATOR, (B) HI-V ELIMINATOR, (C) ZIG-ZAG ELIMINATOR

5.2 Pressure Drop Across Eliminators

Table 5.2.1 is a comparison of the theoretically calculated pressure losses across the three types of drift eliminators with the experimentally measured values at an air speed of 1.5 m/s. Table 5.2.2 presents the same comparison at an air speed of 2.5 m/s. The true air speeds are slightly different for each eliminator, since their flow resistances are different.

The calculated and measured results are in good agreement, and are within the bounds of experimental error. It is clear from the data that as the geometry of the drift eliminator becomes more complex, the pressure loss increases. Since the drift collection efficiency also increases with increasing geometrical complexity (shown in Section 5.3), it is necessary to strike a compromise in designing an eliminator that will achieve an acceptable pressure loss and an acceptable collection efficiency. The values in brackets are the resistances of the eliminators to the air flow expressed in terms of velocity heads corresponding to the nominal air speed. This is an advantageous way to report the data since its numerical value for a particular eliminator is independent of the air speed and the working fluid if the flow is fully turbulent.

The theoretical pressure loss calculations for the Zig-Zag eliminator have been unsuccessful because of the complex eliminator geometry and because of the limitations of the calculational method in describing turbulence (see Chapter 3).

Table 5.2.1

Pressure Drop Across Eliminator at Low Fan Speed

Type of Eliminator	Air Speed (m/s)	Calculated Value (torr)*	Measured Value (torr)	Accuracy of Measurement
Belgian-Wave	1.5	0.02868 (2.82)**	0.03054 (3.00)	13%
Hi-V	1.5	0.03482 (3.43)	0.03734 (3.68)	12%
Zig-Zag	1.5	does not converge	0.07424 (7.31)	8%

* 1 torr = 1 mm Hg = 0.01934 psi.

** Values in parentheses are expressed in units of velocity head, $\Delta P / \frac{1}{2} \rho V^2$.

Table 5.2.2

Pressure Drop Across Eliminator at High Fan Speed

Type of Eliminator	Air Speed (m/s)	Calculated Value (torr)*	Measured Value (torr)	Accuracy of Measurement
Belgian Wave	2.5	0.06546 (2.32)**	0.06279 (2.23)	11%
Hi-V	2.4	0.07663 (2.72)	0.08119 (2.88)	11%
Zig-Zag	2.3	does not converge	0.16079 (5.70)	6%

* 1 torr= 1 mm Hg = 0.01934 psi.

** Values in parentheses are expressed in units of velocity head, $\Delta P/\frac{1}{2}\rho V^2$

However, the agreement of the calculated and measured results for the other two, more simple geometries, demonstrates that the calculations are valuable in reasonably smooth geometries for predicting pressure loss.

Comparing Table 5.2.1 and Table 5.2.2, it is found that the pressure loss increases approximately as the square of the air speed for all three eliminators. The observations made about Table 5.2.1 also apply to Table 5.2.2.

The pressure losses for these eliminators quoted by their vendors are higher than the values presented here (H6, S9). The reason is that in their measurements, the pressure differences with no eliminators installed were not set to zero. This means that their measured data include the pressure loss due to other structures, which are considerable in comparison with just the pressure loss across the eliminators.

5.3 Collection Efficiency Results

In this section, the calculated and measured collection efficiency results are presented. Fig. 5.3.1 shows the droplet collection efficiency as a function of droplet size for the Belgian wave eliminator at an air speed of 1.5 m/s. The measured data are presented as a broken line in the figure. The experimental technique is described in Chapter 4. The calculated results using both no-slip and free-slip boundary conditions are compared with the experimental results. It is found that the calculated and measured droplet capture

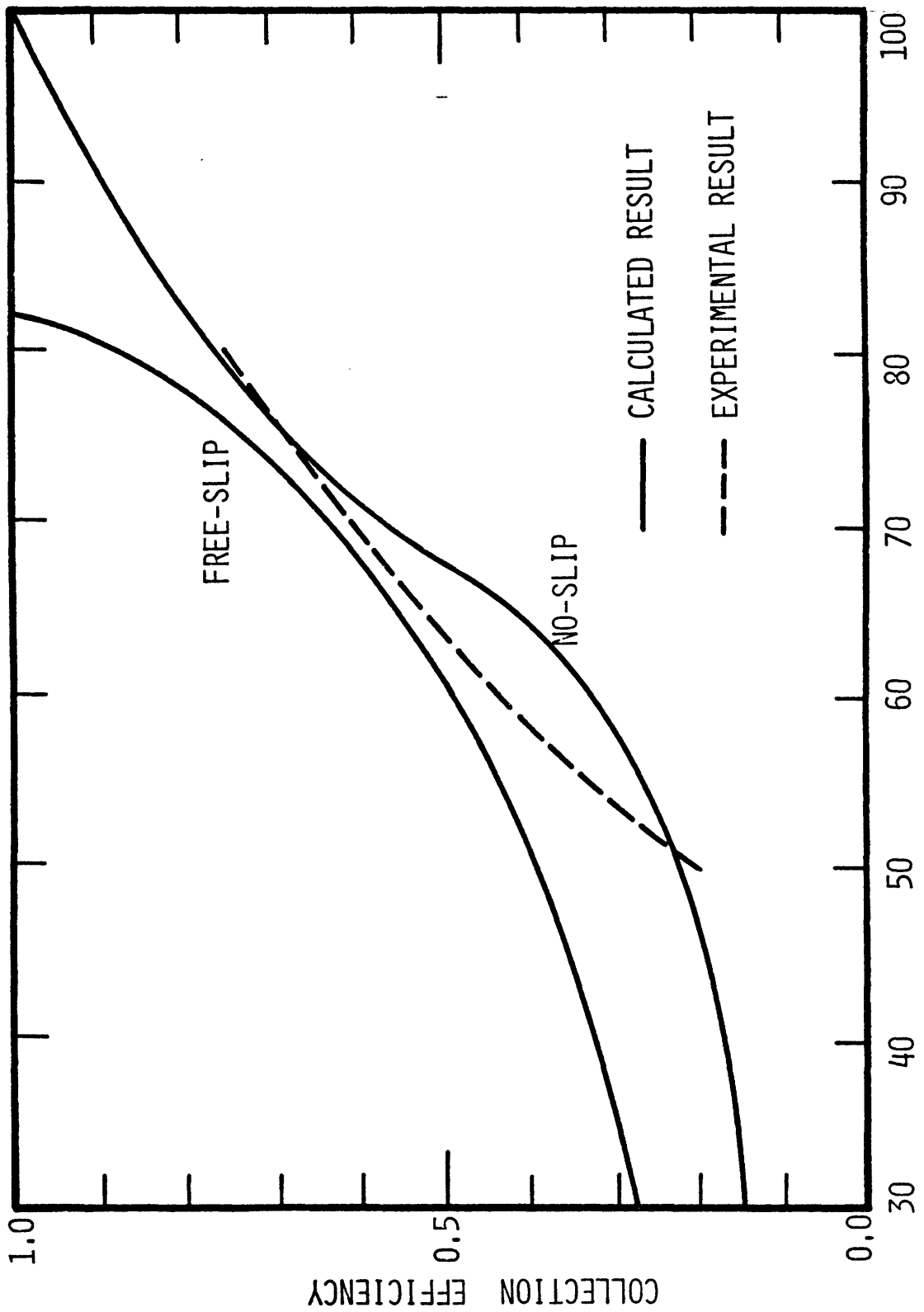

Fig. 5.3.1 Predicted and Measured Droplet Collection Efficiency Functions for Belgian-Wave Eliminator at 1.5 m/s Air Speed

efficiences agree well for this smooth eliminator geometry, with the no-slip boundary results providing more accurate predictions. It is also found that droplets smaller than 60 μm in diameter can easily escape from the eliminator.

The calculated and measured collection efficiency data for the Hi-V eliminator are shown in Fig. 5.3.2. It is found that this eliminator is more efficient in capturing droplets of any size than the Belgian wave eliminator. Also, the agreement between the no-slip prediction and the measurement is reasonably better than the agreement between the free-slip prediction and the measurement. The no-slip result predicts a higher collection efficiency than the measured data, while the free-slip prediction is generally lower than the measured data.

Figure 5.3.3 displays the data for the Zig-Zag eliminator. The calculation of the air velocity distribution for this eliminator failed to achieve asymtoptic values using no-slip boundary conditions, as discussed in Chapter 3. By using the calculated distribution of the nonasymtoptic solution, approximate results of droplet collection efficiency for this eliminator were obtained. This is compared with the free-slip prediction and the measured data in Fig. 5.3.3. This approximate result predicts a higher collection efficiency than the free-slip prediction, and agrees with the measured data better than the free-slip prediction in general.

Figure 5.3.4 shows the data at high fan speed, where the calculated results are no-slip prediction. Similar conclusions can be made from this figure.

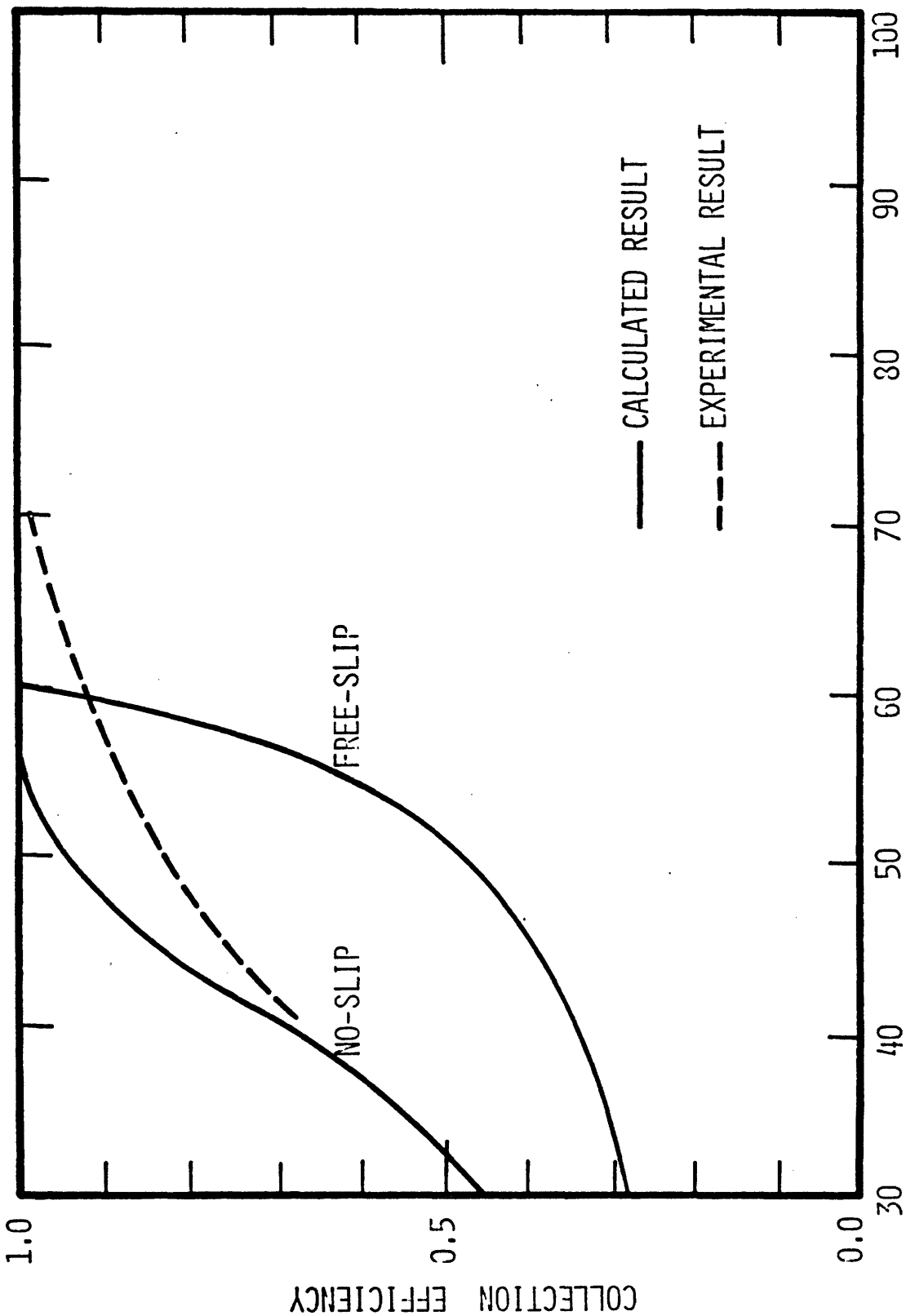

Fig. 5.3.2 Predicted and Measured Droplet Collection Efficiency Functions for Hi-V Eliminator at 1.5 m/s Air Speed

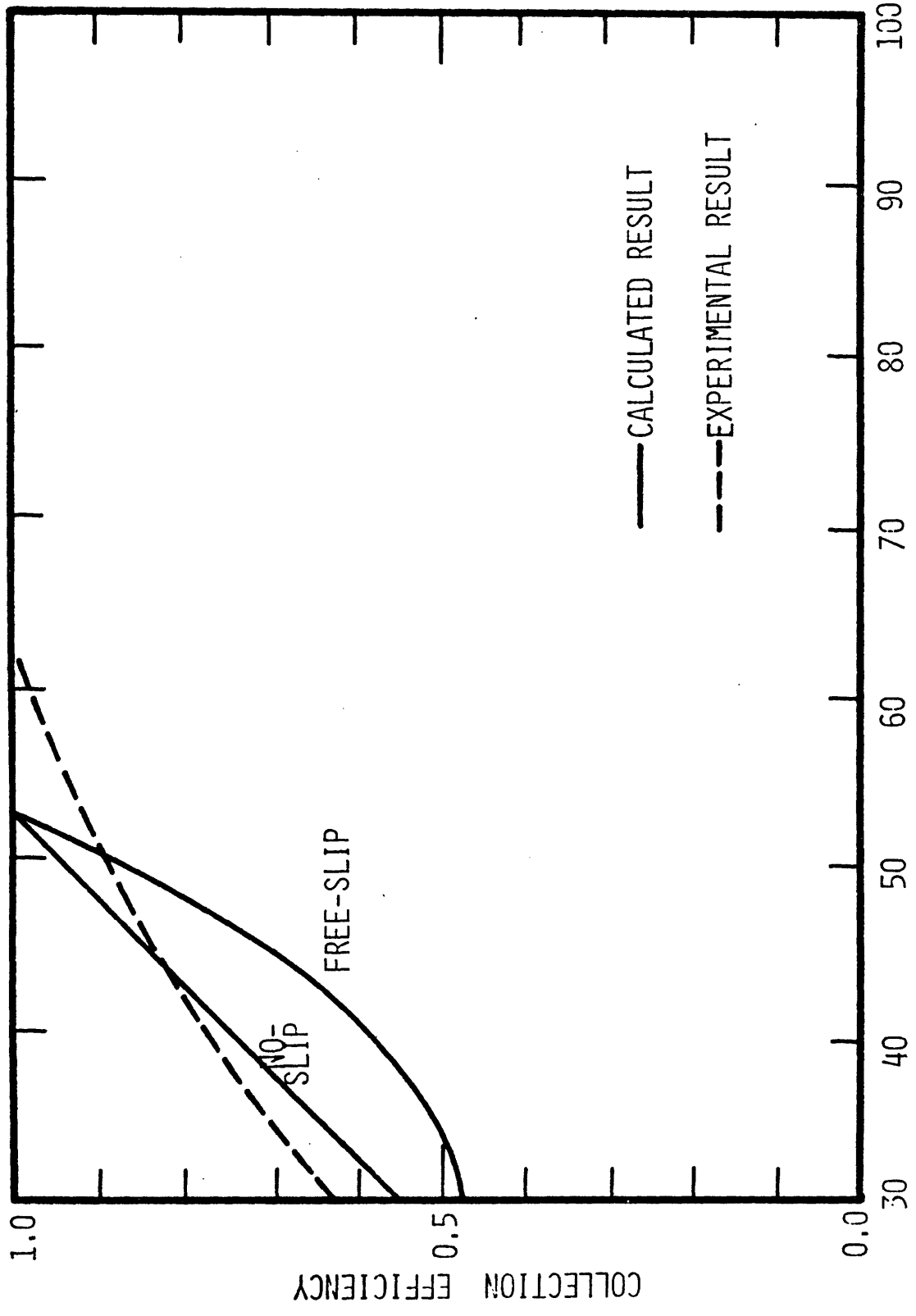

Fig. 5.3.3 Predicted and Measured Droplet Collection Efficiency Functions for Zig-Zag Eliminator at 1.5 m/s Air Speed

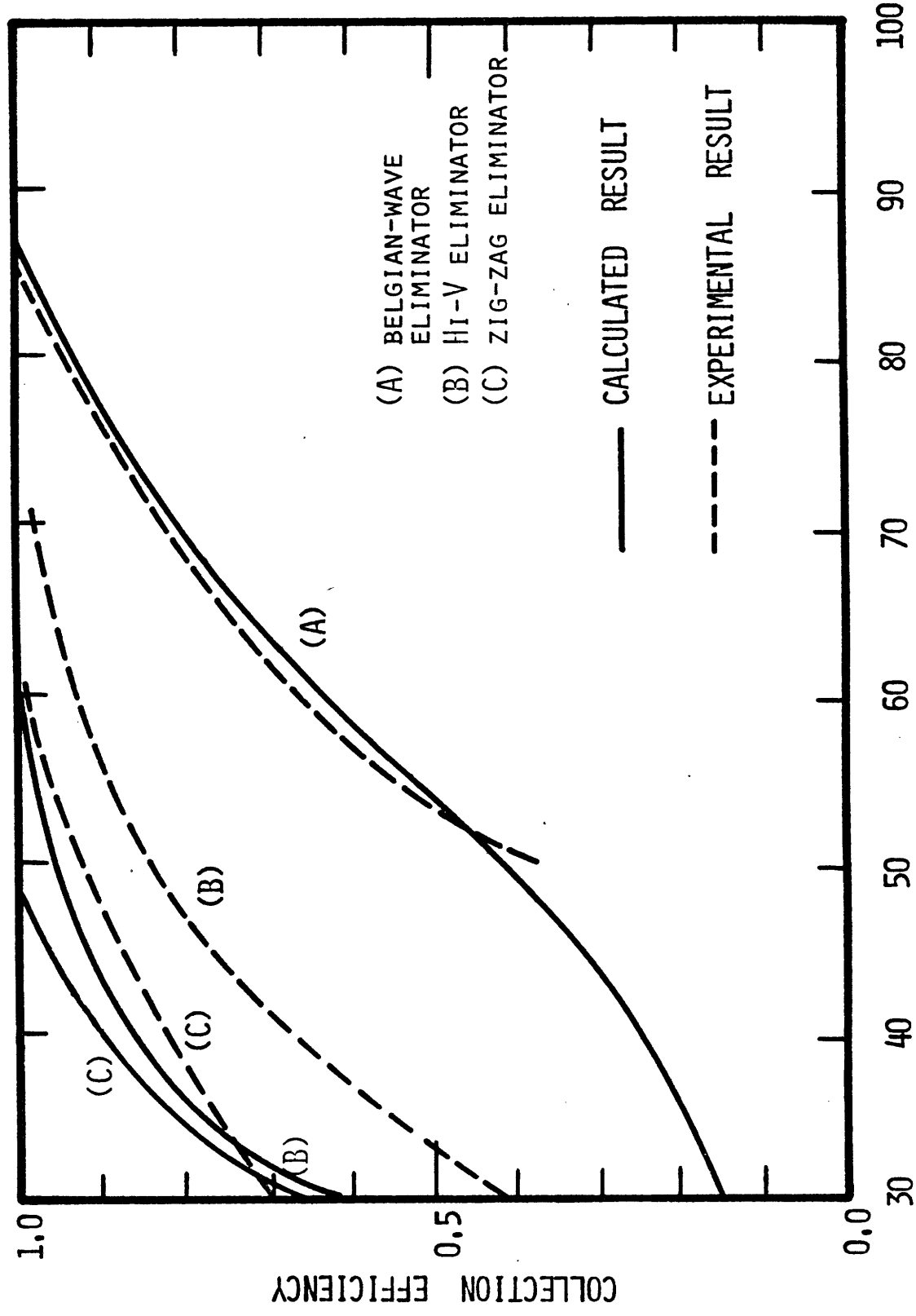

Fig. 5.3.4 Predicted and Measured Droplet Collection Efficiency Functions for Commercial Drift Eliminators at 2.5 m/s Air Speed

5.4 Estimation of Experimental Error

A qualitative discussion of the sources of experimental errors is given in Chapter 4. It was mentioned that the quantitative contributions of those uncertainties in the data are not easily accounted for. In this work only the repeatability of the measured data is established. This is done for each eliminator by repeating the measurements several times under similar conditions.

Table 5.4.1 shows the results of four measurements on the Zig-Zag eliminator at an air speed of 1.5 m/s . The measurements included the calibration run and the droplet size distribution measurements at the inlet and the outlet of the eliminator. The data was taken on different days. From these results it can be seen that the data is repeatable with a maximum standard deviation of about 10% at the smallest droplet size.

The results for the Zig-Zag eliminator are the most consistent among the three eliminators tested in this work. The reason is that this eliminator is constructed in one block so that the pitch and the inclination of the louvres always remains the same even though it was taken out after each measurement. The other two eliminators are furnished in pieces which are installed by using the eliminator holders described in Chapter 4. When taking these eliminators in and out of the test section, it is difficult to repeat the exact pitch and angle of inclination. Therefore, for the Belgian

Table 5.4.1

Measured Collection Efficiencies of the Zig-Zag Eliminator at 1.5 m/s Air Speed

Droplet Diameter (μm)	Measured Collection Efficiency				Mean	Standard Deviation
	Run 1	Run 2	Run 3	Run 4		
30	0.615	0.616	0.529	0.689	0.612	0.065
40	0.718	0.820	0.804	0.785	0.782	0.045
50	0.880	0.926	0.906	0.899	0.903	0.019
60	0.930	0.968	0.929	0.950	0.944	0.019
70	0.951	0.979	0.943	0.963	0.959	0.016
80	0.966	1.0	1.0	1.0	0.992	0.017

wave and the Hi-V eliminators the results are not very repeatable; the maximum standard deviation is as high as 20%.

The discrepancy between the calculated and measured results is discussed further in Chapter 6.

CHAPTER 6
CONCLUSIONS AND RECOMMENDATIONS

6.1 Discussion of Results

It was demonstrated in previous chapters that predictions of collection efficiency and pressure drop for some drift eliminators by the DRIFT code agreed fairly well with measured results. The discrepancies are due to the experimental uncertainties and the calculational and experimental assumptions. The results are discussed in this section.

It was indicated earlier that both the calculated and measured pressure drop results of this work are significantly lower than the values quoted by cooling tower vendors. This is due to a difference in the definition of pressure drop. The vendors include in their definition the pressure loss due to structures other than the eliminators themselves, and this contributes a significant amount to the measured pressure loss.

The collection efficiency results reported in this study are higher than expected because these results generally show 100% efficiency for droplets larger than 100 μm, yet droplets much larger than this have been found to escape actual cooling towers. This is probably due to the assumptions made in the calculations and the simplified conditions in the experiments. Droplet growth effects,water film effects, and flow turbulence are thought to be the main factors. These effects are discussed here.

(1) Water film effects

The droplet collection efficiency calculations have ignored the possible effects of the water film on the eliminator walls. Two effects arise from the drag of the exhaust flow on the water film, and another effect arises from the impacting of captured water droplets on the film. The presence of the water film modifies the exhaust flow boundary conditions from simple no-slip conditions to those of matching the air-water velocities at the gas-liquid interface. Except in the case of a thick film, the effect of this complicated boundary condition on the velocity distribution within the eliminator should be small. Also, drag on the liquid film can lead to droplet generation because water can be drawn off of the trailing edge of the eliminator, or droplets can be stripped from the film surface through the formation of Helmholtz instability waves.

The work of Yao and Schrock (Y1) indicates that at an air speed of 2.0 m/s in a smooth drift eliminator geometry the minimum film thickness required for droplet stripping is 0.2 mm, and that substantially higher air speeds are required for droplet generation via pickup from the peaks of Helmholtz instability waves for a film of this thickness. In the present work, the water film thickness on the eliminator walls was not measured, however, visual observations were unable to detect either droplet stripping at the trailing edge of the eliminator or droplet generation on the interior walls. The

absence of droplet stripping at the outlet is implicit evidence for the absence of wave generated droplets in the interior (Y1).

With sufficiently thick films and with droplets impacting at sufficiently acute angles and high velocities, it has been observed that a droplet can rebound from the film, or "bounce" back into the exhaust flow (J2). This droplet bouncing problem is thought to be significant for drift eliminator performance in actual cooling towers where the water loading on the eliminator is high and the water film is thick. Foster et al. (F3) studied this problem and observed that this effect is indeed significant, however, they found that many droplets meeting the impact conditions established by Jayaratne and Mason (J2) did not bounce. It was concluded that it is not possible to estimate the true importance of droplet bouncing in a real tower environment due to the lack of information about the surface water coverage. Further work on this effect is being carried on by Foster in the Central Electricity Research Laboratories (F5).

(2) Droplet growth effect

It was mentioned that droplets as large as several hundred microns could escape commercial cooling towers outfitted with the drift eliminators being tested in this work. According to the collection efficiency results for these eliminators, these droplets should have been trapped. It is

suggested that the droplets might bypass the eliminators through the openings around the tower structure. It might also be due to the stripping and rebounding effects in the water film as discussed earlier. Another possibility that has so far been overlooked in the literature is droplet growth in cooling towers. It has been suggested that droplet growth is not significant in a cooling tower because a small drift droplet, moving at a velocity approaching that of the air stream, might leave the top of the tallest natural draft tower in less than one minute from the time it passes through the eliminators. If that is true, then even though the air in the surrounding air stream is generally saturated, the time span is too short for any significant droplet growth. However, this is not true for some droplets in cooling towers. Large droplets (>100 μm) do not travel at the air stream speed because their terminal velocities approach that of the air stream speed as shown in Fig. 6.1.1. Therefore they will stay in the tower for a long time. Another factor that causes some water droplets to reside in a cooling tower for a long time is the air flow pattern inside the cooling tower. The turbulent effect, the quiescent region, and the variation of air velocity at the throat of the shell (in the case of a hyperbolic cooling tower) can prolong the residence time of water droplets inside the tower, thus making the growth effect significant. This effect will not only change the size distribution of the escaping drift, it will also change the

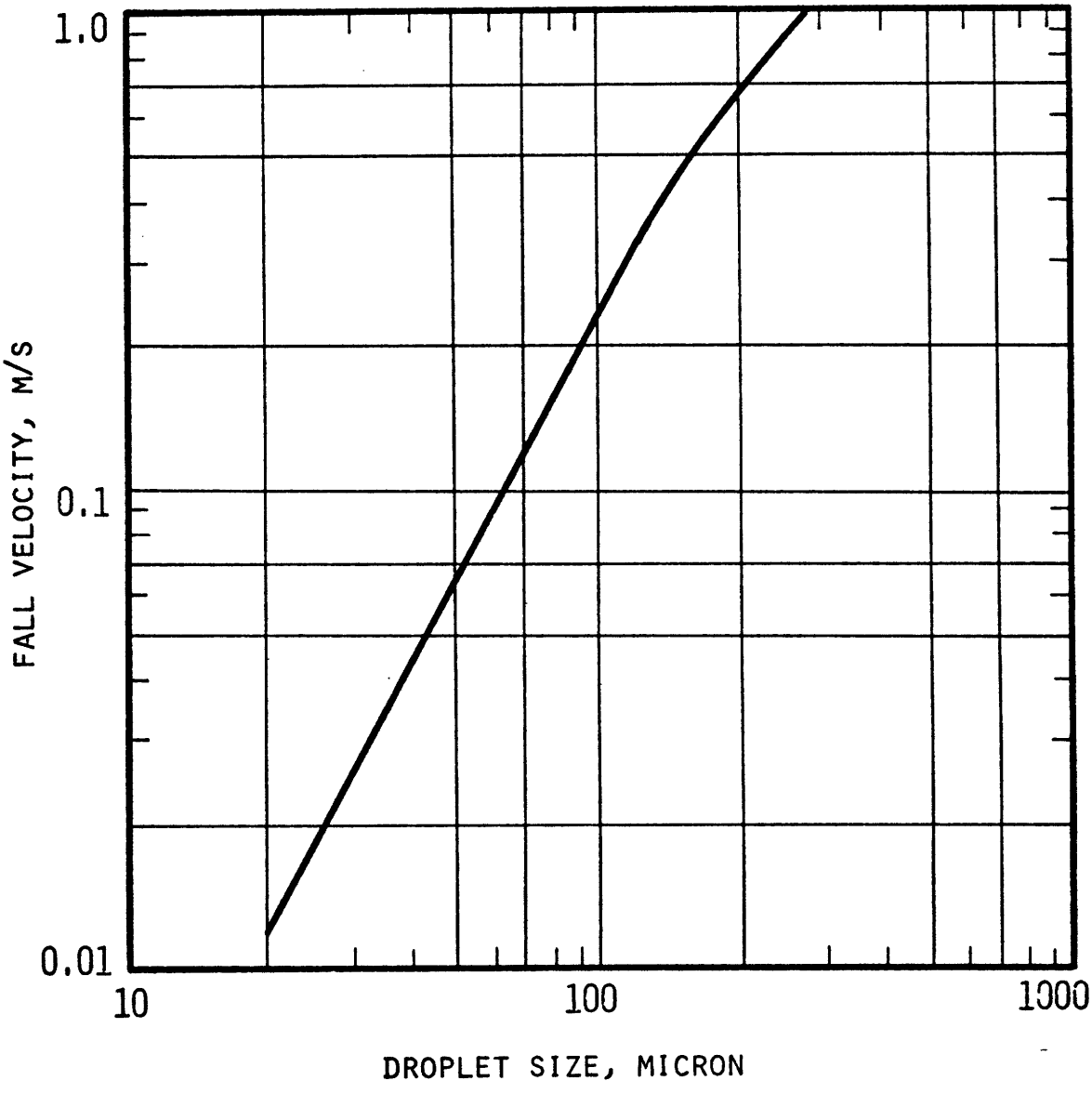

Fig. 6.1.1 Terminal Velocities of Water Droplets

drift chemical concentrations.

(3) Turbulence effects

In the theoretical calculation of the performance of a drift eliminator, it is assumed that the air flow is laminar, and that the turbulent wake region is neglected. However, for some eliminator geometries, this wake region extends over a large portion of the eliminator cross section. In this work, flow visualization is performed for three eliminators: the Belgian wave eliminator, the Hi-V eliminator, and the Zig-Zag eliminator. The flow is established in a long, two foot wide free surface flume. The working fluid is water, instead of air. The water depth is about three inches and the water flow velocity was adjusted to be about 0.1 m/s so that the Reynolds number matches that of a flow of air whose velocity is 1.5 m/s. Blue dye was injected at the eliminator entrance and at the middle of the water depth to get away from the free-surface and boundary layer regions, each of which is about half an inch thick. The dye was injected at the eliminator boundaries so that wake regions could be observed. Photographs were taken of these dye traces for the three eliminators. To observe the general flow pattern within these eliminators, tiny paper chips were sprinkled on to the water surface and time-exposure pictures recorded the trajectories of these chips. The results of these simple experiments were

quite satisfactory.

Figure 6.1.2 displays the wake regions in the Belgian wave eliminator by injecting dye into the flow. The water enters at the right side of the picture where the dye injection tubes are shown. It can be seen that a significant wake region exists at the lower boundary and another wake region exists in the second half of the upper boundary. Fig. 6.1.3 shows the flow pattern by using paper chips. The water enters at the right side of the picture where the dye injection tubes are shown. This picture also shows the wake region at the central portion of the lower boundary where recirculation occurs. The calculated velocity distribution using no-slip boundary conditions shown in Fig. 3.2.5b simulates these regions with almost stagnant regions. These regions are poorly represented if free-slip boundary conditions are used (see Fig. 3.2.5a).

Similar observations can be made for the Hi-V eliminator. Figs. 6.1.4 and 6.1.5 show the wake regions and flow pattern respectively. Again,the wake regions exist at the lower boundary and the second half of the upper boundary. These wake regions are larger than those in the Belgian wave eliminator. In the calculation these regions are represented by stagnant regions if no-slip boundary conditions are used, as shown in Fig. 3.2.6b. Again, the free-slip result cannot account for these regions very well.

Figures 6.1.6 and 6.1.7 show the same set of pictures

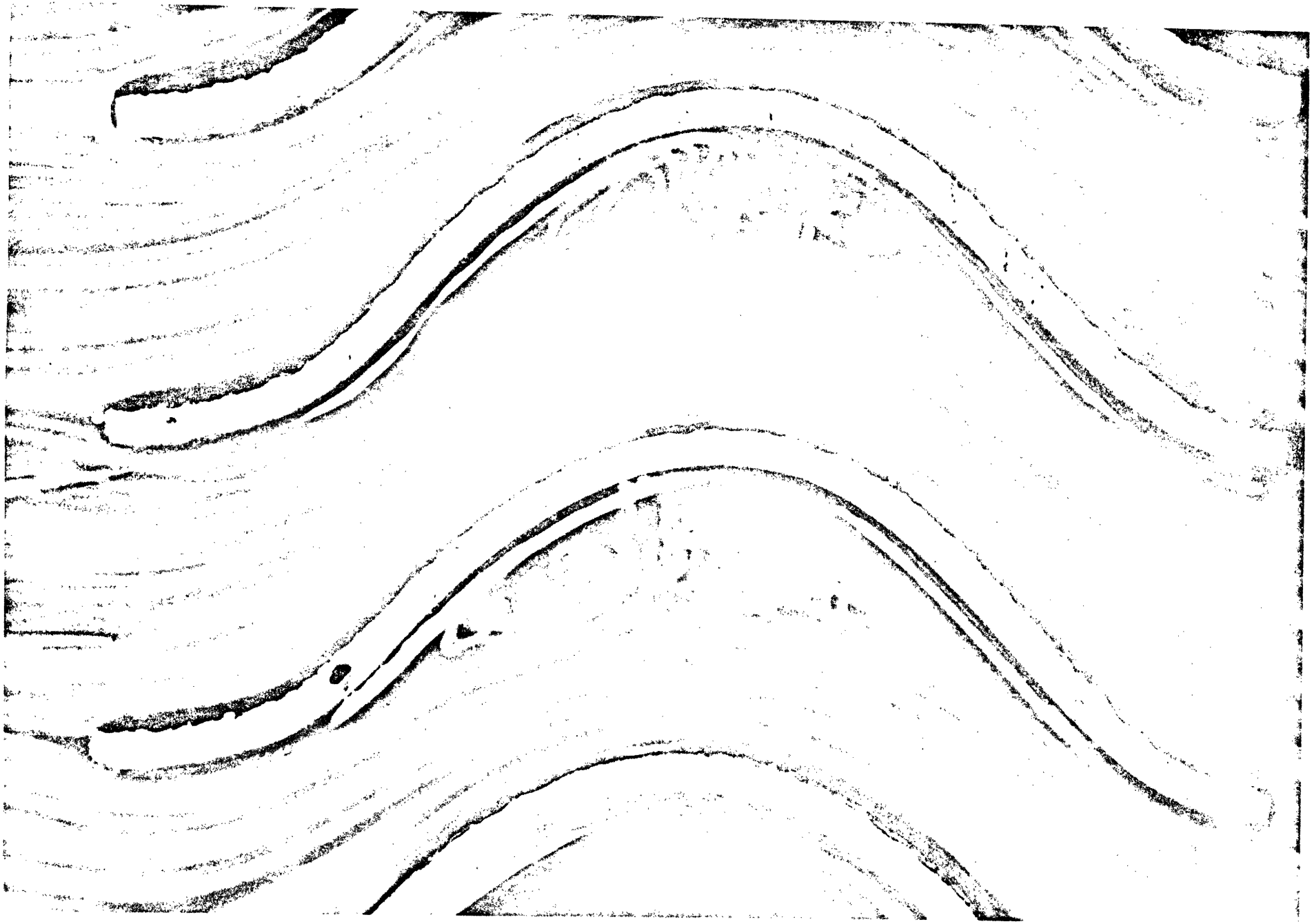

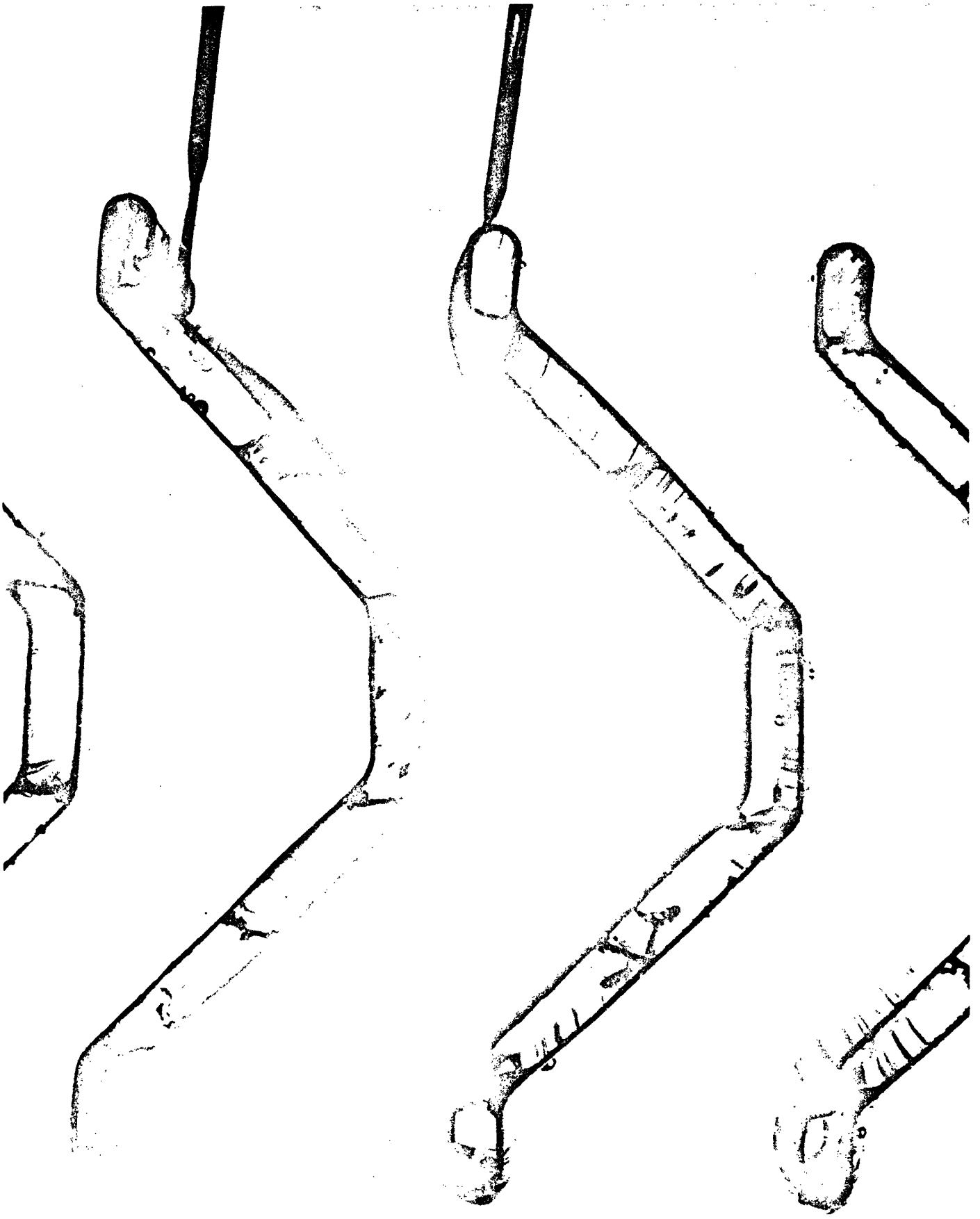

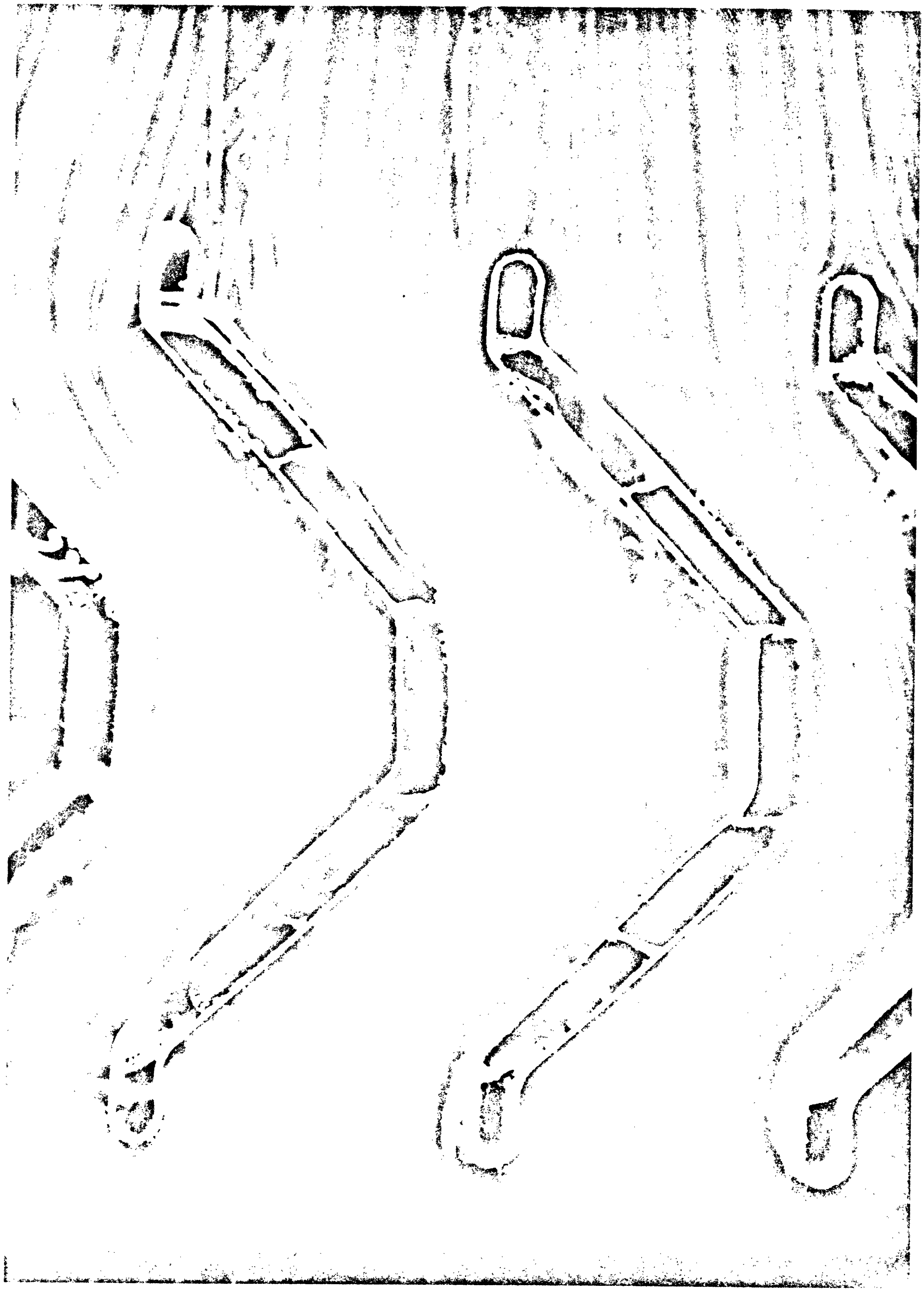

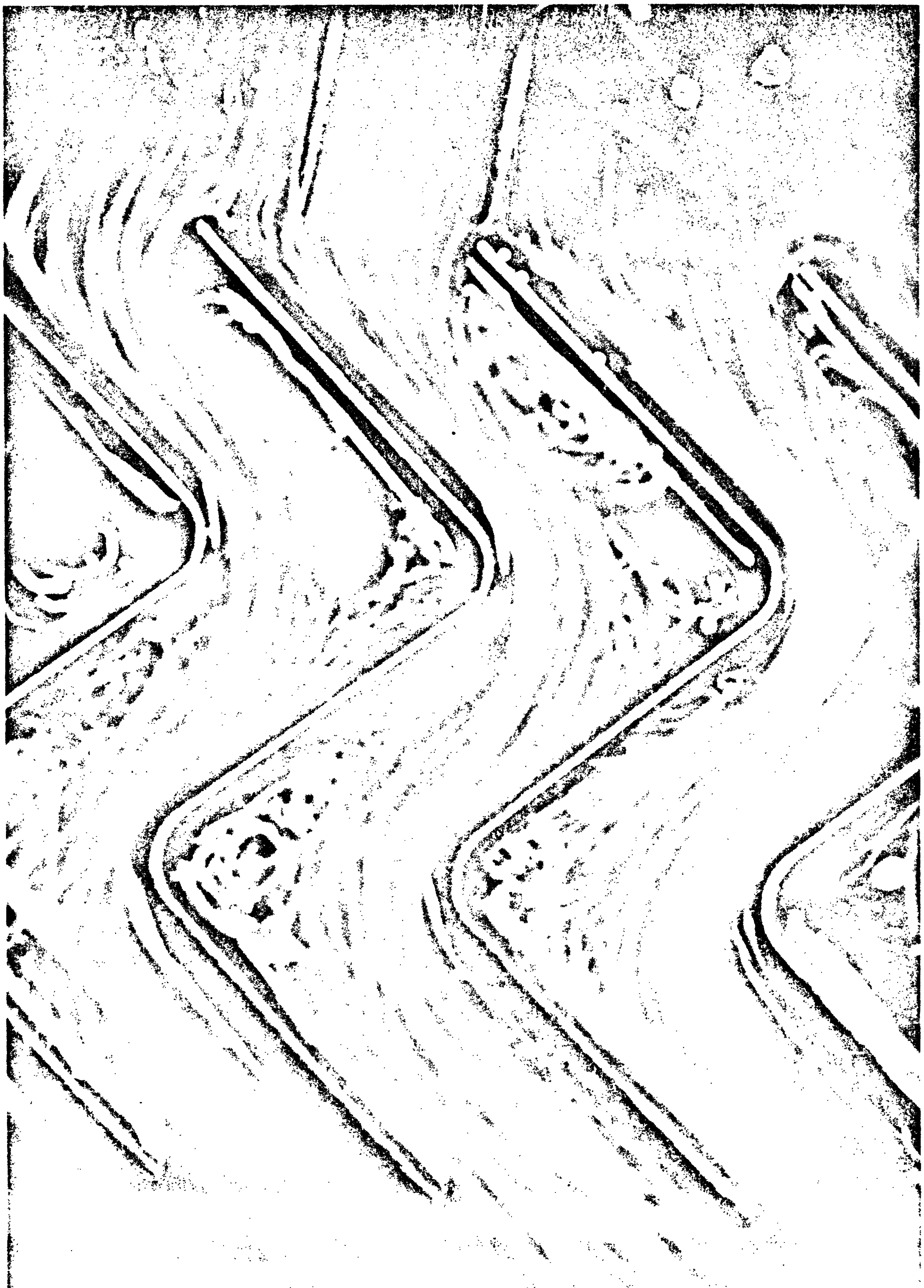

for the Zig-Zag eliminator. It is seen that the wake regions are very large for this eliminator. In fact, the third layer of this eliminator is so turbulent that the dye is well-mixed. Since the flow is so turbulent in this layer, the pressure drop in this layer will be greater than the pressure drop in either of the other two layers. As discussed in Chapter 3 the third layer has little effect on the capture efficiency of this eliminator, and by taking off this layer great savings can be realized in cooling tower operation without producing additional drift.

The calculated velocity distributions using either no-slip or free-slip boundary conditions, as shown in Figs. 3.2.7 and 3.2.8, cannot account for these turbulent wake regions. However, the no-slip prediction gives a better approximation than the free-slip prediction, and the no-slip results predict the flow pattern quite well in the first two layers where most droplets are captured. Therefore, the collection efficiency calculated using these results should be close to the actual result.

For this eliminator it can also be seen that at the entrance of the upper boundary there is flow diversion. This is caused by a pressure difference above and below the eliminator boundary. It is expected that this would not affect the collection efficiency of the eliminator but would certainly increase the pressure drop, and thus it is not desirable. In order to avoid this flow diversion, the eliminator walls at

the entrance should be more parallel to the inlet flow.

From these flow visualization photographs it is concluded that turbulent wake and eddy regions occur in all the eliminators investigated. These effects are especially significant in complex geometries. In the calculations, the turbulence effects are not accounted for and the wakes are not completely resolved. In order to achieve an exact solution, the mesh size should be reduced enough so that recirculating eddies can be fully resolved, and a turbulence model must be included in the equations. However, in view of the success of the present calculation for predicting the experimentally observed behavior of the drift eliminators, it was decided that this more expensive and complicated approach would not be required. The reason for the success of present approximation is that by using no-slip boundary conditions, the calculated velocity distributions represent the actual flow patterns quite well as observed by comparing the flow pattern photographs in this section with the velocity distribution plots in Chapter 3. Although the eddy and turbulent wake regions are not exactly described in the calculated velocity distribution, these regions are approximated by stagnant regions. Moreover, the water droplets seldom travel into these regions as seen in the droplet trajectory plots displayed in Section 3.3. Therefore, using this approach, the collection efficiency can be fairly accurately calculated. However, the pressure drop depends greatly on the existence

of turbulence, and thus it cannot be accurately predicted by these calculations if significant turbulence occurs in the eliminator. For smooth geometries the predictions agree quite well with measurements, but for complicated geometries (such as the Zig-Zag eliminator), the calculation predicts a much smaller pressure drop than the measurement.

Another factor that the calculation does not take into account is the air turbulence inside cooling towers. In order to solve this problem, it is necessary to have a turbulence code to calculate the air velocity distribution inside eliminators, and also to have quantitative information about the nature of air turbulence inside cooling towers. However, this quantitative information is not well known. Martin and Barbar (M3) have indicated the possible variations in the velocity of air approaching an eliminator, but it is also important to know the frequency with which this variation occurs. Some idea of the variation in flow direction was obtained using an ammonium chloride smoke generator (F3). It was suggested that the variation was sensitive to the ambient wind conditions, fluctuating approximately 10° about the vertical with a one second period when the wind was gusting strongly, and remaining steady when the ambient conditions were calm. However, these observations were made close to the tower center, and larger variations would be expected towards its perimeter. The positioning of towers relative to other constructions might also be an important factor in this respect.

The following conclusions are made in this study:

(1) The calculational method can accurately predict the collection efficiencies of cooling tower drift eliminators.

(2) The pressure drop calculations are reasonably good for smooth eliminator geometries. For eliminator geometries with sharp corners the calculation predicts much smaller pressure drops than the actual values.

(3) The design of the Zig-Zag eliminator is economically unsound. The third layer of this eliminator should be removed. By doing this, the drift collection efficiency will not be significantly affected, yet an appreciable savings from the reduced pressure drop will be obtained.

(4) The E-E eliminator designed by Yao and Schrock collects droplets very efficiently as predicted by the designers, yet the pressure drop is much higher due to the occurrence of flow separation. Therefore, this eliminator does not appear as promising as its collection efficiency shows.

(5) In order to achieve a high drift collection efficiency the drift eliminator geometry should be as complex as possible. However, the pressure drop will also increase as the geometry becomes more complex. It is found that an eliminator yielding a higher collection

efficiency will always have a higher pressure drop. Table 6.1.1 demonstrates this point. The table shows the calculated collection efficiency (using no-slip boundary conditions) for some common drift eliminators at an air speed of 1.5 m/s. The values of pressure drop presented in the table are either experimental results, where available, or calculated results. The calculated pressure drop results for complicated geometries with sharp corners might not be reliable. This table shows that more complex geometries have better collection efficiencies yet higher pressure drops.

Up to now, there is no available technique for designing drift eliminators that optimizes between the collection efficiency and the pressure drop. It is therefore suggested that in designing a drift eliminator for a particular cooling tower, a pressure drop limit across the eliminator that can be tolerated should be set first. Then an eliminator geometry should be chosen that has a pressure drop lower than the set limit, yet has the best collection efficiency. This can be done theoretically with the DRIFT code. After selecting the eliminator geometry in this way, it should be constructed and tested in an experimental facility to check that the overall drift emission is lower than the environmental standard set by the Environmental Protection Agency. This approach will

Table 6.1.1

Pressure Drop and Calculated Collection Efficiency Results of Some Drift Eliminators at an Air Speed of 1.5 m/s

	Calculated Collection Efficiency							
Droplet Diameter (μm)	Single Layer (S1)*	Double Layer (D2)	Sinus (N2)	Asbestos Cement (A1)	Hi-V (H1)	E-E (E1)	Zig-Zag (Z1)	Zig-Zag (two layer)
20						0.090		
30	0.115	0.130	0.130	0.070	0.460	0.215	0.540	0.485
40	0.170	0.145	0.155	0.135	0.635	0.675	0.725	0.635
50	0.235	0.155	0.185	0.265	0.895	1.0	0.920	0.910
60	0.330	0.185	0.240	0.485	0.945		1.0	1.0
70	0.400	0.220	0.580	0.710	1.0			
80	0.470	0.260	0.775	0.855				
90	0.525	0.410	0.885	0.945				
100	0.565	0.515	1.0	1.0				
$\Delta P/\frac{1}{2}\rho V^2$	2.35	0.97	3.01**	3.91	4.54**	14.61	7.31**	1.37

* Case number as identified in Table 3.1.1

** Experimental Results

certainly save a lot of unnecessary effort and money while a better eliminator is designed.

6.2 Recommendations

The results from the DRIFT code in this paper suggest that this code is very useful in the evaluation and design of cooling tower drift eliminators. The following future work on this numerical technique is recommended:

(1) It has been shown that the air velocity distribution inside an eliminator calculated by the SOLASUR subroutine using no-slip boundary conditions approximates the actual flow pattern quite well. In order to further validate this calculation, a spatial measurement of the air velocity distribution inside the eliminator would be appropriate. There are many such measurement techniques; a suitable one would be the Laser Doppler Anemometer (LDA) technique which is commercially available. Fig. 6.2.1 shows a recommended test section for this purpose and for the droplet dynamics experiments which are described later. The LDA technique will not only measure the velocity values but also the turbulent flow parameters. These will be very useful for investigating the eliminator performance.

(2) The droplet trajectory calculation performed by the

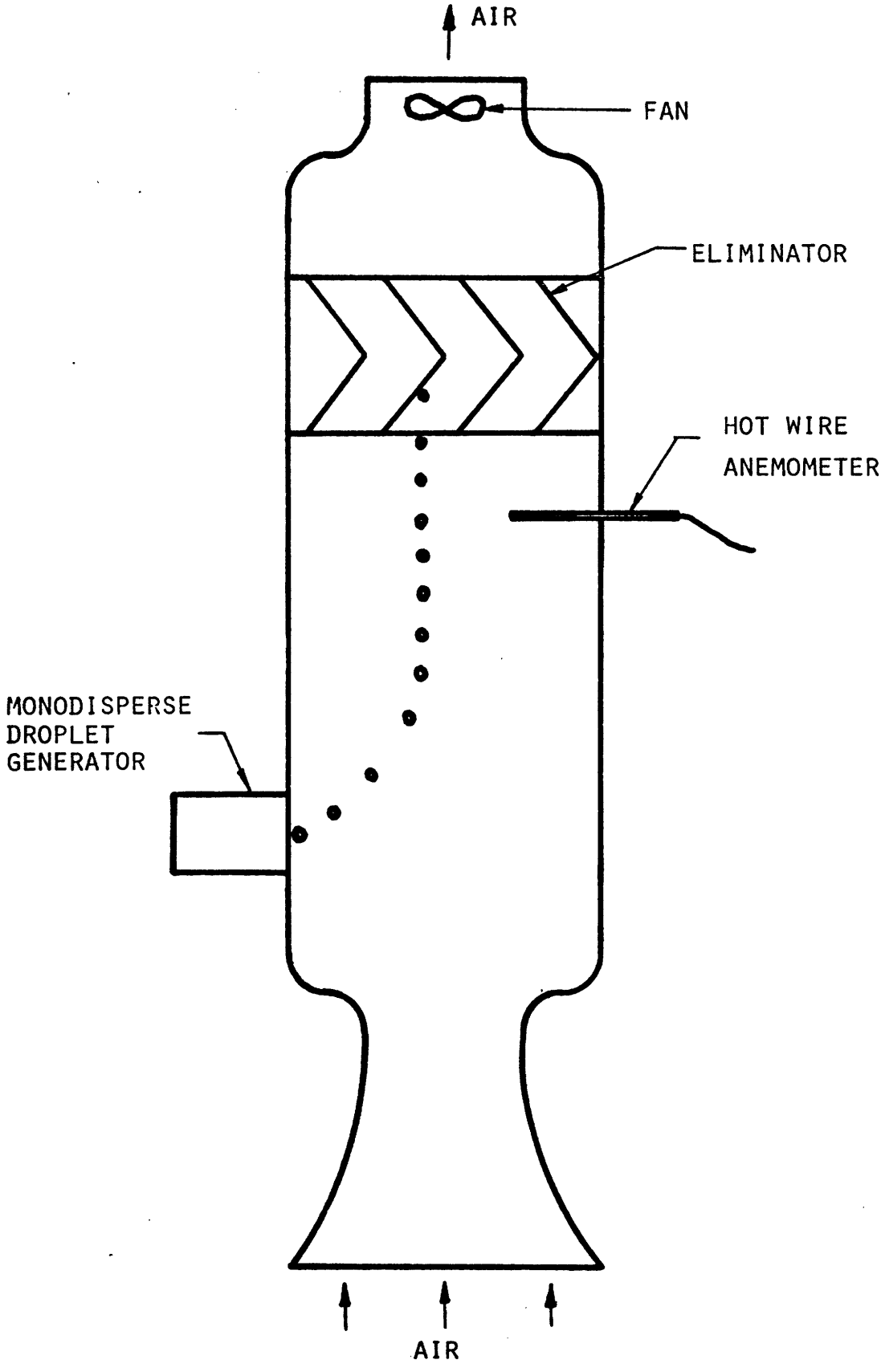

Fig. 6.2.1 Schematic Diagram of the Proposed Experimental Setup for Studying Droplet Trajectory and Air Velocity Distribution in Drift Eliminators

DRIFT code can be checked by a simple experiment. The suggested experimental setup is shown in Fig. 6.2.1. A small exhaust fan will induce the required air flow. Drift eliminators are installed in a test section that consists of plexiglass walls and a flow channel that is several inches thick. The nominal air speed can be measured by hot wire anemometer at the inlet region of the eliminator. Colored water droplets generated by a monodisperse droplet generator are introduced below the eliminator . Their trajectories can be observed with a high-speed cine camera. These trajectories can be compared with calculated results. This experiment can also study the droplet rebounding effect at the walls. Water film effects can also be studied by introducing a water film at the eliminator walls. Since the test section is small, it can be placed either horizontally or vertically. As mentioned in (1), the air velocity distribution inside the eliminator can also be measured by an LDA technique with the eliminators installed in this test section. This basic experiment could validate the present calculation as well as provide improvements to the code concerning the droplet rebounding and water film effects.

For the design of drift eliminators, the following recommendations are made:

(1) It is found from the present calculation that the third layer of the Zig-Zag eliminator serves no purpose in capturing drift droplets, and thus should be removed to reduce the pressure drop across the eliminator. Also, to avoid flow diversion at the eliminator entrance, the boundaries should be reshaped so that they are parallel to the flow. An experimental test of the performance of the Zig-Zag eliminator with only two layers and a smoothed entrance is recommended.

(2) The performances of many common drift eliminator geometries have been evaluated in this work either by numerical simulation or experiments. However, there are still many other eliminator designs that have been used commercially, and some potential designs that are worth investigating. These include the Chevron-type eliminator used by French cooling tower vendors, a helical flow channel design with smooth inlet and outlet nozzles, a "polisher" eliminator design, and many others.

(3) Total drift emission is the most important parameter of the environmental acceptance of cooling tower drift. Therefore, after selecting a particular eliminator design, it is necessary to test the

design for its total drift emission. However, none of the available drift measurement techniques has been proven to be generally satisfactory--to the point of being adopted for general use (A1). A reliable technique for drift emission measurement is needed.

It is proposed that future work should be performed to demonstrate the feasibility of using a radioactive tracer for absolute drift rate measurements. The suggested candidate tracer is Na^{24} ($T_{\frac{1}{2}}$ = 15 hr.; Eγ's = 2.75 Mev and 1.37 Mev) which can be produced from irradiating stable Na^{23} (in NaOH form) in a nuclear reactor. After irradiation, the activated solution will be neutralized with HCl, and injected into the recirculating water flow in the experimental drift facility. Because the air flow in the wind tunnel is recirculated and rapidly becomes saturated, it is expected that droplet evaporation will be negligible. Thus, the salt concentration in the entrained droplets should be the same as in the recirculating water, making possible a direct comparison of drift rates measured by drop-size spectra methods, and by deducing the total salt current using the radioactive tracer. This point has been a problem in the past in intercomparisons between various drift measurement methods -

those methods which observe total salt flow rate (e.g., isokinetic samplers, cyclone samplers, etc.) do not provide a measure of the droplet spectra, and those methods which observe the droplet spectra (e.g., the PILLS system, sensitive paper sampling) do not provide information regarding the total salt current without some assumption being made regarding the salt concentration in the droplets due to evaporation or growth. This is difficult to provide since evaporation and growth rates vary with droplet sizes.

In the test the salt current will be sampled with an array of NaI detectors that scans a transverse section of the experimental drift facility so that the total amount of radiation observed will be directly proportional to the amount of salt that flows past the measurement station.

For a reasonably accurate (2%) experiment it is estimated that the laboratory demonstration will require approximately 10 mCi of activity injected into the recirculating water. For a field test roughly 10 Ci of activity would be required, depending upon the desired accuracy and the extent of the NaI detector array. It is envisioned that this measurement technique would be used sparingly for absolute drift measurements,and that less accurate

methods would be sufficient for routine drift monitoring. In field applications the total amounts of released activity would be no greater than those currently encountered on a chronic basis with boiling water reactors.

In conclusion, the DRIFT code is quite capable of predicting the performance of cooling tower drift eliminators, although some care should be taken in the pressure drop calculations for complex (sharp-cornered) eliminator geometries. This code should be very useful in evaluating drift eliminator performance to aid in the design of drift eliminators for any cooling tower. Provisions for the effect of water film on the eliminator walls, of flow turbulence within the eliminator, and of droplets rebounding from the eliminator walls should be investigated and developed to supplement the DRIFT code.

REFERENCES

A1 "Cooling Tower Plume Modeling and Drift Measurement - A Review of the State-of-the-Art", Sponsored by the Research Committee on Atmospheric Emissions and Plum Behavior from Cooling Towers, ASME, New York, 1975.

B1 Berglund, R.N., and Liu, B.T.H., "Generation of Monodisperse Aerosol Standards," Env. Sci. & Tech., 7, 1973, pp. 147-153.

B2 Bevington, P.R., Data Reduction and Error Analysis in the Physical Sciences, McGraw-Hill Book Company, New York, 1969.

C1 Carnahan, B., Luther, H.A., and Wilkes, J.O., Applied Numerical Method, John Wiley & Sons, Inc., 1969, pp. 363-365.

C2 Campbell, J.C., "A Review of CTI Work on the Measurement of Cooling Tower Drift Loss," TP68A, Cooling Tower Inst., Houston, Texas, 1969.

C3 Chan, J. and Golay, M.W., "Numerical Simulation of Cooling Tower Drift Eliminator Performance," Numerical/Laboratory Computer Methods in Fluid Mechanics, presented at the ASME Annual Winter Meeting, edited by A.A. Pouring and U.L. Shah, ASME, New York, Dec., 1976, pp. 229.

C4 Chilton, H., "Elimination of Carryover from Packed Towers with Special Reference of Natural Draught Water Cooling Towers," Trans. Am. Inst. Chem. Engr., Vol. 30, 1952, pp. 235-250.

C5 Chan, J., and Golay, M.W., "DRIFT-A Numerical Simulation Solution of Cooling Tower Drift Eliminator Performance," MIT Energy Laboratory Report No. MITEL, April,1977.

D1 Dickey, J.B., and Cate, R.E., "Managing Waste Heat with the Water Cooling Tower," The Marley Company, Mission, Kansas, 1970.

D2 Dave, J.V., "Subroutines for Computing the Parameters of the Electromagnetic Radiation Scattered by a Sphere," Report No. 320-3237, IBM Scientific Center, Palo Alto, Calif., May, 1968.

D3 Dave, J.V., "Scattering of Visible Light by Large Water Spheres," Applied Optics, Vol. 8, No.1, January 1969, pp. 155-164.

D4 "Instruction Manual. 1173/1174 Electronic Manometer," Datametrics, Wilmington, Mass.

F1 Fish, B.R., and Duncan, J.R., "Measurement of Liquid Droplet Emissions from Cooling Towers and Process Stacks," Paper No. 72-35 presented at the 65th Annual Meeting of the Air Pollution Control Association, Miami Beach, Florida, June 18-22, 1972.

F2 Foster, P.M., Personal Correspondence, Central Electricity Research Laboratories, Surrey, England, March 17, 1976.

F3 Foster, P.M., Williams, M.I. and Winter, F.T., "Droplet Behavior and Collection by Counterflow Cooling Tower Eliminators," Atmospheric Environment, Vol. 8, No. 4, April 1974, pp. 349-360.

F4 Forsythe, G., and Moler, C.B., Computer Solution of Linear Algebraic Systems, Prentice-Hall, Inc., Englewood Cliffs, N.J., 1967, Chapter 9.

F5 Foster, P.M., Personal Correspondence, Central Electricity Research Laboratories, Surrey, England, February 22, 1977.

G1 Gardner, B.R., and Lowe, H.J., "The Research and Development Background to the Environmental Problems of Natural Draught Cooling Towers," Atmospheric Environment, Vol. 8, No. 4, April 1974, pp. 313-320.

G2 Golay, M.W., "Progress Report - Drift Elimination Project," Jan. 1, 1976, Waste Heat Management Program, MIT Energy Lab., Cambridge, Mass.

G3 Golay, M.W., "Progress Report - Drift Elimination Project," July 1, 1976, Waste Heat Management Program, MIT Energy Lab., Cambridge, Mass.

G4 Golay, M.W., "Progress Report - Drift Elimination Project," Jan. 1, 1977, Waste Heat Management Program, MIT Energy Lab., Cambridge, Mass.

G5 Grolme, M.A., Lambert, G.A., and Fauske, H.K., "Flooding Correlation for Sodium and Cladding Motion in Subassembly Voiding," Trans. Am. Nucl. Soc., Vol. 18, 1974, pp. 209.

H1 Harlow, F.H., and Welch, J.E., "Numerical Calculation of Time-Dependent Viscous Incompressible Flow," Phys. Fluids, Vol. 8, 1965, pp. 2182.

H2 Hirt, C.W., Nichols, B.D., and Romero, N.C., "SOLA - A Numerical Solution Algorithm for Transient Fluid Flows," LA-5832, 1974, Los Alamos Scientific Lab.

H3 Holmberg, J.D., "Drift Management in the Chalk Point Cooling Tower," The Marley Company, Mission, Kansas.

H4 Holmberg, J.D., and Kinney, O.L., "Drift Technology for Cooling Towers," 1973, The Marley Company, Mission, Kansas.

H5 Hosler, C.L., Pena, J., and Pena, R., "Determination of Salt Deposition Rates from Drift from Evaporative Cooling Towers," Journal of Engineering for Power, July, 1974, pp. 283-291.

H6 Holmberg, J.D., Personal Communication, The Marley Company, Mission, Kansas, Jan., 1977.

I1 Ishii, M. and Grolmes, M.A., "Inception Criteria for Droplet Entrainment in Two-Phase Con-current Film Flow," AIChE Journal, Vol. 21, No. 2, 1975, pp. 308-318.

I2 "IMSL Library 1, Edition 4 (FORTRAN IV), S/370-360", International Mathematics and Statistical Libraries, Inc., Houston, Texas, 1975, Vol. II.

J1 Jallouk, P.A., Kidd, G.J., Jr., and Shapiro, T., "Environmental Aspects of Cooling Tower Operation: Survey of Emission, Transport, and Deposition of Drift from the K-31 and K-33 Cooling Towers at ORGDP," K-1859, Oak Ridge Gaseous Diffusion Plant, Oak Ridge, Tenn., 1974.

J2 Jayaratne, O.W., and Mason, B.J., "The Coalescence and Bouncing of Water Drops at an Air/Water Interface," Proc. R. Soc. A , 280, 1964, pp. 545-565.

K1 Knollenberg, R.G., "The Optical Array: An Alternative to Scattering or Extinction for Airborne Particle Size Determination," J. Appl. Meteor., 9, 1970, pp. 86-103.

L1 LeFevre, M., Personal Correspondence, Research Cottrell, Inc.

L2 Lieblein, S., and Roudebush, W., "Theoretical Loss Relations for Low-Speed Two-Dimensional-Cascade Flow," NACA, TN3662, 1956.

L3 Lyerly, R.L., et al., "An Evaluation of the Feasibility of Salt Water Cooling Towers for Turkey Point," Southern Nuclear Engineering, Inc., Report SNE-54 for Florida Power and Light Co., Miami, Feb., 1970.

L4 Levenberg, K., "A Method for the Solution of Certain Non-Linear Problems in Least Squares," Quarterly of Applied Mathematics, Vol. 2, No. 2, 1944, pp. 164-168.

M1 Margetts, M.J., and Shofner, F.M., "Characterization of the Drift Emissions of a Natural Draft Cooling Tower and Examination of Sensitivity to Operational Parameter Variations," presented at the Joint Power Generation Conference, ASME, IEEE, ASCE, New Orleans, Louisiana, Sept. 16-19, 1973.

M2 "Cooling Tower Fundamentals and Application Principles," The Marley Company, Mission, Kansas.

M3 Martin, A., and Barber, F.R., "Some Water Droplet Measurements Inside Cooling Towers," Atmospheric Environment, Vol. 8, No. 4, April 1974, pp. 325-336.

M4 Mason, B.J., The Physics of Clouds, Oxford University Press, Oxford, 1957.

M5 Mie, G., Ann. der Physik., Vol. 25, 1908, pp. 377-445.

M6 Marguardt, D.W., "An Algorithm for Least-Squares Estimation of Nonlinear Parameters," Journal of the Society for Industrial and Applied Mathematics, Vol. 11, No. 2, June 1963, pp. 431-441.

R1 Reisman, J.I., and Ovard, J.C., "Cooling Towers and the Environment - An Overview," presented at the American Power Conference 35th Annual Meeting, Chicago, Illinois, May 1973.

R2 Roffman, A., "Drift Loss from Saltwater Cooling Towers - Some Atmospheric Considerations," Amer. Geophysical Union, 54th Annual Meeting, Washington, D.C., April 16-20, 1973.

R3 Roffman, A., et al., "The State of the Art of Saltwater Cooling Tower for Steam Electric Generating Plants," WASH-1244, Feb. 1973, U.S. Atomic Energy Commission, pp. E.1-E.21.

R4 Roffman, A., and VanVleck, L.D., "The State-of-the Art of Measuring and Predicting Cooling Tower Drift and Its Deposition," Paper No. 73-140, presented at the 66th Air Pollution Control Assoc. Annual Meeting, Chicago, Illinois, 1973.

S1 Schrecker, G.O., Wilber, K.R., Shofner, F.M., "Prediction and Measurement of Airborne Particulate Concentrations from Cooling Device Sources and in the Ambient Atmosphere," presented at the 'Cooling Tower Environment-1974' Symposium, March 4-6, 1974.

S2 Shofner, F.M., "Explicit Calibration of the PILLS II System," EPA Project No. 16130GNK, Environmental Protection Agency, Sept. 1973.

S3 Shofner, F.M., Schrecker, G.O., Carlson, T.B., and Webb, R.O., "Measurement and Interpretation of Drift Particle Characteristics," presented at the 'Cooling Tower Environment-1974' Symposium, March 4-6, 1974.

S4 Shofner, F.M., and Thomas, C.O., "Development and Demonstration of Low-Level Drift Instrumentation," Environmental Protection Agency Report No. 16131GNK, Oct. 1971.

S5 Shofner, F.M., and Thomas, C.O., "Drift Measurement in Cooling Towers," Cooling Tower, AIChE, New York, N.Y., 1971.

S6 Shofner, F.M., Thomas, C.O., Schrecker, G.O., Lyon, C.R., Carlson, T.B., and Bishop, A.O., "Measurement of the Drift and Plume Characteristics of PEPCO's Chalk Point Unit #3 Cooling Tower, Phase One: Experimental Design," Final Report submitted to Maryland Department of Natural Resources, Baltimore, Maryland, August, 1973.

S7 Shofner, F.M., Watanabe, Y., and Carlson, T.B., "Design Considerations for Particulate Instrumentation by Laser Light Scattering (PILLS) Systems," ISA Transactions 12, 1973, pp. 56-61.

S8 "SPRACO Spray Nozzles and Industrial Finishing Equipment," Catalog 73, Spray Engineering Company, Burlington, Mass.

S9 Stewart, Paul B., Personal Communication, Ceramic Cooling Tower Company, Fort Worth, Texas, Jan. 20, 1977.

T1 Thermo-Systems, Inc., The Model 3050 Berglund-Liu Monodisperse Aerosol Generator, Minneapolis, Minnesota, 1974.

T2 Thomas, C.O., and Shofner, F.M., "Cooling Tower Monitoring Systems for Electrical Power Generating Plants," presented at the Midwest Power Symposium in Cincinnati, Ohio, Oct. 22-23, 1973.

T3 Thompson, B.J., and Ward, J.H., "Particle Sizing- The First Direct Use of Holography," Sci. Res., 1, 1966, pp. 37-40.

T4 Thompson, B.J., Parrent, G.B., Ward, J.H., and Justi, B., "A Readout Technique for the Laser Fog Disdrometer," J. of Appl. Meteor., 5, 1966, pp. 343-348.

T5 Thwaites, B., "Approximate Calculation of the Laminar Boundary Layer," Aeronautical Quarterly, Vol. 1, 1949, pp. 245-280.

V1 Van de Hulst, H.C., Light Scattering by Small Particles, Wiley, New York, 1957.

W1 Welch, J.E., Harlow, F.H., Shannon, J.P., and Daly, B.J., "The MAC Method. A Computing Technique for Solving Viscous , Incompressible, Transient Fluid Flow Problems Involving Free Surfaces," LA-3425, March 1966, Los Alamos Scientific Lab.

W2 Wistrom, G.K., and Ovard, J.C., "Cooling Tower Drift, Its Measurement, Control and Environmental Effects," presented at the Cooling Tower Institute Annual Meeting, Houston, Texas, Jan. 1973.

Y1 Yao, S.C., "Investigations on Falling Drop Heat-Mass Transfer and Drift Elimination in Wet Cooling Towers," PhD thesis, University of California, Berkeley, 1974.

Y2 Yao, S.C. and Schrock, V.E., "Aerodynamic Design of Cooling Tower Drift Eliminators," Amer. Soc. Mech. Engrs., Paper No. 75-WA/Pwr-5, Aug. 1975.

APPENDICES

APPENDIX A
DATANA PROGRAM

A.1 Introduction

In the drift measurements by laser light scattering the voltage distribution, $\underline{M}(v)$, recorded by the multichannel analyzer is not the true droplet size distribution, $\underline{P}(d)$, as mentioned in Chapter 4. However, these two distributions can be related by

$$\underline{M}(v) = \underline{\underline{R}}(v;d)\ \underline{P}(d) \quad , \qquad (4.4.1)$$

where $\underline{\underline{R}}(v;d)$ is the voltage response matrix to droplets of diameter d.

In order to recover $\underline{P}(d)$ from the measured distribution $\underline{M}(v)$ in Eq. 4.4.1, a system of linear algebraic equations must be solved. The DATANA program transforms the measured spectra at the inlet and outlet sections of the eliminator to the true droplet size spectra so that the collection efficiency as a function of droplet size can be determined.

This appendix describes this program in detail. The necessary input parameters are described in Section B.3. A listing of the program and a sample problem are also given.

A.2 Description of the Program

The DATANA computer code is written in FORTRAN IV and analyzes the measured voltage pulse height distribution. This

distribution represents the scattered light intensity distribution produced when a spectrum of droplets passes through the scattering volume.

The procedures of the code are listed in the flow chart in Fig. A.2.1. The calibration parameters determined from a calibration check of the drift measuring instrument are used by the program to determine the calibration factors and response function. To transform a voltage pulse height distribution into a droplet size distribution, the measured distribution is first smoothed by a least-squares fitting in the LSMARQ subroutine. This subroutine can use any appropriate fitting function that is supplied by the user through the external function YFCN. It is found that a polynomial of the form

$$f(x) = \sum_{i=1}^{8} \frac{a_i}{x^{i-1}} \qquad (A.2.1)$$

provides the best fit of the typical measured distributions. Guessed values of the parameters a_i are input by user, and best fit values of a_i are calculated by the subroutine. The transformation of the measured distribution to the droplet size distribution is performed either by backward substitution method, if the response function is an upper triangular matrix, or otherwise by the LEQT1F subroutine, which obtains a solution of a system of linear equations. The backward substitution method is the simpler approach and takes less computation time. Collection efficiencies as a function of

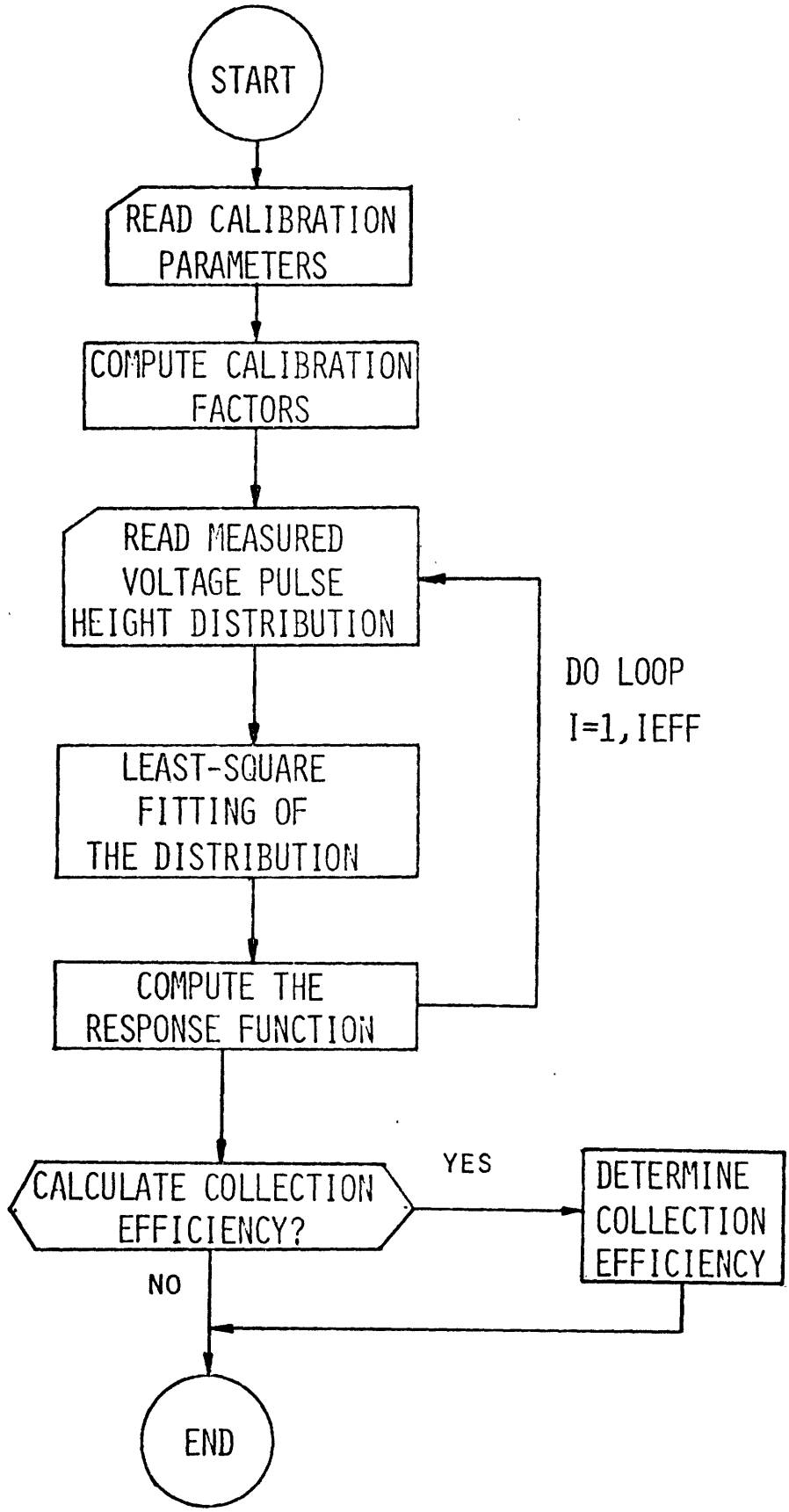

Fig. A.2.1 Flow Chart of the DATANA Code

droplet size can be determined when two measured distributions, one at the inlet and one at the outlet of the eliminator, are provided.

The DATANA code uses several subroutines. They are described below.

(A) LSMARQ

The subprogram LSMARQ computes the solutions of non-linear least-squares curve and surface-fitting problems. That is, LSMARQ finds values of $b_1, b_2, \ldots, b_p$, which minimizes

$$\sum_{i=1}^{n} w_i(y_i - f(x_{i,1}, x_{i,2}, \ldots, x_{i,m}; b_1, b_2, \ldots, b_p)), \quad (A.2.2)$$

where the fitting function f depends on $m > 1$ independent variables $(x_{i,1}, x_{i,2}, \ldots, x_{i,m})$, and on the p unknown parameters, b_j. The i^{th} dependent and independent variables, y_i and $x_{i,1}, \ldots x_{i,m}$, are known values corresponding to the i^{th} data point or observation. The number of data points is n, and the w_i are parameters that weight the errors at each data point.

LSMARQ uses the Levenberg-Marquardt algorithm described in Refs. B2, L4, and M6. It computes the coefficients of a partial Taylor series for the fitting function and then uses the steepest-descent method (or gradient method) to find a "neighborhood" in parameter-space where the series provides an adequate approximation to the data.

This subroutine is called by the main program.

(B) RSIMQ

This is a subroutine called by LSMARQ. It performs forward elimination with partial pivoting.

(C) YFCN

This is a user-supplied FUNCTION subprogram, which computes the function $f(\underline{x},\underline{b})$ of Eq. A.2.2. This external function is called from the main program, the LSMARQ, and RSIMQ subroutines.

(D) LEQT1F

This subprogram solves a set of linear equations, $\underline{\underline{A}}\underline{X}=\underline{B}$, for X, given the NxN matrix $\underline{\underline{A}}$ in full storage mode.

LEQT1F performs Gaussian elimination (Crout algorithm) with equilibration and partial pivoting (F4).

This subroutine is taken from the IMSL library (I2), and is called by the main program.

(E) LUDATF

This subroutine decomposes the N by N matrix $\underline{\underline{A}}$ into the matrices $\underline{\underline{L}}$ $\underline{\underline{U}}$, where $\underline{\underline{L}}$ is lower triangular with one's on the diagonal, and $\underline{\underline{U}}$ is upper triangular.

LUDATF is called by LEQT1F. Its algorithm is described in Ref. I2.

(F) LUELMF

LUELMF performs the elimination part of the solution of a set of simultaneous equations (I2). It is called by LEQT1F.

(G) UERTST

This subprogram prints a message reflecting any error detected by an IMSL subroutine (I2).

A.3 Description of the Input Parameters

Card No. 1

IEFF, IRT
FORMAT (2I5)

IEFF= 1 for data transformation only, no collection efficiency calculation will be performed.

IEFF= 2 for a collection efficiency calculation. In this case two spectra, one at the inlet and one at the outlet of the eliminator, should be provided.

IRT = 0 if the response function is an upper triangular matrix where the simpler transformation method can be used.

IRT ≠ 0 if the response function is not an upper triangular matrix so that the subroutine LEQT1F must be used.

Card No.2

A,B
FORMAT (2E20.6)

A and B convert the channel number to a voltage pulse

height with

voltage = A + B x Channel number.

Card No.3

NC1,NC2,NC3,DC,CC1,CC2

FORMAT (3I5,3F10.3)

These are all calibration parameters and are obtained from a calibration check of the drift measurement instrumentation. DC is the monodisperse droplet size used in the calibration, which is about 80 μm in this work. The meanings of other parameters are found in Fig.A.3.1, which is a calibration curve recorded by the multichannel analyzer for monodisperse droplets.

Card No.4

NC

FORMAT (I5)

NC is the maximum channel number of the data.

Card No. 5 and Card No. 6

(PARAM(I), I = 1, NPARAM)

FORMAT(4E20.6)

PARAM(I) are the guessed values of the least-square fitting parameters. They can be set to be 1.0, however, values closer to the true values will save a lot of computation time.

NPARAM is the number of parameters. It is 8 in the present work.

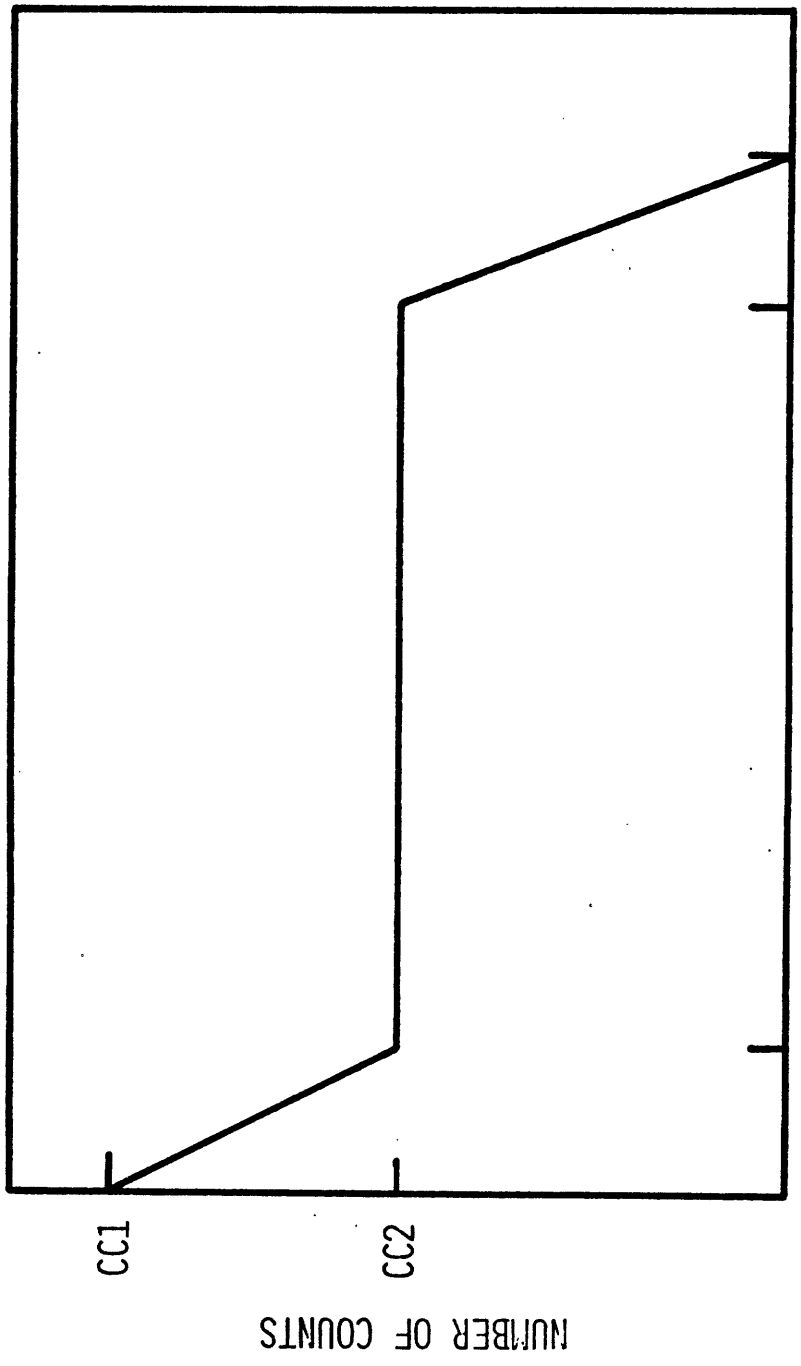

Fig. A.3.1 Approximation of the Calibration Curve

Card No. 7 to Card No. (6+NC/5)

(PV(I), I=1,NC)

FORMAT (4X,5F7.0)

PV(I) is the voltage pulse height distribution measured at the outlet of the eliminator if a collection efficiency calculation is to be performed.

If IEFF equals 2 in Card No. 1, the following insertions are made in the input deck:

Card No. 4A (If IEFF=2)

NC

FORMAT (I5)

NC = the maximum channel number for the distribution measured at the inlet of the eliminator

Card No. 5A and Card No. 6A (If IEFF=2)

(PARAM(I), I = 1, NPARAM)

FORMAT(4E20.6)

PARAM(I) are the guessed values of the least-square fitting parameters for the distribution measured at the inlet of the eliminator.

Card No. 7A to Card No. (6+NC/5)A (If IEFF=2)

(PV(I), I=1,NC)

FORMAT (4X,5F7.0)

PV(I) is the distribution measured at the inlet of the eliminator.

A.4 Listing of the DATANA Code

```
      DIMENSION D(350),PV(350),W(350),W1(350),W2(350),PV1(350)                  MAIN0001
      DIMENSION PARAM(9),W3(9,2),W4(9,9),W5(9),SCALE(9),CURV(9)                 MAIN0002
      DIMENSION EFF(350),PF(350),F(350,350)                                     MAIN0003
      EXTERNAL YFCN                                                             MAIN0004
      NIND=1                                                                    MAIN0005
      NPARAM=8                                                                  MAIN0006
    1 FORMAT(10I5)                                                              MAIN0007
    2 FORMAT(4E20.6)                                                            MAIN0008
    3 FORMAT(3I5,3F10.3)                                                        MAIN0009
    4 FORMAT(5X,5F7.0)                                                          MAIN0010
    5 FORMAT(1H1)                                                               MAIN0011
    6 FORMAT(///,5X,'MEASURED DISTRIBUTION',/)                                  MAIN0012
    7 FORMAT(///,5X,'LEAST SQUARE FITTING PARAMETERS ARE',/)                    MAIN0013
    8 FORMAT(///,5X,'FITTED DISTRIBUTION',/)                                    MAIN0014
    9 FORMAT(///,5X,'LAST CHANNEL NUMBER IS',I5)                                MAIN0015
   10 FORMAT(///,5X,'DIAMETER DISTRIBUTION',/)                                  MAIN0016
   11 FORMAT(///,5X,'TRUE SPECTRUM',/)                                          MAIN0017
   12 FORMAT(///,5X,'EFFICIENCY SPECTRUM',///,8X,'DROPLET DIAMETER(MICRO        MAIN0018
     1N)',5X,'COLLECTION EFFICIENCY',///)                                       MAIN0019
   13 FORMAT(1X,8E15.4)                                                         MAIN0020
   14 FORMAT(///,5X,'VOLTAGE DISTRIBUTION',/)                                   MAIN0021
   15 FORMAT(///,5X,'IER= ',I5)                                                 MAIN0022
   16 FORMAT(10X,E20.6,7X,E20.6)                                                MAIN0023
   17 FORMAT(1H1,///,5X,'IEFF=',                                                MAIN0024
     1     I5,/,5X,'IRT=',I5,//,5X,'A= ',F10.4,/,5X,'B= ',F10.4,//,5X,        MAIN0025
     2'NC1=',I5,/,5X,'NC2=',I5,/,5X,'NC3=',I5,/,5X,'DC= ',F10.2,/,5X,         MAIN0026
     3'CC1=',F10.4,/,5X,'CC2=',F10.4)                                           MAIN0027
C                                                                               MAIN0028
C   IEFF=2 EFFICIENCY CALCULATION IS DONE                                       MAIN0029
C   IEFF=1 NO EFFICIENCY CALCULATION IS DONE                                    MAIN0030
C   IF IRT=0, THE RESPONSE FUNCTION IS AN UPPER TRIANGULAR MATRIX               MAIN0031
C   PARAM(I) ARE THE GUESS OF THE LEAST-SQUARE FITTING PARAMETERS               MAIN0032
C   PV(I) IS THE MEASURED DISTRIBUTION                                          MAIN0033
C   NC1,NC2,NC3,CC1,CC2,DC ARE CALIBRATION PARAMETERS                           MAIN0034
C   VOLTAGE=A+B*CHANNEL NUMBER                                                  MAIN0035
C                                                                               MAIN0036
```

```
  100 READ(5,1,END=1000) IEFF,IRT                                          MAIN0037
      READ 2,A,B                                                           MAIN0038
      READ 3,NC1,NC2,NC3,DC,CC1,CC2                                        MAIN0039
      PRINT 17,              IEFF,IRT,A,B,NC1,NC2,NC3,DC,CC1,CC2           MAIN0040
      VC1=A+B*FLOAT(NC1)                                                   MAIN0041
      VC2=A+B*FLOAT(NC2)                                                   MAIN0042
      VC3=A+B*FLOAT(NC3)                                                   MAIN0043
      XK=VC3/DC**2                                                         MAIN0044
      HPC1=(CC1-CC2)/FLOAT(NC1-1)                                          MAIN0045
      IF(NC3-NC2) 90,85,90                                                 MAIN0046
   85 HPC2=0.0                                                             MAIN0047
      GO TO 105                                                            MAIN0048
   90 HPC2=CC2/FLOAT(NC3-NC2)                                              MAIN0049
  105 CONTINUE                                                             MAIN0050
      DO 600 K=1,IEFF                                                      MAIN0051
      READ 1,NC                                                            MAIN0052
      READ 2,(PARAM(I),I=1,NPARAM)                                         MAIN0053
      READ 4,(PV(I),I=1,NC)                                                MAIN0054
      DO 150 I=2,NC                                                        MAIN0055
      PV(I)=PV(I)/PV(1)*3600.                                              MAIN0056
  150 CONTINUE                                                             MAIN0057
      PV(1)=PV(2)*2.-PV(3)                                                 MAIN0058
      PRINT 5                                                              MAIN0059
      PRINT 6                                                              MAIN0060
      PRINT 13,(PV(I),I=1,NC)                                              MAIN0061
      DO 200 I=1,NC                                                        MAIN0062
  200 D(I)=A+B*FLOAT(I)                                                    MAIN0063
      PRINT 14                                                             MAIN0064
      PRINT 13,(D(I),I=1,NC)                                               MAIN0065
C                                                                          MAIN0066
C   LEAST-SQUARE FIT OF THE MEASURED DISTRIBUTION                          MAIN0067
C                                                                          MAIN0068
      CALL LSMAPO(350,NC,NIND,D,PV,0,W,9,NPARAM,PARAM,YFCN,0.0001,W1,W2,   MAIN0069
     1W3,W4,W5,CURV,SCALF,SSQ,IER)                                         MAIN0070
      PRINT 15,IER                                                         MAIN0071
      PRINT 7                                                              MAIN0072
```

```
      PRINT 13,(PARAM(I),I=1,NPARAM)                                    MAIN0073
      PV1(1) =YFCN(D(1),NIND,PARAM,NPARAM)                              MAIN0074
      DO 300 I=2,NC                                                     MAIN0075
      PV1(I) =YFCN(D(I),NIND,PARAM,NPARAM)                              MAIN0076
      IF(I.LT.50) GO TO 300                                             MAIN0077
      IF(PV1(I).LT.0.) PV1(I)=0.                                        MAIN0078
      PVX=PV1(I-1)-PV1(I)                                               MAIN0079
      IF(PVX.LF.0.) GO TO 320                                           MAIN0080
  300 CONTINUE                                                          MAIN0081
      MC1=NC+1                                                          MAIN0082
      DO 310 I=MC1,350                                                  MAIN0083
      D(I)=D(I-1)+B                                                     MAIN0084
      PV1(I) =YFCN(D(I),NIND,PARAM,NPARAM)                              MAIN0085
      IF(PV1(I).LF.0.0) GO TO 320                                       MAIN0086
      PVX=PV1(I-1)-PV1(I)                                               MAIN0087
      IF(PVX.LE.0.) GO TO 320                                           MAIN0088
  310 CONTINUE                                                          MAIN0089
  320 CONTINUE                                                          MAIN0090
      PRINT 9,I                                                         MAIN0091
      PRINT 8                                                           MAIN0092
      PRINT 13,(PV1(J),J=1,I)                                           MAIN0093
      NC=I-1                                                            MAIN0094
      DO 400 I=1,NC                                                     MAIN0095
  400 D(I)=SQRT(D(I)/XK)                                                MAIN0096
      PRINT 10                                                          MAIN0097
      PRINT 13,(D(I),I=1,NC)                                            MAIN0098
C                                                                       MAIN0099
C   TO GENERATE THE RESPONSE FUNCTION                                   MAIN0100
C                                                                       MAIN0101
      DO 490 JJ=1,NC                                                    MAIN0102
      J=NC-JJ+1                                                         MAIN0103
      NN1=((A+B*FLOAT(J))/XK*VC1/DC**2-A)/B                             MAIN0104
      NN2=((A+B*FLOAT(J))/XK*VC2/DC**2-A)/B                             MAIN0105
      IF(NC3.EQ.NC2) NN2=J                                              MAIN0106
      DO 490 II=1,NC                                                    MAIN0107
      I=NC-II+1                                                         MAIN0108
```

```
      IF(I-J) 440,430,420                                              MAIN0109
  420 R(I,J)=0.0                                                       MAIN0110
      GO TO 490                                                        MAIN0111
  430 R(I,J)=1.0                                                       MAIN0112
      GO TO 490                                                        MAIN0113
  440 IF(I.GE.NN2) R(I,J)=R(J,J)+(J-I)*HPC2                            MAIN0114
      IF(I.LT.NN2.AND.I.GE.NN1) R(I,J)=R(NN2,J)                        MAIN0115
      IF(I.LT.NN1) R(I,J)=R(NN1,J)+(NN1-I)*HPC1                        MAIN0116
  490 CONTINUE                                                         MAIN0117
C                                                                      MAIN0118
C   TO TRANSFORM THE MEASURED DISTRIBUTION TO TRUE DROPLET DISTRIBUTION MAIN0119
C                                                                      MAIN0120
      IF(IRT.EQ.0) GO TO 491                                           MAIN0121
      CALL LEQT1F(R,1,NC,350,PV1,0,W,IER)                              MAIN0122
      PRINT 15,IER                                                     MAIN0123
      GO TO 495                                                        MAIN0124
  491 PV1(NC)=PV1(NC)/R(NC,NC)                                         MAIN0125
      NCC=NC-1                                                         MAIN0126
      DO 494 II=1,NCC                                                  MAIN0127
      I=NCC-II+1                                                       MAIN0128
      S=PV1(I)                                                         MAIN0129
      NM=I+1                                                           MAIN0130
      DO 492 J=NM,NC                                                   MAIN0131
  492 S=S-R(I,J)*PV1(J)                                                MAIN0132
  494 PV1(I)=S/R(I,I)                                                  MAIN0133
  495 CONTINUE                                                         MAIN0134
      NC=NC-1                                                          MAIN0135
      PRINT 11                                                         MAIN0136
      PRINT 13,(PV1(I),I=1,NC)                                         MAIN0137
      IF(K.EQ.2.OR.IEFF.NE.2) GO TO 700                                MAIN0138
      N1=NC                                                            MAIN0139
      DO 500 I=1,NC                                                    MAIN0140
  500 PF(I)=PV1(I)                                                     MAIN0141
  600 CONTINUE                                                         MAIN0142
C                                                                      MAIN0143
C   TO CALCULATE COLLECTION EFFICIENCY                                 MAIN0144
```

```
C
  700 IF(IEFF.NE.2) GO TO 100                                          MAIN0145
      NC=MIN0(N1,NC)                                                   MAIN0146
      DO 720 I=1,NC                                                    MAIN0147
      IF(PV1(I).LE.0.) GO TO 705                                       MAIN0148
      EFF(I)=1.-PF(I)/PV1(I)                                           MAIN0149
  705 IF(PV1(I).LE.0.) EFF(I)=0.                                       MAIN0150
      IF(EFF(I).LT.0.0) EFF(I)=0.0                                     MAIN0151
      IF(PF(I).LT.0.) EFF(I)=0.                                        MAIN0152
      IF(EFF(I).GT.1.0) EFF(I)=1.0                                     MAIN0153
  720 CONTINUE                                                         MAIN0154
      PRINT 12                                                         MAIN0155
      PRINT 16,(D(I),EFF(I),I=1,NC)                                    MAIN0156
      GO TO 100                                                        MAIN0157
 1000 CONTINUE                                                         MAIN0158
      END                                                              MAIN0159
                                                                       MAIN0160
```

```
      FUNCTION YFCN(D,NIND,PARAM,NPARAM)                                YFCN0001
      DIMENSION PARAM(NPARAM)                                           YFCN0002
      YFCN=0.0                                                          YFCN0003
      DO 1 I=1,NPARAM                                                   YFCN0004
    1 YFCN=YFCN+PARAM(I)/D**(I-1)                                       YFCN0005
      RETURN                                                            YFCN0006
      END                                                               YFCN0007
```

```
      SUBROUTINE LSMARQ(NDIM, NPTS, NIND, X, Y, IWEIGH, WEIGHT, NDIM2,   LSMQ0010
     1  NPARAM, PARAM, YFCN, EPSU, WORK1, F, WORK3, A, CHANGE, CURVTR,   LSMQ0020
     2  SCALE, SSQ, IERR)                                               LSMQ0030
C                                                                        LSMQ0040
      REAL A, CHANGE, COSINE, CURVTR, DEL, EPS, EPSU, F, LAMBDA,         LSMQ0050
     1  MACHEP, NU, PARAM, PSAVE, QNORM, RELTOL, SCALE, SMALL,          LSMQ0060
     2  SSQ, STEP, SUMB, SUM1, SUM2, TEM, VARY, WEIGHT, WORK1,          LSMQ0070
     3  WORK3, X, Y, YFCN                                               LSMQ0080
      REAL ABS, AMAX1, AMIN1, SIGN, SQRT                                 LSMQ0090
      INTEGER I, IERR, IM1, IPT, IWEIGH, J, K, NDIM, NDIM2, NIND,        LSMQ0100
     1  NPARAM, NPTS                                                    LSMQ0110
C                                                                        LSMQ0120
      DIMENSION X(NDIM, NIND), Y(NPTS), WEIGHT(NPTS), PARAM(NPARAM),     LSMQ0130
     1  WORK1(NIND), SCALE(NPARAM), CHANGE(NPARAM), A(NDIM2, NPARAM),    LSMQ0140
     2  CURVTR(NDIM2, NPARAM), F(NPTS), WORK3(NDIM2, 2)                 LSMQ0150
      EXTERNAL RSIMQ, YFCN                                               LSMQ0160
C                                                                        LSMQ0170
C  SMALL IS THE SMALLEST FLOATING POINT NUMBER FOR THIS MACHINE.         LSMQ0180
C  MACHEP IS THE SMALLEST FLOATING POINT NUMBER WHICH CAN BE ADDED       LSMQ0190
C  TO 1.0 AND STILL MAKE A DIFFERENCE.                                   LSMQ0200
      DATA SMALL/5.40E-79/, MACHEP/9.55E-7/                              LSMQ0210
C                                                                        LSMQ0220
C  CHECK FOR ARGUMENT ERRORS.                                            LSMQ0230
      IF (NDIM .LT. NPTS .OR. NPTS .LT. NPARAM                           LSMQ0240
     1  .OR. NIND .LE. 0 .OR. NDIM2 .LT. NPARAM                         LSMQ0250
     2  .OR. NPARAM .LE. 0) GO TO 99                                    LSMQ0260
C                                                                        LSMQ0270
      IERR = 0                                                           LSMQ0280
C                                                                        LSMQ0290
C  DEL IS USED IN NUMERICAL DIFFERENTIATION.  DEL SHOULD BE SMALL        LSMQ0300
C  ENOUGH TO GIVE A GOOD APPROXIMATION, BUT NOT SO SMALL THAT THE        LSMQ0310
C  DIFFERENTIATED VALUE IS LOST IN ROUND-OFF NOISE.  THE VALUE           LSMQ0320
C  SQRT(MACHEP) IS AN INTUITIVELY DERIVED COMPROMISE.                    LSMQ0330
      DEL = SQRT(MACHEP)                                                 LSMQ0340
      LAMBDA = 0.1E0                                                     LSMQ0350
      NU = 10.0E0                                                        LSMQ0360
```

```
      EPS = AMAX1(EPSU, MACHEP)                                          LSMQ0370
      RELTOL = SMALL / AMIN1(1.0E0, EPS)                                 LSMQ0380
C                                                                        LSMQ0390
C  COMPUTE SUM OF SQUARES CORRESPONDING TO INITIAL GUESS.                LSMQ0400
      SSQ = 0.0E0                                                        LSMQ0410
      DO 20 I = 1, NPTS                                                  LSMQ0420
         DO 10 K = 1, NIND                                               LSMQ0430
10          WORK1(K) = X(I, K)                                           LSMQ0440
         F(I) = YFCN(WORK1, NIND, PARAM, NPARAM)                         LSMQ0450
C                                                                        LSMQ0460
C  COMPUTE WEIGHTS, IF NECESSARY.                                        LSMQ0470
         IF (IWEIGH .GT. 0) GO TO 15                                     LSMQ0480
         WEIGHT(I) = 1.0E0                                               LSMQ0490
         IF (IWEIGH .LT. 0) WEIGHT(I) = 1.0E0 / AMAX1(Y(I), 1.0E0)       LSMQ0500
15       SSQ = SSQ + WEIGHT(I) *(Y(I) - F(I))**2                         LSMQ0510
20    CONTINUE                                                           LSMQ0520
C                                                                        LSMQ0530
C  TRY A SMALLER VALUE OF LAMBDA.                                        LSMQ0540
30    LAMBDA = LAMBDA / NU                                               LSMQ0550
C                                                                        LSMQ0560
C  ZERO ARRAYS BEFORE ACCUMULATING SUMS.                                 LSMQ0570
      DO 50 I = 1, NPARAM                                                LSMQ0580
         WORK3(I, 2) = 0.0E0                                             LSMQ0590
         DO 40 J = 1, I                                                  LSMQ0600
40          CURVTR(I, J) = 0.0E0                                         LSMQ0610
50    CONTINUE                                                           LSMQ0620
C                                                                        LSMQ0630
      DO 100 IPT = 1, NPTS                                               LSMQ0640
         TEM = WEIGHT(IPT) * (Y(IPT) - F(IPT))                           LSMQ0650
         DO 60 K = 1, NIND                                               LSMQ0660
60          WORK1(K) = X(IPT, K)                                         LSMQ0670
C                                                                        LSMQ0680
         DO 90 I = 1, NPARAM                                             LSMQ0690
C  VARY I-TH PARAMETER, STORING RESULTING CHANGE OF FUNCTION VALUE       LSMQ0700
C  IN WORK3(I, 1).                                                       LSMQ0710
            PSAVE = PARAM(I)                                             LSMQ0720
```

```
            PARAM(I) = PSAVE * (1.0E0 + DEL)                                    LSMQ0730
            IF (PSAVE .EQ. 0.0E0) PARAM(I) = DEL                                LSMQ0740
            WORK3(I, 1) = YFCN(WORK1, NIND, PARAM, NPARAM) - F(IPT)             LSMQ0750
C                                                                               LSMQ0760
C  ACCUMULATE GRADIENT OF SSQ IN WORK3(I, 2).                                   LSMQ0770
            WORK3(I, 2) = WORK3(I, 2) + TEM * WORK3(I, 1)                       LSMQ0780
            PARAM(I) = PSAVE                                                    LSMQ0790
C                                                                               LSMQ0800
C  ACCUMULATE CURVATURE MATRIX.                                                 LSMQ0810
            DO 80 J = 1, I                                                      LSMQ0820
               CURVTR(I, J) = CURVTR(I, J) + WEIGHT(IPT) * WORK3(I, 1)          LSMQ0830
     1            * WORK3(J, 1)                                                LSMQ0840
   80       CONTINUE                                                           LSMQ0850
   90    CONTINUE                                                              LSMQ0860
  100 CONTINUE                                                                  LSMQ0870
C                                                                               LSMQ0880
      QNORM = 0.0E0                                                             LSMQ0890
      DO 120 I = 1, NPARAM                                                      LSMQ0900
C                                                                               LSMQ0910
C  NOW USE WORK3(I, 1) FOR SAVING PARAMETER VALUE.                              LSMQ0920
        WORK3(I, 1) = PARAM(I)                                                  LSMQ0930
C                                                                               LSMQ0940
C  NORMALIZE GRADIENT AND CURVATURE BY PARAMETER VARIATIONS, AND                LSMQ0950
C  SCALE THEM SO THAT CURVATURE DIAGONAL ELEMENTS ARE UNITY.                    LSMQ0960
        VARY = DEL * PARAM(I)                                                   LSMQ0970
        IF (VARY .EQ. 0.0E0) VARY = DEL                                         LSMQ0980
        TEM = SIGN(SQRT(CURVTR(I, I)), VARY)                                    LSMQ0990
        SCALE(I) = VARY / TEM                                                   LSMQ1000
        WORK3(I, 2) = WORK3(I, 2) / TEM                                         LSMQ1010
C                                                                               LSMQ1020
C  ACCUMULATE NORM**2 OF GRADIENT.                                              LSMQ1030
        QNORM = QNORM + WORK3(I, 2)**2                                          LSMQ1040
C                                                                               LSMQ1050
        IF (I .LE. 1) GO TO 120                                                 LSMQ1060
        IM1 = I - 1                                                             LSMQ1070
        DO 110 J = 1, IM1                                                       LSMQ1080
```

```
            VARY = DEL * PARAM(J)                                          LSMQ1090
            IF (VARY .EQ. 0.0E0) VARY = DEL                                LSMQ1100
            CURVTR(I, J) = (CURVTR(I, J) * SCALE(J)) / (TEM * VARY)        LSMQ1110
  110    CONTINUE                                                          LSMQ1120
  120 CONTINUE                                                            LSMQ1130
C                                                                         LSMQ1140
  130 DO 150 I = 1, NPARAM                                                LSMQ1150
C                                                                         LSMQ1160
C  COPY GRADIENT.                                                         LSMQ1170
         CHANGE(I) = WORK3(I, 2)                                          LSMQ1180
C                                                                         LSMQ1190
C  ADD LAMBDA TO CURVATURE DIAGONALS.                                     LSMQ1200
         A(I, I) = 1.0E0 + LAMBDA                                         LSMQ1210
C                                                                         LSMQ1220
C  COPY REST OF CURVATURE MATRIX.                                         LSMQ1230
         IF (I .LE. 1) GO TO 150                                          LSMQ1240
         IM1 = I - 1                                                      LSMQ1250
         DO 140 J = 1, IM1                                                LSMQ1260
            A(I, J) = CURVTR(I, J)                                        LSMQ1270
            A(J, I) = A(I, J)                                             LSMQ1280
  140    CONTINUE                                                         LSMQ1290
  150 CONTINUE                                                            LSMQ1300
C                                                                         LSMQ1310
C  SOLVE FOR BEST DIRECTION OF CHANGE.                                    LSMQ1320
      CALL RSIMQ(NDIM2, NPARAM, A, CHANGE, IERR)                          LSMQ1330
      IF (IERR .NE. 0) RETURN                                             LSMQ1340
C                                                                         LSMQ1350
C  COMPUTE ANGLE BETWEEN CHANGE AND GRADIENT IN SCALED                    LSMQ1360
C  COORDINATES . . .                                                      LSMQ1370
      SUM1 = 0.0EC                                                        LSMQ1380
      SUM2 = 0.0EC                                                        LSMQ1390
      DO 160 I = 1, NPARAM                                                LSMQ1400
         SUM1 = SUM1 + CHANGE(I) * WORK3(I, 2)                            LSMQ1410
         SUM2 = SUM2 + CHANGE(I)**2                                       LSMQ1420
C                                                                         LSMQ1430
C  AND DE-SCALE CHANGE.                                                   LSMQ1440
```

```
         CHANGE(I) = CHANGE(I) * SCALE(I)                                LSMQ1450
  160 CONTINUE                                                           LSMQ1460
C                                                                        LSMQ1470
      COSINE = SUM1 / SQRT(SUM2 * QNORM)                                 LSMQ1480
C                                                                        LSMQ1490
      STEP = 1.0E0                                                       LSMQ1500
C                                                                        LSMQ1510
C  IF STEP*CHANGE IS SMALL FOR ALL COORDINATES, RESTORE PARAMETER        LSMQ1520
C  VALUES AND EXIT.                                                      LSMQ1530
  170 DO 180 I = 1, NPARAM                                               LSMQ1540
         PARAM(I) = WORK3(I, 1)                                          LSMQ1550
         IF (ABS(STEP * CHANGE(I)) .GT. RELTOL + EPS * ABS(PARAM(I)))    LSMQ1560
     1     GO TO 190                                                     LSMQ1570
  180 CONTINUE                                                           LSMQ1580
      RETURN                                                             LSMQ1590
C                                                                        LSMQ1600
C  VARY PARAMETERS BY STEP*CHANGE.                                       LSMQ1610
  190 DO 200 I = 1, NPARAM                                               LSMQ1620
  200    PARAM(I) = STEP * CHANGE(I) + WORK3(I, 1)                       LSMQ1630
C                                                                        LSMQ1640
C  COMPUTE CORRESPONDING SSQ.                                            LSMQ1650
      SUMB = 0.0E0                                                       LSMQ1660
      DO 220 I = 1, NPTS                                                 LSMQ1670
         DO 210 K = 1, NIND                                              LSMQ1680
  210       WORK1(K) = X(I, K)                                           LSMQ1690
         F(I) = YFCN(WORK1, NIND, PARAM, NPARAM)                         LSMQ1700
         SUMB = SUMB + WEIGHT(I) * (Y(I) - F(I))**2                      LSMQ1710
  220 CONTINUE                                                           LSMQ1720
C                                                                        LSMQ1730
      IF (SUMB .LE. SSQ) GO TO 240                                       LSMQ1740
C                                                                        LSMQ1750
C  IF NO REDUCTION, THEN . . .                                           LSMQ1760
      IF (COSINE .LT. 0.866E0) GO TO 230                                 LSMQ1770
C                                                                        LSMQ1780
C  IF CHANGE IS CLOSE TO GRADIENT, REDUCE STEP AND TRY AGAIN.            LSMQ1790
      STEP = 0.5E0 * STEP                                                LSMQ1800
```

```
      GO TO 170                                                          LSMQ1810
C                                                                        LSMQ1820
C  IF CHANGE IS NOT CLOSE TO GRADIENT, INCREASE LAMBDA AND               LSMQ1830
C  RECOMPUTE CHANGE.                                                     LSMQ1840
  230 LAMBDA = LAMBDA * NU                                               LSMQ1850
      GO TO 130                                                          LSMQ1860
C                                                                        LSMQ1870
C  IF REDUCTION, THEN KEEP LAMBDA AND MOVE TO NEW POINT, THEN            LSMQ1880
C  RECOMPUTE GRADIENT AND CURVATURE, AND SO ON.                          LSMQ1890
  240 SSQ = SUMB                                                         LSMQ1900
      GO TO 30                                                           LSMQ1910
C                                                                        LSMQ1920
C  HERE ON ARGUMENT ERROR.                                               LSMQ1930
   99 WRITE (6, 1001) NDIM, NPTS, NINC, NDIM2, NPARAM                    LSMQ1940
      IERR = 3                                                           LSMQ1950
      RETURN                                                             LSMQ1960
C                                                                        LSMQ1970
 1001 FORMAT(24H LSMARQ:  ARGUMENT ERROR, 5I11)                          LSMQ1980
      END                                                                LSMQ1990
```

```
      SUBROUTINE RSIMQ(NDIM, NORDER, COEFF, RHS, IERR)                  RSMQ0010
C                                                                       RSMQ0020
      REAL COEFF, RHS, BIGC, SAVE, TOL, ABS                             RSMQ0030
      INTEGER NORDER, NDIM, I, J, K, IMAX, JP1, JJ, NM1                 RSMQ0040
C                                                                       RSMQ0050
      DIMENSION COEFF(NDIM, NORDER), RHS(NORDER)                        RSMQ0060
C                                                                       RSMQ0070
C  CHECK FOR ARGUMENT ERRORS.                                           RSMQ0080
      IF (NDIM .GE. NORDER .AND. NORDER .GT. 0) GO TO 10                RSMQ0090
      IERR = 2                                                          RSMQ0100
      WRITE (6, 1001) NDIM, NORDER                                      RSMQ0110
      RETURN                                                            RSMQ0120
C                                                                       RSMQ0130
   10 TOL = 0.0E0                                                       RSMQ0140
      IERR = 0                                                          RSMQ0150
C                                                                       RSMQ0160
C  DO FORWARD ELIMINATION, WITH PARTIAL PIVOTING.                       RSMQ0170
      DO 70 J = 1, NORDER                                               RSMQ0180
C                                                                       RSMQ0190
C  CHOOSE LARGEST ELEMENT REMAINING IN THIS COLUMN.                     RSMQ0200
         BIGC = 0.0E0                                                   RSMQ0210
         DO 20 I = J, NORDER                                            RSMQ0220
            IF (ABS(BIGC) .GE. ABS(COEFF(I, J))) GO TO 20               RSMQ0230
            BIGC = COEFF(I, J)                                          RSMQ0240
            IMAX = I                                                    RSMQ0250
   20    CONTINUE                                                       RSMQ0260
C                                                                       RSMQ0270
C  IF ALL ELEMENTS HAVE MAGNITUDES LESS THAN OR EQUAL TO TOL, THEN      RSMQ0280
C  MATRIX IS SINGULAR.                                                  RSMQ0290
         IF (ABS(BIGC) .GT. TOL) GO TO 30                               RSMQ0300
         IERR = 1                                                       RSMQ0310
         WRITE (6, 1002)                                                RSMQ0320
         RETURN                                                         RSMQ0330
C                                                                       RSMQ0340
C  INTERCHANGE ROWS IF NECESSARY, AND DIVIDE NEW CURRENT ROW BY         RSMQ0350
C  PIVOT ELEMENT.                                                       RSMQ0360
```

```
   30     DO 40 K = J, NORDER                                              RSMQ0370
             SAVE = COEFF(IMAX, K)                                         RSMQ0380
             COEFF(IMAX, K) = COEFF(J, K)                                  RSMQ0390
             COEFF(J, K) = SAVE / BIGC                                     RSMQ0400
   40     CONTINUE                                                         RSMQ0410
C                                                                          RSMQ0420
C  DO THE SAME FOR THE RIGHT-HAND SIDE.                                    RSMQ0430
          SAVE = RHS(IMAX)                                                 RSMQ0440
          RHS(IMAX) = RHS(J)                                               RSMQ0450
          RHS(J) = SAVE / BIGC                                             RSMQ0460
C                                                                          RSMQ0470
C  SUBTRACT MULTIPLES OF THIS ROW FROM ANY REMAINING ROWS TO MAKE          RSMQ0480
C  LEADING COEFFICIENTS VANISH.                                            RSMQ0490
          IF (J .GE. NORDER) GO TO 80                                      RSMQ0500
C                                                                          RSMQ0510
          JP1 = J + 1                                                      RSMQ0520
          DO 60 I = JP1, NORDER                                            RSMQ0530
             SAVE = COEFF(I, J)                                            RSMQ0540
             DO 50 K = JP1, NORDER                                         RSMQ0550
   50           COEFF(I, K) = COEFF(I, K) - SAVE * COEFF(J, K)            RSMQ0560
             RHS(I) = RHS(I) - SAVE * RHS(J)                               RSMQ0570
   60     CONTINUE                                                         RSMQ0580
   70  CONTINUE                                                            RSMQ0590
C                                                                          RSMQ0600
C  NOW FIND ELEMENTS OF SOLUTION VECTOR IN REVERSE ORDER BY DIRECT         RSMQ0610
C  SUBSTITUTION.                                                           RSMQ0620
   80  NM1 = NORDER - 1                                                    RSMQ0630
       NP1 = NORDER + 1                                                    RSMQ0640
       DO 100 JJ = 1, NM1                                                  RSMQ0650
          J = NORDER - JJ                                                  RSMQ0660
          JP1 = J + 1                                                      RSMQ0670
          DO 90 KK = 1, JJ                                                 RSMQ0680
             K = NP1 - KK                                                  RSMQ0690
             RHS(J) = RHS(J) - COEFF(J, K) * RHS(K)                        RSMQ0700
   90     CONTINUE                                                         RSMQ0710
  100  CONTINUE                                                            RSMQ0720
```

```
C                                                                       RSMQ0730
      RETURN                                                            RSMQ0740
C                                                                       RSMQ0750
 1001 FORMAT(23H RSIMQ:  ARGUMENT ERROR, 2I11)                          RSMQ0760
 1002 FORMAT(32H RSIMQ:  EQUATIONS ARE SINGULAR.)                       RSMQ0770
      END                                                               RSMQ0780
```

```
C     SUBROUTINE LEQT1F (A,M,N,IA,B,IDGT,WKAREA,IER)                    LE1F0010
C                                                                       LE1F0020
C-LEQT1F--------S/D-----LIBRARY 1---------------------------------------LE1F0030
C                                                                       LE1F0040
C   FUNCTION              - LINEAR EQUATION SOLUTION - FULL STORAGE      LE1F0050
C                             MODE - SPACE ECONOMIZER SOLUTION.         LE1F0060
C   USAGE                 - CALL LEQT1F (A,M,N,IA,B,IDGT,WKAREA,IER)    LE1F0070
C   PARAMETERS    A       - INPUT MATRIX OF DIMENSION N BY N CONTAINING LE1F0080
C                             THE COEFFICIENT MATRIX OF THE EQUATION    LE1F0090
C                             AX = B.                                   LE1F0100
C                           ON OUTPUT, A IS REPLACED BY THE LU          LE1F0110
C                             DECOMPOSITION OF A ROWWISE PERMUTATION OF LE1F0120
C                             A.                                        LE1F0130
C                 M       - NUMBER OF RIGHT-HAND SIDES.(INPUT)          LE1F0140
C                 N       - ORDER OF A AND NUMBER OF ROWS IN B.(INPUT)  LE1F0150
C                 IA      - NUMBER OF ROWS IN THE DIMENSION STATEMENT   LE1F0160
C                             FOR A AND B IN THE CALLING PROGRAM. (INPUT) LE1F0170
C                 B       - INPUT MATRIX OF DIMENSION N BY M CONTAINING LE1F0180
C                             RIGHT-HAND SIDES OF THE EQUATION AX = B.  LE1F0190
C                           ON OUTPUT, THE N BY M SOLUTION X REPLACES B. LE1F0200
C                 IDGT    - INPUT OPTION.                               LE1F0210
C                           IF IDGT IS GREATER THAN 0, THE ELEMENTS OF  LE1F0220
C                             A AND B ARE ASSUMED TO BE CORRECT TO IDGT LE1F0230
C                             DECIMAL DIGITS AND THE ROUTINE PERFORMS   LE1F0240
C                             AN ACCURACY TEST.                         LE1F0250
C                           IF IDGT EQUALS ZERO, THE ACCURACY TEST IS   LE1F0260
C                             BYPASSED.                                 LE1F0270
C                 WKAREA  - WORK AREA OF DIMENSION GREATER THAN OR EQUAL LE1F0280
C                             TO N.                                     LE1F0290
C                 IER     - ERROR PARAMETER                             LE1F0300
C                           TERMINAL ERROR = 128+N.                     LE1F0310
C                             N = 1 INDICATES THAT A IS ALGORITHMICALLY LE1F0320
C                               SINGULAR. (SEE THE CHAPTER L PRELUDE).  LE1F0330
C                           WARNING ERROR = 32+N.                       LE1F0340
C                             N = 2 INDICATES THAT THE ACCURACY TEST    LE1F0350
C                                   FAILED.                             LE1F0360
```

```
C                                  THE COMPUTED SOLUTION MAY BE IN ERROR LE1F0370
C                                  BY MORE THAN CAN BE ACCOUNTED FOR BY  LE1F0380
C                                  THE UNCERTAINTY OF THE DATA.          LE1F0390
C                                  THIS WARNING CAN BE PRODUCED ONLY IF  LE1F0400
C                                  IDGT IS GREATER THAN 0 ON INPUT.      LE1F0410
C                                  SEE CHAPTER L PRELUDE FOR FURTHER     LE1F0420
C                                  DISCUSSION.                           LE1F0430
C   PRECISION            - SINGLE/DOUBLE                                 LE1F0440
C   REQD. IMSL ROUTINES  - LUDATF,LUELMF,UERTST                          LE1F0450
C   LANGUAGE             - FORTRAN                                       LE1F0460
C-----------------------------------------------------------------------LE1F0470
C   LATEST REVISION      - AUGUST 15, 1973                               LE1F0480
C                                                                        LE1F0490
      SUBROUTINE LEQT1F (A,M,N,IA,B,IDGT,WKAREA,IER)                     LE1F0500
C                                                                        LE1F0510
      DIMENSION          A(IA,1),B(IA,1),WKAREA(1)                     LE1F0520
C0    DOUBLE PRECISION   A,B,WKAREA,D1,D2,WA                           LE1F0530
C                                  INITIALIZE IER                        LE1F0540
      IER=0                                                              LE1F0550
C                                  DECOMPOSE A                           LE1F0560
      CALL LUDATF (A,A,N,IA,IDGT,D1,D2,WKAREA,WKAREA,WA,IER)             LE1F0570
      IF (IER .GT. 128) GO TO 9000                                       LE1F0580
C                                  CALL ROUTINE LUELMF (FORWARD AND      LE1F0590
C                                  BACKWARD SUBSTITUTIONS)               LE1F0600
      DO 10 J=1,M                                                        LE1F0610
         CALL LUELMF (A,B(1,J),WKAREA,N,IA,B(1,J))                       LE1F0620
   10 CONTINUE                                                           LE1F0630
      IF (IER .EQ. 0) GO TO 9005                                         LE1F0640
 9000 CONTINUE                                                          LE1F0650
      CALL UERTST (IER,6HLEQT1F)                                         LE1F0660
 9005 RETURN                                                            LE1F0670
      END                                                                LE1F0680
```

```
C      SUBROUTINE LUDATF (A,LU,N,IA,IDGT,D1,D2,IPVT,EQUIL,WA,IER)          LUDA0010
C                                                                          LUDA0020
C-LUDATF--------S/D-----LIBRARY 1-----------------------------------------LUDA0030
C                                                                          LUDA0040
C    FUNCTION              - L-U DECOMPOSITION BY THE CROUT ALGORITHM       LUDA0050
C                            WITH OPTIONAL ACCURACY TEST.                  LUDA0060
C    USAGE                 - CALL LUDATF(A,LU,N,IA,IDGT,D1,D2,IPVT,         LUDA0070
C                                        EQUIL,WA,IER)                     LUDA0080
C    PARAMETERS    A       - INPUT MATRIX OF DIMENSION N BY N CONTAINING    LUDA0090
C                            THE MATRIX TO BE DECOMPOSED                   LUDA0100
C                  LU      - REAL OUTPUT MATRIX OF DIMENSION N BY N         LUDA0110
C                            CONTAINING THE L-U DECOMPOSITION OF A         LUDA0120
C                            ROWWISE PERMUTATION OF THE INPUT MATRIX.      LUDA0130
C                            FOR A DESCRIPTION OF THE FORMAT OF LU, SEE    LUDA0140
C                            EXAMPLE.                                      LUDA0150
C                  N       - INPUT SCALAR CONTAINING THE ORDER OF THE       LUDA0160
C                            MATRIX A.                                     LUDA0170
C                  IA      - INPUT SCALAR CONTAINING THE ROW DIMENSION OF   LUDA0180
C                            MATRICES A AND LU IN THE CALLING PROGRAM.     LUDA0190
C                  IDGT    - INPUT OPTION.                                  LUDA0200
C                            IF IDGT IS GREATER THAN ZERO, THE NON-ZERO    LUDA0210
C                            ELEMENTS OF A ARE ASSUMED TO BE CORRECT TO    LUDA0220
C                            IDGT DECIMAL PLACES.  LUDATF PERFORMS AN      LUDA0230
C                            ACCURACY TEST TO DETERMINE IF THE COMPUTED    LUDA0240
C                            DECOMPOSITION IS THE EXACT DECOMPOSITION      LUDA0250
C                            OF A MATRIX WHICH DIFFERS FROM THE GIVEN ONE  LUDA0260
C                            BY LESS THAN ITS UNCERTAINTY.                 LUDA0270
C                          IF IDGT IS EQUAL TO ZERO, THE ACCURACY TEST IS  LUDA0280
C                            BYPASSED.                                     LUDA0290
C                  D1      - OUTPUT SCALAR CONTAINING ONE OF THE TWO        LUDA0300
C                            COMPONENTS OF THE DETERMINANT. SEE            LUDA0310
C                            DESCRIPTION OF PARAMETER D2, BELOW.           LUDA0320
C                  D2      - OUTPUT SCALAR CONTAINING ONE OF THE            LUDA0330
C                            TWO COMPONENTS OF THE DETERMINANT. THE        LUDA0340
C                            DETERMINANT MAY BE EVALUATED AS (D1)(2**D2)   LUDA0350
C                  IPVT    - OUTPUT VECTOR OF LENGTH N CONTAINING THE       LUDA0360
```

```
C                          PERMUTATION INDICES. SEE DOCUMENT            LUDA0370
C                          (ALGORITHM).                                 LUDA0380
C                  EQUIL   - OUTPUT VECTOR OF LENGTH N CONTAINING       LUDA0390
C                            RECIPROCALS OF THE ABSOLUTE VALUES OF      LUDA0400
C                            THE LARGEST (IN ABSOLUTE VALUE) ELEMENT    LUDA0410
C                            IN EACH ROW.                               LUDA0420
C                  WA      - ACCURACY TEST PARAMETER, OUTPUT ONLY IF    LUDA0430
C                            IDGT IS GREATER THAN ZERO.                 LUDA0440
C                            SEE ELEMENT DOCUMENTATION FOR DETAILS.     LUDA0450
C                  IER     - ERROR PARAMETER                            LUDA0460
C                            TERMINAL ERROR=128+N                       LUDA0470
C                              N = 1 INDICATES THAT MATRIX A IS         LUDA0480
C                                    ALGORITHMICALLY SINGULAR. (SEE THE LUDA0490
C                                    CHAPTER L PRELUDE).                LUDA0500
C                            WARNING ERROR=32+N                         LUDA0510
C                              N = 2 INDICATES THAT THE ACCURACY TEST   LUDA0520
C                                    FAILED.                            LUDA0530
C                                    THE COMPUTED SOLUTION MAY BE IN ERROR LUDA0540
C                                    BY MORE THAN CAN BE ACCOUNTED FOR BY LUDA0550
C                                    THE UNCERTAINTY OF THE DATA.       LUDA0560
C                                    THIS WARNING CAN BE PRODUCED ONLY IF LUDA0570
C                                    IDGT IS GREATER THAN 0 ON INPUT.   LUDA0580
C                                    SEE CHAPTER L PRELUDE FOR FURTHER  LUDA0590
C                                    DISCUSSION.                        LUDA0600
C   PRECISION           - SINGLE/DOUBLE                                 LUDA0610
C   REQD. IMSL ROUTINES - UERTST                                        LUDA0620
C   LANGUAGE            - FORTRAN                                       LUDA0630
C-------------------------------------------------------------------------LUDA0640
C   LATEST REVISION     - AUGUST 15, 1973                               LUDA0650
C                                                                       LUDA0660
      SUBROUTINE LUDATF (A,LU,N,IA,IDGT,D1,D2,IPVT,EQUIL,WA,IER)        LUDA0670
C                                                                       LUDA0680
      DIMENSION          A(IA,1),LU(IA,1),IPVT(1),EQUIL(1)            LUDA0690
C*    DOUBLE PRECISION   A,LU,D1,D2,EQUIL,WA,ZERO,ONE,FOUR,SIXTN,SIXTH, LUDA0700
C1    *                  RN,WREL,BIGA,BIG,P,SUM,AI,WI,T,TEST,Q        LUDA0710
      REAL               LU                                           LUDA0720
```

```
C*    DATA                ZERO,ONE,FOUR,SIXTN,SIXTH/0.D0,1.D0,4.D0,       LUDA0730
C1    *                   16.D0,.0625D0/                                  LUDA0740
      DATA                ZERO,ONE,FOUR,SIXTN,SIXTH/0.0,1.,4.,16.,.0625/ LUDA0750
C                                 INITIALIZATION                          LUDA0760
      IER = 0                                                             LUDA0770
      RN = N                                                              LUDA0780
      WREL = ZERO                                                         LUDA0790
      D1 = ONE                                                            LUDA0800
      D2 = ZERO                                                           LUDA0810
      BIGA = ZERO                                                         LUDA0820
      DO 10 I=1,N                                                         LUDA0830
         BIG = ZERO                                                       LUDA0840
         DO 5 J=1,N                                                       LUDA0850
            P = A(I,J)                                                    LUDA0860
            LU(I,J) = P                                                   LUDA0870
C1          P = DABS(P)                                                   LUDA0880
            P = ABS(P)                                                    LUDA0890
            IF (P .GT. BIG) BIG = P                                       LUDA0900
    5    CONTINUE                                                         LUDA0910
         IF (BIG .GT. BIGA) BIGA = BIG                                    LUDA0920
         IF (BIG .EQ. ZERO) GO TO 110                                     LUDA0930
         EQUIL(I) = ONE/BIG                                               LUDA0940
   10 CONTINUE                                                            LUDA0950
      DO 105 J=1,N                                                        LUDA0960
         JM1 = J-1                                                        LUDA0970
         IF (JM1 .LT. 1) GO TO 40                                         LUDA0980
C                              COMPUTE U(I,J), I=1,...,J-1                LUDA0990
         DO 35 I=1,JM1                                                    LUDA1000
            SUM = LU(I,J)                                                 LUDA1010
            IM1 = I-1                                                     LUDA1020
            IF (IDGT .EQ. 0) GO TO 25                                     LUDA1030
C                                 WITH ACCURACY TEST                      LUDA1040
C1          AI = DABS(SUM)                                                LUDA1050
            AI = ABS(SUM)                                                 LUDA1060
            WI = ZERO                                                     LUDA1070
            IF (IM1 .LT. 1) GO TO 20                                      LUDA1080
```

```
            DO 15 K=1,IM1                                                  LUDA1090
               T = LU(I,K)*LU(K,J)                                         LUDA1100
               SUM = SUM-T                                                 LUDA1110
C1             WI = WI+DABS(T)                                             LUDA1120
               WI = WI+ABS(T)                                              LUDA1130
   15       CONTINUE                                                       LUDA1140
            LU(I,J) = SUM                                                  LUDA1150
C1 20       WI = WI+DABS(SUM)                                              LUDA1160
   20       WI = WI+ABS(SUM)                                               LUDA1170
            IF (AI .EQ. ZERO) AI = BIGA                                    LUDA1180
            TEST = WI/AI                                                   LUDA1190
            IF (TEST .GT. WREL) WREL = TEST                                LUDA1200
            GO TO 35                                                       LUDA1210
C                                   WITHOUT ACCURACY                       LUDA1220
   25       IF (IM1 .LT. 1) GO TO 35                                       LUDA1230
            DO 30 K=1,IM1                                                  LUDA1240
               SUM = SUM-LU(I,K)*LU(K,J)                                   LUDA1250
   30       CONTINUE                                                       LUDA1260
            LU(I,J) = SUM                                                  LUDA1270
   35    CONTINUE                                                          LUDA1280
   40    P = ZERO                                                          LUDA1290
C                                   COMPUTE U(J,J) AND L(I,J), I=J+1,...,LUDA1300
         DO 70 I=J,N                                                       LUDA1310
            SUM = LU(I,J)                                                  LUDA1320
            IF (IDGT .EQ. 0) GO TO 55                                      LUDA1330
C                                   WITH ACCURACY TEST                     LUDA1340
C1          AI = DABS(SUM)                                                 LUDA1350
            AI = ABS(SUM)                                                  LUDA1360
            WI = ZERO                                                      LUDA1370
            IF (JM1 .LT. 1) GO TO 50                                       LUDA1380
            DO 45 K=1,JM1                                                  LUDA1390
               T = LU(I,K)*LU(K,J)                                         LUDA1400
               SUM = SUM-T                                                 LUDA1410
C1             WI = WI+DABS(T)                                             LUDA1420
               WI = WI+ABS(T)                                              LUDA1430
   45       CONTINUE                                                       LUDA1440
```

```
            LU(I,J) = SUM                                                  LUDA1450
C1 50       WI = WI+DABS(SUM)                                              LUDA1460
   50       WI = WI+ABS(SUM)                                               LUDA1470
            IF (AI .EQ. ZERO) AI = BIGA                                    LUDA1480
            TEST = WI/AI                                                   LUDA1490
            IF (TEST .GT. WREL) WREL = TEST                                LUDA1500
            GO TO 65                                                       LUDA1510
C                                     WITHOUT ACCURACY TEST                LUDA1520
   55       IF (JM1 .LT. 1) GO TO 65                                       LUDA1530
            DO 60 K=1,JM1                                                  LUDA1540
               SUM = SUM-LU(I,K)*LU(K,J)                                   LUDA1550
   60       CONTINUE                                                       LUDA1560
            LU(I,J) = SUM                                                  LUDA1570
C1 65       Q = EQUIL(I)*DABS(SUM)                                         LUDA1580
   65       Q = EQUIL(I)*ABS(SUM)                                          LUDA1590
            IF (P .GE. Q) GO TO 70                                         LUDA1600
            P = Q                                                          LUDA1610
            IMAX = I                                                       LUDA1620
   70    CONTINUE                                                          LUDA1630
C                                     TEST FOR ALGORITHMIC SINGULARITY     LUDA1640
         IF (RN+P .EQ. RN) GO TO 110                                       LUDA1650
         IF (J .EQ. IMAX) GO TO 80                                         LUDA1660
C                                     INTERCHANGE ROWS J AND IMAX          LUDA1670
         D1 = -D1                                                          LUDA1680
         DO 75 K=1,N                                                       LUDA1690
            P = LU(IMAX,K)                                                 LUDA1700
            LU(IMAX,K) = LU(J,K)                                           LUDA1710
            LU(J,K) = P                                                    LUDA1720
   75    CONTINUE                                                          LUDA1730
         EQUIL(IMAX) = EQUIL(J)                                            LUDA1740
   80    IPVT(J) = IMAX                                                    LUDA1750
         D1 = D1*LU(J,J)                                                   LUDA1760
C1 85    IF (DABS(D1) .LE. ONE) GO TO 90                                   LUDA1770
   85    IF (ABS(D1) .LE. ONE) GO TO 90                                    LUDA1780
         D1 = D1*SIXTH                                                     LUDA1790
         D2 = D2+FOUR                                                      LUDA1800
```

```
      GO TO 85                                                          LUDA1810
C1 90 IF (DABS(D1) .GE. SIXTH) GO TO 95                                 LUDA1820
   90 IF (ABS(C1) .GE. SIXTH) GO TO 95                                  LUDA1830
      D1 = D1*SIXTN                                                     LUDA1840
      D2 = D2-FOUR                                                      LUDA1850
      GO TO 90                                                          LUDA1860
   95 CONTINUE                                                          LUDA1870
      JP1 = J+1                                                         LUDA1880
      IF (JP1 .GT. N) GO TO 105                                         LUDA1890
C                                  DIVIDE BY PIVOT ELEMENT U(J,J)       LUDA1900
      P = LU(J,J)                                                       LUDA1910
      DO 100 I=JP1,N                                                    LUDA1920
         LU(I,J) = LU(I,J)/P                                            LUDA1930
  100 CONTINUE                                                          LUDA1940
  105 CONTINUE                                                          LUDA1950
C                                  PERFORM ACCURACY TEST                LUDA1960
      IF (IDGT .EQ. 0) GO TO 9005                                       LUDA1970
      P = 3*N+3                                                         LUDA1980
      WA = P*WREL                                                       LUDA1990
C1    IF (WA+10.D0**(-IDGT) .NE. WA) GO TO 9005                         LUDA2000
      IF (WA+10.0**(-IDGT) .NE. WA) GO TO 9005                          LUDA2010
      IER = 34                                                          LUDA2020
      GO TO 9000                                                        LUDA2030
C                                  ALGORITHMIC SINGULARITY              LUDA2040
  110 IER = 129                                                         LUDA2050
      D1 = ZERO                                                         LUDA2060
      D2 = ZERO                                                         LUDA2070
 9000 CONTINUE                                                          LUDA2080
C                                  PRINT ERROR                          LUDA2090
      CALL UERTST(IER,6HLUDATF)                                         LUDA2100
 9005 RETURN                                                            LUDA2110
      END                                                               LUDA2120
```

```
C     SUBROUTINE LUELMF (A,B,IPVT,N,IA,X)                                LUEF0010
C                                                                        LUEF0020
C-LUELMF--------S/D-----LIBRARY 1-----------------------------------------LUEF0030
C                                                                        LUEF0040
C    FUNCTION              - ELIMINATION PART OF SOLUTION OF AX=B -       LUEF0050
C                              FULL STORAGE MODE                         LUEF0060
C    USAGE                 - CALL LUELMF (A,B,IPVT,N,IA,X)               LUEF0070
C    PARAMETERS    A       - THE RESULT, LU, COMPUTED IN THE SUBROUTINE  LUEF0080
C                              'LUDATF', WHERE L IS A LOWER TRIANGULAR   LUEF0090
C                              MATRIX WITH ONES ON THE MAIN DIAGONAL. U IS LUEF0100
C                              UPPER TRIANGULAR. L AND U ARE STORED AS A LUEF0110
C                              SINGLE MATRIX A, AND THE UNIT DIAGONAL OF LUEF0120
C                              L IS NOT STORED                           LUEF0130
C                  B       - B IS A VECTOR OF LENGTH N ON THE RIGHT HAND LUEF0140
C                              SIDE OF THE EQUATION AX=B                 LUEF0150
C                  IPVT    - THE PERMUTATION MATRIX RETURNED FROM THE    LUEF0160
C                              SUBROUTINE 'LUDATF', STORED AS AN N LENGTH LUEF0170
C                              VECTOR                                    LUEF0180
C                  N       - ORDER OF A AND NUMBER OF ROWS IN B          LUEF0190
C                  IA      - NUMBER OF ROWS IN THE DIMENSION STATEMENT   LUEF0200
C                              FOR A IN THE CALLING PROGRAM.             LUEF0210
C                  X       - THE RESULT X                                LUEF0220
C    PRECISION             - SINGLE/DOUBLE                               LUEF0230
C    LANGUAGE              - FORTRAN                                     LUEF0240
C-----------------------------------------------------------------------LUEF0250
C    LATEST REVISICN       - APRIL 11,1975                               LUEF0260
C                                                                        LUEF0270
      SUBROUTINE LUELMF (A,B,IPVT,N,IA,X)                                LUEF0280
C                                                                        LUEF0290
      DIMENSION          A(IA,1),B(1),IPVT(1),X(1)                       LUEF0300
CO    DOUBLE PRECISION   A,B,X,SUM                                       LUEF0310
C                                SOLVE LY = B FOR Y                      LUEF0320
      DO 5 I=1,N                                                         LUEF0330
    5 X(I) = B(I)                                                        LUEF0340
      IW = 0                                                             LUEF0350
      DO 20 I=1,N                                                        LUEF0360
```

```
      IP = IPVT(I)                                                    LUEF0370
      SUM = X(IP)                                                     LUEF0380
      X(IP) = X(I)                                                    LUEF0390
      IF (IW .EQ. 0) GO TO 15                                         LUEF0400
      IM1 = I-1                                                       LUEF0410
      DO 10 J=IW,IM1                                                  LUEF0420
         SUM = SUM-A(I,J)*X(J)                                        LUEF0430
10    CONTINUE                                                        LUEF0440
      GO TO 20                                                        LUEF0450
15    IF (SUM .NE. 0.) IW = I                                         LUEF0460
20 X(I) = SUM                                                         LUEF0470
C                                    SOLVE UX = Y FOR X               LUEF0480
      DO 30 IB=1,N                                                    LUEF0490
         I = N+1-IB                                                   LUEF0500
         IP1 = I+1                                                    LUEF0510
         SUM = X(I)                                                   LUEF0520
         IF (IP1 .GT. N) GO TO 30                                     LUEF0530
         DO 25 J=IP1,N                                                LUEF0540
            SUM = SUM-A(I,J)*X(J)                                     LUEF0550
25    CONTINUE                                                        LUEF0560
30 X(I) = SUM/A(I,I)                                                  LUEF0570
      RETURN                                                          LUEF0580
      END                                                             LUEF0590
```

```
C     SUBROUTINE UERTST (IER,NAME)                                      UERT0010
C                                                                       UERT0020
C-UERTST----------------LIBRARY 1-----------------------------------UERT0030
C                                                                       UERT0040
C    FUNCTION              - ERROR MESSAGE GENERATION                   UERT0050
C    USAGE                 - CALL UERTST(IER,NAME)                      UERT0060
C    PARAMETERS    IER     - ERROR PARAMETER. TYPE + N  WHERE           UERT0070
C                              TYPE= 128 IMPLIES TERMINAL ERROR         UERT0080
C                                    64 IMPLIES WARNING WITH FIX        UERT0090
C                                    32 IMPLIES WARNING                 UERT0100
C                              N   = ERROR CODE RELEVANT TO CALLING ROUTINEUERT0110
C                  NAME    - INPUT VECTOR CONTAINING THE NAME OF THE    UERT0120
C                              CALLING ROUTINE AS A SIX CHARACTER LITERAL UERT0130
C                              STRING.                                  UERT0140
C    LANGUAGE              - FORTRAN                                    UERT0150
C-----------------------------------------------------------------------UERT0160
C    LATEST REVISICN       - JANUARY 18, 1974                           UERT0170
C                                                                       UERT0180
      SUBROUTINE UERTST(IER,NAME)                                       UERT0190
C                                                                       UERT0200
      DIMENSION            ITYP(5,4),IBIT(4)                            UERT0210
      INTEGER*2            NAME(3)                                      UERT0220
      INTEGER              WARN,WARF,TERM,PRINTR                        UERT023C
      EQUIVALENCE          (IBIT(1),WARN),(IBIT(2),WARF),(IBIT(3),TERM) UERT0240
      DATA     ITYP        /'WARN','ING ','    ','    ','    ',        UERT025C
     *                      'WARN','ING(','WITH',' FIX',')   ',        UERT026C
     *                      'TERM','INAL','    ','    ','    ',        UERT0270
     *                      'NON-','DEFI','NED ','    ','    '/,       UERT0280
     *         IBIT         / 32,64,128,0/                               UERT0290
      DATA     PRINTR      / 6/                                         UERT0300
      IER2=IER                                                          UERT031C
      IF (IER2 .GE. WARN) GO TO 5                                       UERT0320
C                                  NON-DEFINED                          UERT0330
      IER1=4                                                            UERT0340
      GO TO 20                                                          UERT035C
   5  IF (IER2 .LT. TERM) GO TO 10                                      UERT036C
```

```
C                                     TERMINAL                          UERT0370
      IER1=3                                                            UERT0380
      GO TO 20                                                          UERT0390
   10 IF (IER2 .LT. WARF) GO TO 15                                      UERT0400
C                                     WARNING(WITH FIX)                 UERT0410
      IER1=2                                                            UERT0420
      GO TO 20                                                          UERT0430
C                                     WARNING                           UERT0440
   15 IER1=1                                                            UERT0450
C                                     EXTRACT 'N'                       UERT0460
   20 IER2=IER2-IBIT(IER1)                                              UERT0470
C                                     PRINT ERROR MESSAGE               UERT0480
      WRITE (PRINTR,25) (ITYP(I,IER1),I=1,5),NAME,IER2,IER              UERT0490
   25 FORMAT(' *** I M S L(UERTST) ***  ',5A4,4X,3A2,4X,I2,             UERT0500
     *   ' (IER = ',I3,')')                                             UERT0510
      RETURN                                                            UERT0520
      END                                                               UERT0530
```

A.5 Sample Problem

Table A.5.1 lists the input data for a sample problem, and Table A.5.2 displays the output from the DATANA code.

Table A.5.1

INPUT DATA FOR DATANA SAMPLE PROBLEM

```
    2    0
   0.6                        0.0333333
   42  215  215  85.394   2.42        1.
  256
   14.85                -310.                1806.                -4744.
  16360.                 -21170.               12000.                -2596.
0512 010000 005520 006089 005820 005642
0517 005373 005049 004685 004508 004323
0522 004036 003772 003622 003311 003129
0527 002995 002728 002620 002525 002255
0532 002260 002092 001882 001852 001696
0537 001683 001483 001481 001322 001327
0542 001249 001121 001106 001029 000950
0547 000956 000880 000880 000811 000760
0552 000725 000728 000650 000677 000616
0557 000564 000574 000517 000498 000516
0562 000459 000417 000418 000407 000367
0567 000377 000365 000336 000322 000307
0572 000284 000290 000272 000253 000244
0577 000233 000223 000222 000178 000212
0582 000185 000166 000165 000167 000160
0587 000146 000129 000127 000126 000121
0592 000106 000100 000095 000089 000084
0597 000080 000091 000075 000073 000091
0602 000065 000057 000065 000081 000068
0607 000062 000056 000071 000054 000043
0612 000052 000063 000052 000050 000051
0617 000049 000041 000045 000032 000033
0622 000039 000033 000036 000021 000024
0627 000033 000032 000021 000031 000031
```

```
0632 000022 000022 000025 000025 000017
0637 000022 000024 000022 000011 000019
0642 000016 000015 000014 000016 000016
0647 000017 000011 000017 000005 000014
0652 000012 000014 000011 000013 000011
0657 000012 000014 000008 000008 000007
0662 000006 000007 000009 000008 000006
0667 000004 000011 000007 000010 000007
0672 000009 000007 000008 000009 000001
0677 000001 000010 000005 000008 000001
0682 000006 000003 000005 000006 000001
0687 000005 000002 000003 000001 000003
0692 000004 000006 000002 000003 000002
0697 000004 000004 000005 000004 000001
0702 000000 000003 000002 000001 000001
0707 000001 000003 000001 000002 000003
0712 000002 000002 000001 000001 000003
0717 000000 000005 000003 000002 000002
0722 000004 000003 000001 000002 000001
0727 000001 000001 000005 000000 000001
0732 000002 000003 000002 000001 000002
0737 000002 000002 000000 000001 000003
0742 000001 000000 000000 000002 000000
0747 000001 000003 000001 000000 000001
0752 000000 000001 000000 000001 000000
0757 000002 000000 000003 000001 000000
0762 000000 000002 000000 000000 000001
0767 000003
  256
  -93.53                -268.8                 15340.                -20700.
  19740.                -17850.                11240.                -2972.
0256 006000 009354 010110 009646 009530
0261 009061 008875 008595 008083 007853
0266 007729 007264 007223 006865 006863
0271 006510 006281 006044 005833 005725
0276 005537 005300 005256 005024 004863
```

0281 004825 004679 004353 004255 004135
0286 004126 004012 003706 003751 003769
0291 003562 003576 003425 003151 003254
0296 003087 003113 003019 002997 002739
0301 002837 002642 002732 002637 002653
0306 002491 002394 002418 002288 002287
0311 002200 002176 002092 002069 002062
0316 002043 001986 001924 001869 001784
0321 001766 001734 001768 001711 001675
0326 001615 001582 001495 001421 001541
0331 001408 001358 001404 001377 001386
0336 001272 001282 001280 001235 001208
0341 001277 001201 001092 001156 001120
0346 001179 001110 001003 001085 001003
0351 001013 000934 000913 000940 000976
0356 000931 000892 000925 000910 000805
0361 000875 000841 000808 000756 000787
0366 000787 000705 000764 000712 000671
0371 000714 000678 000680 000700 000618
0376 000624 000625 000578 000603 000619
0381 000610 000561 000567 000571 000541
0386 000556 000529 000548 000547 000508
0391 000549 000447 000509 000480 000485
0396 000460 000422 000473 000456 000402
0401 000410 000419 000410 000378 000407
0406 000359 000368 000357 000361 000366
0411 000355 000349 000371 000346 000361
0416 000349 000320 000339 000310 000291
0421 000320 000317 000295 000290 000303
0426 000281 000279 000280 000260 000296
0431 000251 000275 000269 000248 000232
0436 000232 000260 000253 000253 000216
0441 000229 000221 000226 000205 000207
0446 000228 000209 000199 000193 000196
0451 000211 000203 000195 000179 000191
0456 000184 000171 000171 000191 000184

```
0461 000162 000168 000168 000172 000134
0466 000158 000152 000131 000145 000142
0471 000141 000136 000137 000133 000148
0476 000135 000124 000136 000142 000122
0481 000108 000124 000113 000134 000128
0486 000113 000126 000116 000122 000102
0491 000117 000103 000102 000112 000114
0496 000082 000089 000082 000088 000094
0501 000096 000074 000108 000110 000073
0506 000092 000080 000078 000073 000067
0511 000094
```

Table A.5.2

Output for DATANA Sample Problem

```
IEFF=    2
IRT=     0

A=       0.6000
B=       0.0333

NC1=    42
NC2=   215
NC3=   215
DC=      85.39
CC1=     2.4200
CC2=     1.0000
```

MEASURED DISTRIBUTION

0.1782E+04	0.1987E+04	0.2192E+04	0.2095E+04	0.2031E+04	0.1934E+04	0.1818E+04	0.1687E+04
0.1623E+04	0.1556E+04	0.1453E+04	0.1358E+04	0.1304E+04	0.1192E+04	0.1126E+04	0.1078E+04
0.9821E+03	0.9432E+03	0.9090E+03	0.8118E+03	0.8136E+03	0.7531E+03	0.6775E+03	0.6667E+03
0.6106E+03	0.6059E+03	0.5339E+03	0.5332E+03	0.4759E+03	0.4777E+03	0.4496E+03	0.4036E+03
0.3982E+03	0.3704E+03	0.3420E+03	0.3442E+03	0.3168E+03	0.3168E+03	0.2920E+03	0.2736E+03
0.2610E+03	0.2521E+03	0.2340E+03	0.2437E+03	0.2219E+03	0.2030E+03	0.2066E+03	0.1961E+03
0.1793E+03	0.1859E+03	0.1652E+03	0.1501E+03	0.1505E+03	0.1465E+03	0.1321E+03	0.1357E+03
0.1314E+03	0.1210E+03	0.1159E+03	0.1105E+03	0.1022E+03	0.1044E+03	0.9792E+02	0.9109E+02
0.8784E+02	0.8388E+02	0.8028E+02	0.7992E+02	0.6408E+02	0.7632E+02	0.6660E+02	0.5976E+02
0.5940E+02	0.6012E+02	0.5760E+02	0.5256E+02	0.4644E+02	0.4572E+02	0.4536E+02	0.4356E+02
0.3816E+02	0.3600E+02	0.3420E+02	0.3204E+02	0.3024E+02	0.2880E+02	0.3276E+02	0.2700E+02
0.2628E+02	0.3276E+02	0.2340E+02	0.2052E+02	0.2340E+02	0.2916E+02	0.2448E+02	0.2232E+02
0.2016E+02	0.2556E+02	0.1944E+02	0.1548E+02	0.1872E+02	0.2268E+02	0.1872E+02	0.1800E+02
0.1836E+02	0.1764E+02	0.1476E+02	0.1620E+02	0.1152E+02	0.1188E+02	0.1404E+02	0.1188E+02
0.1296E+02	0.7560E+01	0.8640E+01	0.1188E+02	0.1152E+02	0.7560E+01	0.1116E+02	0.1116E+02
0.7920E+01	0.7920E+01	0.9000E+01	0.9000E+01	0.6120E+01	0.7920E+01	0.8640E+01	0.7920E+01
0.3960E+01	0.6840E+01	0.5760E+01	0.5400E+01	0.5040E+01	0.5760E+01	0.5760E+01	0.6120E+01
0.3960E+01	0.6120E+01	0.1800E+01	0.5040E+01	0.4320E+01	0.5040E+01	0.3960E+01	0.4680E+01
0.3960E+01	0.4320E+01	0.5040E+01	0.2880E+01	0.2880E+01	0.2520E+01	0.2160E+01	0.2520E+01
0.3240E+01	0.2880E+01	0.2160E+01	0.1440E+01	0.3960E+01	0.2520E+01	0.3600E+01	0.2520E+01
0.3240E+01	0.2520E+01	0.2880E+01	0.3240E+01	0.3600E+00	0.3600E+00	0.3600E+01	0.1800E+01
0.2880E+01	0.3600E+00	0.2160E+01	0.1080E+01	0.1800E+01	0.2160E+01	0.3600E+00	0.1800E+01
0.7200E+00	0.1080E+01	0.3600E+00	0.1080E+01	0.1440E+01	0.2160E+01	0.7200E+00	0.1080E+01
0.7200E+00	0.1440E+01	0.1440E+01	0.1800E+01	0.1440E+01	0.3600E+00	0.0	0.1080E+01
0.7200E+00	0.3600E+00	0.3600E+00	0.3600E+00	0.1080E+01	0.3600E+00	0.7200E+00	0.1080E+01
0.7200E+00	0.7200E+00	0.3600E+00	0.3600E+00	0.1080E+01	0.0	0.1800E+01	0.1080E+01
0.7200E+00	0.7200E+00	0.1440E+01	0.1080E+01	0.3600E+00	0.7200E+00	0.3600E+00	0.3600E+00
0.3600E+00	0.1800E+01	0.0	0.3600E+00	0.7200E+00	0.1080E+01	0.7200E+00	0.3600E+00
0.7200E+00	0.7200E+00	0.7200E+00	0.0	0.3600E+00	0.1080E+01	0.3600E+00	0.0
0.0	0.7200E+00	0.0	0.3600E+00	0.1080E+01	0.3600E+00	0.0	0.3600E+00
0.0	0.3600E+00	0.0	0.3600E+00	0.0	0.7200E+00	0.0	0.1080E+01
0.3600E+00	0.0	0.0	0.7200E+00	0.0	0.0	0.3600E+00	0.1080E+01

VOLTAGE DISTRIBUTION

0.6333E+00	0.6667E+00	0.7000E+00	0.7333E+00	0.7667E+00	0.8000E+00	0.8333E+00	0.8667E+00
0.9000E+00	0.9333E+00	0.9667E+00	0.1000E+01	0.1033E+01	0.1067E+01	0.1100E+01	0.1133E+01
0.1167E+01	0.1200E+01	0.1233E+01	0.1267E+01	0.1300E+01	0.1333E+01	0.1367E+01	0.1400E+01
0.1433E+01	0.1467E+01	0.1500E+01	0.1533E+01	0.1567E+01	0.1600E+01	0.1633E+01	0.1667E+01
0.1700E+01	0.1733E+01	0.1767E+01	0.1800E+01	0.1833E+01	0.1867E+01	0.1900E+01	0.1933E+01
0.1967E+01	0.2000E+01	0.2033E+01	0.2067E+01	0.2100E+01	0.2133E+01	0.2167E+01	0.2200E+01
0.2233E+01	0.2267E+01	0.2300E+01	0.2333E+01	0.2367E+01	0.2400E+01	0.2433E+01	0.2467E+01
0.2500E+01	0.2533E+01	0.2567E+01	0.2600E+01	0.2633E+01	0.2667E+01	0.2700E+01	0.2733E+01
0.2767E+01	0.2800E+01	0.2833E+01	0.2867E+01	0.2900E+01	0.2933E+01	0.2967E+01	0.3000E+01
0.3033E+01	0.3067E+01	0.3100E+01	0.3133E+01	0.3167E+01	0.3200E+01	0.3233E+01	0.3267E+01
0.3300E+01	0.3333E+01	0.3367E+01	0.3400E+01	0.3433E+01	0.3467E+01	0.3500E+01	0.3533E+01
0.3567E+01	0.3600E+01	0.3633E+01	0.3667E+01	0.3700E+01	0.3733E+01	0.3767E+01	0.3800E+01
0.3833E+01	0.3867E+01	0.3900E+01	0.3933E+01	0.3967E+01	0.4000E+01	0.4033E+01	0.4067E+01
0.4100E+01	0.4133E+01	0.4167E+01	0.4200E+01	0.4233E+01	0.4267E+01	0.4300E+01	0.4333E+01
0.4367E+01	0.4400E+01	0.4433E+01	0.4467E+01	0.4500E+01	0.4533E+01	0.4567E+01	0.4600E+01
0.4633E+01	0.4667E+01	0.4700E+01	0.4733E+01	0.4767E+01	0.4800E+01	0.4833E+01	0.4867E+01
0.4900E+01	0.4933E+01	0.4967E+01	0.5000E+01	0.5033E+01	0.5067E+01	0.5100E+01	0.5133E+01

0.5167E+01	0.5200E+01	0.5233E+01	0.5267E+01	0.5300E+01	0.5333E+01	0.5367E+01	0.5400E+01
0.5433E+01	0.5467E+01	0.5500E+01	0.5533E+01	0.5567E+01	0.5600E+01	0.5633E+01	0.5667E+01
0.5700E+01	0.5733E+01	0.5767E+01	0.5800E+01	0.5833E+01	0.5867E+01	0.5900E+01	0.5933E+01
0.5967E+01	0.6000E+01	0.6033E+01	0.6067E+01	0.6100E+01	0.6133E+01	0.6167E+01	0.6200E+01
0.6233E+01	0.6267E+01	0.6300E+01	0.6333E+01	0.6367E+01	0.6400E+01	0.6433E+01	0.6467E+01
0.6500E+01	0.6533E+01	0.6567E+01	0.6600E+01	0.6633E+01	0.6667E+01	0.6700E+01	0.6733E+01
0.6767E+01	0.6800E+01	0.6833E+01	0.6867E+01	0.6900E+01	0.6933E+01	0.6967E+01	0.7000E+01
0.7033E+01	0.7067E+01	0.7100E+01	0.7133E+01	0.7167E+01	0.7200E+01	0.7233E+01	0.7267E+01
0.7300E+01	0.7333E+01	0.7367E+01	0.7400E+01	0.7433E+01	0.7467E+01	0.7500E+01	0.7533E+01
0.7567E+01	0.7600E+01	0.7633E+01	0.7667E+01	0.7700E+01	0.7733E+01	0.7767E+01	0.7800E+01
0.7833E+01	0.7867E+01	0.7900E+01	0.7933E+01	0.7967E+01	0.8000E+01	0.8033E+01	0.8067E+01
0.8100E+01	0.8133E+01	0.8167E+01	0.8200E+01	0.8233E+01	0.8267E+01	0.8300E+01	0.8333E+01
0.8367E+01	0.8400E+01	0.8433E+01	0.8467E+01	0.8500E+01	0.8533E+01	0.8567E+01	0.8600E+01
0.8633E+01	0.8667E+01	0.8700E+01	0.8733E+01	0.8767E+01	0.8800E+01	0.8833E+01	0.8867E+01
0.8900E+01	0.8933E+01	0.8967E+01	0.9000E+01	0.9033E+01	0.9067E+01	0.9100E+01	0.9133E+01

IER= 0

LEAST SQUARE FITTING PARAMETERS ARE

0.2192E+02	-0.3854E+03	0.2008E+04	-0.8842E+04	0.1622E+05	-0.2110E+05	0.1207E+05	-0.2631E+04

LAST CHANNEL NUMBER IS 178

FITTED DISTRIBUTION

0.1776E+04	0.2048E+04	0.2119E+04	0.2093E+04	0.2021E+04	0.1930E+04	0.1831E+04	0.1731E+04
0.1632E+04	0.1538E+04	0.1448E+04	0.1362E+04	0.1282E+04	0.1206E+04	0.1134E+04	0.1066E+04
0.1003E+04	0.9439E+03	0.8883E+03	0.8362E+03	0.7874E+03	0.7418E+03	0.6990E+03	0.6591E+03
0.6216E+03	0.5866E+03	0.5538E+03	0.5231E+03	0.4944E+03	0.4675E+03	0.4422E+03	0.4186E+03
0.3964E+03	0.3756E+03	0.3560E+03	0.3377E+03	0.3204E+03	0.3042E+03	0.2890E+03	0.2746E+03
0.2611E+03	0.2484E+03	0.2364E+03	0.2251E+03	0.2144E+03	0.2043E+03	0.1948E+03	0.1858E+03
0.1773E+03	0.1692E+03	0.1616E+03	0.1543E+03	0.1475E+03	0.1410E+03	0.1349E+03	0.1290E+03
0.1234E+03	0.1182E+03	0.1132E+03	0.1084E+03	0.1039E+03	0.9953E+02	0.9542E+02	0.9150E+02
0.8777E+02	0.8421E+02	0.8081E+02	0.7757E+02	0.7448E+02	0.7152E+02	0.6870E+02	0.6600E+02
0.6342E+02	0.6095E+02	0.5859E+02	0.5632E+02	0.5416E+02	0.5209E+02	0.5010E+02	0.4819E+02
0.4637E+02	0.4462E+02	0.4294E+02	0.4132E+02	0.3977E+02	0.3829E+02	0.3686E+02	0.3549E+02
0.3417E+02	0.3290E+02	0.3168E+02	0.3051E+02	0.2939E+02	0.2830E+02	0.2726E+02	0.2625E+02
0.2528E+02	0.2435E+02	0.2345E+02	0.2259E+02	0.2176E+02	0.2095E+02	0.2018E+02	0.1943E+02
0.1871E+02	0.1802E+02	0.1735E+02	0.1670E+02	0.1608E+02	0.1547E+02	0.1489E+02	0.1433E+02
0.1379E+02	0.1327E+02	0.1276E+02	0.1227E+02	0.1180E+02	0.1135E+02	0.1091E+02	0.1048E+02
0.1007E+02	0.9674E+01	0.9290E+01	0.8919E+01	0.8560E+01	0.8214E+01	0.7878E+01	0.7554E+01
0.7241E+01	0.6938E+01	0.6645E+01	0.6362E+01	0.6088E+01	0.5823E+01	0.5566E+01	0.5318E+01
0.5079E+01	0.4847E+01	0.4623E+01	0.4406E+01	0.4196E+01	0.3993E+01	0.3797E+01	0.3607E+01
0.3424E+01	0.3247E+01	0.3075E+01	0.2910E+01	0.2749E+01	0.2594E+01	0.2445E+01	0.2300E+01
0.2160E+01	0.2025E+01	0.1895E+01	0.1768E+01	0.1647E+01	0.1529E+01	0.1416E+01	0.1306E+01
0.1200E+01	0.1098E+01	0.9995E+00	0.9045E+00	0.8128E+00	0.7245E+00	0.6393E+00	0.5573E+00
0.4783E+00	0.4022E+00	0.3289E+00	0.2584E+00	0.1906E+00	0.1253E+00	0.6268E-01	0.2482E-02
0.0	0.0						

DIAMETER DISTRIBUTION

0.2439E+02	0.2502E+02	0.2564E+02	0.2626E+02	0.2683E+02	0.2741E+02	0.2797E+02	0.2853E+02
0.2907E+02	0.2960E+02	0.3013E+02	0.3064E+02	0.3115E+02	0.3165E+02	0.3214E+02	0.3262E+02
0.3310E+02	0.3357E+02	0.3403E+02	0.3449E+02	0.3494E+02	0.3538E+02	0.3582E+02	0.3626E+02
0.3668E+02	0.3711E+02	0.3753E+02	0.3794E+02	0.3835E+02	0.3876E+02	0.3916E+02	0.3956E+02
0.3995E+02	0.4034E+02	0.4073E+02	0.4111E+02	0.4149E+02	0.4186E+02	0.4224E+02	0.4261E+02
0.4297E+02	0.4333E+02	0.4369E+02	0.4405E+02	0.4440E+02	0.4475E+02	0.4510E+02	0.4545E+02
0.4579E+02	0.4613E+02	0.4647E+02	0.4681E+02	0.4714E+02	0.4747E+02	0.4780E+02	0.4812E+02
0.4845E+02	0.4877E+02	0.4909E+02	0.4941E+02	0.4972E+02	0.5004E+02	0.5035E+02	0.5066E+02
0.5097E+02	0.5127E+02	0.5158E+02	0.5188E+02	0.5218E+02	0.5248E+02	0.5278E+02	0.5307E+02
0.5337E+02	0.5366E+02	0.5395E+02	0.5424E+02	0.5453E+02	0.5481E+02	0.5510E+02	0.5538E+02
0.5566E+02	0.5594E+02	0.5622E+02	0.5650E+02	0.5678E+02	0.5705E+02	0.5732E+02	0.5760E+02
0.5787E+02	0.5814E+02	0.5841E+02	0.5867E+02	0.5894E+02	0.5921E+02	0.5947E+02	0.5973E+02
0.5999E+02	0.6025E+02	0.6051E+02	0.6077E+02	0.6103E+02	0.6128E+02	0.6154E+02	0.6179E+02
0.6204E+02	0.6230E+02	0.6255E+02	0.6280E+02	0.6305E+02	0.6329E+02	0.6354E+02	0.6379E+02
0.6403E+02	0.6427E+02	0.6452E+02	0.6476E+02	0.6500E+02	0.6524E+02	0.6548E+02	0.6572E+02
0.6596E+02	0.6619E+02	0.6643E+02	0.6666E+02	0.6690E+02	0.6713E+02	0.6736E+02	0.6760E+02
0.6783E+02	0.6806E+02	0.6829E+02	0.6852E+02	0.6874E+02	0.6897E+02	0.6920E+02	0.6942E+02
0.6965E+02	0.6987E+02	0.7010E+02	0.7032E+02	0.7054E+02	0.7076E+02	0.7098E+02	0.7120E+02
0.7142E+02	0.7164E+02	0.7186E+02	0.7208E+02	0.7229E+02	0.7251E+02	0.7273E+02	0.7294E+02
0.7316E+02	0.7337E+02	0.7358E+02	0.7379E+02	0.7401E+02	0.7422E+02	0.7443E+02	0.7464E+02
0.7485E+02	0.7506E+02	0.7526E+02	0.7547E+02	0.7568E+02	0.7589E+02	0.7609E+02	0.7630E+02
0.7650E+02	0.7671E+02	0.7691E+02	0.7711E+02	0.7732E+02	0.7752E+02	0.7772E+02	0.7792E+02
0.7812E+02							

TRUE SPECTRUM

-0.2765E+03	-0.7414E+02	0.2347E+02	0.6935E+02	0.8974E+02	0.9742E+02	0.9865E+02	0.9678E+02
0.9333E+02	0.8915E+02	0.8465E+02	0.8010E+02	0.7556E+02	0.7118E+02	0.6693E+02	0.6286E+02
0.5898E+02	0.5532E+02	0.5184E+02	0.4857E+02	0.4549E+02	0.4259E+02	0.3988E+02	0.3732E+02
0.3495E+02	0.3273E+02	0.3065E+02	0.2872E+02	0.2691E+02	0.2523E+02	0.2366E+02	0.2219E+02
0.2082E+02	0.1954E+02	0.1835E+02	0.1724E+02	0.1621E+02	0.1525E+02	0.1435E+02	0.1351E+02
0.1273E+02	0.1200E+02	0.1132E+02	0.1068E+02	0.1008E+02	0.9526E+01	0.9005E+01	0.8515E+01
0.8058E+01	0.7629E+01	0.7226E+01	0.6848E+01	0.6493E+01	0.6160E+01	0.5847E+01	0.5552E+01
0.5275E+01	0.5014E+01	0.4768E+01	0.4536E+01	0.4319E+01	0.4112E+01	0.3917E+01	0.3734E+01
0.3561E+01	0.3396E+01	0.3241E+01	0.3094E+01	0.2956E+01	0.2824E+01	0.2699E+01	0.2581E+01
0.2469E+01	0.2362E+01	0.2261E+01	0.2165E+01	0.2074E+01	0.1987E+01	0.1905E+01	0.1826E+01
0.1752E+01	0.1680E+01	0.1613E+01	0.1548E+01	0.1487E+01	0.1428E+01	0.1372E+01	0.1318E+01
0.1267E+01	0.1218E+01	0.1172E+01	0.1127E+01	0.1085E+01	0.1044E+01	0.1005E+01	0.9677E+00
0.9320E+00	0.8977E+00	0.8649E+00	0.8335E+00	0.8034E+00	0.7743E+00	0.7467E+00	0.7201E+00
0.6946E+00	0.6700E+00	0.6464E+00	0.6239E+00	0.6021E+00	0.5812E+00	0.5611E+00	0.5417E+00
0.5231E+00	0.5052E+00	0.4880E+00	0.4714E+00	0.4554E+00	0.4399E+00	0.4252E+00	0.4108E+00
0.3971E+00	0.3838E+00	0.3709E+00	0.3587E+00	0.3467E+00	0.3352E+00	0.3241E+00	0.3134E+00
0.3030E+00	0.2930E+00	0.2833E+00	0.2740E+00	0.2650E+00	0.2563E+00	0.2479E+00	0.2397E+00
0.2319E+00	0.2242E+00	0.2168E+00	0.2097E+00	0.2028E+00	0.1961E+00	0.1897E+00	0.1834E+00
0.1773E+00	0.1714E+00	0.1657E+00	0.1602E+00	0.1549E+00	0.1497E+00	0.1447E+00	0.1398E+00
0.1351E+00	0.1305E+00	0.1261E+00	0.1218E+00	0.1176E+00	0.1135E+00	0.1096E+00	0.1058E+00
0.1021E+00	0.9852E-01	0.9500E-01	0.9165E-01	0.8835E-01	0.8515E-01	0.8205E-01	0.7902E-01
0.7610E-01	0.7326E-01	0.7051E-01	0.6782E-01	0.6522E-01	0.6267E-01	0.6020E-01	0.2482E-02

MEASURED DISTRIBUTION

0.5159E+04	0.5612E+04	0.6066E+04	0.5788E+04	0.5718E+04	0.5837E+04	0.5325E+04	0.5157E+04
0.4859E+04	0.4712E+04	0.4637E+04	0.4358E+04	0.4334E+04	0.4119E+04	0.4118E+04	0.3906E+04
0.3769E+04	0.3626E+04	0.3500E+04	0.3435E+04	0.3322E+04	0.3180E+04	0.3154E+04	0.3014E+04
0.2919E+04	0.2895E+04	0.2807E+04	0.2612E+04	0.2553E+04	0.2481E+04	0.2476E+04	0.2407E+04
0.2224E+04	0.2251E+04	0.2261E+04	0.2137E+04	0.2146E+04	0.2055E+04	0.1891E+04	0.1952E+04
0.1852E+04	0.1869E+04	0.1811E+04	0.1798E+04	0.1643E+04	0.1702E+04	0.1585E+04	0.1619E+04
0.1582E+04	0.1592E+04	0.1495E+04	0.1436E+04	0.1451E+04	0.1373E+04	0.1372E+04	0.1320E+04
0.1306E+04	0.1255E+04	0.1241E+04	0.1237E+04	0.1226E+04	0.1192E+04	0.1154E+04	0.1121E+04
0.1070E+04	0.1060E+04	0.1040E+04	0.1061E+04	0.1027E+04	0.1005E+04	0.9690E+03	0.9492E+03
0.8970E+03	0.8526E+03	0.9246E+03	0.8448E+03	0.8148E+03	0.8424E+03	0.8262E+03	0.8316E+03
0.7632E+03	0.7692E+03	0.7680E+03	0.7410E+03	0.7248E+03	0.7662E+03	0.7206E+03	0.6552E+03
0.6936E+03	0.6720E+03	0.7074E+03	0.6660E+03	0.6018E+03	0.6510E+03	0.6018E+03	0.6078E+03
0.5604E+03	0.5478E+03	0.5640E+03	0.5856E+03	0.5586E+03	0.5352E+03	0.5550E+03	0.5460E+03
0.4830E+03	0.5250E+03	0.5046E+03	0.4848E+03	0.4536E+03	0.4722E+03	0.4722E+03	0.4230E+03
0.4584E+03	0.4272E+03	0.4026E+03	0.4284E+03	0.4068E+03	0.4080E+03	0.4200E+03	0.3708E+03
0.3744E+03	0.3750E+03	0.3468E+03	0.3618E+03	0.3714E+03	0.3660E+03	0.3366E+03	0.3402E+03
0.3426E+03	0.3246E+03	0.3336E+03	0.3174E+03	0.3288E+03	0.3282E+03	0.3048E+03	0.3294E+03
0.2682E+03	0.3054E+03	0.2880E+03	0.2910E+03	0.2760E+03	0.2532E+03	0.2838E+03	0.2736E+03
0.2412E+03	0.2460E+03	0.2514E+03	0.2460E+03	0.2268E+03	0.2442E+03	0.2154E+03	0.2208E+03
0.2142E+03	0.2166E+03	0.2196E+03	0.2130E+03	0.2094E+03	0.2226E+03	0.2076E+03	0.2166E+03
0.2094E+03	0.1920E+03	0.2034E+03	0.1860E+03	0.1746E+03	0.1920E+03	0.1902E+03	0.1770E+03
0.1740E+03	0.1818E+03	0.1686E+03	0.1674E+03	0.1680E+03	0.1560E+03	0.1776E+03	0.1506E+03
0.1650E+03	0.1614E+03	0.1488E+03	0.1392E+03	0.1392E+03	0.1550E+03	0.1518E+03	0.1518E+03
0.1296E+03	0.1374E+03	0.1326E+03	0.1356E+03	0.1230E+03	0.1242E+03	0.1368E+03	0.1254E+03
0.1194E+03	0.1158E+03	0.1176E+03	0.1266E+03	0.1218E+03	0.1170E+03	0.1074E+03	0.1146E+03
0.1104E+03	0.1026E+03	0.1026E+03	0.1146E+03	0.1104E+03	0.9720E+02	0.1008E+03	0.1008E+03
0.1032E+03	0.8040E+02	0.9480E+02	0.9120E+02	0.7860E+02	0.8700E+02	0.8520E+02	0.8460E+02
0.8160E+02	0.8220E+02	0.7980E+02	0.8880E+02	0.8100E+02	0.7440E+02	0.8160E+02	0.8520E+02
0.7320E+02	0.6480E+02	0.7440E+02	0.6780E+02	0.8040E+02	0.7680E+02	0.6780E+02	0.7560E+02
0.6960E+02	0.7320E+02	0.6120E+02	0.7020E+02	0.6180E+02	0.6120E+02	0.6720E+02	0.6840E+02
0.4920E+02	0.5340E+02	0.4920E+02	0.5280E+02	0.5640E+02	0.5760E+02	0.4440E+02	0.6480E+02
0.6600E+02	0.4380E+02	0.5520E+02	0.4860E+02	0.4680E+02	0.4380E+02	0.4020E+02	0.5640E+02

VOLTAGE DISTRIBUTION

0.6333E+00	0.6667E+00	0.7000E+00	0.7333E+00	0.7667E+00	0.8000E+00	0.8333E+00	0.8667E+00
0.9000E+00	0.9333E+00	0.9667E+00	0.1000E+01	0.1033E+01	0.1067E+01	0.1100E+01	0.1133E+01
0.1167E+01	0.1200E+01	0.1233E+01	0.1267E+01	0.1300E+01	0.1333E+01	0.1367E+01	0.1400E+01
0.1433E+01	0.1467E+01	0.1500E+01	0.1533E+01	0.1567E+01	0.1600E+01	0.1633E+01	0.1667E+01
0.1700E+01	0.1733E+01	0.1767E+01	0.1800E+01	0.1833E+01	0.1867E+01	0.1900E+01	0.1933E+01
0.1967E+01	0.2000E+01	0.2033E+01	0.2067E+01	0.2100E+01	0.2133E+01	0.2167E+01	0.2200E+01
0.2233E+01	0.2267E+01	0.2300E+01	0.2333E+01	0.2367E+01	0.2400E+01	0.2433E+01	0.2467E+01
0.2500E+01	0.2533E+01	0.2567E+01	0.2600E+01	0.2633E+01	0.2667E+01	0.2700E+01	0.2733E+01
0.2767E+01	0.2800E+01	0.2833E+01	0.2867E+01	0.2900E+01	0.2933E+01	0.2967E+01	0.3000E+01
0.3033E+01	0.3067E+01	0.3100E+01	0.3133E+01	0.3167E+01	0.3200E+01	0.3233E+01	0.3267E+01
0.3300E+01	0.3333E+01	0.3367E+01	0.3400E+01	0.3433E+01	0.3467E+01	0.3500E+01	0.3533E+01
0.3567E+01	0.3600E+01	0.3633E+01	0.3667E+01	0.3700E+01	0.3733E+01	0.3767E+01	0.3800E+01
0.3833E+01	0.3867E+01	0.3900E+01	0.3933E+01	0.3967E+01	0.4000E+01	0.4033E+01	0.4067E+01
0.4100E+01	0.4133E+01	0.4167E+01	0.4200E+01	0.4233E+01	0.4267E+01	0.4300E+01	0.4333E+01
0.4367E+01	0.4400E+01	0.4433E+01	0.4467E+01	0.4500E+01	0.4533E+01	0.4567E+01	0.4600E+01
0.4633E+01	0.4667E+01	0.4700E+01	0.4733E+01	0.4767E+01	0.4800E+01	0.4833E+01	0.4867E+01
0.4900E+01	0.4933E+01	0.4967E+01	0.5000E+01	0.5033E+01	0.5067E+01	0.5100E+01	0.5133E+01

0.5167E+01	0.5200E+01	0.5233E+01	0.5267E+01	0.5300E+01	0.5333E+01	0.5367E+01	0.5400E+01
0.5433E+01	0.5467E+01	0.5500E+01	0.5533E+01	0.5567E+01	0.5600E+01	0.5633E+01	0.5667E+01
0.5700E+01	0.5733E+01	0.5767E+01	0.5800E+01	0.5833E+01	0.5867E+01	0.5900E+01	0.5933E+01
0.5967E+01	0.6000E+01	0.6033E+01	0.6067E+01	0.6100E+01	0.6133E+01	0.6167E+01	0.6200E+01
0.6233E+01	0.6267E+01	0.6300E+01	0.6333E+01	0.6367E+01	0.6400E+01	0.6433E+01	0.6467E+01
0.6500E+01	0.6533E+01	0.6567E+01	0.6600E+01	0.6633E+01	0.6667E+01	0.6700E+01	0.6733E+01
0.6767E+01	0.6800E+01	0.6833E+01	0.6867E+01	0.6900E+01	0.6933E+01	0.6967E+01	0.7000E+01
0.7033E+01	0.7067E+01	0.7100E+01	0.7133E+01	0.7167E+01	0.7200E+01	0.7233E+01	0.7267E+01
0.7300E+01	0.7333E+01	0.7367E+01	0.7400E+01	0.7433E+01	0.7467E+01	0.7500E+01	0.7533E+01
0.7567E+01	0.7600E+01	0.7633E+01	0.7667E+01	0.7700E+01	0.7733E+01	0.7767E+01	0.7800E+01
0.7833E+01	0.7867E+01	0.7900E+01	0.7933E+01	0.7967E+01	0.8000E+01	0.8033E+01	0.8067E+01
0.8100E+01	0.8133E+01	0.8167E+01	0.8200E+01	0.8233E+01	0.8267E+01	0.8300E+01	0.8333E+01
0.8367E+01	0.8400E+01	0.8433E+01	0.8467E+01	0.8500E+01	0.8533E+01	0.8567E+01	0.8600E+01
0.8633E+01	0.8667E+01	0.8700E+01	0.8733E+01	0.8767E+01	0.8800E+01	0.8833E+01	0.8867E+01
0.8900E+01	0.8933E+01	0.8967E+01	0.9000E+01	0.9033E+01	0.9067E+01	0.9100E+01	0.9133E+01

IER= 0

LEAST SQUARE FITTING PARAMETERS ARE

-0.9527E+02	-0.2618E+03	0.1535E+05	-0.2074E+05	0.1976E+05	-0.1784E+05	0.1123E+05	-0.2971E+04

LAST CHANNEL NUMBER IS 302

FITTED DISTRIBUTION

0.5134E+04	0.5733E+04	0.5893E+04	0.5842E+04	0.5695E+04	0.5509E+04	0.5312E+04	0.5117E+04
0.4930E+04	0.4752E+04	0.4584E+04	0.4425E+04	0.4276E+04	0.4134E+04	0.3999E+04	0.3871E+04
0.3749E+04	0.3632E+04	0.3520E+04	0.3413E+04	0.3310E+04	0.3211E+04	0.3116E+04	0.3025E+04
0.2937E+04	0.2853E+04	0.2771E+04	0.2693E+04	0.2617E+04	0.2545E+04	0.2475E+04	0.2407E+04
0.2342E+04	0.2279E+04	0.2218E+04	0.2159E+04	0.2103E+04	0.2048E+04	0.1996E+04	0.1945E+04
0.1895E+04	0.1848E+04	0.1802E+04	0.1757E+04	0.1714E+04	0.1673E+04	0.1632E+04	0.1593E+04
0.1556E+04	0.1519E+04	0.1484E+04	0.1449E+04	0.1416E+04	0.1384E+04	0.1352E+04	0.1322E+04
0.1293E+04	0.1264E+04	0.1236E+04	0.1209E+04	0.1183E+04	0.1158E+04	0.1133E+04	0.1109E+04
0.1086E+04	0.1063E+04	0.1041E+04	0.1019E+04	0.9986E+03	0.9782E+03	0.9585E+03	0.9392E+03
0.9204E+03	0.9022E+03	0.8844E+03	0.8670E+03	0.8501E+03	0.8337E+03	0.8176E+03	0.8019E+03
0.7867E+03	0.7719E+03	0.7572E+03	0.7430E+03	0.7292E+03	0.7157E+03	0.7024E+03	0.6896E+03
0.6770E+03	0.6647E+03	0.6526E+03	0.6409E+03	0.6294E+03	0.6182E+03	0.6072E+03	0.5965E+03
0.5860E+03	0.5757E+03	0.5657E+03	0.5558E+03	0.5462E+03	0.5368E+03	0.5276E+03	0.5186E+03
0.5097E+03	0.5011E+03	0.4926E+03	0.4843E+03	0.4762E+03	0.4682E+03	0.4604E+03	0.4527E+03
0.4452E+03	0.4379E+03	0.4307E+03	0.4236E+03	0.4167E+03	0.4099E+03	0.4032E+03	0.3967E+03
0.3903E+03	0.3840E+03	0.3778E+03	0.3717E+03	0.3657E+03	0.3599E+03	0.3542E+03	0.3485E+03
0.3430E+03	0.3376E+03	0.3322E+03	0.3270E+03	0.3218E+03	0.3168E+03	0.3118E+03	0.3069E+03
0.3021E+03	0.2974E+03	0.2927E+03	0.2882E+03	0.2837E+03	0.2793E+03	0.2749E+03	0.2707E+03
0.2665E+03	0.2624E+03	0.2583E+03	0.2543E+03	0.2504E+03	0.2465E+03	0.2427E+03	0.2390E+03
0.2353E+03	0.2317E+03	0.2281E+03	0.2246E+03	0.2211E+03	0.2177E+03	0.2144E+03	0.2111E+03
0.2078E+03	0.2046E+03	0.2015E+03	0.1983E+03	0.1953E+03	0.1923E+03	0.1893E+03	0.1864E+03
0.1835E+03	0.1807E+03	0.1779E+03	0.1751E+03	0.1724E+03	0.1697E+03	0.1671E+03	0.1645E+03
0.1619E+03	0.1594E+03	0.1569E+03	0.1544E+03	0.1520E+03	0.1496E+03	0.1472E+03	0.1449E+03
0.1426E+03	0.1403E+03	0.1381E+03	0.1359E+03	0.1337E+03	0.1316E+03	0.1295E+03	0.1274E+03
0.1253E+03	0.1233E+03	0.1213E+03	0.1193E+03	0.1173E+03	0.1154E+03	0.1135E+03	0.1116E+03
0.1097E+03	0.1079E+03	0.1061E+03	0.1043E+03	0.1025E+03	0.1008E+03	0.9908E+02	0.9738E+02

0.9570E+02	0.9404E+02	0.9241E+02	0.9079E+02	0.8919E+02	0.8761E+02	0.8605E+02	0.8451E+02
0.8299E+02	0.8148E+02	0.8000E+02	0.7853E+02	0.7708E+02	0.7564E+02	0.7423E+02	0.7282E+02
0.7144E+02	0.7007E+02	0.6872E+02	0.6738E+02	0.6606E+02	0.6475E+02	0.6346E+02	0.6218E+02
0.6092E+02	0.5967E+02	0.5844E+02	0.5722E+02	0.5601E+02	0.5482E+02	0.5364E+02	0.5247E+02
0.5132E+02	0.5017E+02	0.4904E+02	0.4793E+02	0.4682E+02	0.4573E+02	0.4465E+02	0.4358E+02
0.4252E+02	0.4147E+02	0.4044E+02	0.3941E+02	0.3840E+02	0.3740E+02	0.3640E+02	0.3542E+02
0.3445E+02	0.3349E+02	0.3254E+02	0.3159E+02	0.3066E+02	0.2974E+02	0.2883E+02	0.2792E+02
0.2703E+02	0.2614E+02	0.2526E+02	0.2440E+02	0.2354E+02	0.2269E+02	0.2184E+02	0.2101E+02
0.2018E+02	0.1937E+02	0.1856E+02	0.1776E+02	0.1696E+02	0.1618E+02	0.1540E+02	0.1463E+02
0.1386E+02	0.1311E+02	0.1236E+02	0.1162E+02	0.1088E+02	0.1016E+02	0.9437E+01	0.8723E+01
0.8017E+01	0.7316E+01	0.6623E+01	0.5936E+01	0.5255E+01	0.4581E+01	0.3913E+01	0.3251E+01
0.2595E+01	0.1946E+01	0.1302E+01	0.6640E+00	0.3200E-01	-0.5943E+00		

DIAMETER DISTRIBUTION

0.2439E+02	0.2502E+02	0.2564E+02	0.2624E+02	0.2683E+02	0.2741E+02	0.2797E+02	0.2853E+02
0.2907E+02	0.2960E+02	0.3013E+02	0.3064E+02	0.3115E+02	0.3165E+02	0.3214E+02	0.3262E+02
0.3310E+02	0.3357E+02	0.3403E+02	0.3449E+02	0.3494E+02	0.3538E+02	0.3582E+02	0.3626E+02
0.366PE+02	0.3711E+02	0.3753E+02	0.3794E+02	0.3835E+02	0.3876E+02	0.3916E+02	0.3956E+02
0.3995E+02	0.4034E+02	0.4073E+02	0.4111E+02	0.4149E+02	0.4186E+02	0.4224E+02	0.4261E+02
0.4297E+02	0.4333E+02	0.4369E+02	0.4405E+02	0.4440E+02	0.4475E+02	0.4510E+02	0.4545E+02
0.4579E+02	0.4613E+02	0.4647E+02	0.4681E+02	0.4714E+02	0.4747E+02	0.4780E+02	0.4812E+02
0.4845E+02	0.4877E+02	0.4909E+02	0.4941E+02	0.4972E+02	0.5004E+02	0.5035E+02	0.5066E+02
0.5097E+02	0.5127E+02	0.5158E+02	0.5188E+02	0.5218E+02	0.5248E+02	0.5278E+02	0.5307E+02
0.5337E+02	0.5366E+02	0.5395E+02	0.5424E+02	0.5453E+02	0.5481E+02	0.5510E+02	0.5538E+02
0.5566E+02	0.5594E+02	0.5622E+02	0.5650E+02	0.5678E+02	0.5705E+02	0.5732E+02	0.5760E+02
0.5787E+02	0.5814E+02	0.5841E+02	0.5867E+02	0.5894E+02	0.5921E+02	0.5947E+02	0.5973E+02
0.5999E+02	0.6025E+02	0.6051E+02	0.6077E+02	0.6103E+02	0.6128E+02	0.6154E+02	0.6179E+02
0.6204E+02	0.6230E+02	0.6255E+02	0.6280E+02	0.6305E+02	0.6329E+02	0.6354E+02	0.6379E+02
0.6403E+02	0.6427E+02	0.6452E+02	0.6476E+02	0.6500E+02	0.6524E+02	0.6548E+02	0.6572E+02
0.6596E+02	0.6619E+02	0.6643E+02	0.6666E+02	0.6690E+02	0.6713E+02	0.6736E+02	0.6760E+02
0.6783E+02	0.6806E+02	0.6829E+02	0.6852E+02	0.6874E+02	0.6897E+02	0.6920E+02	0.6942E+02
0.6965E+02	0.6987E+02	0.7010E+02	0.7032E+02	0.7054E+02	0.7076E+02	0.7099E+02	0.7120E+02
0.7142E+02	0.7164E+02	0.7186E+02	0.7208E+02	0.7229E+02	0.7251E+02	0.7273E+02	0.7294E+02
0.7316E+02	0.7337E+02	0.7358E+02	0.7379E+02	0.7401E+02	0.7422E+02	0.7443E+02	0.7464E+02
0.7485E+02	0.7506E+02	0.7526E+02	0.7547E+02	0.7568E+02	0.7589E+02	0.7609E+02	0.7630E+02
0.7650E+02	0.7671E+02	0.7691E+02	0.7711E+02	0.7732E+02	0.7752E+02	0.7772E+02	0.7792E+02
0.7812E+02	0.7832E+02	0.7852E+02	0.7872E+02	0.7892E+02	0.7912E+02	0.7931E+02	0.7951E+02
0.7971E+02	0.7990E+02	0.8010E+02	0.8029E+02	0.8049E+02	0.8068E+02	0.8088E+02	0.8107E+02
0.8126E+02	0.8145E+02	0.8165E+02	0.8184E+02	0.8203E+02	0.8222E+02	0.8241E+02	0.8260E+02
0.8279E+02	0.8298E+02	0.8317E+02	0.8335E+02	0.8354E+02	0.8373E+02	0.8392E+02	0.8410E+02
0.8429E+02	0.8447E+02	0.8466E+02	0.8484E+02	0.8503E+02	0.8521E+02	0.8539E+02	0.8558E+02
0.8576E+02	0.8594E+02	0.8612E+02	0.8631E+02	0.8649E+02	0.8667E+02	0.8685E+02	0.8703E+02
0.8721E+02	0.8739E+02	0.8757E+02	0.8774E+02	0.8792E+02	0.8810E+02	0.8828E+02	0.8845E+02
0.8863E+02	0.8881E+02	0.8898E+02	0.8916E+02	0.8933E+02	0.8951E+02	0.8968E+02	0.8986E+02
0.9003E+02	0.9021E+02	0.9038E+02	0.9055E+02	0.9073E+02	0.9090E+02	0.9107E+02	0.9124E+02
0.9141E+02	0.9158E+02	0.9175E+02	0.9192E+02	0.9209E+02	0.9226E+02	0.9243E+02	0.9260E+02
0.9277E+02	0.9294E+02	0.9311E+02	0.9328E+02	0.9344E+02	0.9361E+02	0.9378E+02	0.9395E+02
0.9411E+02	0.9428E+02	0.9444E+02	0.9461E+02	0.9477E+02	0.9494E+02	0.9510E+02	0.9527E+02
0.9543E+02	0.9560E+02	0.9576E+02	0.9592E+02	0.9609E+02	0.9625E+02	0.9641E+02	0.9657E+02
0.9674E+02	0.9690E+02	0.9706E+02	0.9722E+02	0.9738E+02	0.9754E+02	0.9770E+02	0.9786E+02
0.9802E+02	0.9818E+02	0.9834E+02	0.9850E+02	0.9866E+02	0.9882E+02	0.9897E+02	0.9913E+02
0.9929E+02	0.9945E+02	0.9960E+02	0.9976E+02	0.9992E+02			

TRUE SPECTRUM

-0.6405E+03	-0.1993E+03	0.1546E+02	0.1141E+03	0.1559E+03	0.1693E+03	0.1690E+03	0.1632E+03
0.1553E+03	0.1469E+03	0.1388E+03	0.1314E+03	0.1247E+03	0.1187E+03	0.1132E+03	0.1080E+03
0.1036E+03	0.9938E+02	0.9550E+02	0.9190E+02	0.8847E+02	0.8526E+02	0.8219E+02	0.7915E+02
0.7637E+02	0.7372E+02	0.7117E+02	0.6875E+02	0.6641E+02	0.6417E+02	0.6202E+02	0.5996E+02
0.5790E+02	0.5600E+02	0.5417E+02	0.5243E+02	0.5075E+02	0.4912E+02	0.4758E+02	0.4609E+02
0.4466E+02	0.4324E+02	0.4192E+02	0.4065E+02	0.3944E+02	0.3827E+02	0.3715E+02	0.3607E+02
0.3504E+02	0.3400E+02	0.3305E+02	0.3213E+02	0.3124E+02	0.3039E+02	0.2957E+02	0.2878E+02
0.2802E+02	0.2729E+02	0.2656E+02	0.2589E+02	0.2524E+02	0.2461E+02	0.2400E+02	0.2333E+02
0.2269E+02	0.2206E+02	0.2146E+02	0.2089E+02	0.2032E+02	0.1978E+02	0.1926E+02	0.1875E+02
0.1827E+02	0.1780E+02	0.1734E+02	0.1690E+02	0.1647E+02	0.1606E+02	0.1566E+02	0.1528E+02
0.1490E+02	0.1454E+02	0.1419E+02	0.1385E+02	0.1352E+02	0.1320E+02	0.1289E+02	0.1259E+02
0.1230E+02	0.1202E+02	0.1175E+02	0.1148E+02	0.1123E+02	0.1097E+02	0.1073E+02	0.1050E+02
0.1027E+02	0.1004E+02	0.9828E+01	0.9618E+01	0.9414E+01	0.9214E+01	0.9022E+01	0.8834E+01
0.8651E+01	0.8473E+01	0.8299E+01	0.8131E+01	0.7968E+01	0.7807E+01	0.7652E+01	0.7500E+01
0.7353E+01	0.7209E+01	0.7069E+01	0.6932E+01	0.6799E+01	0.6669E+01	0.6544E+01	0.6419E+01
0.6299E+01	0.6182E+01	0.6067E+01	0.5955E+01	0.5847E+01	0.5740E+01	0.5636E+01	0.5534E+01
0.5435E+01	0.5339E+01	0.5244E+01	0.5152E+01	0.5062E+01	0.4974E+01	0.4888E+01	0.4803E+01
0.4722E+01	0.4641E+01	0.4562E+01	0.4485E+01	0.4410E+01	0.4336E+01	0.4264E+01	0.4194E+01
0.4126E+01	0.4058E+01	0.3992E+01	0.3928E+01	0.3865E+01	0.3803E+01	0.3742E+01	0.3683E+01
0.3625E+01	0.3568E+01	0.3512E+01	0.3458E+01	0.3405E+01	0.3352E+01	0.3301E+01	0.3250E+01
0.3201E+01	0.3153E+01	0.3106E+01	0.3059E+01	0.3014E+01	0.2969E+01	0.2925E+01	0.2882E+01
0.2841E+01	0.2799E+01	0.2759E+01	0.2719E+01	0.2680E+01	0.2642E+01	0.2604E+01	0.2568E+01
0.2531E+01	0.2496E+01	0.2461E+01	0.2427E+01	0.2394E+01	0.2361E+01	0.2328E+01	0.2296E+01
0.2265E+01	0.2235E+01	0.2204E+01	0.2175E+01	0.2146E+01	0.2117E+01	0.2089E+01	0.2062E+01
0.2034E+01	0.2008E+01	0.1982E+01	0.1956E+01	0.1931E+01	0.1906E+01	0.1882E+01	0.1857E+01
0.1834E+01	0.1811E+01	0.1788E+01	0.1765E+01	0.1743E+01	0.1721E+01	0.1700E+01	0.1679E+01
0.1658E+01	0.1638E+01	0.1618E+01	0.1598E+01	0.1579E+01	0.1560E+01	0.1541E+01	0.1523E+01
0.1504E+01	0.1486E+01	0.1469E+01	0.1451E+01	0.1434E+01	0.1417E+01	0.1401E+01	0.1385E+01
0.1368E+01	0.1353E+01	0.1337E+01	0.1322E+01	0.1307E+01	0.1292E+01	0.1277E+01	0.1263E+01
0.1248E+01	0.1234E+01	0.1221E+01	0.1207E+01	0.1194E+01	0.1180E+01	0.1167E+01	0.1154E+01
0.1142E+01	0.1129E+01	0.1117E+01	0.1105E+01	0.1093E+01	0.1081E+01	0.1070E+01	0.1058E+01
0.1047E+01	0.1036E+01	0.1025E+01	0.1014E+01	0.1003E+01	0.9926E+00	0.9823E+00	0.9720E+00
0.9619E+00	0.9519E+00	0.9421E+00	0.9323E+00	0.9228E+00	0.9133E+00	0.9041E+00	0.8948E+00
0.8858E+00	0.8769E+00	0.8680E+00	0.8593E+00	0.8507E+00	0.8422E+00	0.8339E+00	0.8256E+00
0.8174E+00	0.8093E+00	0.8014E+00	0.7936E+00	0.7858E+00	0.7782E+00	0.7706E+00	0.7632E+00
0.7558E+00	0.7485E+00	0.7414E+00	0.7343E+00	0.7273E+00	0.7204E+00	0.7135E+00	0.7068E+00
0.7001E+00	0.6936E+00	0.6870E+00	0.6806E+00	0.6743E+00	0.6680E+00	0.6618E+00	0.6557E+00
0.6497E+00	0.6437E+00	0.6378E+00	0.6320E+00				

EFFICIENCY SPECTRUM

DROPLET DIAMETER(MICRON)	COLLECTION EFFICIENCY
0.243852E+02	0.0
0.250197E+02	0.0
0.256365E+02	0.0
0.262398E+02	0.392013E+00
0.268296E+02	0.424369E+00
0.274066E+02	0.424715E+00
0.279717E+02	0.416173E+00
0.285257E+02	0.407109E+00
0.290691E+02	0.398954E+00
0.296025E+02	0.393025E+00
0.301265E+02	0.390285E+00
0.306415E+02	0.390602E+00

0.311480E+02	0.394059E+00
0.316464E+02	0.400281E+00
0.321371E+02	0.408922E+00
0.326204E+02	0.418210E+00
0.330966E+02	0.430392E+00
0.335661E+02	0.443317E+00
0.340291E+02	0.457153E+00
0.344859E+02	0.471461E+00
0.349367E+02	0.485865E+00
0.353814E+02	0.500457E+00
0.358213E+02	0.514836E+00
0.362555E+02	0.528451E+00
0.366846E+02	0.542361E+00
0.371087E+02	0.556085E+00
0.375280E+02	0.569355E+00
0.379427E+02	0.582275E+00
0.383529E+02	0.594821E+00
0.387588E+02	0.606873E+00
0.391604E+02	0.618587E+00
0.395580E+02	0.629977E+00
0.399516E+02	0.640510E+00
0.403414E+02	0.651078E+00
0.407274E+02	0.661232E+00
0.411099E+02	0.671118E+00
0.414888E+02	0.680546E+00
0.418643E+02	0.689610E+00
0.422364E+02	0.698416E+00
0.426053E+02	0.706925E+00
0.429710E+02	0.714963E+00
0.433336E+02	0.722472E+00
0.436932E+02	0.730316E+00
0.440499E+02	0.737293E+00
0.444037E+02	0.744323E+00
0.447548E+02	0.751079E+00
0.451031E+02	0.757622E+00
0.454487E+02	0.763925E+00
0.457917E+02	0.770008E+00
0.461322E+02	0.775659E+00
0.464701E+02	0.781342E+00
0.468057E+02	0.786943E+00
0.471388E+02	0.792157E+00
0.474696E+02	0.797298E+00
0.477981E+02	0.802289E+00
0.481244E+02	0.807096E+00
0.484485E+02	0.811773E+00
0.487704E+02	0.816282E+00
0.490902E+02	0.820506E+00
0.494079E+02	0.824762E+00
0.497236E+02	0.828862E+00
0.500374E+02	0.832985E+00
0.503491E+02	0.836775E+00
0.506590E+02	0.839960E+00
0.509668E+02	0.843054E+00
0.512730E+02	0.846072E+00
0.515773E+02	0.848973E+00
0.518798E+02	0.851815E+00
0.521806E+02	0.854567E+00
0.524798E+02	0.857243E+00
0.527770E+02	0.859855E+00
0.530726E+02	0.862388E+00

0.533667E+02	0.864861E+00
0.536591E+02	0.867265E+00
0.539499E+02	0.869603E+00
0.542392E+02	0.871888E+00
0.545269E+02	0.874106E+00
0.548132E+02	0.876282E+00
0.550979E+02	0.878394E+00
0.553812E+02	0.880454E+00
0.556630E+02	0.882471E+00
0.559435E+02	0.884443E+00
0.562225E+02	0.886356E+00
0.565001E+02	0.888235E+00
0.567764E+02	0.890061E+00
0.570514E+02	0.891862E+00
0.573250E+02	0.893611E+00
0.575973E+02	0.895323E+00
0.578684E+02	0.897005E+00
0.581382E+02	0.898640E+00
0.584067E+02	0.900249E+00
0.586740E+02	0.901825E+00
0.589401E+02	0.903363E+00
0.592050E+02	0.904870E+00
0.594687E+02	0.906354E+00
0.597313E+02	0.907804E+00
0.599927E+02	0.909226E+00
0.602530E+02	0.910627E+00
0.605121E+02	0.911996E+00
0.607702E+02	0.913339E+00
0.610271E+02	0.914659E+00
0.612830E+02	0.915969E+00
0.615378E+02	0.917234E+00
0.617916E+02	0.918481E+00
0.620443E+02	0.919708E+00
0.622960E+02	0.920929E+00
0.625467E+02	0.922115E+00
0.627964E+02	0.923275E+00
0.630451E+02	0.924434E+00
0.632929E+02	0.925560E+00
0.635396E+02	0.926681E+00
0.637854E+02	0.927777E+00
0.640302E+02	0.928861E+00
0.642741E+02	0.929923E+00
0.645171E+02	0.930972E+00
0.647592E+02	0.931996E+00
0.650004E+02	0.933023E+00
0.652407E+02	0.934034E+00
0.654801E+02	0.935017E+00
0.657187E+02	0.935999E+00
0.659564E+02	0.936958E+00
0.661932E+02	0.937912E+00
0.664292E+02	0.938861E+00
0.666643E+02	0.939774E+00
0.668986E+02	0.940699E+00
0.671322E+02	0.941600E+00
0.673649E+02	0.942497E+00
0.675967E+02	0.943370E+00
0.678278E+02	0.944253E+00
0.680581E+02	0.945110E+00
0.682877E+02	0.945970E+00
0.685164E+02	0.946809E+00

0.687445E+02	0.947641E+00
0.689717E+02	0.948469E+00
0.691982E+02	0.949283E+00
0.694240E+02	0.950093E+00
0.696490E+02	0.950893E+00
0.698734E+02	0.951686E+00
0.700970E+02	0.952473E+00
0.703198E+02	0.953238E+00
0.705420E+02	0.954018E+00
0.707635E+02	0.954771E+00
0.709843E+02	0.955519E+00
0.712044E+02	0.956283E+00
0.714239E+02	0.957019E+00
0.716426E+02	0.957755E+00
0.718607E+02	0.958479E+00
0.720781E+02	0.959206E+00
0.722949E+02	0.959913E+00
0.725110E+02	0.960635E+00
0.727265E+02	0.961341E+00
0.729413E+02	0.962034E+00
0.731555E+02	0.962730E+00
0.733691E+02	0.963424E+00
0.735821E+02	0.964104E+00
0.737945E+02	0.964782E+00
0.740062E+02	0.965446E+00
0.742174E+02	0.966130E+00
0.744279E+02	0.966788E+00
0.746379E+02	0.967447E+00
0.748472E+02	0.968109E+00
0.750560E+02	0.968755E+00
0.752642E+02	0.969414E+00
0.754718E+02	0.970040E+00
0.756789E+02	0.970687E+00
0.758854E+02	0.971322E+00
0.760913E+02	0.971952E+00
0.762967E+02	0.972595E+00
0.765015E+02	0.973212E+00
0.767058E+02	0.973929E+00
0.769095E+02	0.974442E+00
0.771127E+02	0.975058E+00
0.773154E+02	0.975669E+00
0.775175E+02	0.976280E+00
0.777191E+02	0.976884E+00
0.779202E+02	0.999033E+00

APPENDIX B
DAMIE PROGRAM

B.1 Introduction

DAMIE (D2) is a FORTRAN subroutine which computes the so-called "Efficiency Factors" and Stokes parameters for electromagnetic radiation scattered by a sphere. The formulas calculated in this subroutine were first derived by G. Mie (M5), and thus this scattering process is referred to as Mie scattering.

Mie's expressions for the radiation scattered by a sphere are valid when the radius of the sphere is comparable to or greater than the wavelength of the incident radiation. The index of refraction of the material of the sphere is assumed to have the form $n_1 - in_2$. In the DAMIE subroutine, all functions are computed with an upward recurrence procedure. This procedure is stable for non-absorbing ($n_2=0$), moderate or large-sized spheres. For partially-absorbing ($n_2>0$) spheres, the DBMIE subroutine (D2), which uses a downward recurrence procedure, gives more reliable results.

In the present study, the scattered intensity of water droplets is found as a function of droplet size. Since water is essentially a non-absorbing medium, and the droplet sizes under consideration are large, the DAMIE subroutine is used, requiring much less computer storage.

This appendix describes the part of the DAMIE code that finds the relationship between the scattered light intensity and droplet size. Other features of the subroutine will not be presented here. They are described in Ref. D2. A listing of the program and a sample problem are included at the end of this appendix.

B.2 Description of the Program

The expressions for Mie scattering can be written as

$$\underline{I}_s = \underline{\underline{F}}' \cdot \underline{I}_i \quad , \qquad \text{(B.2.1)}$$

where $\underline{I}_i$ and $\underline{I}_s$ respectively represent the Stokes parameters of the incident and scattered radiation, and F' is a four-by-four matrix referred to as a "transformation matrix". It has the following form:

$$\underline{\underline{F}}' = \begin{bmatrix} M_2 & 0 & 0 & 0 \\ 0 & M_1 & 0 & 0 \\ 0 & 0 & S_{21} & -D_{21} \\ 0 & 0 & D_{21} & S_{21} \end{bmatrix} \qquad \text{(B.2.2)}$$

The DAMIE subroutine calculates the elements in this transformation matrix at any scattering angle. The scattered intensity, I_s, at any scattering angle, can simply be expressed as

$$I_s(\Theta) = \frac{1/2(M_1(\Theta) + M_2(\Theta))}{k^2 \cdot L^2} I_i \quad , \qquad \text{(B.2.3)}$$

where

$$k = \frac{2\pi}{\lambda} \quad , \qquad \text{(B.2.4)}$$

where λ is the wavelength of the incident radiation, and L is the distance from the scattering location. In the program output, the value of $(1/2)(M_1+M_2)$ is also given under the heading "INTENSITY" for each scattering angle, as shown in Section B.5. The only purpose of using this subroutine in the present study is to find this value as a function of droplet size.

All of the necessary information for this computation are input through the main program. These include the refractive index of water, the wavelength of the incident radiation, the scattering angle, and the droplet size. The subroutine is called to compute the transformation matrix elements, which are then used to compute the scattered intensity factor.

B.3 Description of the Input Parameters

Card No. 1

RFR, RFI, ALAM

FORMAT (4D15.5)

RFR is n_1, the real part of the refractive index of the material of the sphere. RFR equals 1.341 for water.

RFI is n_2, the imaginary part of the refractive index of the material of the sphere. RFI equals 0.0 for water.

ALAM is the wavelength of the incident light source expressed in microns.

Card No.2

THETD(1), AJX, JX

FORMAT(2D15.5, I5)

THETD(1) is θ_1, the smallest angle between the direction of the scattered light and the direction of the incident light in the calculations. It is expressed in degrees, and its value should not exceed 90°.

AJX is $\Delta\theta$, the interval between successive θ's for calculations.

JX is the total number of θ's for calculations of a scattered intensity. Its value should not exceed 100, unless the dimensions in all related statements are appropriately changed. It must be greater than or equal to 1.

Card No. 3 and Onward

X

FORMAT (D15.5)

X is the water droplet radius expressed in microns, for the calculations. Execution will be terminated when there are no more data cards.

B.4 Listing of the DAMIE Code

```
C                                                                       MAIN0001
C   DAMIE - CALCULATION OF SCATTERED INTENSITY AS A FUNCTION            MAIN0002
C           OF DROPLET SIZE                                             MAIN0003
C                                                                       MAIN0004
C    RFR=REAL PART OF THE REFRACTIVE INDEX OF THE MATERIAL              MAIN0005
C        OF THE SPHERE                                                  MAIN0006
C    RFI=IMAGINARY PART OF THE REFRACTIVE INDEX OF THE MATERIAL         MAIN0007
C        OF THE SPHERE                                                  MAIN0008
C    ALAM=WAVE LENGTH OF THE LIGHT SOURCE IN MICRO                      MAIN0009
C    THETD(1)=SCATTERING ANGLE IN DEGREE                                MAIN0010
C    AJX=INTERVAL BETWEEN SCATTERING ANGLES FOR WHICH COMPUTATION       MAIN0011
C        IS PERFORMED                                                   MAIN0012
C    JX=TOTAL NUMBER OF SCATTERING ANGLES FOR WHICH COMPUTATION         MAIN0013
C       WILL BE PERFORMED                                               MAIN0014
C    X=DROPLET SIZE IN MICRON                                           MAIN0015
C                                                                       MAIN0016
  100 FORMAT(4D15.5)                                                    MAIN0017
  101 FORMAT(2D15.5,I5)                                                 MAIN0018
  105 FORMAT(1H1)                                                       MAIN0019
  110 FORMAT(////,T10,6D15.5,I5)                                        MAIN0020
  200 FORMAT(//T10,'ELEMENTS OF THE TRANSFORMATION MATRIX FOR A SPHERE  MAIN0021
     1 WITH SIZE PARAMETER = ',F15.5)                                   MAIN0022
  300 FORMAT(//T10,'REFRACTIVE INDEX. REAL = ',D15.5,T60,'IMAGINARY =',  MAIN0023
     1D15.5//)                                                          MAIN0024
  400 FORMAT(T3,'ANGLE',T17,'M SUB 2 ',T32,'M SUB 1',T46,' S SUB 21',   MAIN0025
     1T61,'D SUB 21',T76,'INTENSITY',T91,'POLARIZATION'//)              MAIN0026
  500 FORMAT(F10.4,5E15.6,F15.4)                                        MAIN0027
  600 FORMAT(//T10,' EFFICIENCY FACTOR FOR EXTINCTION',E15.6)           MAIN0028
  700 FORMAT(//T10,' EFFICIENCY FACTOR FOR SCATTERING',E15.6)           MAIN0029
  800 FORMAT(//T10,' EFFICIENCY FACTOR FOR ABSORPTION',E15.6)           MAIN0030
  900 FORMAT(//T10,' ASYMMETRY FACTOR',E15.6)                           MAIN0031
      REAL*8 RFR,RFI,X,QEXT,QSCAT,QABS,THETD(100),ELTRMX(4,100,2)       MAIN0032
      REAL*8 ALAM,CON,CTBRQS,AVCSTH                                     MAIN0033
      REAL*4 AIN(100,2),POLR(100,2)                                     MAIN0034
      CON=3.14159265358979320+0                                         MAIN0035
      READ 100,RFR,RFI,ALAM                                             MAIN0036
```

```
      READ 101,THETD(1),AJX,JX                                          MAIN0037
      THETD(2)=180.0D0-THETD(1)                                         MAIN0038
   10 READ(5,100,END=1000) X                                            MAIN0039
      PRINT 105                                                         MAIN0040
      PRINT 110,X,RFR,RFI,ALAM,THETD(1),AJX,JX                          MAIN0041
      X= (2.0D0*CON*X)/ALAM                                             MAIN0042
      CALL DAMIE(X,RFR,RFI,THETD,JX,QEXT,QSCAT,CTBRQS,ELTRMX)           MAIN0043
      QABS=QEXT-QSCAT                                                   MAIN0044
      AVCSTH=CTBRQS/QSCAT                                               MAIN0045
      DO 2 K=1,2                                                        MAIN0046
      DO 2 J=1,JX                                                       MAIN0047
      AIN(J,K)=ELTRMX(1,J,K)+ELTRMX(2,J,K)                              MAIN0048
      POLR(J,K)=(ELTRMX(2,J,K)-ELTRMX(1,J,K))/AIN(J,K)                  MAIN0049
      AIN(J,K)=0.5*AIN(J,K)                                             MAIN0050
    2 CONTINUE                                                          MAIN0051
      PRINT 200,X                                                       MAIN0052
      PRINT 300,RFR,RFI                                                 MAIN0053
      PRINT 400                                                         MAIN0054
      PRINT 500,((THETD(J),(ELTRMX(I,J,1),I=1,4),AIN(J,1),POLR(J,1)),   MAIN0055
     1J=1,JX)                                                           MAIN0056
      PRINT 500,(THETD( 2),(ELTRMX(I,JX,2),I=1,4),AIN(JX,2),POLR(JX,2)) MAIN0057
      PRINT 600,QEXT                                                    MAIN0058
      PRINT 700,QSCAT                                                   MAIN0059
      PRINT 800,QABS                                                    MAIN0060
      PRINT 900,AVCSTH                                                  MAIN0061
      GO TO 10                                                          MAIN0062
 1000 CONTINUE                                                          MAIN0063
      END                                                               MAIN0064
```

```
      SUBROUTINE DAMIE (X,RFR,RFI,THETD,JX,QEXT,QSCAT,CTBRQS,ELTRMX)
    5 FORMAT(T10,'THE VALUE OF THE SCATTERING ANGLE IS GREATER THAN
     1 90.0 DEGREES. IT IS ',D15.4)
    6 FORMAT(//T10,' PLEASE READ COMMENTS '//)
    7 FORMAT(//T10,'THE VALUE OF THE ARGUMENT JX IS GREATER THAN 100')
    8 FORMAT(//T10,'THE VALUE OF RFI*X IS GREATER THAN 80.0. IT IS',
     1 D15.4,//)
      REAL*8 X,RX,RFR,RFI,QEXT,QSCAT,T(5),TA(4),TB(2),TC(2)
      REAL*8 TD(2),TE(2),CTBRQS
      REAL*8 ELTRMX(4,100,2),PI(3,100),TAU(3,100),CSTHT(100),SI2THT(100)
     1,THETD(100)
      COMPLEX*16 RF,RRF,RRFX,WM1,FNA,FNB,TC1,TC2,WFN(2),ACAP(2)
      COMPLEX*16 FNAP,FNBP
      EQUIVALENCE (WFN(1),TA(1)),(FNA,TB(1)),(FNB,TC(1))
      EQUIVALENCE (FNAP,TD(1)),(FNBP,TE(1))
      IF ( JX .LE. 100 ) GO TO 20
      WRITE(6,7)
      WRITE(6,6)
      CALL EXIT
   20 RF=DCMPLX(RFR,-RFI)
      RRF=1.0D0/RF
      RX=1.0D0/X
      RRFX=RRF*RX
      DO 30 J=1,JX
      IF ( THETD(J).LT.0.0D0 ) THETD(J)=DABS(THETD(J))
      IF ( THETD(J).GT.0.0D0) GO TO 23
      CSTHT(J)=1.0D0
      SI2THT(J)=0.0D0
      GO TO 30
   23 IF ( THETD(J).GE.90.0D0 ) GO TO 25
      T(1)=(3.1415926535897932 * THETD(J))/180.0D0
      CSTHT(J)=DCOS(T(1))
      SI2THT(J)=1.0D0-CSTHT(J)**2
      GO TO 30
   25 IF(THETD(J).GT.90.0D0) GO TO 28
      CSTHT(J)=0.0D0
```

```
      SI2THT(J)=1.0D0                                                   DMIF0037
      GO TO 30                                                          DMIE0038
   28 WRITE(6,5) THETD(J)                                               DMIE0039
      WRITE(6,6)                                                        DMIE0040
      CALL EXIT                                                         DMIE0041
   30 CONTINUE                                                          DMIE0042
      DO 35 J=1,JX                                                      DMIF0043
      PI(1,J)=0.0D0                                                     DMIE0044
      PI(2,J)=1.0D0                                                     DMIE0045
      TAU(1,J)=0.0D0                                                    DMIE0046
      TAU(2,J)=CSTHT(J)                                                 DMIE0047
   35 CONTINUE                                                          DMIE0048
      T(1)=DCOS(X)                                                      DMIE0049
      T(2)=DSIN(X)                                                      DMIE0050
      WM1=DCMPLX(T(1),-T(2))                                            DMIF0051
      WFN(1)=DCMPLX(T(2),T(1))                                          DMIE0052
      WFN(2)=RX*WFN(1)-WM1                                              DMIE0053
      T(1)=RFI*X                                                        DMIF0054
      IF(T(1).GT.80.0D0) GO TO 40                                       DMIE0055
      T(3)=0.5D0*DEXP(T(1))                                             DMIF0056
      T(4)=0.25D0/T(3)                                                  DMIE0057
      T(1)=T(3)+T(4)                                                    DMIE0058
      T(2)=T(3)-T(4)                                                    DMIE0059
      T(3)=T(2)**2                                                      DMIE0060
      T(2)=T(1)*T(2)                                                    DMIE0061
      T(1)=T(3)                                                         DMIF0062
      T(3)=RFR * X                                                      DMIF0063
      T(4)=DSIN(T(3))                                                   DMIE0064
      T(3)=DCOS(T(3))                                                   DMIE0065
      T(1)=T(1)+T(4)**2                                                 DMIE0066
      T(3)=T(3)*T(4)                                                    DMIF0067
      ACAP(1)=DCMPLX(T(3),T(2))/T(1)                                    DMIE0068
      GO TO 50                                                          DMIE0069
   40 ACAP(1)=DCMPLX(0.0D0,1.0D0)                                       DMIF0070
      WRITE(6,8) T(1)                                                   DMIE0071
      WRITE(6,6)                                                        DMIF0072
```

```
50 ACAP(2)=-RRFX+(1.0D0/(RRFX-ACAP(1)))                                          DMIE0073
   TC1=ACAP(2)*RRF+RX                                                            DMIE0074
   TC2=ACAP(2)*RF+RX                                                             DMIE0075
   FNA=(TC1*TA(3)-TA(1))/(TC1*WFN(2)-WFN(1))                                     DMIE0076
   FNB=(TC2*TA(3)-TA(1))/(TC2*WFN(2)-WFN(1))                                     DMIE0077
   FNAP=FNA                                                                      DMIE0078
   FNBP=FNB                                                                      DMIE0079
   T(1)=1.50D0                                                                   DMIE0080
   TB(1)=T(1)*TB(1)                                                              DMIE0081
   TB(2)=T(1)*TB(2)                                                              DMIE0082
   TC(1)=T(1)*TC(1)                                                              DMIE0083
   TC(2)=T(1)*TC(2)                                                              DMIE0084
   DO 60 J=1,JX                                                                  DMIE0085
   ELTRMX(1,J,1)=TB(1)*PI(2,J)+TC(1)*TAU(2,J)                                    DMIE0086
   ELTRMX(2,J,1)=TB(2)*PI(2,J)+TC(2)*TAU(2,J)                                    DMIE0087
   ELTRMX(3,J,1)=TC(1)*PI(2,J)+TB(1)*TAU(2,J)                                    DMIE0088
   ELTRMX(4,J,1)=TC(2)*PI(2,J)+TB(2)*TAU(2,J)                                    DMIE0089
   ELTRMX(1,J,2)=TB(1)*PI(2,J)-TC(1)*TAU(2,J)                                    DMIE0090
   ELTRMX(2,J,2)=TB(2)*PI(2,J)-TC(2)*TAU(2,J)                                    DMIE0091
   ELTRMX(3,J,2)=TC(1)*PI(2,J)-TB(1)*TAU(2,J)                                    DMIE0092
   ELTRMX(4,J,2)=TC(2)*PI(2,J)-TB(2)*TAU(2,J)                                    DMIE0093
60 CONTINUE                                                                      DMIE0094
   QEXT=2.0D0*(TB(1)+TC(1))                                                      DMIE0095
   QSCAT=(TB(1)**2+TB(2)**2+TC(1)**2+TC(2)**2)/0.75D0                            DMIE0096
   CTBRQS=0.0D0                                                                  DMIE0097
   N=2                                                                           DMIE0098
65 T(1)=2*N-1                                                                    DMIE0099
   T(2)=N-1                                                                      DMIE0100
   T(3)=2*N+1                                                                    DMIE0101
   DO 70 J=1,JX                                                                  DMIE0102
   PI(3,J)=(T(1)*PI(2,J)*CSTHT(J)-N*PI(1,J))/T(2)                                DMIE0103
   TAU(3,J)=CSTHT(J)*(PI(3,J)-PI(1,J))-T(1)*SI2THT(J)*PI(2,J)+TAU(1,J            DMIE0104
  1)                                                                             DMIE0105
70 CONTINUE                                                                      DMIE0106
   WM1=WFN(1)                                                                    DMIE0107
   WFN(1)=WFN(2)                                                                 DMIE0108
```

```
      WFN(2)=T(1)*RX*WFN(1)-WM1                                          DMIE0109
      ACAP(1)=ACAP(2)                                                    DMIE0110
      ACAP(2)=-N*RRFX+(1.0D0/(N*RRFX-ACAP(1)))                           DMIE0111
      TC1=ACAP(2)*RRF+N*RX                                               DMIE0112
      TC2=ACAP(2)*RF+N*RX                                                DMIE0113
      FNA=(TC1*TA(3)-TA(1))/(TC1*WFN(2)-WFN(1))                          DMIE0114
      FNB=(TC2*TA(3)-TA(1))/(TC2*WFN(2)-WFN(1))                          DMIE0115
      T(5)=N                                                             DMIE0116
      T(4)=T(1)/(T(5)*T(2))                                              DMIE0117
      T(2)=(T(2)*(T(5)+1.0D0))/T(5)                                      DMIE0118
      CTBRQS=CTBRQS+T(2)*(TD(1)*TB(1)+TD(2)*TB(2)+TE(1)*TC(1)+           DMIE0119
     1TE(2)*TC(2))+T(4)*(TD(1)*TE(1)+TD(2)*TE(2))                        DMIE0120
      QEXT=QEXT+T(3)*(TB(1)+TC(1))                                       DMIE0121
      T(4)=TB(1)**2+TB(2)**2+TC(1)**2+TC(2)**2                           DMIE0122
      QSCAT=QSCAT+T(3)*T(4)                                              DMIE0123
      T(2)=N*(N+1)                                                       DMIE0124
      T(1)=T(3)/T(2)                                                     DMIE0125
      K=(N/2)*2                                                          DMIE0126
      DO 80 J=1,JX                                                       DMIE0127
      ELTRMX(1,J,1)=ELTRMX(1,J,1)+T(1)*(TB(1)*PI(3,J)+TC(1)*TAU(3,J))    DMIE0128
      ELTRMX(2,J,1)=ELTRMX(2,J,1)+T(1)*(TB(2)*PI(3,J)+TC(2)*TAU(3,J))    DMIE0129
      ELTRMX(3,J,1)=ELTRMX(3,J,1)+T(1)*(TC(1)*PI(3,J)+TB(1)*TAU(3,J))    DMIE0130
      ELTRMX(4,J,1)=ELTRMX(4,J,1)+T(1)*(TC(2)*PI(3,J)+TB(2)*TAU(3,J))    DMIE0131
      IF(K.EQ.N) GO TO 75                                                DMIE0132
      ELTRMX(1,J,2)=ELTRMX(1,J,2)+T(1)*(TB(1)*PI(3,J)-TC(1)*TAU(3,J))    DMIE0133
      ELTRMX(2,J,2)=ELTRMX(2,J,2)+T(1)*(TB(2)*PI(3,J)-TC(2)*TAU(3,J))    DMIE0134
      ELTRMX(3,J,2)=ELTRMX(3,J,2)+T(1)*(TC(1)*PI(3,J)-TB(1)*TAU(3,J))    DMIE0135
      ELTRMX(4,J,2)=ELTRMX(4,J,2)+T(1)*(TC(2)*PI(3,J)-TB(2)*TAU(3,J))    DMIE0136
      GO TO 80                                                           DMIE0137
   75 ELTRMX(1,J,2)=ELTRMX(1,J,2)+T(1)*(-TB(1)*PI(3,J)+TC(1)*TAU(3,J))   DMIE0138
      ELTRMX(2,J,2)=ELTRMX(2,J,2)+T(1)*(-TB(2)*PI(3,J)+TC(2)*TAU(3,J))   DMIE0139
      ELTRMX(3,J,2)=ELTRMX(3,J,2)+T(1)*(-TC(1)*PI(3,J)+TB(1)*TAU(3,J))   DMIE0140
      ELTRMX(4,J,2)=ELTRMX(4,J,2)+T(1)*(-TC(2)*PI(3,J)+TB(2)*TAU(3,J))   DMIE0141
   80 CONTINUE                                                           DMIE0142
      IF(T(4).LT.1.0D-14) GO TO 100                                      DMIE0143
      N=N+1                                                              DMIE0144
```

```
      DO 90 J=1,JX                                                      DMIE0145
      PI(1,J)=PI(2,J)                                                   DMIE0146
      PI(2,J)=PI(3,J)                                                   DMIE0147
      TAU(1,J)=TAU(2,J)                                                 DMIE0148
      TAU(2,J)=TAU(3,J)                                                 DMIE0149
   90 CONTINUE                                                          DMIE0150
      FNAP=FNA                                                          DMIE0151
      FNBP=FNB                                                          DMIE0152
      GO TO 65                                                          DMIE0153
  100 DO 120 J=1,JX                                                     DMIE0154
      DO 120 K=1,2                                                      DMIE0155
      DO 115 I=1,4                                                      DMIE0156
      T(I)=ELTRMX(I,J,K)                                                DMIE0157
  115 CONTINUE                                                          DMIE0158
      ELTRMX(2,J,K)=T(1)**2+T(2)**2                                     DMIE0159
      ELTRMX(1,J,K)=T(3)**2+T(4)**2                                     DMIE0160
      ELTRMX(3,J,K)=T(1)*T(3)+T(2)*T(4)                                 DMIE0161
      ELTRMX(4,J,K)=T(2)*T(3)-T(4)*T(1)                                 DMIE0162
  120 CONTINUE                                                          DMIE0163
      T(1)=2.0D0*RX**2                                                  DMIE0164
      QEXT=QEXT*T(1)                                                    DMIE0165
      QSCAT=QSCAT*T(1)                                                  DMIE0166
      CTBRQS=2.0D0*CTBRQS*T(1)                                          DMIE0167
      RETURN                                                            DMIE0168
      END                                                               DMIE0169
```

B.5 Sample Problem

A sample problem is given here to demonstrate the use of the DAMIE code. The material of the scattering medium is pure water which has a refractive index of 1.34-i0. The wavelength of the incident light source is 0.6328 μm. The scattering angle is set to be 26.5°. The radii of the water droplets for this computation are listed in the input section of the sample problem.

The output of the code gives the input information as well as the elements of the transformation matrix for the input scattering angle and its complementary angle. In the present study only the values of the intensity are used. All of this information is repeated for each input droplet size.

```
C          INPUT OF SAMPLE PROBLEM FOR DAMIE PROGRAM                    INPU0001
   1.3420D0      0.0D0           0.6328                                 INPU0002
  26.50D0         0.D0              1                                   INPU0003
  5.0D0                                                                 INPU0004
  10.0D0                                                                INPU0005
  20.0D0                                                                INPU0006
  30.0D0                                                                INPU0007
  40.0D0                                                                INPU0008
  50.0D0                                                                INPU0009
  60.0D0                                                                INPU0010
  70.0D0                                                                INPU0011
  80.0D0                                                                INPU0012
  90.0D0                                                                INPU0013
 100.0D0                                                                INPU0014
```

0.50000D+01 0.13420D+01 0.0 0.63280D+00 0.26500D+02 0.0 1

ELEMENTS OF THE TRANSFORMATION MATRIX FOR A SPHERE WITH SIZE PARAMETER = 49.64590

REFRACTIVE INDEX. REAL = 0.13420D+01 IMAGINARY = 0.0

ANGLE	M SUB 2	M SUB 1	S SUB 21	D SUB 21	INTENSITY	POLARIZATION
26.5000	0.190689D+04	0.123446D+04	0.150990D+04	0.272378D+03	0.157067E+04	-0.2141
153.5000	0.394814D+03	0.352423D+02	-0.793190D+02	0.873078D+02	0.215028E+03	-0.8361

EFFICIENCY FACTOR FOR EXTINCTION 0.205035D+01

EFFICIENCY FACTOR FOR SCATTERING 0.205035D+01

EFFICIENCY FACTOR FOR ABSORPTION 0.0

ASYMMETRY FACTOR 0.853527D+00

0.10000D+02 0.13420D+01 0.0 0.63280D+00 0.26500D+02 0.0 1

ELEMENTS OF THE TRANSFORMATION MATRIX FOR A SPHERE WITH SIZE PARAMETER = 99.29180

REFRACTIVE INDEX. REAL = 0.13420D+01 IMAGINARY = 0.0

ANGLE	M SUB 2	M SUB 1	S SUB 21	D SUB 21	INTENSITY	POLARIZATION
26.5000	0.219803D+05	0.240829D+05	0.229522D+05	-0.159597D+04	0.230316E+05	0.0456
153.5000	0.178566D+03	0.145557D+04	0.185881D+03	0.474726D+03	0.817070E+03	0.7815

EFFICIENCY FACTOR FOR EXTINCTION 0.214774D+01

EFFICIENCY FACTOR FOR SCATTERING 0.214774D+01

EFFICIENCY FACTOR FOR ABSORPTION 0.0

ASYMMETRY FACTOR 0.878025D+00

0.20000D+02 0.13420D+01 0.0 0.63280D+00 0.26500D+02 0.0 1

ELEMENTS OF THE TRANSFORMATION MATRIX FOR A SPHERE WITH SIZE PARAMETER = 198.58361

REFRACTIVE INDEX. REAL = 0.13420D+01 IMAGINARY = 0.0

ANGLE	M SUB 2	M SUB 1	S SUB 21	D SUB 21	INTENSITY	POLARIZATION
26.5000	0.788699D+05	0.885268D+05	0.831022D+05	-0.872497D+04	0.836984E+05	0.0577
153.5000	0.193841D+04	0.212137D+04	0.116681D+04	0.165850D+04	0.202989E+04	0.0451

EFFICIENCY FACTOR FOR EXTINCTION 0.208603D+01

EFFICIENCY FACTOR FOR SCATTERING 0.208603D+01

EFFICIENCY FACTOR FOR ABSORPTION 0.0

ASYMMETRY FACTOR 0.870171D+00

0.30000D+02 0.13420D+01 0.0 0.63280D+00 0.26500D+02 0.0 1

ELEMENTS OF THE TRANSFORMATION MATRIX FOR A SPHERE WITH SIZE PARAMETER = 297.87541

REFRACTIVE INDEX. REAL = 0.13420D+01 IMAGINARY = 0.0

ANGLE	M SUB 2	M SUB 1	S SUB 21	D SUB 21	INTENSITY	POLARIZATION
26.5000	0.154489D+06	0.164404D+06	0.159151D+06	-0.835008D+04	0.159447E+06	0.0311
153.5000	0.112530D+05	0.539753D+03	0.885705D+03	-0.229987D+04	0.589639E+04	-0.9085

EFFICIENCY FACTOR FOR EXTINCTION 0.203613D+01

EFFICIENCY FACTOR FOR SCATTERING 0.203613D+01

EFFICIENCY FACTOR FOR ABSORPTION 0.0

ASYMMETRY FACTOR 0.869208D+00

0.40000D+02 0.13420D+01 0.0 0.63280D+00 0.26500D+02 0.0 1

ELEMENTS OF THE TRANSFORMATION MATRIX FOR A SPHERE WITH SIZE PARAMETER = 397.16721

REFRACTIVE INDEX. REAL = 0.13420D+01 IMAGINARY = 0.0

ANGLE	M SUB 2	M SUB 1	S SUB 21	D SUB 21	INTENSITY	POLARIZATION
26.5000	0.253297D+06	0.251485D+06	0.252116D+06	-0.117470D+05	0.252391E+06	-0.0036
153.5000	0.140381D+04	0.326051D+05	0.841257D+03	-0.671294D+04	0.170044E+05	0.9174

EFFICIENCY FACTOR FOR EXTINCTION 0.201977D+01

EFFICIENCY FACTOR FOR SCATTERING 0.201977D+01

EFFICIENCY FACTOR FOR ABSORPTION 0.0

ASYMMETRY FACTOR 0.873835D+00

0.50000D+02 0.13420D+01 0.0 0.63280D+00 0.26500D+02 0.0 1

ELEMENTS OF THE TRANSFORMATION MATRIX FOR A SPHERE WITH SIZE PARAMETER = 496.45902

REFRACTIVE INDEX. REAL = 0.13420D+01 IMAGINARY = 0.0

ANGLE	M SUB 2	M SUB 1	S SUB 21	D SUB 21	INTENSITY	POLARIZATION
26.5000	0.379813D+06	0.342664D+06	0.360461D+06	-0.147120D+05	0.361239E+06	-0.0514
153.5000	0.189627D+05	0.163937D+05	0.343393D+03	0.176281D+05	0.176782E+05	-0.0727

EFFICIENCY FACTOR FOR EXTINCTION 0.203422D+01

EFFICIENCY FACTOR FOR SCATTERING 0.203422D+01

EFFICIENCY FACTOR FOR ABSORPTION 0.0

ASYMMETRY FACTOR 0.873846D+00

0.60000D+02 0.13420D+01 0.0 0.63280D+00 0.26500D+02 0.0 1

ELEMENTS OF THE TRANSFORMATION MATRIX FOR A SPHERE WITH SIZE PARAMETER = 595.75082

REFRACTIVE INDEX. REAL = 0.13420D+01 IMAGINARY = 0.0

ANGLE	M SUB 2	M SUB 1	S SUB 21	D SUB 21	INTENSITY	POLARIZATION
26.5000	0.575563D+06	0.482253D+06	0.523860D+06	-0.560139D+05	0.528908E+06	-0.0882
153.5000	0.260394D+05	0.163721D+04	0.642192D+04	-0.117941D+04	0.138383E+05	-0.8817

EFFICIENCY FACTOR FOR EXTINCTION 0.204117D+01

EFFICIENCY FACTOR FOR SCATTERING 0.204117D+01

EFFICIENCY FACTOR FOR ABSORPTION 0.0

ASYMMETRY FACTOR 0.876979D+00

0.70000D+02 0.13420D+01 0.0 0.63280D+00 0.26500D+02 0.0 1

ELEMENTS OF THE TRANSFORMATION MATRIX FOR A SPHERE WITH SIZE PARAMETER = 695.04262

REFRACTIVE INDEX. REAL = 0.13420D+01 IMAGINARY = 0.0

ANGLE	M SUB 2	M SUB 1	S SUB 21	D SUB 21	INTENSITY	POLARIZATION
26.5000	0.726696D+06	0.636103D+06	0.674361D+06	-0.865502D+05	0.681400E+06	-0.0665
153.5000	0.338620D+05	0.277975D+05	0.133752D+04	-0.306511D+05	0.308297E+05	-0.0984

EFFICIENCY FACTOR FOR EXTINCTION 0.203400D+01

EFFICIENCY FACTOR FOR SCATTERING 0.203400D+01

EFFICIENCY FACTOR FOR ABSORPTION 0.0

ASYMMETRY FACTOR 0.879728D+00

0.80000D+02 0.13420D+01 0.0 0.63280D+00 0.26500D+02 0.0 1

ELEMENTS OF THE TRANSFORMATION MATRIX FOR A SPHERE WITH SIZE PARAMETER = 794.33443

REFRACTIVE INDEX. REAL = 0.13420D+01 IMAGINARY = 0.0

ANGLE	M SUB 2	M SUB 1	S SUB 21	D SUB 21	INTENSITY	POLARIZATION
26.5000	0.888014D+06	0.799425D+06	0.836368D+06	-0.101925D+06	0.843719E+06	-0.0525
153.5000	0.503774D+04	0.110838D+06	-0.387128D+04	0.233106D+05	0.579378E+05	0.9130

EFFICIENCY FACTOR FOR EXTINCTION 0.202200D+01

EFFICIENCY FACTOR FOR SCATTERING 0.202200D+01

EFFICIENCY FACTOR FOR ABSORPTION 0.0

ASYMMETRY FACTOR 0.877414D+00

0.90000D+02 0.13420D+01 0.0 0.63280D+00 0.26500D+02 0.0 1

ELEMENTS OF THE TRANSFORMATION MATRIX FOR A SPHERE WITH SIZE PARAMETER = 893.62623

REFRACTIVE INDEX. REAL = 0.13420D+01 IMAGINARY = 0.0

ANGLE	M SUB 2	M SUB 1	S SUB 21	D SUB 21	INTENSITY	POLARIZATION
26.5000	0.103699D+07	0.937279D+06	0.980783D+06	-0.100051D+06	0.987133E+06	-0.0505
153.5000	0.882246D+05	0.772380D+04	-0.923185D+04	0.244173D+05	0.479742E+05	-0.8390

EFFICIENCY FACTOR FOR EXTINCTION 0.201132D+01

EFFICIENCY FACTOR FOR SCATTERING 0.201132D+01

EFFICIENCY FACTOR FOR ABSORPTION 0.0

ASYMMETRY FACTOR 0.878113D+00

0.10000D+03 0.13420D+01 0.0 0.63280D+00 0.26500D+02 0.0 1

ELEMENTS OF THE TRANSFORMATION MATRIX FOR A SPHERE WITH SIZE PARAMETER = 992.91803

REFRACTIVE INDEX. REAL = 0.13420D+01 IMAGINARY = 0.0

ANGLE	M SUB 2	M SUB 1	S SUB 21	D SUB 21	INTENSITY	POLARIZATION
26.5000	0.119919D+07	0.104623D+07	0.111688D+07	-0.849762D+05	0.112271E+07	-0.0681
153.5000	0.513284D+05	0.197524D+05	0.190377D+05	-0.255231D+05	0.355404E+05	-0.4442

EFFICIENCY FACTOR FOR EXTINCTION 0.201675D+01

EFFICIENCY FACTOR FOR SCATTERING 0.201675D+01

EFFICIENCY FACTOR FOR ABSORPTION 0.0

ASYMMETRY FACTOR 0.878813D+00